



Universiteit
Leiden
The Netherlands

Gochlear implants from model to patients

Briaire, J.J.

Citation

Briaire, J. J. (2008, November 11). *Gochlear implants from model to patients*. Retrieved from <https://hdl.handle.net/1887/13251>

Version: Corrected Publisher's Version

License: [Licence agreement concerning inclusion of doctoral thesis in the Institutional Repository of the University of Leiden](#)

Downloaded from: <https://hdl.handle.net/1887/13251>

Note: To cite this publication please use the final published version (if applicable).

COCHLEAR IMPLANTS

FROM MODEL TO PATIENTS

COCHLEAR IMPLANTS

FROM MODEL TO PATIENTS

PROEFSCHRIFT

ter verkrijging van
de graad van Doctor aan de Universiteit Leiden,
op gezag van de Rector Magnificus prof. mr. P.F. van der Heijden,
volgens besluit van College voor Promoties
te verdedigen op dinsdag 11 November 2008
te klokke 11:15 uur

door
Jeroen Johannes Briaire
geboren te Nootdorp
in 1974

Promotiecommissie

Promotor: Prof.Dr.Ir. J.H.M. Frijns
Referent: Prof.Dr. J. Wouters (KU Leuven)
Overige leden: Prof.Dr. P. van Dijk (UMC Groningen)
Prof.Dr. J.G. van Dijk
Dr. W. Soede
Dr. B. van Zanten (UMC Utrecht)

ISBN 978-90-9023555-4

The printing of this thesis was financially sponsored by: Advanced Bionics,
Stichting Atze Spoor Fonds, Med-El and Veenhuis Medical Audio B.V.

Aan Saskia, Pascal en Lianne

Contents

1	Introduction	13
1.1	The first bursts of electric sound	16
1.2	Industry comes into play	21
1.3	Different CI devices	23
1.4	Overview of the present study	23
2	Integrated Use of Volume Conduction and Neural Models to Simulate the Response to Cochlear Implants	27
2.1	Introduction	29
2.2	Electrical volume conduction in the cochlea	31
2.3	Simulating the auditory nerve fibre responses	36
2.4	Results	38
2.4.1	Potential distributions due to intra-cochlear electrodes	38
2.4.2	Model validation: the dependence of the neural responses on the electrode position	40
2.4.3	Applications	46
2.5	Conclusions and future directions	49
2.A	The generalised SEF auditory nerve fibre model	51
3	3D Mesh Generation to Solve the Electrical Volume Conduction Problem in the Implanted Inner Ear.	55

3.1	Introduction	57
3.2	Numerical method selection	59
3.2.1	Lumped parameter models	60
3.2.2	Finite element method (FEM)	61
3.2.3	Finite difference method (FDM)	61
3.2.4	Boundary element method (BEM)	62
3.3	A 3D cochlea mesh	64
3.4	Constructing meshes of implants and the surrounding area	66
3.5	Calculated potential distributions	71
3.6	Discussion and Conclusions	73
4	Field Patterns in a 3D Tapered Spiral Model of the Electrically Stimulated Cochlea	77
4.1	Introduction	79
4.2	Materials and Methods	81
4.2.1	Numerical method to calculate the potential distribution in the cochlea	81
4.2.2	Models of the cochlea	82
4.3	Results	88
4.3.1	Potential and current distributions in the cochlea	88
4.3.2	Neural responses	95
4.4	Discussion	97
4.5	Acknowledgements	102
5	The Importance of Human Cochlear Anatomy for the Results with Modiolus Hugging Multi-Channel Cochlear Implants	103
5.1	Introduction	105
5.2	Materials and Methods	108
5.2.1	Three-dimensional volume conduction model of the human and guinea pig cochlea	108

5.2.2	Simulated electrode configurations	111
5.2.3	Calculating the neural responses	113
5.3	Results	114
5.4	Discussion and Conclusions	118
5.5	Acknowledgement	124
6	Initial evaluation of the Clarion CII cochlear implant: Speech perception and neural response imaging	125
6.1	Introduction	127
6.2	Patients, Materials and Methods	128
6.2.1	The Clarion CII Cochlear Implant	128
6.2.2	Patient Demographics and Follow-Up	130
6.2.3	Neural Response Imaging	133
6.3	Results	134
6.3.1	Speech Perception in Quiet and in Background Noise	136
6.3.2	Neural Responses	140
6.4	Discussion and Conclusions	145
6.5	Acknowledgement	152
7	The relative value of predictive factors of cochlear implant performance depends on follow-up time	153
7.1	Introduction	156
7.2	Materials and Methods	157
7.2.1	Participants	157
7.2.2	Profile fitting method	161
7.2.3	Statistical Analysis	162
7.3	Results	163
7.3.1	Group comparisons	163
7.3.2	Bivariate regression analyses	166

7.3.3	Multiple regression analysis	170
7.4	Discussion	174
7.5	Conclusions	177
7.6	Acknowledgement	178
8	Unraveling the Electrically Evoked Compound Action Potential	179
8.1	Introduction	181
8.2	Materials and methods	184
8.2.1	The forward problem: simulating neural excitation in the human cochlea	184
8.2.2	The backward problem: calculation of the compound action potential	187
8.2.3	The use of an artifact rejection scheme	188
8.3	Results	190
8.4	Discussion	200
8.5	Acknowledgement	207
9	The consequences of neural degeneration regarding optimal cochlear implant position in scala tympani: A model approach	209
9.1	Introduction	211
9.2	Materials and Methods	214
9.3	Results	218
9.4	Discussion	224
9.5	Acknowledgment	229
10	Concept and initial testing of a new, basally perimodiolar electrode design	231
10.1	Introduction	233
10.2	Materials and methods	234
10.3	Results	236

10.4 Discussion	236
10.5 Acknowledgment	237
11 The model as a clinical tool: General discussion and future perspectives	239
11.1 Tuning the implant	241
11.2 The individual patient's cochlear model	241
11.3 Objective measures	242
11.4 Keeping up the pace	244
11.5 The future of cochlear implants	244
Bibliography	249
Summary	269
Samenvatting	275
Curriculum vitae	281

Chapter 1

Introduction

Cochlear implant users regain part of their hearing by direct electrical stimulation of the auditory nerve. In the last decade, cochlear implantation has become an established mode of rehabilitation for adults and children with severe to profound hearing loss (NIH Consensus Statement, 1995). As described below, various different cochlear implant designs have been developed and used over time to rehabilitate profoundly deaf patients. All modern multi channel cochlear implant systems, however, have the same basic components and functions in common (figure 1.1) with the “Chorimac”, developed by Bertin for Chouard in the mid-Seventies.

Every auditory device needs a microphone to capture the incoming sounds. This sound signal is then processed in a speech processor. The speech processors can be divided into two groups, the body worn processors and the behind the ear (BTE) processors. Although there are only small functional differences between the two processors, in some cases, the BTE has a limited processing capability. Basically, the speech processor divides the auditory signal into separate frequency bands, one for each active channel of the cochlear implant. A so-called envelope extraction mechanism usually determines the amplitudes of the various frequency bands. This amplitude information is then coded according to a specific speech coding strategy.

Subsequently, the coded auditory signal is sent to the internal implant via a radio frequency signal. For this purpose a transmitter coil is placed on top of the skin directly over a receiver coil underneath the skin. The transmitter is held in place by a small magnet linked to a similar implanted magnet, automatically aligning both coils on top of each other. The information is then further processed by the internal electronics. The internal electronics are either encased in ceramics or in titanium. In the latter situation the receiver coil is outside the (en)casing in a thin Silastic cover. In the implanted processor, the amplitude information is converted to an electric current, which is in most cases a charge balanced bi-phasic pulse, with a regulated amplitude. This current pulse is sent to a specific channel. In the clinically most used configuration each channel corresponds with a single electrode contact combined with a distant reference electrode. One can, however, also use other configurations with multiple electrodes per channel, with the aim to focus or steer the excitation area, in such a way bipoles or tripoles are created. The electrode array is implanted into the cochlea, usually in the scala tympani, through a cochleostomy in the vicinity of the round window membrane. In this way the electrode contacts are distributed along the cochlear duct. The purpose of this is that each electrode contact stimulates a separate sub-population of nerve fibers and, due to the tonotopic organization of the cochlea, the patient

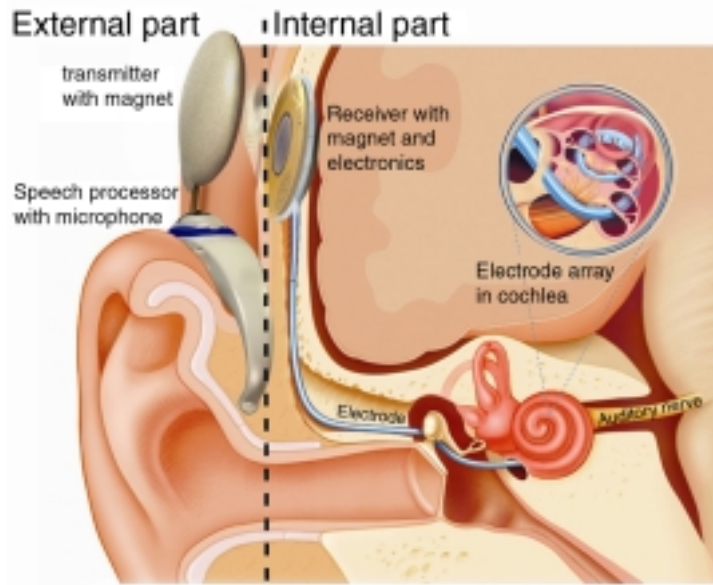


Figure 1.1: Graphical representation of the basic components of a cochlear implant system.

perceives a different auditory perception.

The main design changes of the electrode array and variations in speech coding strategies are made on the basis of insights gained by clinical experience. As Kiang already indicated in the 1970s; at first a lot of guesswork is applied, followed by animal experiments and clinical trials. The opinion was that work in this field would benefit from a more fundamental approach to the problem, an approach based on insights into the mechanisms of electrical stimulation. Computational modeling has become a powerful research and development tool in various fields, from fluid flow in the oil industry to electromagnetism in chip-design. In the field of cochlear implants some initial trials were performed but without an active neural model (Finley et al., 1990; Suesserman and Spelman, 1993). In order to investigate whether a three dimensional computer model of an implanted cochlea including time varying stimulation patterns was feasible, a study was performed with an emphasis on combining an electrical conduction model and an active nerve fiber model. (Frijns, 1995).

In this study a cylindrical symmetrical approximation of a guinea pig cochlea

was used with infinitely small point current sources to represent the electrode array. It appeared to be possible to link an active auditory nerve fiber model to a model of the cochlea, and to simulate, with high accuracy, an outcome resembling that of animal experiments (Shepherd et al., 1993; Frijns et al., 1995). The conclusion of this study was that it is possible to use model simulations in order to predict outcomes of cochlear implantation. Based on these initial findings, the aim of this thesis was to improve the computer model to a degree such that predictions of the outcomes of the implanted human cochlea can be made. This includes realistic representations of the human cochlea and models of clinically used implant devices. Parallel to this study the clinical program at our centre was started. For this reason it is also described in this thesis, how the new insights from our model studies have greatly influenced this clinical program.

1.1 The first bursts of electric sound

Electrical stimulation from the auditory nerve fiber can be traced back to 1790 to the inventor of the battery, the Italian scientist Alessandro Volta. He used the battery to demonstrate that electrical stimulation could directly evoke auditory, visual, olfactory and touch sensations in humans (Volta, 1800). For this purpose, he placed the two ends of a 50 volt battery in each of his ears and described the sensation as follows:

. . . at the moment when the circuit was completed, I received a shock in the head and after some moments I began to hear a sound or rather a noise in the ears, which I cannot define well: it was some crackling with shocks, as if some paste or tenacious matter was boiling . . . This disagreeable sensation, which I believed might be dangerous because of the shock in the brain, prevented me from repeating this experiment

The second report of electrical hearing comes from Duchenne of Boulogne in 1855, a neurologist who did pioneering work on muscular diseases, electrodiagnostics and electrical stimulation. He tried, using an alternating current, to stimulate his hearing and described what he heard, as a sound like an insect trapped between a glass pane and a curtain. During the 1930s, a number of research groups started to investigate the generation of acoustic effects by electrical stimulation of the ear. These studies were based on the above

mentioned early reports of electrical stimulation and on reports of electrical phenomena involved in the mechanism of hearing (Davis, 1935) (Figure 1.2).

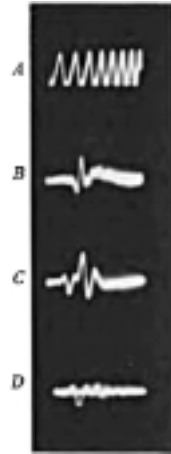


Figure 1.2: Oscillogram of nerve impulses and cochlear responses. A. 1000 Hz wave to show time scale. B. Nerve impulses from the eighth nerve in response to single acoustic clicks. C. Response to single clicks as recorded from the round window, consisting of cochlear response followed by nerve impulse complex. D. The same, except for increase in strength of stimulus, after death of animal showing persistence of cochlear responses and loss of nerve impulses. No response is obtained from the nerve after death (Davis, 1935).

The first direct evidence of electrical stimulation of the auditory nerve was presented by Andreev et al. (1935), who reported hearing sensations during electrical stimulation in a deaf patient whose middle and inner ears were damaged. Experiments at Harvard University involved an electrical circuit, in which one electrode was a copper wire coated with solder inserted into a saline-filled ear, while the ground electrode was attached to the arm. Various AC and DC currents were used. Depending upon the characteristics of the circuits and the ear, various acoustic sensations could be induced in a normal hearing subject. Two subjects were able to hear a tone as low as 125 Hz on one occasion and as high as 12 kHz on two occasions. The sound, however, tended to be distorted. To demonstrate this distortion the electrodes were attached to the output of a radio:

Music can be heard and popular tunes identified, but the quality

is definitely poor – “tin pan” music. Speech can easily be recognized as speech, but only occasionally words can be understood. “Clearly, electrical stimulation does not promise much as an alternative means of hearing so long as so much distortion is present” (Stevens, 1937).

The mechanisms inducing the sound effects in these subjects appeared not only to be due to direct stimulation of the auditory nerve. It was therefore hypothesized that the cochlear microphonic was responsible for the generation of (the) pure tones (Jones et al., 1940).

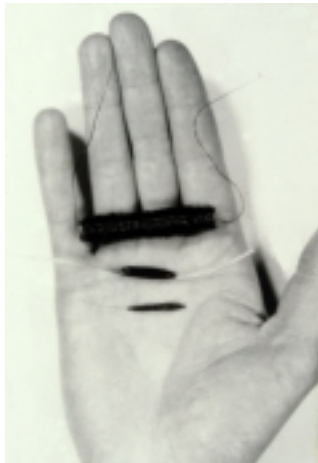


Figure 1.3: First handmade cochlear implant system covered in Araldite

The first attempts to restore hearing through electrical stimulation were made by Djourno and Eyries on February 25 1957. They used a handmade receiver made of insulated silver wire around an iron core (approx. 2000 turns) covered in Araldite (figure 1.3). The electrode contacts were made of stainless steel, soldered to the silver coils. The first patient used the implant (with one reimplantation needed due to electrode fracture) for 20 months until a failure of the second device. This patient noticed changes in amplitude, but not of pitch. The patient demonstrated improved lip-reading capabilities with the use of this implant. The second patient was forced into the surgery by her father and has never been a happy and frequent user. After some time this patient stopped using the device (Graham, 2003; Djourno and Eyries, 1957). This first

success, however, was dampened by the considerable concerns about the safety risks of the patients when an external device is inserted into the inner ear.

The American otologist House, together with a collaborating engineer Doyle, was inspired by the above mentioned French report. In 1961 House implanted a new electrode array, which was designed to stimulate the cochlea at five different positions along its length into the scala tympani. Unfortunately, it appeared that the silicone that was used contained toxic substances and after

about three weeks the electrode was rejected, which led to explantation. Although the subjects perceived some pleasant and useful hearing sensations, active work on cochlear implantation was temporarily suspended at this point (Doyle et al., 1964; House and Urban, 1973).

At the same time, Simmons from Stanford Medical School became interested in cochlear implantation. His first experiment in 1962 was aimed to control the pitch, based on differences in rate of stimulation (Simmons et al., 1964). In 1964 Simmons implanted a 6-electrode array directly into the modiolus of a volunteer who was totally deaf in the right ear and suffered from progressive hearing loss in the left ear. The patient underwent extensive testing to investigate the subject's ability to discriminate between a pitch encoded by place or by rate (Simmons et al., 1965). After being refused permission to present his work at the American Otological Society meeting and being refused a grant from the National Institute of Health (NIH), Simmons stopped working with humans and returned to animal experimental work.

While skepticism engendered by claimed miracles is healthy, outright denial that a genuine research problem exists is not. While my 1964-65 experiments were in progress I contacted a least six of the most prominent researchers in speech coding, and others in auditory psychophysics. None of these persons were willing or interested in suggesting experiments which might have helped define speech coding strategies for the future. I got the distinct impression, perhaps colored by a little personal paranoia after the first few rejections, that everyone was either incapable of thinking about the many problems involved or would rather not risk tainting their scientific careers. I do not believe this problem has disappeared completely in the subsequent 20 years (Simmons, 1985).

The prospects of developing a safe cochlear implant improved in the late 1960s because of the new inventions within various fields such as the space industry (smaller electronics and the transistor) and cardiac pacemakers (the knowledge of biocompatible materials and the effects of electrical stimulation). With these new technologies the implants could be used during a prolonged period in the patients. The attitude and willingness of technologists to collaborate in this area also improved, thereby creating a basis for clinical application of cochlear implants.

In 1968, William House restarted his work on cochlear implants, together with Jack Urban, president of a small brand in medical electronics. In this study

three patients were implanted with a 5-channel array in the scala tympani. After extensive work on speech coding strategies the first wearable speech processor (which could be taken home), was produced mid-1972 (House and Urban, 1973). At the same time the House group changed the multichannel system to a single channel implant system, because it appeared that the multichannel system offered no significant advantage over a single-channel implant. Moreover, they were more difficult to produce.

So Jack and I decided to make an entirely implantable device and to implant 8 or 10 patients that I had selected and who had talked to Graser (one of the first three patients). Because we had discovered that the best sound, as reported to us by our first few patients, was produced when the same signal was injected into all the electrodes, we decided to use only a single, short electrode. By all the evidence we had, nothing more was needed (House, 1995)

In 1971 Simmons and White received a grant from the NIH for the development of cochlear implants. Unlike the House group, Simmons aimed to develop the optimal multichannel implant system. In September 1977 the first patients were implanted with a 4-contact device which was placed directly into the cochlear nerve. The direct contact with the nerve would give lower thresholds, less spread of excitation and less interference due to neural degeneration (Blume, 1995). At the same time an electronic link system was developed in order to replace the then commonly used transcutaneous plug. There was, however, still a lot of opposition to cochlear implants, and particular to “human experimentation”. This view was particularly expressed by Kiang of the Massachusetts Institute of Technology and the Massachusetts Eye and Ear Infirmary. In his opinion, speech perception through electrical stimulation might be possible but not with a single channel device. In addition, there were still physiological and surgical limitations to be overcome for multichannel devices to yield more satisfactory results.

When information available at the level of the nerve is improperly coded, it may prove difficult, even with training, to use a prosthetic device in communication tasks (Kiang and Moxon, 1972).

Kiang stressed that, at that time, prosthesis design was based on nothing more than guesswork, because too little was known about the way the central nervous system processed auditory information (Blume, 1995).

By this time the work of House and his colleagues attracted interest among European clinicians. The controversy between Simmons and House also arose in Europe. In 1973, in France, Chouard implanted his first three patients with a 7 electrode device. Because of the problems with the transcutaneous Teflon plug, Chouard found an industrial partner, Bertin, who wanted to develop (and to construct) a better device based on electro-magnetic coupling (the *Chorimac*). Like House, Chouard believed in the clinical value of the implant device and implanted as many devices as his resources permitted (approximately 1 per month). From 1976 he even started with implantations in children. Meanwhile, in London, a different approach was used. Douek placed the electrode contacts on the outside of the cochlea, extra-cochlear, and obtained similar results to those of House. This (theoretically) safer technique was combined with the idea of Fourcin that implants should be used to supplement information available from lip reading. In this setting, the fundamental frequency is provided instead of the whole speech signal (Fourcin et al., 1979). Like Simmons, the London-Cambridge group main focus was to performed research and had no intention to implant large numbers of devices.

In the late Seventies there was a tendency, based on the early experiments, to apply direct electrical stimulation of the auditory nerve more systematically in a clinical setting. Then, in the period 1978-1982, a turnabout took place when industry became involved. In 1982 a group of experts in the United Kingdom recommended establishment of a limited number of implant centers. (Ballantyne et al., 1982) Remarkably, a few years before, the same group advised caution (Ballantyne et al., 1978). The experimental status of the cochlear implant changed completely in 1984, when the Food and Drug Administration (FDA) in the United States approved the cochlear implant for adults.

1.2 Industry comes into play

The successes of the implants in the late 1970s provided impetus for more research and development. At the same time industry picked up interest and started developing various more or less commercial implants. Several implants and companies appeared on the market: 3M started producing both the Vienna device and the House single channel implant. In Antwerp, the LAURA (Leuven Antwerp University Research Auditory prosthesis) multiple-electrode was developed (Peeters et al., 1989). The Chorimac-8 was updated to the Chorimac-12 by Bertin in France. The first reports appeared, demonstrating relatively good speech understanding using a cochlear implant. This was

shown by the performance (45% correct for words in the Everyday CID Sentences) of 50 patients implanted with the 4 contacts Symbion Ineraid multiple-channel device (Eddington, 1980; Dorman et al., 1989).

At that period, not all implants were placed in the scala tympani. For instance, a large number of patients were implanted with an extracochlear multiple-electrode device developed in Cologne-Düren, Germany (Banfai et al., 1985).

The Australian Nucleus electrode array with 22 contacts was developed by Clark and colleagues for Nucleus Limited. Clinical trials were started in 1982, followed by an international trial in 1983 for the FDA. A study of 40 users showed significant and substantial improvement in speech reading, and in speech understanding with electrical stimulation alone (Dowell et al., 1986).

In the last half of the eighties, this implant became the single-most used implant in the world. The commercial success of the Nucleus device indicated the final acceptance of implants as assistive devices (House, 1995).

The Nucleus implant was a breakthrough in electrode design and device safety, but the introduction of Continuous Interleaved Sampling (CIS) was a major improvement in speech coding strategies (Wilson et al., 1991). Especially, when compared to the speech coding strategies used at that time for instance the Compressed Analog (CA) strategy and feature-extraction (F0/F2 and F0/F1/F2) strategies. The CIS strategy reduced the electrode interaction by presenting the signal in brief pulses to each electrode in a non-overlapping sequence. This resulted in large improvements in speech understanding (Wilson et al., 1991). Almost all modern speech coding strategies are based on the CIS principle.

From animal experiments it was learned that it was possible to record electrically evoked compound action potentials (Charlet de Sauvage et al., 1983). Data from patients implanted with the Ineraid device, with the percutaneous plug, indicated that it was also possible to make these recordings in humans (Brown et al., 1990). With such a method it is expected to obtain data on the neural status and to gain objective indicators for device fitting, especially in young children. These findings initiated the inclusion of the Neural Response Telemetry (NRT) recording system into the Nucleus CI24M implant (Brown et al., 1998). The other implant devices followed with similar capabilities. Neural Response Imaging (NRI) was introduced in the Advanced Bionics CII device (Frijns et al., 2002) and Auditory Nerve Response Telemetry (ART) in the MedEl PulsarCI¹⁰⁰ device.

1.3 Different CI devices

The currently available scala tympani cochlear implants show various differences between the capabilities of the electronics, the number of current sources or contacts and the electrode design. For instance, the Nucleus Freedom implant with the Contour Advance electrode from Cochlear, has one current source and 22 contacts, while the HiRes90K with the HiFocus electrode from Advanced Bionics has 16 current sources and 16 contacts. These differences have their consequences in developing the optimal speech coding strategies to run on the different processors. The large number of contacts and the single current source in the Nucleus device led to a strategy in which the dominant spectral cues are selected and stimulated while the Clarion device, with less electrodes but more current sources, tries to improve the speech signal by using simultaneous stimulation.

The electrode designs differ not only in the number of contacts but more importantly, in geometry. The most implanted electrode design is the precursor of the Contour Advance electrode, the Nucleus banded array, consisting of 22 rings around a Silastic carrier. Another design option is the Clarion pre-curved array with 16 ball electrodes, which are alternately directed toward the modiolus and the basilar membrane. All implants of the latest generation have their contacts directed towards the modiolus. The length of the array is another variable and as a consequence of this there is a variation in the desired insertion depth. The device from MedEl aims for very deep insertions, up to two cochlear turns, where the Cochlear and the Advanced Bionics devices aim for insertions of up to 1.5 cochlear turns. Although there are large differences among electrode designs, there is no definite proof which position, or insertion depth is optimal. Next to these “standard” arrays there are also numerous designs for special situations for instance an array for drilled out cochleas consisting of two shorter arrays, shorter and thinner arrays with the aim of preserving residual hearing in the lower frequencies and arrays on flat surfaces to be placed on the brainstem for when there is no auditory nerve fibre.

1.4 Overview of the present study

This thesis describes the development of a realistic computer model of the implanted human. **Chapter 2** describes the basic principle of modeling cochlear implants with a two step model. The first step is the modeling of the electrical

conduction through the cochlea, also known as the volume conduction problem. The second step is to model the behavior of the nerve fibers in response to the potential distribution calculated in the first step. The potential fields generated by longitudinal dipoles at various locations in a spiral shaped cochlea model are described.

In **chapter 3** a detailed description is given of the volume conduction model including how cochlear meshes are generated. Throughout this thesis, the meshes are spiral shaped and implanted with realistic representations of cochlear implants. To get an accurate representation of the current flow through the guinea pig cochlea for both intra- and extra-cochlear electrode contacts, an air filled bulla was included, surrounding the cochlear mesh. Differences in potential distributions between the cylindrically symmetric and the spiral shaped cochlea model are presented.

In **chapter 4** the current pathways through the cochlea are investigated. The scala tympani is always presumed to be a leaky transmission line, because of its insulating boundaries. The influence of the insulating membranes surrounding the scala tympani as well as the preferable pathways of current conduction through the cochlea are described. The consequences of using a simplification of the spiral shape like a cylindrical symmetric model on the potential distribution and on neural excitation patterns are presented in this chapter.

In **chapter 5** a comparison is made between the outcomes of a guinea pig computer model and a realistic model of the human cochlea, both implanted with a realistic model representation of the HiFocus cochlear implant. Since the beginning of electrical stimulation of the cochlea, a lot of research has been done with animals, implanted with miniaturized electrode arrays placed in the basal turn. The human basal turn is, however, essentially different from other species. By using both a human and a guinea pig cochlea model, a bridge is made between experimental and clinical data.

chapter 6 describes the first clinical evaluation in 10 postlingually deafened adult patients of the HiFocus CII electrode array with the electrode positioning system. This new implant system had the goals as the modiolar electrode used by Simmons in 1977: to produce lower thresholds and less spread of excitation than that now achieved from within the scala tympani. One of the new features of the HiFocus CII implant is neural response imaging (NRI), i.e. the implant has the capability to record the electrically evoked compound action potential (eCAP) without any additional recording electrodes. These eCAP recordings, now available in all modern implant devices, can give indications

of the threshold and other neural properties. The first clinical tests with NRI system are presented in this study.

Chapter 7 recounts the 2 year follow-up of 91 patients implanted between 2000 and 2005 with the CII and HiRes90K cochlear implant presented in chapter 6. Correlation with the duration of deafness, age at implantation and pre-operative CVC scores were calculated directly and with multiple regression analysis using the Iowa predictive model directly or extended to contain age at implantation or the presence of an electrode positioner. The analysis were performed for various periods of implant use to study the consequence of follow-up time on outcome predictors. With the same patient population the consequence of age at implantation and the use of the electrode positioning system are investigated.

Chapter 8 aims at deriving a fundamental understanding of the processes underlying eCAP recordings in humans, both in terms of the contributions of the individual nerve fibers to the overall signal as well as to what extent this signal yields clinically relevant information about functional aspects of electrical stimulation. This chapter describes the expansion of the computational model with the capability to record the eCAP response, similar to the clinical NRI system described in chapter 6. At the same time the neural model has been extended to incorporate an unmyelinated cell body and an unmyelinated pre-somatic region, a specific characteristic of the human auditory nerve fibre.

Chapter 9 describes an extensive model study on the consequences of the choice of location of the electrode array. The electrode positioning system and precurving of the contour electrode array are designed to bring the electrode contacts in close proximity to the nerve fibers by aligning the array against the modiulus. In this chapter the objective is to find the optimal placement of the array in the scala tympani for both, degenerated and non-degenerated cochleae. In the same study, the benefits of eCAP recordings are investigated in order to determine on the basis of these recordings, whether it is possible to make decisions about the optimal location, for instance during surgery.

In **chapter 10** shows a design change, based on the outcomes described in chapter 9, proposed for the HiFocus electrode array, i.e. to position the electrode array against the modiolar wall of the scala tympani at the basal end of the cochlea and along the lateral wall in the more apical regions. In collaboration with Advanced Bionics, prototypes of the new electrode design have been made. The preliminary tests with this design, in temporal bones are described.

In **chapter 11** the capabilities of the current model are described as well as

future steps needed for the creation of a patient specific model with direct clinical implications for the individual patient. Some of the ongoing developments leading to a new generation of cochlear implants are highlighted.

Chapter 2

Integrated Use of Volume Conduction and Neural Models to Simulate the Response to Cochlear Implants

Johan H.M. Frijns, Jeroen J. Briaire and
Ruurd Schoonhoven
Simulation Practice and Theory (2000), 8 (1-2), 75-97

Abstract

Cochlear implants are electronic devices intended to restore the sense of hearing in deaf people by direct electrical stimulation of the auditory nerve fibres that are still present in the deaf inner ear. Unfortunately, the clinical outcome is not very predictable. In this study a computational model is presented that can predict the neural response to an arbitrary cochlear implant. It first computes the potential distribution set up in a 3-dimensional, spiralling volume conduction model of the auditory part of the inner ear (cochlea) and then applies a nerve fibre model to construct input/output curves and excitation profiles of the auditory nerve. As an initial validation the results are compared with experimentally induced electrically evoked auditory brainstem responses. In the light of the favourable results, we conclude that the model can serve as a tool for designing future cochlear implants. In combination with electrophysiological measurements in the individual patient it is applicable as an implant fitting tool.

2.1 Introduction

In normal hearing, air pressure variations with frequencies between 20 Hz and 20 kHz are translated into neural information (action potentials) on the auditory nerve. This nerve conveys the information to the brainstem and higher auditory pathways. For this purpose the sound energy is picked up by the external ear and transmitted via the eardrum and the middle ear ossicles (malleus, incus and stapes) to the inner ear (cochlea). In the cochlea the final transduction from mechanical vibration into action potentials takes place. It is shaped as a tapered tube (the membranous labyrinth) that is wound in a spiralling fashion around the modiolus that contains the central axons of the auditory nerve fibres in their course to the brain stem. In humans the cochlea has $2\frac{3}{4}$ turns and is fully embedded in the solid petrous bone, while it has $3\frac{1}{2}$ turns and protrudes into the air-filled bulla (middle ear) in our experimental animal, the guinea pig. In physiological hearing the nerve fibres are arranged tonotopically, i.e. the nerve fibres located at the base of the cochlea (i.e. near the stapes) encode for the higher frequencies, whereas the more apical ones respond to the lower frequencies. In fact, the normal cochlea acts more or less as a mechanical Fourier analyser (Dallos et al., 1996), where each place along the basilar membrane (and thus each nerve fibre) is sharply tuned to respond to a specific frequency.

Hearing impairment, resulting from damage to the cochlea (usually to the outer or inner hair cells), is called sensorineural hearing loss. This induces elevated hearing thresholds and loss of tuning, resulting, e.g., in difficulties in understanding speech. Patients having mild to moderate sensorineural hearing loss can be helped with conventional hearing aids, which are basically sound amplifiers. In cases of profound sensorineural hearing loss (deafness) such conventional hearing aids are insufficient. For this group of patients cochlear implants have been developed. These are electronic devices that can give a sense of hearing to profoundly deaf patients by direct electrical stimulation of the spiral ganglion cells (primary auditory nerve fibres) that are still present in the damaged cochlea (Balkany, 1986). At present, over 16000 patients have been implanted world-wide with several devices of varying designs, most of which apply electrode arrays inserted into the scala tympani through the round window membrane at the basal end of it or through a so-called cochleostomy through the surrounding bone. In spite of promising results in approximately 25% of recently implanted patients, which are more or less able to take part in normal conversation without the help of lip reading, it is very difficult to identify the parameters that are crucial to predict the clinical outcome pre-operatively.

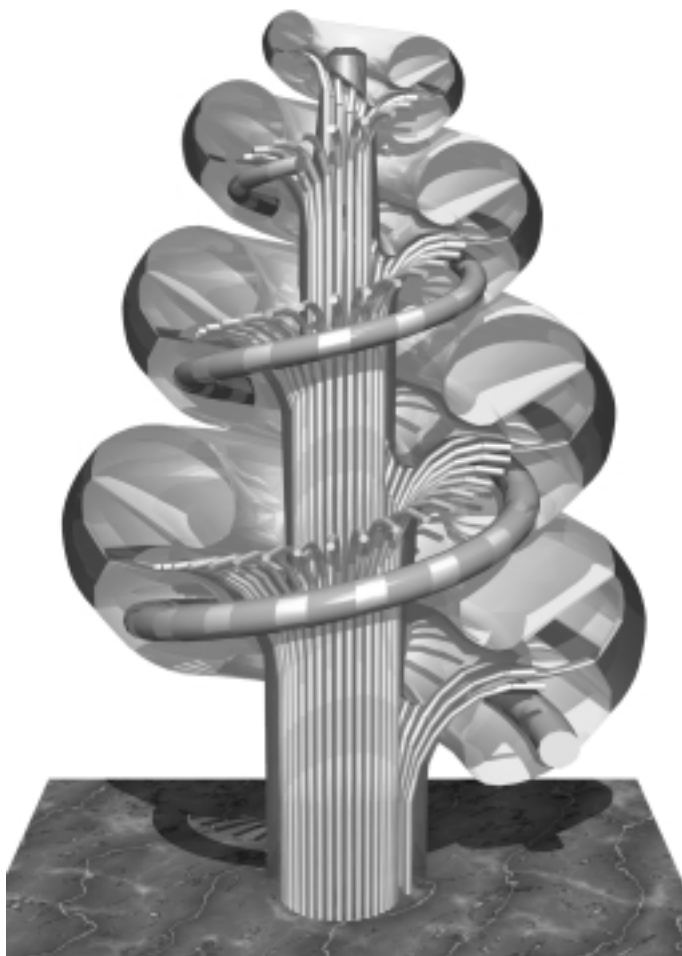


Figure 2.1: An artist's impression of a Nucleus®-like cochlear implant inserted into the scala tympani of a guinea pig cochlea. The banded electrode array consists of Platinum contacts on a silastic carrier.

This outcome appears to be the result of a complex interplay between various patient and device related factors, which are not yet fully understood (Gantz et al., 1993). Initial research in this field was primarily defined in terms of clinical concerns. It established the feasibility of the approach and documented the beneficial effects and possible risks. However, in order to achieve a further improvement of the clinical results by more sophisticated implant designs, more information from basic research is needed to identify the key factors that need optimisation. Modern multichannel cochlear implants try to take advantage of the tonotopy in the cochlea by trying to stimulate localised sub-populations of nerve fibres by each electrode combination in the electrode array. The resulting configuration is illustrated in Fig. 2.1, which shows an artist's impression of a typical multichannel implant in a guinea pig cochlea. The spatial selectivity thus aimed at, is the electrical counterpart of the mechanical tuning, present in the normal cochlea.

This paper focuses on the development of a computational model of the implanted cochlea, which is intended to provide more insight in the fundamentals of functional electrical stimulation of the auditory nerve. This problem not only involves simulating the response of a nerve fibre to an externally applied potential field, but also the calculation of this potential distribution from the currents on the stimulating electrodes (Fig. 2.2). This is especially intricate in the case of cochlear implants due to the complex geometry of the inner ear. In previous studies we used a rotationally symmetric cochlear geometry to calculate neural excitation patterns and the spatial selectivity for different electrode configurations and stimulation patterns (Frijns et al., 1995; Frijns et al., 1996a). We showed that the simulation results were in good accordance with experimental data despite the use of a simplified geometry. In this paper, we will present and validate a more refined, helical representation of the cochlea. We will show how this model can be applied to give insight in the performance of various multichannel electrode designs.

2.2 Electrical volume conduction in the cochlea

Measurements of the *in vivo* electrical properties of a cochlea implanted with an electrode array confirmed that there is a strong influence of the cochlear electro-anatomy on the neural excitation patterns induced by cochlear implants (Black et al., 1983; Ifukube and White, 1987). An analytic solution of such a 3D volume conduction problem is restricted to geometries that are

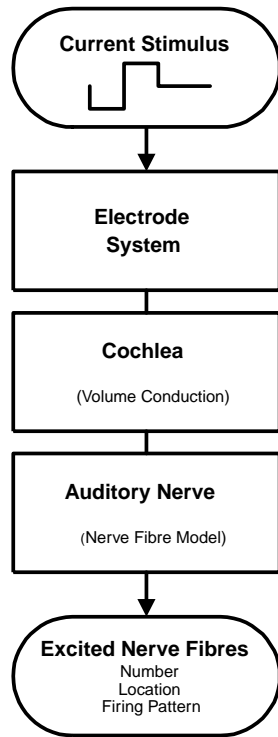


Figure 2.2: The conceptual framework behind the model of the electrically stimulated ear. The input signal is the current stimulus in the top-most panel, which is delivered by the speech processor. This current induces a potential field in the cochlea via the electrode system. This potential field, as computed by the volume conduction model, forms the input of the nerve fibre model that predicts which auditory nerve fibres will be excited. The information conveyed to the brain is characterised by the number, location and firing pattern of these fibres, the model's output.

much simpler than the cochlea, and the first theoretical models on the (actually three-dimensional) potential pattern set up in the cochlea by the stimulating current sources assumed an exponential decay of current from its source to the nerve fibres along the cochlea, modelled in one dimension (O'Leary et al., 1985). Sapozhnikov (Sapozhnikov, 1990) computed potential distributions with a finite difference method in a linear, unrolled cochlear geometry, incorporating two cochlear turns. Girzon (Girzon, 1987) also used a finite difference method to compute the potential distribution in an anatomically-based three-dimensional volume conductor that included a continuously spiralling cochlear duct, and showed that the scala tympani acts in part as a terminated leaky transmission line. The limited spatial resolution of his model, however, did not permit the computation of neural excitation functions. Finley et al. (Finley et al., 1990) were the first to present an integrated three-dimensional neuron-field model of a segment of an unrolled cochlea, using the finite element method (FEM) and a passive nerve fibre model based upon activating functions (Rattay, 1993) for most of their computations. Suesserman and Spelman (Suesserman and Spelman, 1993) developed a so-called lumped-parameter model of the unrolled first turn of a guinea pig cochlea in which they incorporated resistive and capacitive components but did not include any neural element. Using the Boundary Element Method (BEM) (van Oosterom, 1991), we developed a rotationally symmetric volume conduction model of the second turn of the guinea pig cochlea, coupled with an active nerve fibre model (Frijns et al., 1995; Frijns et al., 1996a). Unlike the other models, the model preserved the contiguity in the modiolus of the auditory nerve fibres coming from different places in the cochlea. It was shown to give a more accurate description of the neural recruitment characteristics, especially for higher stimulus currents where excitation of nerve fibres in the modiolus takes place.

The BEM is also used in the present study, as it offers the advantages of a relative ease of mesh generation and the opportunity to perform calculations with multiple current source configurations instead of one, with a limited additional amount of computational effort. It requires discretisation of the boundaries between volumes with different conductivity rather than discretisation of these volumes themselves. To increase the numerical accuracy and to obtain a more realistic shape of the modelled cochlea we tessellated all boundaries with quadratically curved triangular surface elements on which the potential was also interpolated quadratically (Frijns et al., 2000b). The mesh was generated by spiralling the cross-section shown in Fig. 2.3 around the central axis the modiolus of and scaling it (Briaire and Frijns, 2000a). The resulting mesh is completely embedded in bone (the potential is defined to be 0 in infinity),

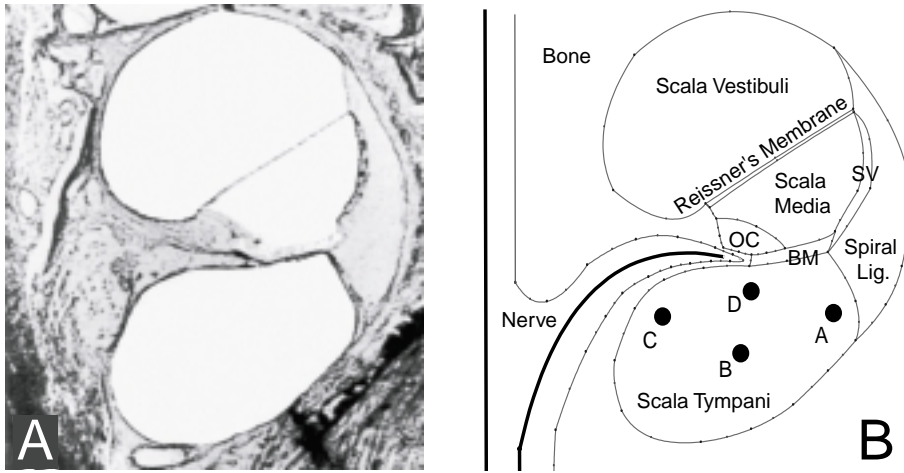


Figure 2.3: A Photomicrograph of the cross-section at the beginning of the second turn of a left guinea pig cochlea that was used to construct the boundary element mesh in (B). B. The modelled cross-section of the second turn of the guinea pig cochlea, showing how the contours of the cross-section in (A) can be represented adequately with parabolic line elements. The various compartments with different conductivities (see Table 2.1) are indicated (with BM=Basilar Membrane; SV=Stria Vascularis; OC=Organ of Corti) as well as the four electrode sites (A = near the outer wall; B = central in the scala tympani; C = near the spiral ganglion; and D = underneath the dendrites). The course of two nerve fibres, one ending in the modelled second turn and one in a more apical turn, is displayed.

and contains three turns (Fig. 2.4). It is locally refined in the vicinity of the current sources in order to minimise computational errors in regions of high potential gradients. The fact that the mesh does not include a helicotrema (the interconnection of the scala tympani and the scala vestibuli at the apex) is not expected to influence the results in this study since all current sources are placed at a relatively large distance from the apex.

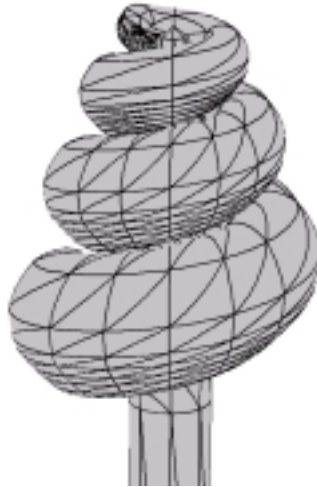


Figure 2.4: The 3D boundary element mesh of the cochlea used in the volume conduction calculations. It has local mesh refinements around the sites where the current sources are situated. In contrast to the in vivo situation the mesh spirals up to an apical closure point, so it does not have a so-called helicotrema where the scala tympani and scala vestibuli are interconnected.

Table 2.1 illustrates the large differences in electrical conductivity between the various cochlear tissues: The fluid-filled scalae are highly conductive compared to the surrounding bone and membranes. In all simulations capacitive effects are neglected, as measurements have shown that this assumption is valid for frequencies up to 100 kHz (F. Spelman, personal communication).

Table 2.1: The conductivities of the various cochlear tissues as used in the computations (the data were compiled from Frijns et al. (1995)).

Tissue	Conductivity (Ωm) ⁻¹
Scala tympani	1.43
Scala vestibuli	1.43
Scala media	1.67
Stria vascularis	0.0053
Spiral ligament	1.67
Reißner's membrane	0.00098
Basilar membrane	0.0625
Organ of Corti	0.012
Bone	0.156
Nerve tissue	0.3

2.3 Simulating the auditory nerve fibre responses

Fig. 2.5^A shows the anatomy of the primary auditory nerve fibres. These are thin bipolar nerve fibres, which are myelinated, i.e. the axon is covered by a highly insulating layer of Schwann cells. This layer is interrupted at more or less regularly spaced intervals, in the so-called nodes of Ranvier. In these nodes, the cell membrane contains voltage-dependent sodium and potassium channels that are responsible for the excitability of the nerve fibres. When elicited electrically, the action potentials propagate from node to node in both directions from their initiation point (so-called saltatory conduction) (Rattay, 1993). Basically, there exist two types of primary auditory nerve fibres. The majority are so-called high spontaneous rate (HSR) fibres, which have an axon diameter of 3 μm in guinea pigs and cats, while low spontaneous rate fibres have thinner peripheral processes (axon diameter 2 μm) (Gleich and Wilson, 1993; Liberman and Oliver, 1984). In a previous paper (Frijns et al., 1996a) we performed simulations with both types of fibres and concluded that these physiological variations in size of the auditory nerve fibres are not expected to have substantial influence on the performance after cochlear implantation. Therefore, we will here just perform calculations with a model equivalent of the HSR fibres.

In an attempt to model the behaviour of these fibres Colombo and Parkins (Colombo and Parkins, 1987) developed a model of the mammalian auditory-nerve neurone based on the classical work on amphibian nerve fibres of Frankenhæuser and Huxley (Frankenhæuser and Huxley, 1994). In order

to fine tune the model to represent physiological data obtained from single auditory-nerve fibre experiments in squirrel monkeys they had to adapt the modelled nerve fibre's anatomy significantly. Rattay and co-workers (Motz and Rattay, 1986; Rattay, 1993) used a single-node model to investigate the time structure of the response of the auditory nerve to electrical stimuli and concluded that the Hodgkin and Huxley (Hodgkin and Huxley, 1952) model of unmyelinated squid giant axon membrane simulates the electrically stimulated (myelinated!) auditory nerve best in time behaviour. We developed the so-called MSEN (Frijns and ten Kate, 1994) and SEF (Frijns et al., 1994) models which are non-linear cable models which represent essential mammalian nerve fibre properties, including spike conduction velocity, refractory behaviour and repetitive firing, better than previous models and can deal with arbitrary stimulus wave forms. The SEF model is based upon voltage clamp measurements in rat and cat motor nerve fibres at mammalian body temperature performed by Schwarz and Eikhof (Schwarz and Eikhof, 1987). In this paper, we will use a generalised version of the SEF model, which also describes the prolonged duration of action potentials and refractory periods in nerve fibres of smaller diameter like primary auditory nerve fibres (Fig. 2.5^B) (Frijns et al., 1994; Frijns, 1995). The model treats the internodal myelin sheet as a perfect insulator, as it was in the original SEF model.

The simulations involved 365 nerve fibres, uniformly distributed along the three cochlear turns, each representing approximately 85 actual nerve fibres that are present in a real cochlear segment of 3° (± 0.6 mm along the basilar membrane). To fit the nerve fibres into the tapered cochlea model we applied a linear scaling factor to the lengths of the three internodes of the peripheral process of the fibres in such a way that the relative position of the soma and the unmyelinated terminal to the membranous labyrinth was constant throughout the cochlea. This scaling factor ranged from 1.3 at the basal end of the cochlea to 0.43 at the apex, while it was 1.0 at the base of the second turn.

For each nerve fibre a system of 100 coupled non-linear differential equations (i.e. four equations for each of the 25 included active nodes of Ranvier) had to be solved. The details of the model equations and the parameters used are summarised in Appendix 2.A.

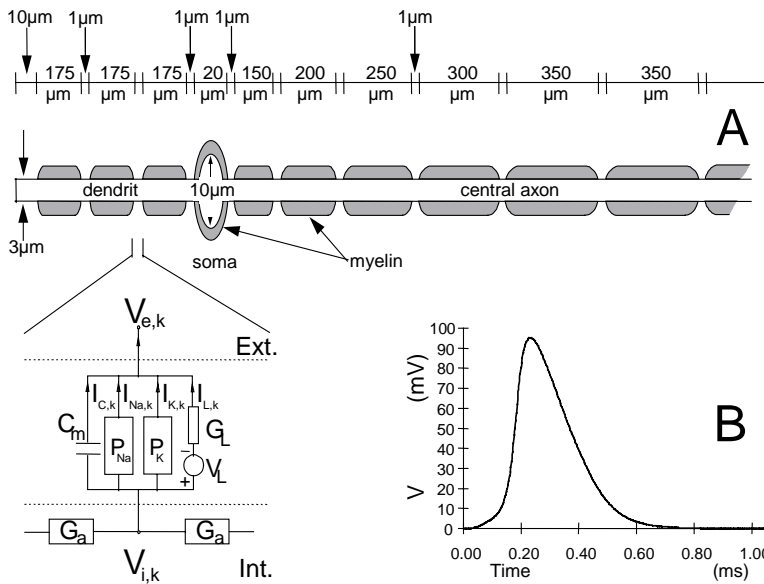


Figure 2.5: The form and function of the auditory nerve fibre model. Excitation of the fibre results in the production of an action potential (B) that is conducted to the brain along the axon. The electrical analogue of the mechanism in the so-called node of Ranvier that is responsible for the generation and propagation of the action potentials is shown in the lower left of (A).

2.4 Results

2.4.1 Potential distributions due to intra-cochlear electrodes

Fig. 2.6 shows the equipotential lines in a cross-section near the anode as computed for a longitudinal bipolar point current source of 1 mA (750 μm distance between the sources, called 'Bipolar+1', see below) at four representative positions in the scala tympani. It demonstrates the insulating effects of the highly resistive membranes surrounding the scala media, resulting in a relatively limited effect of the injected current on the nerve terminals in more apical turns. It is also clear that the potential distribution on the peripheral processes of fibres in the vicinity of the electrodes strongly depends upon the exact position of the electrode in the scala tympani. This is further illustrated in Fig. 2.7.

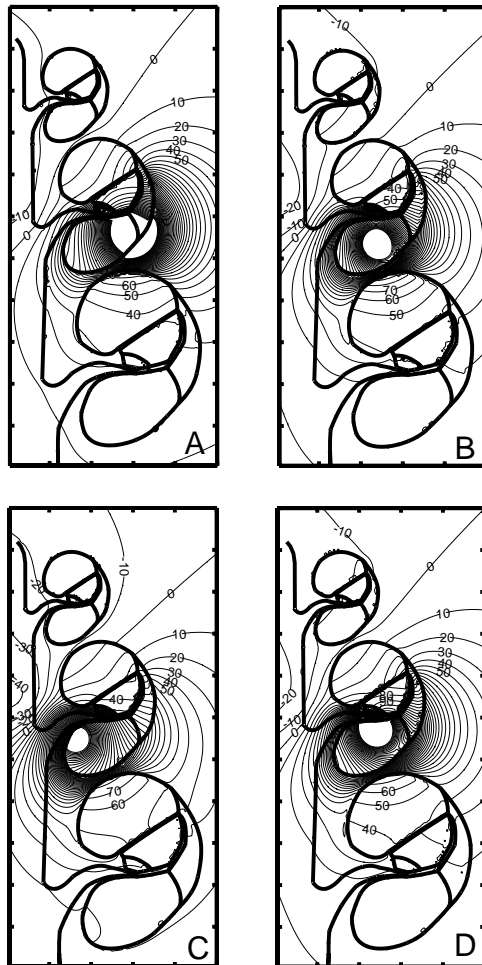


Figure 2.6: The potential distribution close to the anode due to a longitudinal current dipole (inter-electrode distance $750 \mu\text{m}$) at four sites in the scala tympani, $1 \frac{1}{4}$ turns from the basal end of the cochlea (A = near the outer wall; B = central in the scala tympani; C = near the spiral ganglion; and D = underneath the dendrites). The potentials are in mV for a 1mA source.

This figure shows for the electrode position in the centre of the scala tympani (B in Fig. 2.6) how the potentials vary along four representative nerve fibres, at the base, at the beginning of the second and the third turn and at the apex of the cochlea. It demonstrates that fibres in the implanted turn (1 in Fig. 2.7) experience the highest stimulating potentials in their peripheral process, and therefore they are most likely to be excited there. On the other hand, fibres from more apical turns (2 and 3 in Fig. 2.7) have their highest potentials in their modiolar part, i.e. where they pass by at the level of the electrodes. As contrasted with the widely spread concept based upon unrolled geometries (O'Leary et al., 1985; Suesserman and Spelman, 1993), this means that for the excitation of these fibres the current flow along the scala tympani (which would lead to elevated potentials at their peripheral processes) is less important than the current flowing directly into the modiolus. In other words, the electrode in the second turn will probably excite fibres originating in more apical turns in the modiolus rather than at their peripheral processes, giving rise to so-called ectopic or cross-turn stimulation (see below).

2.4.2 Model validation: the dependence of the neural responses on the electrode position

It was shown experimentally in cats that both the threshold currents and the slope of the input-output curves of the electrically evoked auditory brainstem response (EABR, an objective measure of the hearing sensation brought about by the electrical stimulus) depend upon the exact location of bipolar scala tympani electrodes (Shepherd et al., 1993). As these differences must be reflected in the excitation patterns of the auditory nerve at the level of the cochlea, these data are applicable to validate our model predictions against experimental results.

For this purpose we computed potential distributions in our volume conduction model of the cochlea for longitudinally directed bipolar electrodes at four locations (A=near the outer wall, B=in the middle of the scala tympani, C=adjacent to the modiolus and D=underneath the dendrites) comparable to the ones used experimentally (see Fig. 2.3^B). We used the same biphasic current pulses (pulse width 200 μ s/phase, the more apical electrode of the electrode pair acting as the cathode during the first stimulus phase) in our simulations as in the experiments, but all electrode spacings were scaled down by a factor 2 to account for the difference in size between the modelled guinea pig cochlea and the feline cochlea used in the experiments. For the so-called 'bipolar'

stimulus mode this resulted in a $375 \mu\text{m}$ inter-electrode distance, whereas it was 0.75 mm and 1.125 mm for the situations that will be referred to as 'bipolar+1' and 'bipolar+2', respectively (a terminology that was adopted from the Nucleus[®] cochlear implant that was used experimentally (Shepherd et al., 1993)).

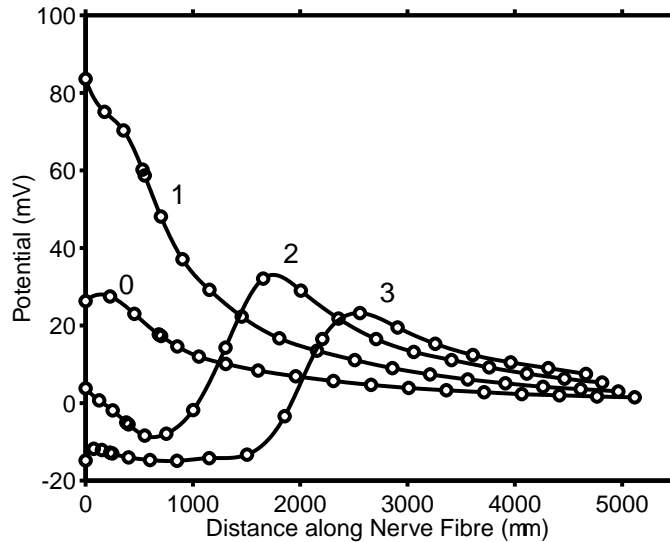


Figure 2.7: The potential along the nerve fibres, at the base (0), at the beginning of the second (1) and the third (2) turn and at the apex (3) of the cochlea for electrode pair B in Fig. 2.6. The symbols indicate the position of the nodes of Ranvier. The cell body (soma) has a short length of $20 \mu\text{m}$ (see Fig. 2.5) and its position, which depends on the scaling of the peripheral process, can therefore be recognised by the two intersecting circles on each curve.

Using the potential distributions computed this way, we determined the excitation threshold for all 365 nerve fibres in the model, while we also recorded the node of Ranvier in which the initial excitation occurred. For the four 'bipolar+1' electrode configurations the results are presented as so-called threshold profiles in Fig. 2.8. For all four electrode pairs this figure shows a bimodal distribution of excitation thresholds in the vicinity of the implanted electrodes, and this pattern is repeated to some extent in the cochlear regions 1 turn more basal and 1 turn more apical than the stimulation current sources. This bimodality is a consequence of the fact that there is a zero-potential plane in between the

electrodes constituting the dipole and that the fibres run approximately parallel to this plane. The global threshold (defined as the level at which the first fibre starts firing) varies significantly among the four electrode positions, as we already expected from the potential distributions in Figs. 2.6 and 2.7.

The threshold profiles also show that above this global threshold there is a gradual spread of excitation around the site of current injection with increasing stimulus levels. This gradual recruitment of neurones is most likely to be perceived as an increasing loudness of the stimulus. At currents above ± 0.5 mA (position C) to ± 1.7 mA (position A) also fibres in higher cochlear turns are excited in the modiolus rather than at their peripheral processes. On the basis of the tonotopic organisation of the auditory nerve, this cross-turn stimulation, already alluded to above when describing Fig. 2.7, is expected to produce sensations corresponding with far lower frequencies than those associated with the place of the stimulating electrodes and therefore must be considered as an unwanted effect.

The data shown in a threshold profile can be summarised by plotting the number of excited nerve fibres as a function of stimulus level. This yields the so-called I/O-curves, shown in Fig. 2.9 for the same four 'bipolar+1' electrode configurations. In this plot, the excitation threshold is visible as the intersection of each curve with the abscissa. The slope of the I/O-curve is a measure of the spatial selectivity, since a steeper slope indicates that more fibres get excited with increasing stimulus levels. In accordance with this notion, the stimulus level at which cross-turn stimulation occurs can be recognised as a sudden increase of the slope of the I/O-curve.

From the results shown in Fig. 2.9 it is clear that -like in the experiments- also in the simulations both the excitation threshold and the slope of the I/O-curve depend upon the exact place of the electrode in the scala tympani. With other electrode spacings ($375 \mu\text{m}$ = 'Bipolar' and $1125 \mu\text{m}$ = 'Bipolar+2') we found similar effects. The results are summarised and compared against Shepherd's experimental findings (Shepherd et al., 1993) in Table 2.2. It appears that the average ratio between the experimental and simulated current thresholds is approximately 3, rather than 1, which would obviously have been the ideal result. However, the fact that this ratio is fairly independent from electrode site and electrode spacing, implies that the model gives realistic predictions of the relative threshold shifts between the various electrode configurations. The main exception to this finding is the bipolar electrode in the C position, for which the ratio is even 6.6! This exception may be explained by the notion that the solution for this position is particularly sensitive to numerical limitations of

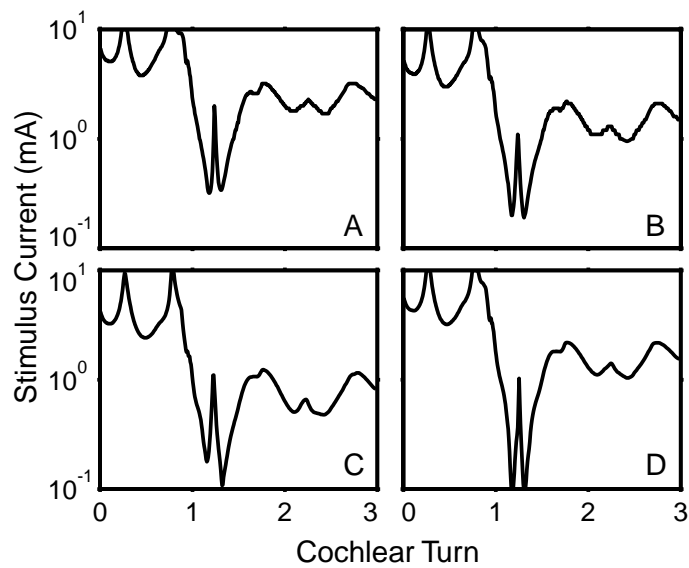


Figure 2.8: Threshold profiles, showing the excitation thresholds of all fibres from the base (turn=0) to the apex (turn=3) of the cochlea for symmetric biphasic pulses with a duration of $200 \mu\text{s}/\text{phase}$ on so-called 'bipolar+1' electrode configurations (inter-electrode distance $750 \mu\text{m}$) located $11/4$ turns from the basal end of the cochlea. Stimuli were cathodic-first, which means that the more apical electrode acts as the cathode during the first stimulus phase. (A)-(D) indicate the same electrode pairs as used in Fig. 2.6.

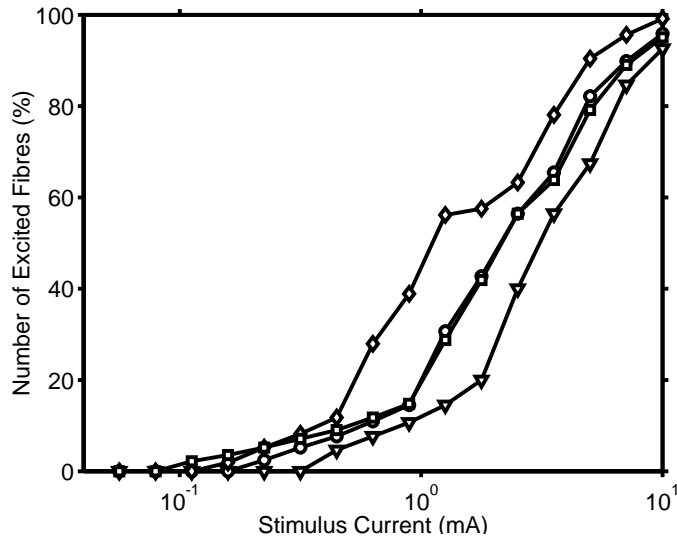


Figure 2.9: I/O-curves, showing the percentage of nerve fibres that is excited as a function of the stimulus current (cathodic-first biphasic stimuli, $200 \mu\text{s}/\text{phase}$). These data were computed from the threshold curves in Fig. 2.8.

the BEM method due to the close vicinity of 3 media with large steps in conductivity (nerve tissue, bone and perilymph). Other explanations of the discrepancies between the model and the experiments include the experimental uncertainty about the actual electrode positions and the biological variability between cats, clearly shown in Shepherd's results. Furthermore, the anatomical differences between the cat cochlea and our guinea pig model are obvious, especially with respect to the exact location of the nerve fibres in relation to the medial wall of the scala tympani.

Table 2.2 also compares the slope of the I/O-curves (computed by counting the auditory nerve fibres that are excited 12 dB above the computed thresholds) against Shepherd's data (Shepherd et al. (1993), Table V) on the slope of EABR I/O-curves. Ideally, the ratio between the EABR slope (in $\mu\text{V}/\text{dB}$) and the slope of the computed I/O-curve (expressed as the percentage of excited nerve fibres per dB) would have a constant value, as the relative contribution of each actual fibre to the amplitude of the EABR-response is believed to be constant. As shown in Table 2.2, this is largely the case for all 12 electrode configurations tested.

When comparing the results of these validation steps with those obtained with

Table 2.2: Comparison of the computed thresholds (I_{th}) and I/O-curve gradients for the first 12 dB above I_{th} (G_{IO} , expressed as the percentage of modelled fibres that is excited) with corresponding experimental EABR data [28], I_{th}^{exp} and G_{IO}^{exp} for all electrode spacings and electrode sites A-D. The values between brackets were computed with the omission of the data for the bipolar C position, which are most likely influenced by numerical errors (See text).

Electrode Site	I_{th} (mA)	I_{th}^{exp} (mA)	I_{th}^{exp}/I_{th}	G_{IO} (%fibres/ dB)	G_{IO}^{exp} (μV / dB)	G_{IO}^{exp}/G_{IO}
Bipolar						
A	0.50	1.10	2.20	0.98	0.42	0.43
B	0.27	0.99	3.67	0.73	0.48	0.65
C	0.10	0.66	6.60	0.66	0.33	0.50
D	0.13	0.32	2.39	0.41	0.19	0.47
Mean \pm SD			3.71 \pm 2.03 (2.75 \pm 0.80)			0.51 \pm 0.10 (0.51 \pm 0.12)
Bipolar+1						
A	0.32	0.59	1.84	1.21	0.47	0.39
B	0.19	0.55	2.89	0.91	0.46	0.50
C	0.11	0.34	3.15	0.98	0.38	0.39
D	0.08	0.26	3.07	0.59	0.31	0.52
Mean \pm SD			2.74 \pm 0.61			0.45 \pm 0.07
Bipolar+2						
A	0.26	0.47	1.81	1.26	0.50	0.40
B	0.18	0.41	2.28	1.19	0.46	0.39
C	0.09	0.31	3.64	1.00	0.45	0.45
D	0.11	0.24	2.10	0.87	0.35	0.40
Mean \pm SD			2.46 \pm 0.81			0.41 \pm 0.03
<i>All spacings</i>						
Mean \pm SD			2.97 \pm 1.31 (2.64 \pm 0.68)			0.46 \pm 0.08 (0.45 \pm 0.08)

the previous, rotationally symmetric model (Frijns et al., 1995), it is clear that the predicted thresholds are largely the same. This is not surprising, since the electrode configurations involved are relatively closely spaced bipolar current sources for which the difference between the local dimensions of both cochlear models is very limited. The predictions for the slopes of the I/O-curves, however, are better in the spiral model, which represents the modiolar structure better (in the rotationally symmetric model we had to exclude the responses for higher cochlear turns to obtain a good match between experimental and simulation data).

As a test of the sensitivity of the model to uncertainties in the conductivity of the various media, we varied the individual conductivities up and down by a factor 2. It turned out that the changes to the computed neural excitation patterns were negligible for all media, except for perilymph and bone. The main effect of reducing the conductivity of the bone by 50% was an increase of the thresholds for ectopic stimulation by 1-3 dB depending on the electrode site. A decreased conductivity of the perilymph (comparable to fibrous tissue or bone formation in the scalae as quite often occurs after electrode insertion) results in an approximately proportionate decrease of the excitation thresholds, as well as a slight increase of the slope of the I/O-curves. As the conductivity of the perilymph is known within a few percent, and the conductivity of cochlear bone has been measured with an accuracy of approximately 30% (Suesserman, 1992), we concluded that the model predictions are relatively insensitive to uncertainties in all conductivities.

2.4.3 Applications

All computations shown thus far involved point current sources. Actual cochlear implants, however, have electrode arrays with dimensions that are not negligible relative to the size of the scala tympani. As described in the companion paper (Briaire and Frijns, 2000a), the meshing software, developed to construct the mesh of the cochlea, also enables us to construct meshes of such clinically used electrodes. As these electrodes are intended to be inserted into the scala tympani without disruption of the cochlear tissues, the resulting situation can be modelled by simple addition of the meshes of the cochlea and the electrode. Then, the various electrode combinations can be simulated by the insertion of point current sources in the centres of the highly conducting ($\sigma = 10^7(\Omega m)^{-1}$) areas representing the electrode contacts. Examples of such electrode meshes are shown in Fig. 2.10.

Preliminary simulations with a Nucleus[®]-like electrode (Figs. 2.1 and 2.10^A) in the guinea-pig cochlea have shown results that are highly comparable with the ones shown in Table 2.2 provided that the cross-sectional area of the electrode is small (< 10%, like in the clinical situation) relative to that of the scala tympani (Briaire and Frijns, 1998a). With bipolar stimulation thick electrodes result in reduced thresholds and current densities, while the spatial selectivity is comparable to that obtained with thin ones. The simulations also indicated that tripolar stimulation with this electrode is only favourable (i.e. highly selective) if it is thin, and that the associated high global excitation thresholds easily lead to high current densities at the electrode surfaces. This is an undesirable

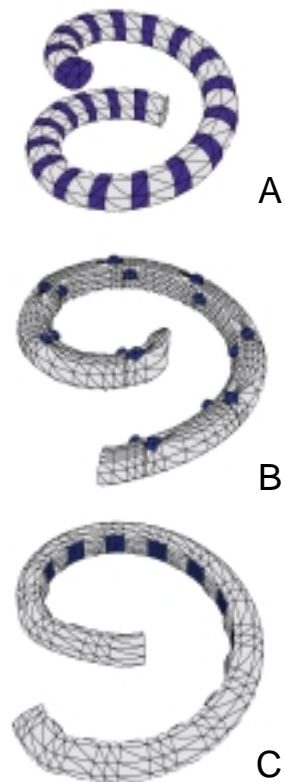


Figure 2.10: Some examples of boundary element meshes of clinically applied electrodes. The black areas are Platinum surface contacts, the grey areas represent the silastic carrier. A. The Nucleus[®] electrode, the most commonly used electrode in clinical practice. It consists of 22 regularly spaced Platinum bands on a silastic carrier. B. The Clarion[®] electrode, which has 16 Platinum ball contacts (eight on the medial side, eight on top) that are partly recessed into the silastic carrier. C. The Clarion[®] Hi-Focus[®] electrode, which has 16 square Platinum contacts located medially, separated by silastic blebs, protruding from the carrier. It is intended to be displaced against the modiolar wall by a silastic positioner that is inserted laterally, against the outer wall.

condition, as electrical stimulation can lead to damage to biological tissues if the charge density per phase exceeds a certain critical level (Brummer and Turner, 1977).

Our group is especially interested in the use of extra-cochlear electrodes, which are placed in the bony labyrinth, just outside the cochlea. Such electrodes can be placed over the apex (the upper end of the cochlear spiral), which is inaccessible for scala tympani electrodes. This is particularly interesting in the light of the fact that many patients suffering from severe sensorineural hearing loss have relatively many intact auditory nerve fibres in this region. In addition, these low and middle frequency nerve fibres are important for the understanding of speech in normally hearing subjects, while these fibres also play an important role in directional hearing by detection of interaural time differences. An important drawback of the extra-cochlear location of electrodes is the fact that the distance between the stimulating electrodes and the excitable neural elements is relatively large. This is expected to result in higher stimulation thresholds and less selective stimulation. The higher stimulus currents involved may also impose limitations on the dynamic range, e.g., due to stimulation of the facial nerve. One of the ways we conceived to deal with the latter problem is to combine intra- and extra-cochlear electrodes as radial bipolar pairs. The fact that the electrodes are oriented radially eliminates the bimodal character seen in the threshold profiles for longitudinal dipoles (Fig. 2.8). In an earlier study (Frijns et al., 1996a) we demonstrated this for radially oriented scala tympani electrodes. We also found that the spatial selectivity with such electrodes can be higher than with longitudinal ones, but at the cost of a very limited range of useful stimulus levels since the threshold for cross-turn stimulation is very low. It is not surprising that with combined intra- and extra-cochlear ball electrodes similar effects are observed (Fig. 2.11^{A,C}). The explanation for the relatively low thresholds for cross-turn stimulation follows from the potential distribution in the modiolus shown in Fig. 2.11^A. The fibres from higher cochlear turns passing by in the modiolus, the leftmost part of the figure, will cross many equipotential lines. The main excitatory component for myelinated nerve fibres like these is the activating function (Rattay, 1993), i.e. the second order difference quotient of the nodal potentials to the place, and therefore this will result in a very large tendency of the fibres to start firing as soon as the stimulus current reaches even moderate levels. In this respect the situation in Fig. 2.11^B is quite different. This figure displays the potential distribution set up by the same extra-cochlear ball electrode and an intra-cochlear wire electrode inserted over approximately the full length of the scala tympani, passing by through the centre of the ball electrode. In this case the

potential distribution around the extra-cochlear electrode is comparable to the one shown in Fig. 2.11^A, but the potentials in the modiolus are varying only very smoothly. In fact, the wire electrode acts more or less a Faradaic cage, protecting the modiolar parts of the fibres from being excited. The functional impact of this is reflected by the I/O-curves for both situations as depicted by Fig. 2.11^C, which shows that the introduction of the line electrode increases the useful range of stimulus levels (i.e. without cross-turn stimulation) to a large extent.

2.5 Conclusions and future directions

The method presented in this paper, which combines a helical 3D volume conduction model of the electrically implanted cochlea with an active neural excitation model, allows the prediction of excitation thresholds and spatial selectivity in cochlear implants. In accordance with electrophysiological experiments, it predicts that the excitation pattern depends on the exact location of the electrodes in the scala tympani (Frijns, 1995). These predictions are at least comparable with the ones obtained with a rotationally symmetric model, but the new geometry allows a wider variability of electrode geometries, including clinically applied designs like the ones shown in Fig. 2.10 to be included in the simulations. Therefore, the method is also applicable to develop and evaluate electrode configurations for future cochlear implant designs. An example of such a design, which we are currently evaluating in animal experiments in our laboratory, is the extra-cochlear ball vs. wire electrode demonstrated above (Fig. 2.11).

As there are large (size and shape) differences between the guinea pig cochlea and the human one, the next step in our project will be the construction of a mesh of the human cochlea. This not only will enable us to simulate human situations more realistically, but also will give us a tool to assess the validity of the (commonly carried out) extrapolation of data obtained in animal experiments to the clinical situation in humans. In doing so, one should be aware of the fact that -in contrast to all other species- in humans 90% of the cell bodies of the primary auditory nerve fibres are not myelinated. This means that human fibres carry an enlarged capacitive load which will have implications for excitation thresholds and spike timing, especially if degeneration of the peripheral processes due to prolonged deafness has occurred.

The results obtained thus far make us confident that this modelling approach

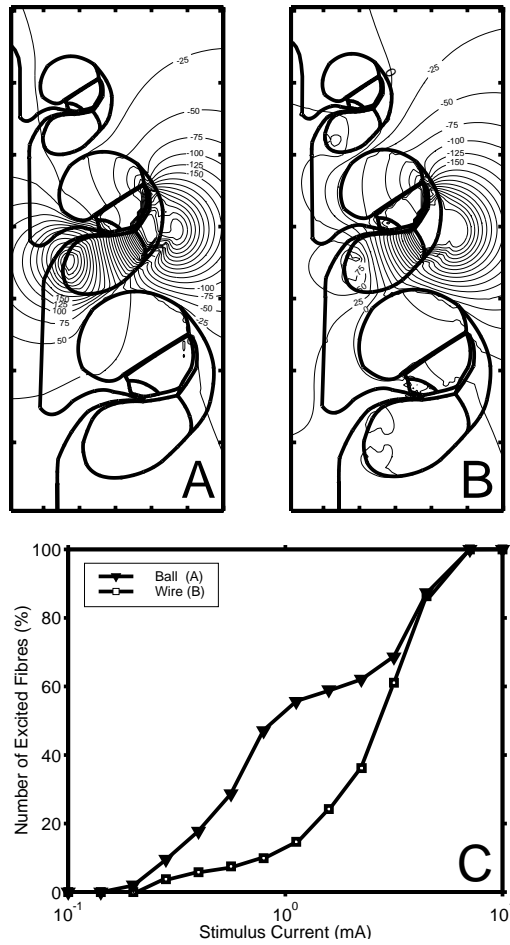


Figure 2.11: A. Potential distribution in a mid-modiolar cross-section in the vicinity of the electrodes, computed for the situation that an extra-cochlear electrode is stimulated against a ball electrode in the scala tympani (current strength 1 mA), in such a way that the electrodes form a radial bipolar pair. B. The same as (A), now with the scala tympani ball electrode replaced by a wire following the medial wall of the cochlea. C. I/O-curves computed for the situations in (A) and (B).

will help us in identifying the biophysical constraints imposed on restoring hearing by electrically stimulating the inner ear. This insight, in turn, combined with electrophysiological responses obtained in an implantee will be useful to optimise stimulation strategies for this implantee.

Appendix 2.A The generalised SEF auditory nerve fibre model

The auditory nerve fibre model used in the present paper (Fig. 2.5) is an active cable model of a guinea pig high spontaneous rate fibre, based on an extension of the SEF model (Frijns et al., 1994) to fibres of smaller diameter. Here we will only summarise the model equations and parameters of this auditory nerve fibre model. For symbols that are not explained in the text Table 2.3 will provide additional information. For further details we refer to the literature (Frijns et al., 1994; Schwarz and Eikhof, 1987). In Frijns et al. (1994) we showed that the model equations of a uniform finite-length active cable model with N nodes can be written as an equation with time-independent matrices **A**, **B** and **C** and time-dependent vectors describing the status of all nodes:

$$\frac{d\vec{V}}{dt} = \mathbf{A}\vec{V} + \mathbf{B}\vec{V}_e + \mathbf{C} [\vec{I}_{act} + \vec{I}_L] \quad (2.A.1)$$

where: $\vec{V} = (V_1, \dots, V_N)$ - the deviation from the resting membrane potential, $\vec{V}_e = (V_{e,1}, \dots, V_{e,N})$ - the extracellular potentials due to the stimulating electrodes, $\vec{I}_{act} = (I_{act,1}, \dots, I_{act,N})$ - the sum of the active sodium and potassium current per node, and $\vec{I}_L = -G_L V_L \cdot (1, \dots, 1)$ with G_L the nodal leak conductance, and V_L the leak current equilibrium potential.

For non-uniform fibres like the present auditory nerve fibre the structure of the matrices **A**, **B** and **C** given in Frijns et al. (1994) requires a slight modification, to account for the variation with segment number k of the nodal gap width l_k , the internodal length L_k and axon diameter d_k . This leads to the following dependence on k of the nodal membrane capacitance $C_{m,k}$, the nodal leak conductance and the axoplasmic conductance $G_{a,k}$:

$$C_{m,k} = c_m \pi d_k l_k, \quad (2.A.2)$$

Table 2.3: The parameters of the generalised SEF high spontaneous rate auditory nerve fibre model.

Parameter	Unit	Symbol	Value
axoplasm resistivity	Ωm	ρ_i	0.7
nodal membrane capacitance	pF	C_m	0.189
nodal leak conductance	$\text{n}\Omega^{-1}$	G_L	2.43
nodal sodium permeability	$(\mu\text{m})^3\text{s}^{-1}$	P_{Na}	172
nodal potassium permeability	$(\mu\text{m})^3\text{s}^{-1}$	P_K	6.68
intracellular sodium concentration	mol m^{-3}	$[\text{Na}^+]_i$	10
extracellular sodium concentration	mol m^{-3}	$[\text{Na}^+]_o$	142
intracellular potassium concentration	mol m^{-3}	$[\text{K}^+]_i$	141
extracellular potassium concentration	mol m^{-3}	$[\text{K}^+]_o$	4.2
Temperature	K	T	310.15 (= 37°C)

$$G_L = \pi d_k l_k g_L, \quad (2.A.3)$$

and

$$G_{a,k} = \frac{\pi d_k^2}{4\rho_i L_k}, \quad (2.A.4)$$

where c_m is the membrane capacitance per unit area, g_L the leak conductance per unit area, and ρ_i is the axoplasm resistivity.

This results in the following expressions for **A**, **B** and **C**:

A =

$$\left(\begin{array}{cccc} \frac{G_{a,1} + G_{L,1}}{C_{m,1}} & \frac{G_{a,1}}{C_{m,1}} & & \\ \dots & \dots & \dots & \\ & \frac{G_{a,k-1}}{C_{m,k}} & -\frac{G_{a,k-1} + G_{L,k} + G_{a,k}}{C_{m,k}} & \frac{G_{a,k}}{C_{m,k}} \\ & & \dots & \dots \\ & & & \frac{G_{a,N-1}}{C_{m,N}} - \frac{G_{a,N-1} + G_{L,N}}{C_{m,N}} \end{array} \right), \quad (2.A.5)$$

$$\mathbf{B} = \begin{pmatrix} -\frac{G_{a,1}}{C_{m,1}} & \frac{G_{a,1}}{C_{m,1}} & & & \\ \dots & \dots & \dots & & \\ & \frac{G_{a,k-1}}{C_{m,k}} & -\frac{G_{a,k-1} + G_{a,k}}{C_{m,k}} & \frac{G_{a,k}}{C_{m,k}} & \\ & & \dots & \dots & \dots \\ & & & \frac{G_{a,N-1}}{C_{m,N}} & -\frac{G_{a,N-1}}{C_{m,N}} \end{pmatrix}, \quad (2.A.6)$$

$$\mathbf{C} = \frac{1}{C_m} \begin{pmatrix} 1 & & & 0 \\ & \dots & & \\ & & 1 & \\ & & & \dots \\ 0 & & & & 1 \end{pmatrix}. \quad (2.A.7)$$

In the high spontaneous rate auditory nerve fibre model used in the present paper (Fig. 2.5) the nodal gap width l is fixed throughout the fibre. Also the axonal diameter d is identical on both sides of the cell body. The cell body itself has a larger internal diameter ($10 \mu\text{m}$ instead of $3 \mu\text{m}$). We could, however, not detect any influence of the soma thickness on the computed I/O-curves nor on the excitation profiles of the auditory nerve, but a large discontinuity in the axon diameter resulted in up to ten-fold increased computation times, due to the much smaller integration step-sizes required to maintain numerical stability. Therefore we decided to perform some of our computations with a $3 \mu\text{m}$ soma thickness.

The generalised SEF model equations describing the active nodal sodium and potassium currents $I_{Na,k}$ for each node k are:

$$I_{Na,k} = P_{Na,k} h_k m_k^3 \cdot \frac{E_k F^2}{RT} \cdot \frac{[Na^+]_0 - [Na^+]_i \exp\left(\frac{E_k F}{RT}\right)}{1 - \exp\left(\frac{E_k F}{RT}\right)}, \quad (2.A.8)$$

$$I_{K,k} = P_{K,k} n_k^2 \cdot \frac{E_k F^2}{RT} \cdot \frac{[K^+]_0 - [K^+]_i \exp\left(\frac{E_k F}{RT}\right)}{1 - \exp\left(\frac{E_k F}{RT}\right)}, \quad (2.A.9)$$

where T is the absolute temperature, F Faraday's constant, R the gas constant, E_k is the transmembrane potential in node k , and m_k , h_k and n_k are dimensionless variables describing the kinetics of the ionic channels of node k . For $\vec{m} = (m_1, \dots, m_N)$ the matrix-vector equation describing the set of first order differential equations that controls its time course reads:

$$\frac{d\vec{m}}{dt} = \begin{pmatrix} \alpha_{m,1} \\ \dots \\ \alpha_{m,N} \end{pmatrix} + \begin{pmatrix} \alpha_{m,1} + \beta_{m,1} & & 0 \\ & \dots & \\ 0 & & \alpha_{m,N} + \beta_{m,N} \end{pmatrix} \cdot \vec{m}. \quad (2.A.10)$$

Similar equations apply for $\vec{h} = (h_1, \dots, h_N)$ and $\vec{n} = (n_1, \dots, n_N)$. The way the α and β parameters in Eq. 2.A.10 depend on voltage and temperature is described in detail in our previous paper (Frijns et al., 1994). The equations are initialised with starting values \vec{m}_0 , \vec{h}_0 and \vec{n}_0 respectively, that ensure that the nerve fibre is at rest at its resting potential V_r , i.e. $d\vec{m}/dt = d\vec{h}/dt = d\vec{n}/dt = \vec{0}$ at $\vec{V} = \vec{0}$. The value of V_r is computed with the Goldman equation to account for variations in the ionic content of the extracellular medium:

$$V_r = \frac{RT}{F} \cdot \ln \left(\frac{P_K n_0^2 [K^+]_0 + P_{Na} h_0 m_0^3 [Na^+]_0}{P_K n_0^2 [K^+]_i + P_{Na} h_0 m_0^3 [Na^+]_i} \right). \quad (2.A.11)$$

In summary, for the 25 nodes of Ranvier included in the auditory nerve fibre model a system of 100 coupled non-linear first order differential equations had to be solved (viz. Eqs. 2.A.1 and 2.A.10 and the equivalent equations for \vec{h} and \vec{n}). These equations were integrated by means of a fourth order Runge-Kutta algorithm with adaptive step-size control with step-sizes varying between 0.001 and 1s. These small integration steps were necessary because of the large range (over 40 dB) of stimulus strengths applied. As explained in Frijns and ten Kate (1994), a simple and robust threshold criterion is formed by the rise of the m parameter (describing the sodium channel activation) above 0.7.

Chapter 3

3D Mesh Generation to Solve the Electrical Volume Conduction Problem in the Implanted Inner Ear.

Jeroen J. Briaire and Johan H.M. Frijns
Simulation Practice and Theory (2000), 8 (1-2), 57-73

Abstract

Cochlear implants are used to restore hearing in the profoundly deaf [Th.J. Balkany, *Otolaryngol. Clin. North. Am.* 19 (2) (1986) 215-449] by direct electrical stimulation of the auditory nerve. To study the working mechanism of cochlear implants and to provide a tool to develop better ones, a Boundary Element electrical volume conduction model of the cochlea (the auditory part of the inner ear) has been constructed. In this paper first a short comparison of the available numerical methods is given, then an algorithm is presented with which different cochlear geometries can be constructed and fitted with different types of cochlear implants. With the resulting model the potential distributions induced by the implant can be calculated, and a prediction of the effect of the implant can be made. The use of the meshing algorithm is not restricted to cochlear implants, but is also applicable in other fields.

3.1 Introduction

The cochlea is the snail-house shaped organ that in normal hearing converts mechanical auditory vibrations into a neural response (Dallos et al., 1996). It is a tapering tube that winds around the beginning of the auditory nerve, positioned in the modiolus. In the majority of profoundly deaf people this conversion is defective but the neural pathways are still (partially) intact. The nerve fibres at the base of the cochlea respond to high frequencies and the fibres at the top (apex) to the low frequencies. The cochlea acts more or less as a mechanical Fourier transformer. This is called the tonotopic organisation of the cochlea.

A cochlear implant is a device that is implanted into the deaf inner ear, and stimulates the auditory nerve directly by injecting small currents into the cochlea, preferably making use of the tonotopic organisation of the nerve fibres. To get a better understanding of the way cochlear implants function and as a tool in developing future generations of cochlear implants we have built a 3D boundary element mesh of the inner ear. With this volume conducting model we can calculate the potential distributions in the cochlea from which a nerve fibre model can predict the response of the auditory nerve induced by the cochlear implant under study. In our previous studies (Frijns et al., 1995; Frijns et al., 1996a) a rotationally symmetric model with point current sources was used, this model has been extended to a 3D tapered spiral with macro electrodes.

In Fig. 3.1, a cross-section of a guinea pig cochlea is shown. In the centre of the picture you can see the bundle of nerve fibres, entering the skull towards the brain in the lower right corner, this fibre compartment is called the modiolus. The cochlea itself consists of three main fluid-filled compartments with relative good conductivity, separated by membranes with a much lower conductivity (Finley et al., 1990; Suesserman, 1992; Strelhoff, 1973) (Fig. 3.2, Table 3.1). In most cases, the cochlear implant is inserted from basis to apex into the lower of the three compartments, the scala tympani. To get comparable results with experimental data from our laboratory we have built a model of the guinea pig cochlea. This cochlea differs from the human form in several ways: It is approximately two times smaller (the length of the basilar membrane in the guinea pig 18.8 mm (Fernández, 1952) is in humans approximately 35 mm (Békésy, 1960)) and it has more turns, $3\frac{1}{2}$ compared to $2\frac{3}{4}$ turns in the human situation. Furthermore, the cochlea of the guinea pig protrudes into the equivalent of the human middle ear, the air filled bulla, whereas in humans the cochlea is embedded in the solid petrous bone. This makes the

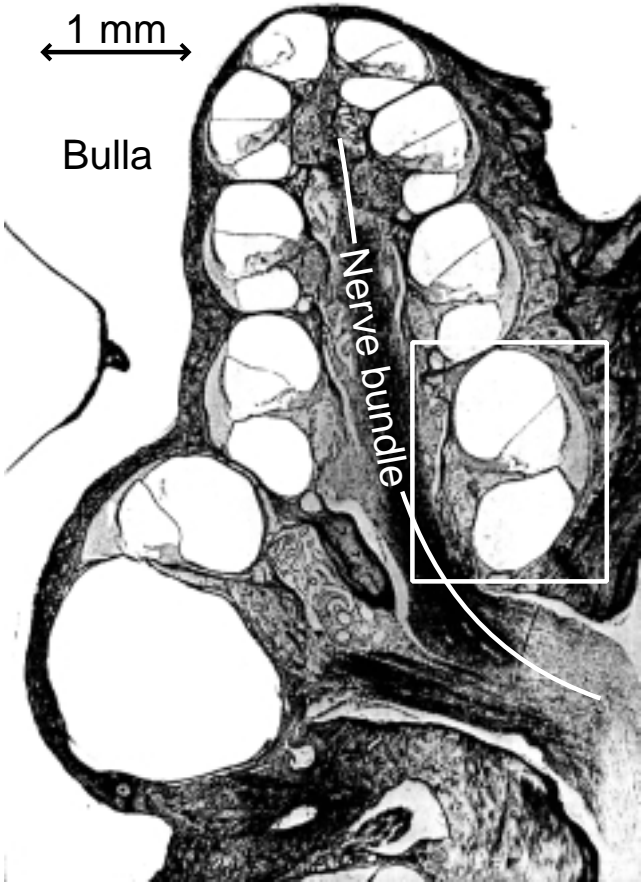


Figure 3.1: Mid-modiolar cross-section of a guinea pig cochlea. The rectangle indicates the turn to which the basic slice used in the meshing algorithm is fitted. In the centre the nerve bundle is indicated, which enters the skull in the lower right corner, travelling towards the brain stem. This fibre compartment is called the modiulus.

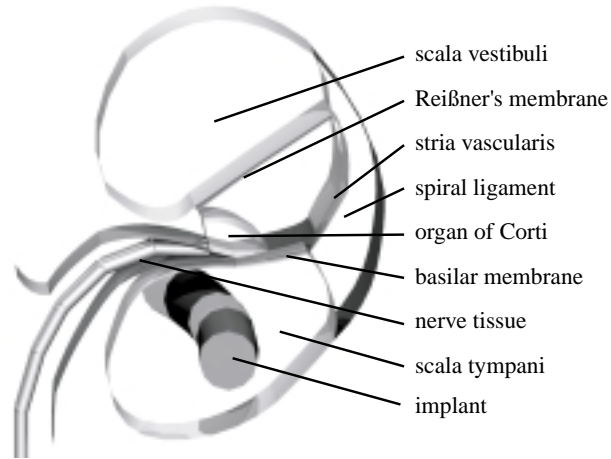


Figure 3.2: The basic slice of the cochlea used to construct the mesh. It is based upon the histological section of Fig. 3.1. An example of a cochlear implant is visible in the scala tympani.

guinea pig a good experimental animal for auditory experiments and a large amount of electrophysiological data are available.

In this paper, we will discuss in Section 3.2 the reasons to use the boundary element method for our calculations in perspective to the numerical methods used previously in the literature to model cochlear implants. One of our main demands of the method is that it must offer sufficient spatial resolution and accuracy to couple the results to a neural model. Another important aspect is the ease with which meshes of the cochlea with different types of implants inserted can be generated. Sections 3.3 and 3.4 deal with the algorithm we developed to generate the 3D cochlea mesh and the models of the cochlear implants. In Section 3.5, the results of some representative calculations are given.

3.2 Numerical method selection

The current injected into the inner ear by the cochlear implant induces a potential distribution. The calculation of this distribution is called the volume

conduction problem and requires the solution of the Poisson equation:

$$\nabla^2 \phi = -\frac{i}{\sigma}, \quad (3.1)$$

with ϕ the potential, i the current source distribution and σ the conductivity of the medium. In the past numerous numerical methods have been used to solve the electrical volume conduction problem of cochlear implants, each with some strong points. Below, a short description of these methods will be given on the basis of which we had to make a choice for the model we wanted to construct. The demands for the model are the possibility to calculate a potential distribution with sufficient accuracy to couple the results with a nerve fibre model and to position realistic cochlear implant electrodes into the cochlea model.

Table 3.1: The conductivities of the various cochlear tissues as used in the computation. The conductivities are derived from Finley et al.(1990), Suesserman (1992) and Strelhoff (1973). We have enlarged the thickness of Reißner's membrane and of the basilar membrane and consequently also enlarged their conductivities by a factor 10 and 5 respectively.

Tissue	Conductivity $(\Omega m)^{-1}$
Scala tympani	1.43
Scala vestibuli	1.43
Scala media	1.67
Stria vascularis	0.0053
Spiral ligament	1.67
Reißner's membrane	0.00098
Basilar membrane	0.0625
Organ of Corti	0.012
Bone	0.156
Nerve tissue	0.3

3.2.1 Lumped parameter models

In lumped parameter models, the geometric properties are represented by an electrical network of resistors and capacitors. It is relatively easy to incorporate capacitive effects in this kind of models due to the network structure. Such models have been used for the study of cochlear implants (Suesserman and

Spelman, 1993; Black et al., 1983), but the models were not refined enough to incorporate a neural model and they have so far been limited to unrolled cochlea models. These models predict an exponential decay of the potential and current along the scala tympani as a result of an injected current.

We concluded that this class of models is not refined enough for our research because of our goal to couple the electrical conduction model with nerve fibre models, although they can give good global insights in the functioning of cochlear implants.

3.2.2 Finite element method (FEM)

In the FEM the solution is found by minimisation of the energy in a volume. For the electrical volume conduction problem this leads to minimisation of the power dissipation P :

$$P = \int_v \left(\frac{\nabla\phi \cdot \sigma\phi}{2} + i_v\phi \right) dV, \quad (3.2)$$

where σ is the conductivity, i_v the current source distribution and ϕ the electrical potential. For this method the volume has to be discretised by subdividing the space in small volumes (Davies, 1980). Finley and co-workers (Finley et al., 1990) used this method to construct an unrolled cochlea model coupled with a passive neural model based on the activation function (Rattay, 1989). This method is able to incorporate capacitive effects and anisotropic media and uses little computational resources, memory and CPU-time, relative to the other methods. The drawback of the method is the difficult mesh generation, as the volume, including the surrounding area, has to be discretised into small volumes. When a change is made to the geometry, e.g. by the introduction of an electrode, the entire volume has to be discretised.

3.2.3 Finite difference method (FDM)

The FDM computes the potentials by a Taylor expansion of the Poisson equation along a fixed structure of points, which is solved through an iterative process. The mesh of the FDM has a simple structure, but it is hard to fit a complexly detailed structure, like the cochlea, on such a fixed grid. The membranes in the cochlea are very thin (a few μ m) and due to their relatively low conductivity important to the geometry. These membranes can leak easily in

a FDM mesh. To overcome this problem and to approximate the geometry adequately small mesh elements have to be used which leads to large memory requirements and long computation times.

In our group we used a finite difference model as a test case to investigate the effects of volume conduction in the inner ear (Aarnink, 1991) and coupled this model to a nerve fibre model (Mooij, 1992). The geometry used for this study is comparable with the structure used by Finly and co-workers (Finley et al., 1990). Sapozhnikov (Sapozhnikov, 1990) used the FDM to simulate an unrolled cochlea but was not able to link the results with a nerve fibre model. Girzon (Girzon, 1987) build a fully 3D cochlea but was also not able to incorporate a neural model due to insufficient spatial resolution.

To summarise, this method has the possibility to be linked with a neural model, the implementation is relatively easy, but the mesh generation has a drawback which can lead to errors in the results unless large computational efforts are accepted. The mesh has to be redefined for every implant geometry and position.

3.2.4 Boundary element method (BEM)

The BEM uses Green's second theorem to calculate the potential distribution due to a current source distribution in a piece-wise homogeneous volume conductor (van Oosterom, 1991). The equation to be solved reads:

$$\phi(\vec{x}_p) = \frac{4\pi}{\Psi} \phi_h - \frac{1}{\Psi\sigma} \sum_{k=1}^{n_s} (\delta\sigma_k \int_{S_k} \phi(\vec{x}) \nabla\left(\frac{1}{r}\right) \cdot \vec{d}\vec{a}), \quad (3.3)$$

where ϕ is the electrical potential, \vec{x}_p the observation point, Ψ the boundary representation function, ϕ_h the potential due to the current sources in a homogeneous unbounded volume, σ the conductivity, $\delta\sigma_k$ the conductivity difference between the two sides of the surface S_k and $\vec{d}\vec{a}$ a vector perpendicular to an infinitesimal surface element. Boundary element meshes differ from finite element and finite difference meshes in that only the boundaries between the volumes with different conductivities are tessellated in stead of the entire volume. This leads to an easy mesh generation and it gives the possibility to add different meshes together, as long as they do not intersect with each other. In this way the mesh of the cochlear implant can be added to the cochlea model afterwards and it is not necessary to rebuild the entire geometry. Eq. (3.3) leads to a set of N linear equations of N variables where N is the number of

nodes (i.e. calculation points on the boundaries). This matrix is a representation of the distortion of the homogenous electric field by the areas with different conductivities and can be used for every source position. To solve this problem the inverse of the matrix has to be calculated involving N^3 operations. The grounding problem is solved by defining the potential in infinity to be zero. The BEM is more difficult to implement than the other methods and it requires very much computational effort because of the surface integrals in the equation and the need to calculate the inverse of the solution matrix. However, once the inverse of the solution matrix has been calculated, the potential distribution of every electrode combination can be calculated with a minimum of extra computer effort. This is useful in the situation of multi-electrode cochlear implants. The use of anisotropic media is possible with the BEM, although limited to a single direction (Zhou and Oosterom, 1994). Alternatively, it is possible to combine the BEM with the FEM (Pullan, 1996) in case of anisotropy.

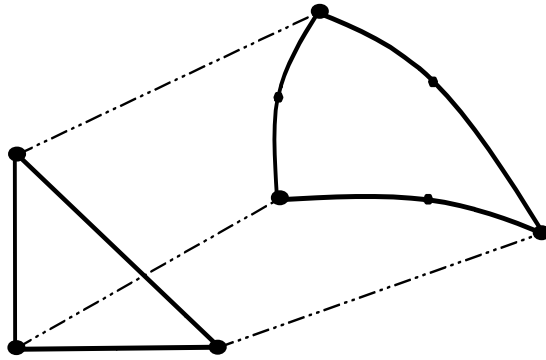


Figure 3.3: A quadratically curved triangle is subtended by six points while three points subtend a flat triangle.

Despite the need for a lot of computational resources and the more complicated implementation we chose the boundary element method to generate an inner ear model because of the ease in mesh generation, the possibility to vary the implant without rebuilding the complete mesh and the calculation of potential distributions of extra electrode positions with hardly any computational effort. To increase the numerical accuracy and to give a better description of the curved nature of biological structures, especially the inner ear, we use quadratically curved triangular surface elements to define the volume boundaries. These triangles are subtended by the three vertex points and by three

extra point in the middle of the sides (Fig. 3.3). This imposes extra constraints on the meshing algorithm. On the surfaces, the potentials are calculated using second-order interpolation functions. This results in an accuracy that is roughly inversely proportional to the third power of the length of the sides of the surface elements (Frijns et al., 2000b).

3.3 A 3D cochlea mesh

As can be seen in Fig. 3.1 the generation of a cochlea mesh is not trivial due to the complex geometry. Therefore, simplifications are unavoidable but they should not have major impact on the outcome of the simulations. All previous models of the inner ear used some simplification of the geometry. The most commonly used approximation is the unrolled and sometimes even unscaled cochlea model. In these models a slice of the cochlea like the one shown in Fig. 3.2, is translated to get a straight tube. One step further to an accurate representation of the cochlea is the rotationally symmetric model previously used in our simulations (Frijns et al., 1995). This is a model where a slice of the cochlea is rotated around a central axis. Unrolled and rotationally symmetric meshes have as a common feature that they are constructed from congruent slices. In this paper, this concept is extended with scaling and a combination of translation and rotation to create a tapered spiralling mesh (Fig. 3.4). The same scaling paradigm, which is a linear function of the rotational angle, is also used for both horizontal and vertical dimensions. The scaling function has been derived from anatomical data (Fernández, 1952) and reads:

$$S = -0.29 \cdot \theta + 1.29, \quad (3.4)$$

with S the scale factor and θ the rotational position defined as the number of turns between the position and the basal end of the cochlea. Note that $S = 1$ for $\theta = 1$ (i.e. at the base of the second turn where the slice of Fig. 3.2 was fitted on). To increase the accuracy, the mesh is locally refined around the positions of the electrode, where the electrical gradients are large. To be able to use different tessellation densities in the membranous labyrinth (including the fluid-filled compartments) and the modiolus (the neural compartment) we separated the mesh in two individual meshes. By doing this, the labyrinth has become a straightforward spiralling set of slices that only have to be interconnected with triangular surface elements, and there are no connections between each slice and other ones than its direct neighbours. This tube can

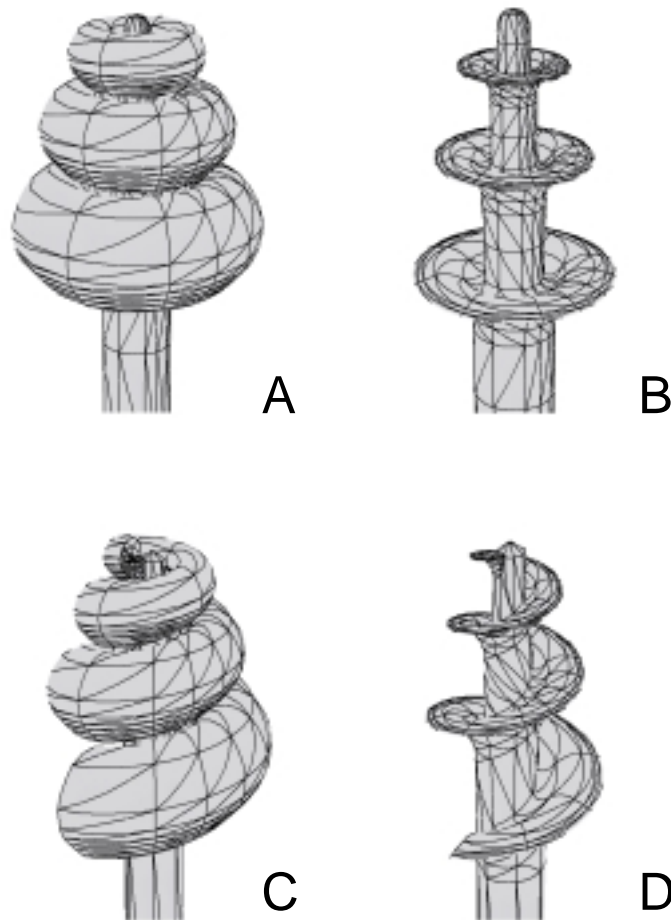


Figure 3.4: (A) Rotationally symmetric representation of the guinea pig cochlea. (B) The modiolus of the rotationally symmetric cochlea model. (C) The spiralling representation of a guinea pig cochlea. (D) The modiolus structure of the spiralling cochlea model. Both models have refinements in the first and second turn.

easily be refined locally by adding an extra slice. The problem of the six sub-tension points required for the integration method to be used (Section 3.2.4) is solved by using quadratically curved line elements, subtended by three points, in the slices and alternating these slices with slices consisting of only middle points. This will result in two quadratically curved triangles in between two line elements of two subsequent slices (Fig. 3.6).

The modiolus mesh is build up in a similar way with the extra difficulty that every slice is also connected to the slice one turn above and below its position. This problem is solved by indicating in every slice which points should be connected to the turn above and below, respectively. First the subsequent slices are interconnected and then the turns are connected to each other. The shape of the modiolus is such that an extension containing the peripheral processes of the nerve fibres is radiating into the labyrinth (Fig. 3.4^A). In our initial work (Frijns et al., 1995) the top of the extension was sharp. However, sharp edges give rise to numerical errors in the boundary element method (Ferguson and Stroink, 1997). This problem was reduced by placing a quadratically curved element at the tip (Fig.3.5) of the extension. As a result the volume conduction problem at this edge is dealt with by smoothly varying interpolation and integration functions and there is no sharp edge in the BEM mesh causing numerical errors.

As explained in Section 3.2.4, the size of the numerical problem is defined by the number of nodes in the mesh. The cochlea mesh used in this study has 4711 nodes subtending 2508 quadratically curved triangles. This results in a matrix with 22,193,521 elements of approximately 169 Mbytes. Custom made software written in Borland® Delphi® was used for generating the meshes, displaying them (e.g. Fig. 3.4) and performing the BEM calculations. POV-ray was used to create ray-traced images of the mesh like Fig. 3.7 .

3.4 Constructing meshes of implants and the surrounding area

Most clinically used cochlear implants have electrodes that can be considered as a repetition of (scaled) segments with the same geometry. An example, the Nucleus® electrode which is the most widely applied one world-wide, is shown in Fig. 3.7. As a first step in creating the meshes of the electrodes, the basic segment of the electrode is defined with the same algorithm as used for constructing the cochlea mesh, it is constructed out of slices and these slices

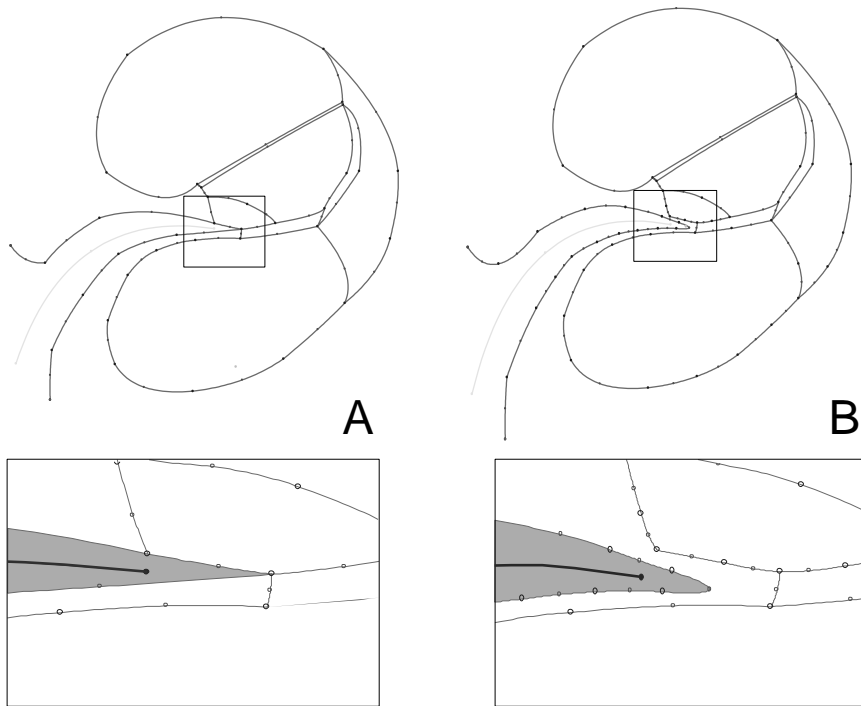


Figure 3.5: (A) The original cross-section of the modelled cochlea in which the modiolus mesh (gray) has a sharp tip and is attached to the membranous labyrinth. (B) The improved cross-section with a loose modiolus. The sharp tip is replaced by a parabolic element. The black line in the modiolus represents the position of the nerve fibre.

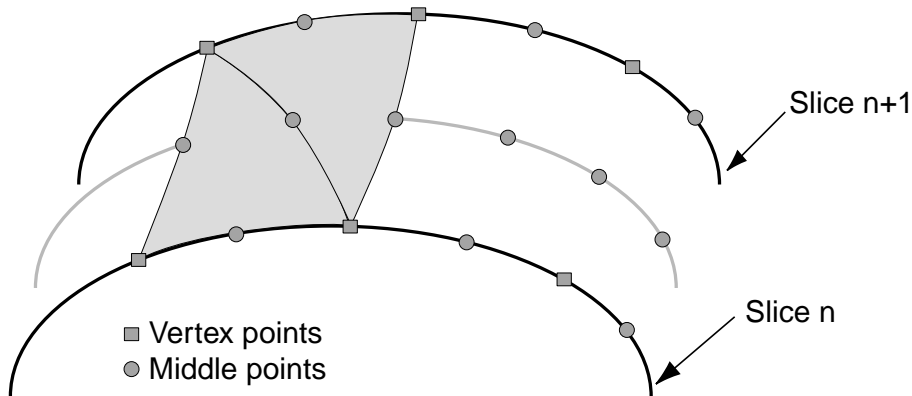


Figure 3.6: Two subsequent slices n and $n+1$ are connected with quadratically curved triangles by placing a slice with middle points in between the two slices.

are then interconnected with triangles as was described for the cochlea mesh in the Section 3.3. A series of these segments is placed on a positioning line in the cochlea, defined by position points placed in the slices while constructing the cochlea mesh. In this way the placement and curvature of the implant can be controlled very accurately. This procedure ensures that the implant model has automatically the right shape and curvature to fit in the cochlea model without intersections or collisions.

As already mentioned in Section 3.1, there is an air filled bulla outside the cochlea of the guinea pig. This bulla is expected to influence the volume conduction process, for in an infinite space filled for the half with insulator, the insulator will block the currents and thus increase the potentials in the conducting areas. To study the influence of this phenomenon on the outcome with cochlear implants, a bulla was constructed around the cochlea. The basis for this mesh was a toroidal structure. All the slices of this structure were fitted to anatomical cross-sections like the one in Fig. 3.1 and cross sections of the cochlea mesh (Fig. 3.8). In the end these slices were interconnected with triangles and this mesh was added to the cochlea mesh. Because the slices were fitted to cross-sections of the inner ear model there were no intersections.



Figure 3.7: An artist's impression of the cochlea model with the nerve fibres radiating from the modiolus and a Nucleus[®]-like implant, an insulating carrier with banded electrodes, in the scala tympani.

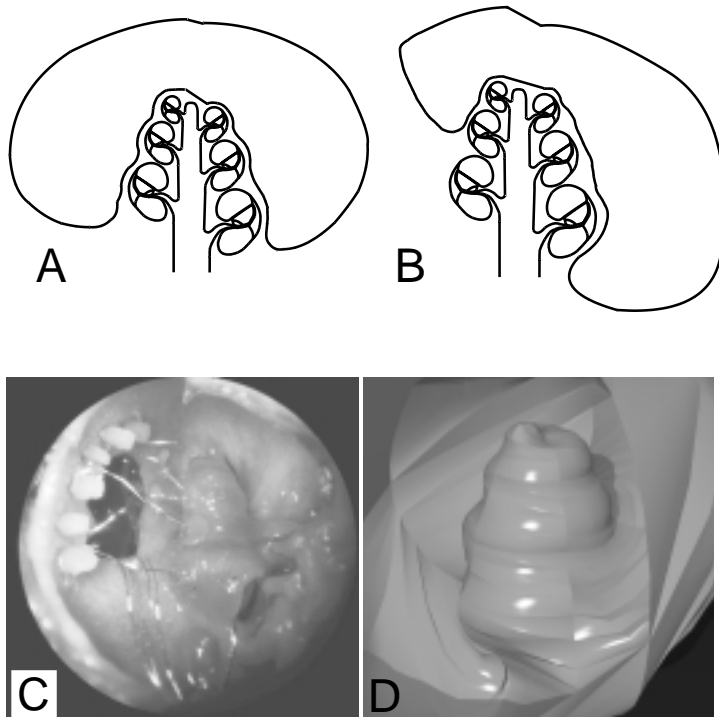


Figure 3.8: The model of the bulla (the equivalent of the human middle ear) that has been constructed from a toroidal structure, where all the slices are fitted to anatomical data. The bulla is located in the petrous bone around the cochlea model. (A,B) Two perpendicular mid-modiolar cross-sections of the bulla with the cochlea model. (C) A photograph of the bulla of guinea pig. The cochlea has been implanted with wired electrodes. (D) A 3D representation of the bulla model.

3.5 Calculated potential distributions

Fig. 3.9 compares the potential distribution in the rotationally symmetric (Fig. 3.4^{A,B}) and the spiralling mesh (fig 3.4^{C,D}) set up by a longitudinal bipolar point current source of 1 mA. It shows the distribution of the equipotential lines in a plane that is constructed by rotating or spiralling a radial line at the level of the current sources. In these plots it can be seen that the scala tympani, which has a relatively high conductivity compared with the surrounding structures, is a favourable current pathway. Except for some small differences due to asymmetry inherent to the spiralling mesh, the results are quite comparable.

For the interpretation of the results in terms of the clinical application of cochlea implants the potentials on the nerve fibres are of primary importance as these potentials are the driving force behind the neural responses that can be computed with the neural sub-model, described in the companion paper (Frijns et al., 2000a). To be able to show the potential distribution along the nerve fibres the nerve bundle is unrolled, resulting in a plane of fibres. The potential along every fibre is now plotted against the cochlear turn from base to apex (Fig. 3.10). In the modiolus, the nerve fibres from turns above the stimulation position run through the level of the electrodes. This means that for these fibres not the tip but a more central part is closest to the current sources, as can be seen from the elevation of the potentials one turn from the electrode position. These fibres are consequently more likely to be excited. These repetitions cause the so-called cross-turn or ectopic stimulation for higher stimulation strengths. This means that when the current through the cochlea becomes too large, fibres from other turns start to respond. These fibres correspond with completely different frequencies and are likely to confuse the implantee. This puts an upper limit to the useful range of current levels in the cochlear implant.

From the calculation with the bulla added to the cochlea model we found that the neural responses for intracochlear electrodes were almost identical with the situation without the bulla, and only for very large currents the influence of the bulla became evident (Briaire and Frijns, 1998b). The same result was found when we filled the bulla with fluid, to simulate otitis media with effusion. For extracochlear electrodes, which are electrodes placed in the bulla just outside the cochlea, the addition of the bulla resulted in a slight upward shift of the threshold (the minimum current causing excitation of fibres), but no other changes were observed.

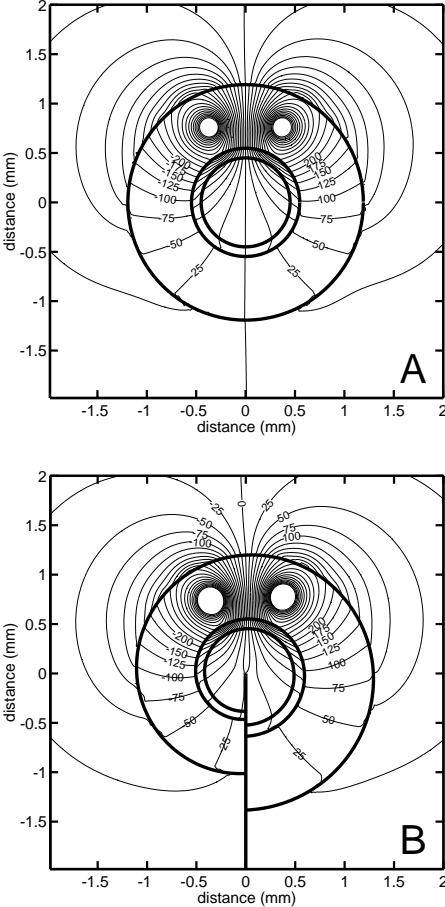


Figure 3.9: Equipotential lines in horizontal cross-sections of the rotationally symmetric (A) and a spiralling model (B) as induced by a longitudinal current dipole of 1 mA. The numbers indicate the potential in mV. The bold lines represent the boundaries between the different tissues in the cochlea (for inside to outside: nerve, inner wall bone, scala tympani and outer wall bone).

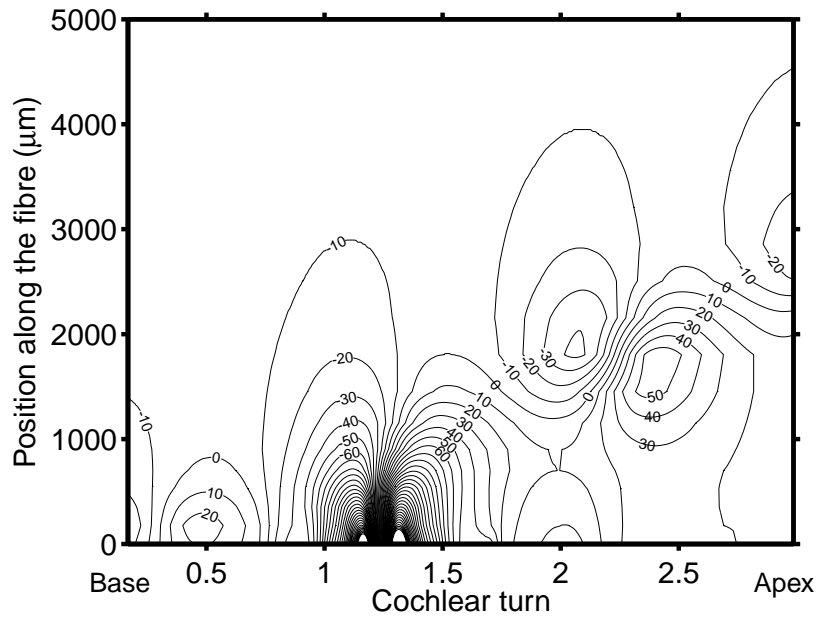


Figure 3.10: Equipotential lines (in mV) on the nerve fibres of the spiral model as induced by a 1mA current dipole with a distance between the electrodes of $375 \mu\text{m}$, positioned at 1.25 turn. The dipole distribution reappears on the nerve fibres one turn above and one turn below the actual stimulation site (see text).

3.6 Discussion and Conclusions

The meshing algorithms presented in this paper, which have the common property of repeating a cross-section, are capable of constructing cochlear meshes of different geometries. They also allow to create cochlear implants of arbitrary design and place these with the appropriate curvature in the cochlea model. For closely spaced bipolar current sources the previously used rotationally symmetric mesh gives potential distributions comparable with those computed with the new spiralling mesh, and we conclude that our previous results (Frijns et al., 1996a) are still valid. This conclusion is substantiated by the neural responses calculated in the companion paper (Frijns et al., 2000a). For situations, where the electrodes are moved further apart or with monopolar electrodes we expect that the spiralling nature of our new mesh becomes more important. The extension of the model with a bulla is only necessary

for extracochlear electrodes because of its very small influence. This effect is expected to be even smaller in the human situation where the bone layer surrounding the cochlea is much thicker.

We conclude that the BEM enables us to get the accuracy needed to link the results with a neural model. As it yields a large flexibility of mesh generation we can create a cochlea model and realistic implants. As shown in Section 3.2 it is also possible with the FDM to create a cochlea mesh (Girzon, 1987; Sapozhnikov, 1990; Aarnink, 1991) but at the expense of very large computational effort. Although the meshes for this method are of an easy structure for applying a fixed grid it is hard to build a detailed cochlea geometry and the desired variety of electrode models within such a fixed grid. The FEM also offers the possibility to link with a neural model (Finley et al., 1990), and it has the advantage of a reduced computational effort in comparison with the other methods. Although this may seem unlogical at first sight for a 3D method, the FEM generates large, but sparse matrices with just 21 non-zero bands and the equations can be solved iteratively using for example Gauss-Seidel iteration. This means that both memory and CPU requirements are less than with the BEM, which generates relatively small but full matrices. However, the mesh generation for the FEM is much more complicated and less flexible and the whole procedure has to be repeated for each electrode position. Therefore we chose to apply the BEM, giving adequate accuracy to link the calculated potentials with neural models and very flexible meshing opportunities because of the possibility to add meshes together without having to do any rebuilding of the mesh.

The algorithm described is developed to create meshes for the BEM but the algorithm can be extended to create FEM meshes. In that situation the slices contain the sides of the discretisation volumes instead of the sides of triangles. This means that the areas of homogeneous conductivity in the slices (such as the scala tympani) have to be tessellated also. For that purpose general tessellation algorithms are applicable. The algorithm can also be used to construct meshes for other geometries than the cochlea e.g., a spinal cord. Electrical stimulation of the spinal cord is used in pain management and to revalidate patients who lost control of e.g., the urinary bladder. The spinal cord can be viewed as a repetition of scaled segments along a predefined line and a mesh for it can thus be defined in a way comparable with the one we used to construct cochlear implant meshes. The demonstrated use of the BEM was electrical volume conduction, but the same method can be used for different areas like heat radiation or mechanical stresses (Brebbia and Dominguez, 1992), and the meshing methods presented here are likewise applicable.

The ultimate goal of our research is to develop a clinically applicable tool in human cochlear implantation. As mentioned in Section 3.1, the human cochlea is fairly different from the guinea pig counterpart. It can not be defined adequately by taking the cross-section of one turn and a scaling parameter, for the internal structure of membranous labyrinth changes much more than in the guinea pig. This means that all the slices have to be fitted to histological or MRI data to get a realistic representation. We do this by keeping the basic structure of all slices identical so that the same interconnecting algorithm can be used as in the guinea pig cochlea. However the individual slices are not only scaled, translated and rotated but also distorted. For this purpose the software package also allows repositioning of the individual points, thereby stretching the elements they subtend.

In summary, the volume conduction model presented here is a valuable tool in understanding the behaviour of the electrically implanted cochlea, especially when combined with a neural excitation model. We intend to use it in designing better future implant geometries, and in identifying the parameters that are crucial to predict the clinical outcome.

Chapter 4

Field Patterns in a 3D Tapered Spiral Model of the Electrically Stimulated Cochlea

Jeroen J. Briare and Johan H.M. Frijns
Hearing Research (2000), 148, 18-30

Abstract

Despite the fact that cochlear implants are widely and successfully used in clinical practice, relatively little is known to date about the electric field patterns they set up in the cochlea. Based upon the available measurements and modelling results the scala tympani is usually considered to be a preferential current pathway that acts like a leaky transmission line. Therefore, most authors assume the current thresholds to decay exponentially along the length of the scala tympani. Here we present potential distributions calculated with a fully 3-dimensional, spiralling volume conduction model of the guinea pig cochlea, and try to identify its preferential current pathways. The relatively well conducting scala tympani turns out to be the main one indeed, but the exponential decay ($J \sim e^{-z}$) of current is only a good description of the far-field behaviour. In the vicinity of the electrodes, i.e. near the fibres that are most easily excited, higher current densities are found, that are best described by a spherical spread of the current ($J \sim \frac{1}{R^2}$). The results are compared with those obtained with a variant of our previous, rotationally symmetric, model and with measurements in the literature. The implications of the findings are discussed in the light of simulated neural responses.

4.1 Introduction

Cochlear implants are now firmly established as effective options in the habilitation and rehabilitation of individuals with profound hearing impairment (Balkany, 1986; NIH Consensus Statement, 1995). They directly stimulate the primary auditory nerve fibres by injecting electric currents into the inner ear. In order to get more insight in the processes involved in this type of stimulation, many experimental and computational model studies have been performed. Conceptually, the working principle of these prostheses can be divided into two separate processes: first, the electrical conduction of the current through the geometry of the cochlea, and second, the generation of the neural response. In the present study, we will focus on the volume conduction of the current through the cochlea, leading to an excitatory potential field. Due to the small geometry of the cochlea, experimental data of current flow through the cochlea are hard to obtain. Classical measurements focussed on the field patterns on the outside of the cochlea (Ifukube and White, 1987). With the recording techniques build into modern cochlear implants, some *in vivo* measurements of the potential distribution in the scala tympani (Kral et al., 1998) and even neural response telemetry (Abbas et al., 1999) have become possible. Computational modelling as applied in this study is a way to study electrical field patterns induced by cochlear implants more fundamentally.

Most model studies focus on one of the two parts involved in cochlear stimulation and fully integrated neuron and field models are scarce. The majority of the model studies on electrical conduction are based on lumped-parameter models (Black et al., 1983; O'Leary et al., 1985; Suesserman and Spelman, 1993; Jolly et al., 1996; Kral et al., 1998). The models used in these studies work under the assumption that the turns of the cochlea can be unrolled and can be considered electrically uncoupled. These studies indicate that the scala tympani acts more or less as a leaky transmission line through the cochlea and that the potential (V) and the current (I) decay along the scala tympani as an exponential function with a length constant λ ($V \sim e^{-z/\lambda}$). Lumped parameter models give insight in the flow of the current through the cochlear duct but do not provide the detailed information necessary to couple the model to neural models. Sapozhnikov (1990) used a finite difference model in a linear unrolled cochlear geometry, incorporating two turns. He concluded that the less conductive parts induce a channelling through the cochlea and that there is limited influence on the potential in other turns. Girzon (1987) made the extension to a full three-dimensional (3D) finite difference model of the cochlea but a limited spatial resolution prohibited the computation of neural

excitation functions. He arrived at the conclusion that the cochlea acts more or less as a leaking transmission line.

Other studies focus mainly on the neural response (Colombo and Parkins, 1987; Bruce et al., 1999a; Bruce et al., 1999b; Rubinstein et al., 1999b), making assumptions about the potential distribution through the cochlea, based upon the models described above. The exponential decay along the scala tympani is commonly used to calculate the distribution along the nerve fibres.

Finley et al. (1990) were the first to present an integrated 3D neuron-field model of a segment of an unrolled cochlea, using the finite element method (FEM) and a passive nerve fibre model based upon the activation function (Rattay, 1989). In our previous work (Frijns et al., 1995; Frijns et al., 1996a) we used a rotationally symmetric boundary element model to calculate the potential distribution in the cochlea and coupled these results to an active nerve fibre model (Frijns et al., 1994). The computed I/O curves for several bipolar electrode configurations were shown to be in good agreement with experimental data (Shepherd et al., 1993), and a study of the spatial selectivity of stimulation with different sources was performed.

In this study, we present a realistic 3D tapered spiral model of the guinea pig cochlea and give a more detailed description of the potential distribution and the current flow through it. In doing so, we will test the validity of the assumption that the scala tympani acts as a transmission line while also the validity and limitations of the use of a rotationally symmetric cochlear geometry will be tested. For this purpose, we will use two geometrical models of the cochlea, viz. a rotationally symmetric model similar to the one used in our previous studies (Frijns et al., 1995; Frijns et al., 1996a) with the extension to three turns and a more realistic tapered spiral model constructed from the same histological cross-section as its rotationally symmetric counterpart. To investigate the magnitude of the transmission line effect, we will for some computations change the conductivity of certain parts of the cochlea model to that of bone, which can also be viewed as a way to test the electrical effects of ossification. Furthermore, the current along the central axis of the modiolus will be described as well as the potential distribution along the nerve fibres in conjunction with its functional consequences in terms of neural excitation patterns.

4.2 Materials and Methods

4.2.1 Numerical method to calculate the potential distribution in the cochlea

To solve electrical conduction problems in a complex 3D geometry, such as the cochlea, various computational methods exist (Binns et al., 1992). In the present study, the boundary element method (BEM) (Meijs et al., 1989; van Oosterom, 1991; Brebbia and Dominguez, 1992) is used to calculate the potential distribution set up by current sources in the cochlea. This method which we also used in our previous studies (Frijns et al., 1995; Frijns et al., 1996a; Frijns et al., 2000a) has the advantage of a relative ease of mesh generation as it requires only the tessellation of the boundaries between the volumes with different conductivities rather than the discretisation of the volumes themselves as is necessary with the FEM and the finite difference method. An other advantage of the BEM is that it leads to an inverse matrix with which the potential distribution of any electrode configuration in the same volume conductor can be calculated with a minimum of extra calculation time. In this way, the geometry has to be dealt with only once to compute the results for multiple electrode configurations in a multi-channel cochlear implant.

The requirement to be able to couple the results of the volume conduction model to a nerve fibre model increases the demands put on the accuracy of the solution, not only of the computed potential field but also of the first and second derivatives to the place of the potential field. This results from the fact that the driving force for the excitation of a nerve fibre at a node far from its end point is roughly proportional to the second order difference quotient of the extracellular potential along the axon (Rattay, 1989; Warman et al., 1992). To increase the accuracy of our model in these respects, quadratically curved triangles on which potential is also interpolated quadratically have been used to tessellate the mesh. Each curved triangle is subtended by 6 nodes (3 vertex points and 3 intermediate points). The application of second order interpolation functions implies that the error terms in the calculations are of the order three and above, and therefore the accuracy of the calculated potentials is inversely proportional to the third power of the length of the sides of the surface elements (Meijs et al., 1989; Frijns et al., 1995; Frijns et al., 2000b; Ferguson and Stroink, 1997).

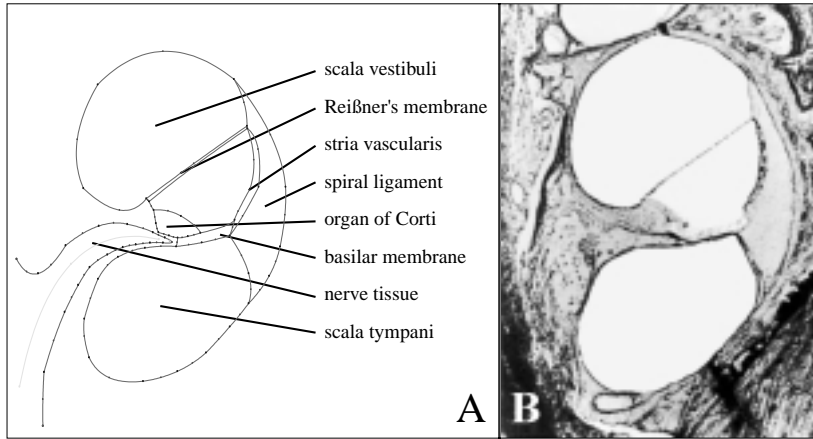


Figure 4.1: **A:** The model representation of a cross-section of the guinea pig cochlea as used to construct the boundary element meshes. **B:** A histological cross-section at the basal end of the second turn of a left guinea pig cochlea that was used to construct the slice in A.

4.2.2 Models of the cochlea

The model geometry is constructed from the cochlea of the guinea pig, our laboratory animal. To generate the mesh we used a histological cross-section of the guinea pig cochlea from the basal part of the second turn (figure 4.1^B). In figure 4.1^A the model representation of the boundaries between the areas with different conductivities is shown. The conductivity data for the three scalae were adopted from Finley et al. (1990), who compiled their values from several authors. For the conductivity of the bony tissue, more accurate data from Suesserman (1992) were used. The conductivity of the stria vascularis, the spiral ligament, the organ of Corti, Reißner's membrane and the basilar membrane were computed from resistance data of Strelhoff (1973), combined with morphologic data from Nijdam (1982) and Fernández (1952), using the dimensions in the second turn of the guinea pig cochlea at 10 mm from the stapes. This set of conductivity parameters was also used in our previous studies (Frijns et al., 1995; Frijns et al., 1996a). As before, we have enlarged the thickness of Reißner's membrane and of the basilar membrane (and consequently also enlarged their conductivities) by a factor 10 and 5, respectively, to prevent excessive numerical errors inherent to the BEM (Table

Table 4.1: The conductivities of the various cochlear tissues as used in the computation. The conductivities are derived from Finley et al.(1990), Suesserman (1992) and Strelhoff (1973), see text. We have enlarged the thickness of Reißner's membrane and of the basilar membrane and consequently also enlarged their conductivities by a factor 10 and 5, respectively.

Tissue	Conductivity (Ωm) ⁻¹
Scala tympani	1.43
Scala vestibuli	1.43
Scala media	1.67
Stria vascularis	0.0053
Spiral ligament	1.67
Reißner's membrane	0.00098
Basilar membrane	0.0625
Organ of Corti	0.012
Bone	0.156
Nerve tissue	0.3

4.1). It is assumed throughout this paper that the impedances of all the media in the cochlea are purely resistive, as this allows to evaluate time-varying stimuli by means of scaling the calculated potentials. The capacitive effects are neglected, the validity of which is supported by the findings of Spelman et al. (1982), who showed that the potentials in the scala tympani are virtually frequency-independent for all frequencies tested (up to 12.5 kHz).

A part of the guinea pig cochlea protrudes in an air-filled bulla, with only a thin bone layer separating the labyrinth from the air. In the models used in this paper (and previous ones) the cochlea is imbedded in bone, which increases the similarity with the human/feline situation. Previous studies (Briaire and Frijns, 1998b), showed that the influence of the bulla for intra cochlear electrodes is negligible.

In the present study we compare two different model geometries, a rotationally symmetric model (Fig. 4.2^{A,B}) and a tapered spiral model (Fig. 4.2^{C,D}) based upon the same cross-section (Fig. 4.1). The rotationally symmetric model is an extension of the one used in the previous studies, as it incorporates three scaled segments representing the three modelled turns rather than just one single segment as in our previous studies (Frijns et al., 1995; Frijns et al., 1996a). The spiral model is built by scaling, rotating and translating the cross-section to form a tapered spiral (Briaire and Frijns, 2000a). The scaling factors used to create the tapering are derived from Fernández (1952). In

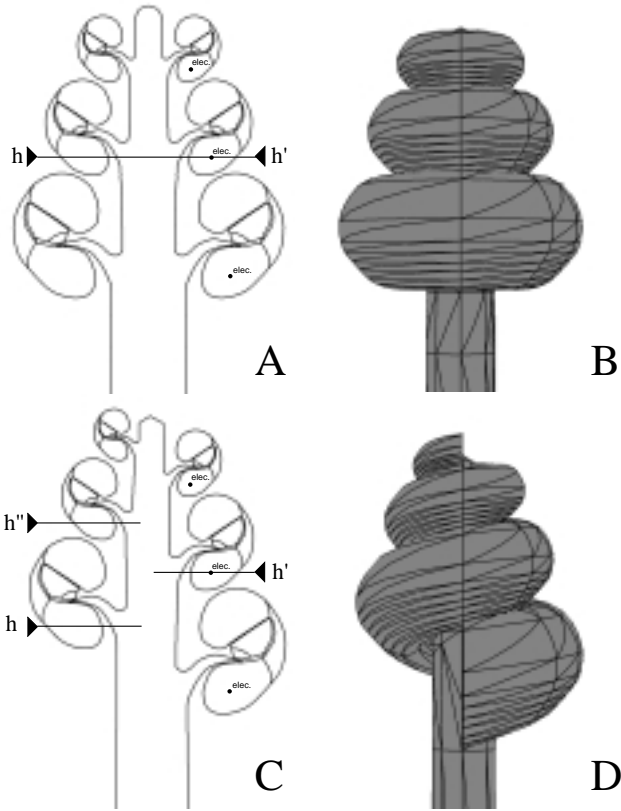
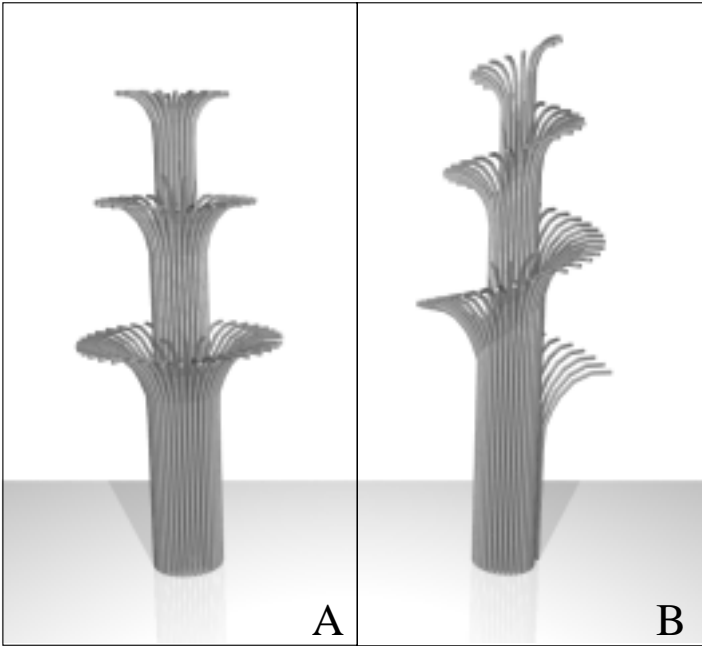


Figure 4.2: **A:** Mid-modiolar cross-section of the rotationally symmetric model . The line $h-h'$ represents the location of the cross-section used for potential distributions in a horizontal plane (cf. Fig. 4.6). **B:** A 3D side view of the rotationally symmetric model . **C:** Mid-modiolar cross-section of the spiral model . The cross-section used for the potential distribution on a horizontal plane (Fig. 4.6) is constructed by spiralling a radial line from h through h' to h'' . **D:** A 3D side view of the spiral model. Note that the right parts of A and C ($\Upsilon = 0.25, 1.25$ and 2.25 , i.e. where the electrodes are placed, as indicated by dots) are identical.

the current paper, every position in the cochlea is referred to in terms of its rotational position Υ , defined as the number of turns between that position and the basal end of the cochlea. This implies that the rotational position of the apex of this three turn model is 3.00. The scaling factor at $\Upsilon = 1.00$ is equal to unity in the spiral model. In the rotationally symmetric model the position jumps from the first to the second segment at $\Upsilon = 1.00$, and from the second to the third segment at $\Upsilon = 2.00$ to get a position measure that is comparable with the spiral model.

The positions of the current sources in the spiral model are chosen at $\Upsilon = 0.25$, 1.25 and 2.25, respectively (Fig. 4.2^{A,C}), to avoid influence of the closure of the cochlea at the base and the apex, while $\Upsilon = 1.25$ is still close to rotational position 1.00, where the fit to the histological cross-section is best. The cross-sections of the three segments of the rotationally symmetric model are identical to the cross-sections in the spiral model at these three rotational positions to be able to compare the results from the two models. To increase the numerical accuracy of the results, the tessellation density is increased in the vicinity of the current sources. In the rotationally symmetric model, the rotational position of the sources obviously has no influence on the potential distribution due to the symmetry, as long as the sources stay within the same segment. In the model we used $\Upsilon = 0.50$ and 1.50 to place the electrodes to avoid problems with the discontinuity in the rotational position measure at $\Upsilon = 1.00$ and 2.00. As electrode configuration, we use point current sources with a strength of 1 mA placed at the centre of the scala tympani. They are configured as both (i) monopolar electrodes and (ii) longitudinal bipolar electrode pairs separated by 375 μm , and centred on the location of the monopolar electrode.

The auditory nerve fibres are located in the modiolus, the neural compartment. In the in vivo situation and in both models, more apical fibres take a more central course in this modiolus. The exact position of the nerve fibres in the modelled modiolus is different for the two models because of the different geometry: the fibres in the rotationally symmetric model are placed in a rotationally symmetric fashion (Fig. 4.3^A) while the fibres in the spiral model are arranged spirally (Fig. 4.3^B). To minimise numerical errors in the potential distribution on these nerve fibres, in both models a higher tessellation density is used on the modiolus than on the surrounding labyrinth (Briaire and Frijns, 2000a). The size of the resulting meshes is 2540 triangles and 4802 nodes for the rotationally symmetric mesh and 2508 triangles and 4711 nodes for the spiral mesh.



*Figure 4.3: The configuration of the nerve fibres in the modiolus for the two different models. **A**: Rotationally symmetric model . **B**: Spiral model. The configuration at the position of the electrodes is identical in both situations.*

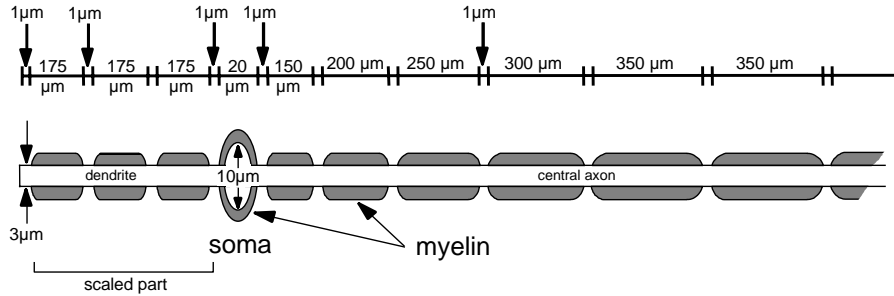


Figure 4.4: The morphology of the auditory nerve fibre model used in the calculations. The length of the myelinated internodes in peripheral process ('dendrite') are scaled to hold the position of the soma constant relative to the basilar membrane. The scale factor is equal to unity at the beginning of the second turn.

mammals (Schwarz and Eikhof, 1987), are described in detail elsewhere (Frijns et al., 1994; Frijns et al., 1995) and will not be reproduced here.

The morphology of the bipolar primary auditory nerve fibres is shown in Fig 4.4. It is based upon the findings of Liberman and Oliver (1984) in the cat and Brown (1987) and Gleich and Wilson (1993) in the guinea pig, taking into account a shrinkage of approximately 10% due to labelling with horseradish peroxidase. The simulated high spontaneous rate fibres consist of a peripheral and a modiolar axon with a diameter of $3 \mu\text{m}$, interconnected by a cell body with a diameter of $10 \mu\text{m}$. The gap width in the nodes of Ranvier is $1 \mu\text{m}$. The unmyelinated terminal of the nerve fibres is positioned under the organ of Corti. The lengths of the myelinated internodes in the peripheral process are scaled in such a way that the cell body and the unmyelinated terminal remain at the same relative position to the basilar membrane throughout the cochlea. The scaling factor changes from 1.29 at the base to 0.43 at the apex and is equal to unity at $\Upsilon = 1.00$, the beginning of the second turn of the spiralling model.

The fibres are placed in such a way that the terminals are separated $40 \mu\text{m}$ from each other. In the rotationally symmetric model, this leads to 168 nerve fibres in the first turn, 128 in the second and 88 in the most apical turn (384 in total). In the spiral model 365 fibres are placed equidistantly from base to

apex. This means that both models incorporate approximately 60 fibres per octave, or equivalently, 210 fibres per decade and each modelled nerve fibre represents about 60 actual nerve fibres.

4.3 Results

4.3.1 Potential and current distributions in the cochlea

Fig. 4.5 shows the potential distribution (in mV for a current source of 1 mA) as in a mid-modiolar cross-section through the electrode position induced by a monopolar electrode. The potential distributions have been constructed with 44.000 observation points placed on a square grid with 20 μm spacing. In Fig.4.5^{A,B}, the data are shown for the rotationally symmetric model and the spiral model, respectively. Fig. 4.5^{C,D} gives an enlarged view of the field for the section around the electrodes for both models in the same order. In spite of the geometrical differences, the potential distributions in both models are very similar. The highly resistive organ of Corti and the basilar membrane virtually block the current flow out of the scala tympani, as can be seen from the fact that the equipotential lines are closely together there. The bone layer between the turns also works to confine the current flow to the scala tympani. The spiral ligament on the other hand, acts as a pathway through which the current can leak out of the scala tympani.

To get insight in the field patterns along the course of the scala tympani, so-called horizontal cross-sections have been taken at the level of the electrodes through one turn starting 0.50 turn basally and ending 0.50 turn apically from these electrodes (Fig.4.6). In the rotationally symmetric model, this is the horizontal plane indicated by the line h h' in Fig. 4.2^A. In the case of the spiral model the level of this plane shifts up with the scala tympani as indicated in Fig.4.2^C by the lines from the centre of the modiolus to h, h', and h'' respectively. Consequently, the boundaries between the various structures in the cochlea (indicated by the thick solid lines in Fig. 4.6) shift to a more central position as a result of the tapering of the mesh. From inside to outside, these structures are nerve tissue, inner wall bone, scala tympani and outer wall bone. Fig. 4.6^{A,B} show that the scala tympani functions as a favourable current pathway, as the potentials in the scala tympani due to monopolar current sources are higher than in the surrounding bone. In Fig.4.6^{C,D} the potential distribution is plotted for a bipolar electrode pair (spacing 375 μm). Expectedly, the potential change is much more localised around the electrodes

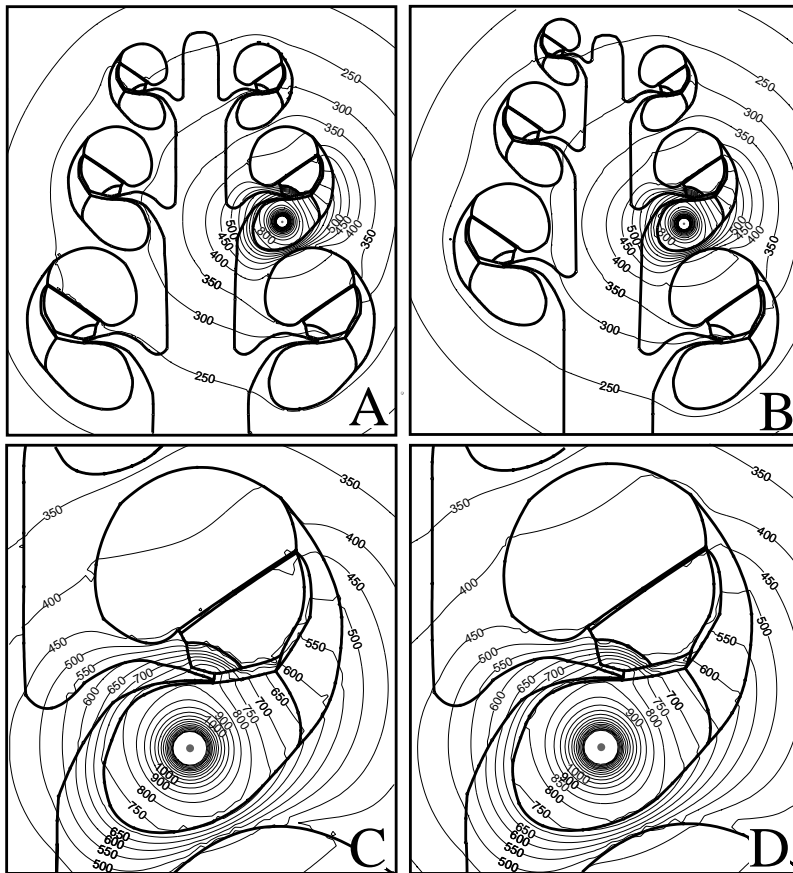


Figure 4.5: Equipotential lines for a monopolar electrode (1mA) in the second turn of the cochlear models. **A**: The rotationally symmetric model. **B**: The spiral model. **C** and **D**: Enlargements of A and B, respectively, in the vicinity of the electrodes. The potentials are in mV.

than was the case with the monopolar electrodes (Fig.4.6^{A,B}), and there is a zero-potential plane in between the electrodes. As contrasted with Fig. 4.5, Fig.4.6 shows some asymmetry in the potential distribution in the spiral mesh, but again, the differences are limited at first sight (see Section 3.2)

As a next step, the current densities (\vec{J}) in the cochlea have been calculated by taking the first spatial derivative of the potential field ($\vec{J} = -\sigma\nabla V$, with σ the conductivity and V the potential). Fig. 4.7^A shows the current densities for the first apical quarter of a turn (from $\Upsilon = 1.25$ to $\Upsilon = 1.50$) in the spiral model as induced by a monopolar electrode with a current strength of 1 mA, placed at $\Upsilon = 1.25$. As with the potential distributions, the current densities for the rotationally symmetric model are almost identical to the ones for the spiral model despite the geometrical differences and are not presented here. It turned out that the amount of current going through the scala tympani is larger than the current along the same pathway in a homogenous medium (solid line). From this, we can conclude that the scala tympani indeed acts as a favourable current pathway through the cochlea.

To investigate the influence on the transmission line effect of the different compartments of the electrical volume conductor, we have set the conductivities of certain parts of the cochlea equal to that of bone. This process can also be viewed as a way to model the electrical effects of ossification of a part of the inner ear due to, e.g., meningitis. In this way, we constructed two additional spiral models, one with a ossified scala tympani and one where the complete labyrinth is replaced by bone. In the vicinity of the electrode the current densities are the same for all three models and also equal to the homogenous solution (Fig.4.7^A). This means that the current drops with $1/R^2$ (with R the distance from the electrode). Somewhat further away from the electrode the results differ from each other as follows: the complete model gives a larger current density than the homogenous solution, indicating ('transmission line like') preferential conduction along the scala tympani. The current densities in the model with the ossified scala tympani are smaller than the homogenous solution. And, expectedly, the results from the model with a completely ossified labyrinth are almost identical with the homogenous solution.

To visually enhance the differences in current conduction the ratio between the homogenous field solution and the currents from the different models has been plotted in Fig.4.7^B. From this figure, it is evident that the transmission line effect results in an up to a factor four larger current than the homogenous field solution. With an ossified scala tympani the current density decreases to levels that are smaller than the homogenous case by a factor of two. From

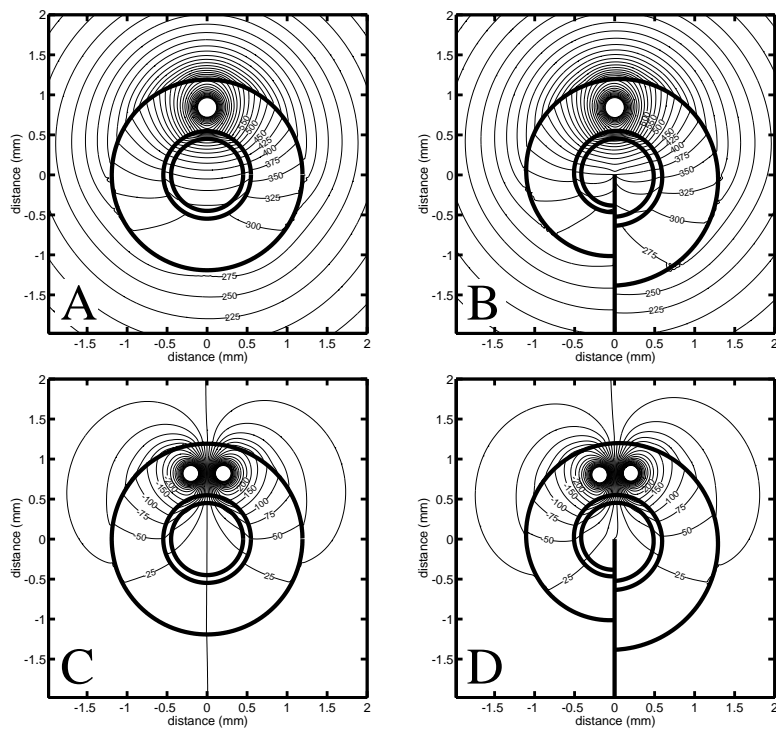


Figure 4.6: Potential distribution on a horizontal plane at the level of the current sources. In the spiral model the plane spirals up with the cochlea (cf. Fig. 4.2). The potentials at the equipotential lines are in millivolts for a 1 mA current source. **A**: Potential distribution due to monopolar stimulation in the rotationally symmetric model. **B**: Potential distribution due to monopolar stimulation in the spiral model. **C**: Potential distribution due to bipolar stimulation in the rotationally symmetric model. **D**: Potential distribution due to bipolar stimulation in the spiral model.

similar calculations (not shown here) of the current densities in the radial and vertical directions, it followed that with an ossified scala tympani the current densities in vertical and radial direction tend to approach the homogenous field solutions. The current fluxes in the direction of the spiral ligament and the scala vestibuli of the underlying turn are slightly larger than that resulting in a decrease of the current component directed along the scala tympani. This is in agreement with the findings of figure 4.5 where we observed that the spiral ligament functions as an other preferential current pathway.

One of the major points of interest from a functional point of view is the field pattern in the neural compartment where the electrical information is conveyed to the nerve fibres. These nerve fibres run predominantly in the vertical direction and the derivative of the current along the fibres is a rough approximation of the activation function (Rattay, 1989) and therefore a first indication for the neural response. For this purpose, the vertical component J_z of the current density through the centre of the modiolus is shown in the Fig. 4.8^A (rotationally symmetric model) and Fig. 4.8^B (spiral model) as induced by a monopolar current source of 1 mA positioned in the first turn of the cochlea at $\Upsilon = 0.25$. The current density in the direction of the apex has been taken positive. For comparison, the analytical solution for a homogenous medium is added. In addition curves are shown for the situations where only the modiolus is present, and where only the membranous labyrinth is taken into account. The latter two situations were included with the objective to identify the part of the cochlea that influences the results most.

At first sight, the differences between Fig.4.8^A and 4.8^B are limited. On the other hand, there are considerable differences between the four curves in each sub-figure. Especially the full solution and the situation with only the membranous labyrinth show a clear asymmetry in amplitude on both sides of the source. The largest amplitudes are found for the situation with only the modiolus due to the fact that the relatively high conductivity of the modiolus creates a preferential current pathway along the modiolus which parallels the z-axis. Similarly, the tendency of current to flow along the scala tympani (Fig.4.7) and the spiral ligament (Fig.4.5) leads to a reduced amplitude in the case of only the membranous labyrinth. For this particular situation, the superposition of both effects leads to a result that is to some extent comparable with the homogenous solution. An important difference between the homogenous solution and the full model results is, of course, the asymmetry mentioned above, and the ripple in J_z on the apical side of the electrode which is more clearly visible in the rotationally symmetric variant of the model.

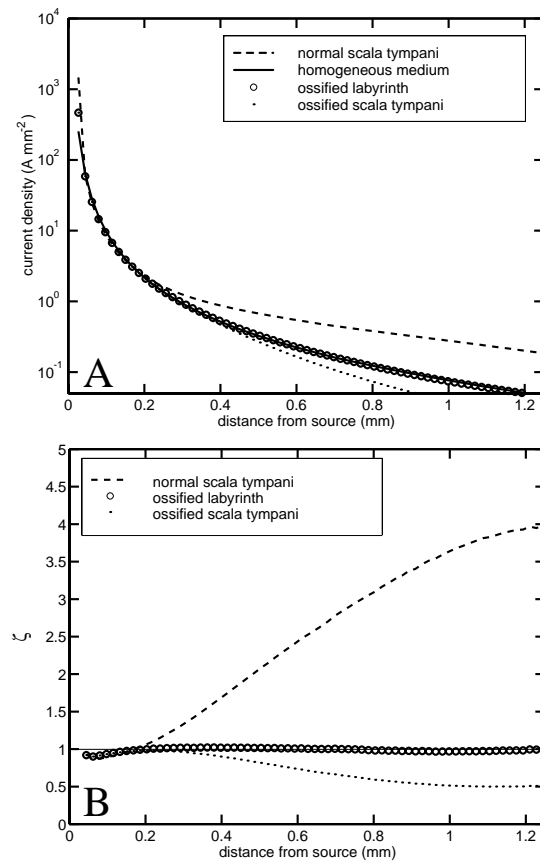


Figure 4.7: **A:** The current density through the scala tympani set up by a 1 mA monopolar current source as a function of the distance from the electrode in apical direction. The solid line representing the solution for a homogeneous medium is an analytically calculated curve. The other three curves are model simulations. **B:** The ratio ζ between the homogeneous solution and the model calculations shown in A as a function of the distance from the electrode in apical direction.

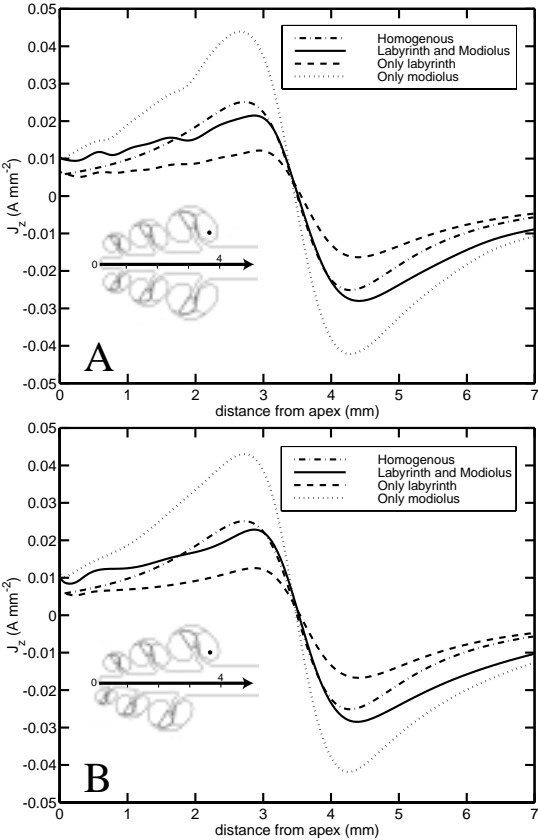


Figure 4.8: **A**: The vertical component of the current flux J_z through the centre of the modiolus as indicated by the insert in the rotationally symmetric model for a monopolar current source of 1 mA in the first turn. **B**: As A, now for the spiral model with a monopolar current source of 1 mA in the first turn at $\Upsilon = 0.25$.

4.3.2 Neural responses

As shown in Fig.4.9 the potential distribution on the nodes of Ranvier of the primary auditory nerve fibres can be plotted as a function of the rotational position Υ and the distance of the node from the peripheral ending of each nerve fibre. Such a plot gives general insight in the groups of nerve fibres that are most likely to be excited, but as explained in Section 2.3 we use an active neural response model to calculate the cochlear excitation patterns from the potential distribution on the nodes of Ranvier. This neural model takes time-varying fields into account. Its output is plotted as a so-called excitation profile (Fig.4.10), showing the position of all excited fibres in the cochlea for each stimulus level. In addition, the excitation profile shows the part of the fibre where the initial excitation occurs (in the peripheral process, in the soma or in the modiolar axon) as a grey shading.

The potential distribution on the nerve fibres in the spiral model is plotted in Fig.4.9^B for the same bipolar electrode pair with an interelectrode distance of 375 μm as used in Fig.4.6^{C,D}. The most basal electrode is positive, the more apical electrode is cathodic. In this plot the peripheral processes of the fibres close to the electrodes ($\Upsilon = 1.25$) experience large potential variations as a result of the current injected nearby. The fibres originating from one turn above the electrodes ($\Upsilon = 2.25$) experience a similar potential variation at their central axons. This originates from the fact that these fibres pass by the electrode position in their way to the brainstem through the modiolus. The potentials are lower and less localised because the fibres from the higher turns run more centrally in the modiolus than the more basal fibres. Therefore, their distance to the stimulating electrodes is relatively large but with higher stimulus levels these fibres are likely to get excited, leading to so-called cross-turn stimulation.

Fig.4.10^B shows the excitation profile for the situation of Fig.4.9^B, calculated with a biphasic signal of 200 μs /phase (basal electrode cathodic first). Around $\Upsilon = 1.25$ the reaction to the potential variation of the peripheral processes of the fibres close to the site of implantation is visible as a bimodal peak. Each lobe of this peak corresponds with the exact location of the current sources in the bipolar pair, and fibres in the plane midway between these electrodes have higher excitation thresholds. The asymmetry in the grey shading of the lobes is due to the fact that the site of excitation around the most apical electrode shifts towards the modiolus with increasing stimulus levels. As expected, this peak is repeated more or less around $\Upsilon = 2.25$ as a result of the cross-turn stimulation explained above. The mechanism behind the bimodal excitation

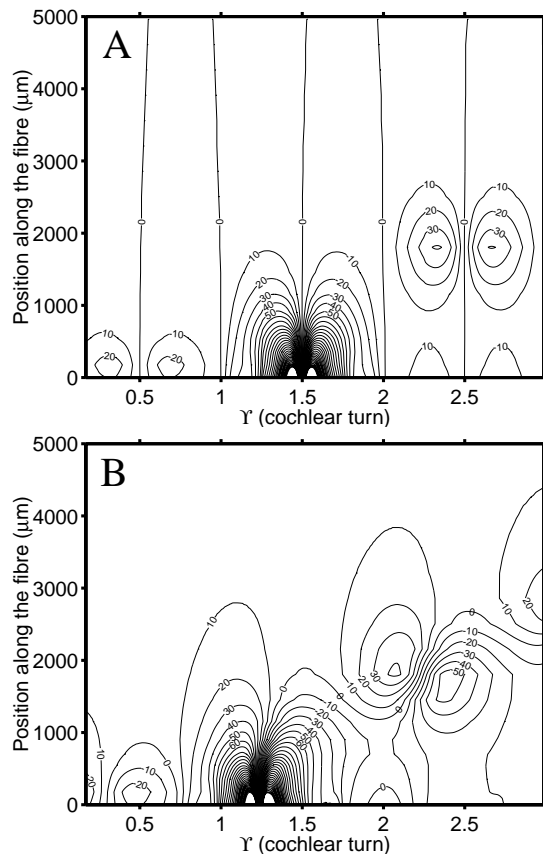


Figure 4.9: Potential distribution as induced by a bipolar current source of 1 mA (interelectrode distance 375 μm) on the nodes of Ranvier of the nerve fibres plotted as a function of their rotational position Υ and the distance of the node from the peripheral ending of each nerve fibre. **A:** The rotationally symmetric model with electrode at position $\Upsilon = 1.5$. **B:** The spiral model with electrode at position $\Upsilon = 1.25$.

peak at even higher stimulation levels around $\Upsilon = 0.25$ is somewhat different. It results from direct excitation of peripheral processes by the potential field in the basal turn (cf. Fig.4.9^B). From the fact that this peak is bimodal, it follows that it is a result of current flow across turns rather than from current flow through the scala tympani.

As explained in Section 2.2, the rotational position of the sources within a turn does not basically influence the potential distribution in the rotationally symmetric model, allowing us to avoid discontinuities in the potential distribution by placing the source dipole around $\Upsilon = 1.5$ instead of $\Upsilon = 1.25$. Fig. 4.9^A pertains to this situation and it is clear that this potential distribution is to a large extent comparable to the one found in the spiral model (Fig.4.9^B). The rotationally symmetric model (Fig.4.9^A) has roughly the same variation in potential near the electrode site as the spiral model. This is reflected in the excitation profile (Fig.4.10) where the bimodal excitation peak around the electrodes is almost equal in shape from threshold to approximately 1 mA. At higher stimulus levels, also in the rotationally symmetric model cross-turn stimulation occurs. The threshold for this phenomenon is slightly higher than in the spiral model for the apical as well as for the basal fibres. As contrasted with the spiral model the bimodality of the peak of the cross-turn stimulation through the modiolus is very distinct. This can be explained from Fig. 4.9^A where a 0 mV equipotential line parallels the course of the nerve fibres for $\Upsilon = 2.5$. Moreover, the symmetry of the mesh is also reflected in the symmetry of the potentials around this line. In Fig. 4.9^B, these equipotential lines are distorted due to the spiralling geometry, resulting in a more smeared aspect of the bimodal distribution.

4.4 Discussion

In this paper, the current and potential fields in an electrically stimulated cochlea were studied in a realistic 3D spiral model of the guinea pig cochlea. The BEM was used to solve the volume conduction problem. The neural response to the electrical stimulus was calculated with the active GSEF cable model (Frijns et al., 1995). The results were compared with ones obtained with a three turn rotationally symmetric geometry, which was constructed to match the spiral model as closely as possible.

In Section 3.1 we tried to identify preferential current pathways from the field patterns shown in Figs. 4.5 and 4.6. We found that current flow out of the scala tympani is limited by the less conductive media surrounding it. Superiorly, the

highly resistive membranes adjacent to the scala media virtually block the current flow while medially, inferiorly and laterally the bone, which has a 10-fold lower conductivity than perilymph, tends to confine the current to the scala tympani. The spiral ligament, located superolaterally, was identified as a major leakage pathway which consequently will increase neural excitation thresholds, especially for electrodes placed near the outer wall. The magnitude of this effect depends on the conductivity of the spiral ligament itself, for which accurate data are lacking. However, the spiral ligament consists of loose connective tissue and its actual conductivity will be within the order of magnitude of the value used in the calculations. In a previous study (Frijns et al., 1995), the sensitivity of the model to the uncertainties in the conductivity of the various tissues was tested, which showed that changing the conductivity induces surprisingly insignificant changes to the calculated neural excitation pattern for all media with the exception of the perilymph and the bone.

Most new intracochlear electrode arrays are designed to reach a position near the modiolus. Apart from reducing the threshold levels by decreasing the distance to the nerve fibres, such modiolus-hugging electrodes will suffer less from current leakage through the outer wall. An example of this situation is the Clarion[®] implant when medialised with the so-called positioner (Firtsz et al., 1999). Placement of the electrode contacts on the medial side of the implant carrier (as is the case for the Clarion[®] Hi-Focus[®] (Kuzma and Balkany, 1999) and the new precurved intracochlear electrode with stilet from Cochlear corporation (Aschendorff et al., 1999) helps to minimise the current loss through the lateral wall further. This will result in a reduction of the power consumption and probably a more selective stimulation. Whether this is really the case and under which circumstances is the subject of research currently going on in our laboratory.

The fact that the scala tympani acts as a preferential current pathway is further substantiated by Fig.4.7. In this figure the current along the scala tympani progressively deviates from the solution in a homogenous medium for distances above 0.2 mm. In the far field the current drops almost exponentially as is illustrated by the fact that the dashed curve in Fig.4.7^A is almost linear in this region. In the near field however, this curve closely follows the solution for the homogenous situation, which is theoretically described by

$$J = \frac{I_0}{4\pi R^2} \quad (4.1)$$

were I_0 is the current injected by the electrode and R the distance from the source.

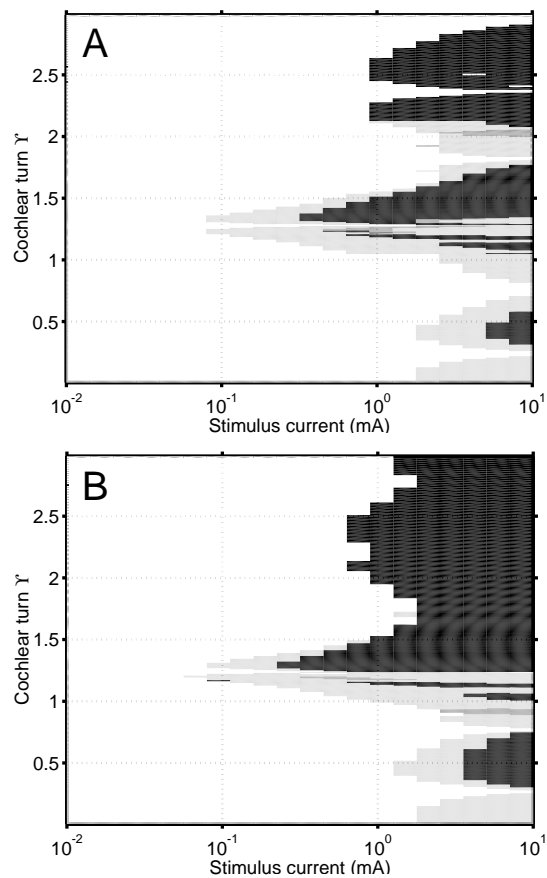


Figure 4.10: Excitation profiles for a bipolar electrode configuration (anodic-first biphasic current pulses, $200 \mu\text{s}/\text{phase}$). The location of the node of ranvier where the initial excitation of each nerve fibre takes place is indicated by the degree of shading: the peripheral processes are indicated by light grey, the nodes surrounding the soma by dark grey and in the modiolar axon by black. **A**: Computed in the rotationally symmetric model. **B**: Computed in the spiral model.

Therefore, it is plausible to postulate the following formula that gives an overall description of the current density along the scala tympani in both near and far field:

$$J = \frac{I_0}{4\pi R^2} + Ae^{-\frac{R}{\lambda}} \quad (4.2)$$

Here the parameter A is a constant determined by the magnitude of the transmission line and λ is a length constant. Both parameters are dependent on the rotational position of the source. If their values are chosen correctly, the fit obtained with eq. ?? matches the solution found in the spiral model so closely that both curves are indiscernible on the scale of Fig.4.7. The fact that the value of A increases with increasing Υ is in accordance with the findings of Kral et al. (1998) who found that the ratio between the potential and the injected current increases in the apical direction (see his figures 6 and 7).

Our simulations for the near field deviate substantially from the results obtained with lumped parameter models (Black et al., 1983; Suesserman, 1992), which only exhibit the exponential decay, characteristic for a leaky transmission line and traditionally applied to calculate the potential on the nerve fibres by authors that do not have access to a volume conduction model (O'Leary et al., 1985; Bruce et al., 1999a; Bruce et al., 1999b). The results from the present study and experimental data in squirrel monkeys (Ch. Parkins, pers. comm.) show that an exponential decay is incorrect in the vicinity of the electrode, which has important implications since the fibres excited at threshold and above are in the near field. This even holds for fibres in more apical and basal turns as the potential and the current density have a relative maximum exactly one turn under and above the electrode due to direct volume conduction. At these locations, this effect is much larger than the transmission through the scala tympani and it is the main determinant for excitation of the nerve fibres. The results from the rotationally symmetric model in this study further corroborate this conclusion. By definition, there is no transmission line effect through the scala tympani into other turns in this model, but the main phenomena of excitation and cross-turn excitation do exist at just slightly higher current levels than in the spiral model. Therefore, we can conclude that the transmission line effect through the scala tympani, although present, has a very limited influence on the neural excitation in other turns. These results are comparable to the results from Girzon (1987) who also found the combination of a transmission line effect and direct current pathways to the different turns. He, however, predicted a more prominent role for the transmission line effect as he did not recognise the existence of cross-turn stimulation via the modiolus. Ifukube and White (1987) measured the current in the modiolus due to intracochlear electrodes in a cadaveric human temporal bone. They found

a non-monotonous decline of this current when their measuring electrodes moved from the apex to the base of the cochlea and interpreted this result as caused by the current flowing along the scala tympani. Their experimental setup is comparable to the first 3 mm in the simulation shown in Fig.4.8, which also shows a non-monotonous behaviour of the current through the modiolus. From the fact that this effect is even more salient in the rotationally symmetric model than in the spiral model we conclude that it is caused by current pathways across the different turns rather than by a transmission line effect along the scala tympani.

In line with this observation is the fact that the rotationally symmetric model and the spiral model give very similar results in the vicinity of the electrodes in the potential fields in the cross-sections (Figs.4.5 and 4.6), the current along the scala tympani (Fig.4.7) and in the excitation profiles (Fig.4.10) as far as current levels below 1 mA are concerned. In previous studies, we compared the neural recruitment characteristics in the rotationally symmetric model (Frijns et al., 1996a) and the spiral model (Frijns et al., 2000a) with measurements done in cats (Shepherd et al., 1993). The experimental data limited a quantitative comparison to the excitation threshold and the spread of excitation in the first 12 dB above threshold. These outcomes are almost the same for both models, and the conclusion that they are equally valuable is still valid. From Fig. 4.9, however, it is evident that there are differences in the fields set up in both geometries. Further away from the electrode position and at higher current levels, these differences become clearly visible in the neural responses (Fig.4.10) as differences in cross-turn stimulation thresholds and saturation currents. We conclude that the rotationally symmetric model, for which the mesh is relatively easy to generate, is a useful model to study gross effects for electrodes that are spaced closely together. This means that most predictions made in previous studies are still valid, e.g., the elevated thresholds and reduced spatial selectivity with longitudinal dipoles if the peripheral processes are absent (Frijns et al., 1996a). For electrodes that are placed further apart or if more detailed information is desired, the full spiral model will do a better job.

In the current study, only point current sources rather than macro-electrodes have been used. This simplification has been introduced on purpose as the presence of large conductors and insulators in the cochlea will change the field patterns and make their interpretation less straightforward. Expectedly, the observed current flow along the scala tympani will no longer match Eq.?? that closely. As already pointed out above, the effect of the shape and placement of macro-electrodes in the cochlea will be the subject of future studies.

The human cochlea not only differs from the guinea pig cochlea by its size. It is among others deeply embedded in the petrous bone rather than protruding in an air-filled bulla, and ,more important, in humans the second and third turns are more or less embedded in the basal one and each turn has its own shape, whereas in the guinea pig all turns are stacked on top of one another and almost uniformly shaped. In the simulations shown here we have used the guinea pig cochlea but placed it in a bony environment. We have also performed simulations which include a representation of the bulla and found that its influence on the neural excitation patterns is negligible, at least for intracochlear electrodes. From preliminary simulations with a human cochlea model, we expect that the conclusions of the present study are also valid for the human situation, despite known geometrical differences. The influence of species differences on neural recruitment characteristics with different macro electrode configurations is the subject of one of our future studies.

4.5 Acknowledgements

This research was financially supported by grants from the Hoogenboom-Beck-Fund and the Heinsius Houbolt Fund. We wish to thank Prof. Dr. J.J. Grote, head of our department, for his continuing support of the modelling work on cochlear implants.

Chapter 5

The Importance of Human Cochlear Anatomy for the Results with Modiolus Hugging Multi-Channel Cochlear Implants

Johan H.M. Frijns, Jeroen J. Briaire and Jan J. Grote
Otology and Neurotology (2001), 22, 340-349

Abstract

Hypothesis: The fact that the anatomy of the basal turn of the human cochlea, especially, is essentially different from that of other species is likely to influence the outcome of cochlear implantation.

Background: Multichannel cochlear implants give better speech understanding than single-channel devices. They are intended to make use of the tonotopic organization of the cochlea by selectively stimulating subpopulations of the auditory nerve. At higher stimulus levels and with monopolar stimulation, excitation of nerve fibers from other turns may interfere with this concept, especially with modiolus-hugging electrodes.

Methods: A three-dimensional spiraling computer model of the human cochlea, based on histological data, was used to test the spatial selectivity and the dynamic range before cross-turn stimulation takes place for the Clarion HiFocus implant with and without a positioner. The results were compared with a similar model of the guinea pig cochlea.

Results: In humans (in contrast to the guinea pig), a well-designed modiolus-hugging electrode yielded reduced current thresholds and high spatial selectivity without reduction of the useful dynamic range. The apical turn of the human cochlea, however, is largely comparable in this respect with the guinea pig cochlea, where cross-turn stimulation reduces the dynamic range substantially.

Conclusion: The clinical success of cochlear implantation in humans and the favorable results with modiolus-hugging devices depend on the anatomy of the human cochlea.

5.1 Introduction

The successful application of multichannel devices is the main factor contributing to the breakthrough in performance by cochlear prostheses for the totally deaf during the last decade. In contrast to single-channel designs, multichannel cochlear implants take advantage of the tonotopic organization in the cochlea by trying to stimulate localized subpopulations of nerve fibers with each electrode or electrode combination in the electrode array. The spatial selectivity thus achieved is the electrical counterpart of the mechanical tuning present in the normal cochlea. The continuous interleaved sampling strategy (Wilson et al., 1991) and various strategies used with the Nucleus (Cochlear Corp., Melbourne, Australia) device, which that use sequential, nonsimultaneous stimulation of the electrodes, have thereby proved important in avoiding the problems associated with direct electrical interaction between electrodes. There is still, however, a mismatch between the small number of independent input channels and the thousands of surviving nerve fibers to be stimulated. Therefore, the need is perceived for further refinement of the electrode array to include many more electrodes to stimulate small groups of auditory nerve fibers (Clark, 1999). For this to be feasible, even with nonsimultaneous stimulation, the regions of the cochlea excited by the various electrodes must not overlap excessively, i.e., the electrodes must have sufficient spatial selectivity. Some recent experiments suggest, however, that changes in the peak or edge of the excitation pattern are more important than the relative amount of nonoverlap of the excitation areas from the two electrodes, at least for discrimination tasks (McKay et al., 1999).

In previous articles, we addressed the question of neural excitation and spatial selectivity with cochlear implants, using a computational model of the electrically implanted guinea pig cochlea (Frijns et al., 1995; Frijns et al., 1996a). As validation, we compared the results with experimental evoked auditory brainstem responses (Shepherd et al., 1993) and single-fiber (van den Honert and Stypulkowski, 1987) data in the literature and found a good agreement with the model predictions. It was shown that both the excitation threshold and the spatial selectivity depend strongly upon on the exact position of the stimulating current sources in the scala tympani. Moreover, the simulations, including more recent ones with a truly spiraling cochlear model (Frijns et al., 2000a; Briare and Frijns, 2000b), demonstrated that the upper range of useful stimulus levels is limited by so-called ectopic or cross-turn stimulation rather than by current spread along the scala tympani, as is widely assumed. This

cross-turn stimulation occurs when the stimulating electrodes excite the modiolar part of the auditory nerve fibers originating in more apical turns, i.e., those fibers physiologically associated with lower frequencies. Therefore, this phenomenon is expected to cause substantially different percepts at higher stimulation levels.

Several advantages are associated with a reduction of the current threshold. First, this increases the safety margin before the electrochemical processes at the electrodes can produce potentially noxious products. Because these processes are primarily controlled by the current density at the electrode surface (Brummer and Turner, 1977), it is necessary to limit the stimulating currents if larger numbers of smaller electrode contacts are to be used in future cochlear implants. Also, total power consumption, important with behind-the-ear or fully implantable devices (Maniglia et al., 1999), is beneficially affected by reducing stimulus levels. With currently available cochlear implants, many patients are programmed in monopolar stimulation modes, because this leads not only to lower thresholds but also to saturation at lower stimulus levels than, for example, bipolar or quadripolar configurations (Chatterjee, 1999). To increase selectivity with such broadly spreading current sources, several methods have been proposed to move the electrode array toward the modiolus (Gstoettner et al., 1999; Kuzma and Balkany, 1999; Aschendorff et al., 1999), i.e., closer to the fibers to be stimulated. This modiolus-hugging principle is also expected to yield further reduced threshold levels and will lead to a deeper insertion if the same length of the electrode carrier is bent along the modiolar rather than the outer wall of the scala tympani.

If however, this modiolus-hugging principle is viewed in the light of the results obtained in our simulations with the guinea pig model, it is doubtful whether it will be as beneficial as might initially be thought. Moving the current source toward the modiolus means not only that it approaches the fibers it should stimulate, but that it will also come closer to the modiolar parts of the fibers from more apical turns. The risk of early cross-turn stimulation is therefore increased, and the overall gain associated with modiolus-hugging depends on the recruitment characteristics of the different fiber populations. These recruitment characteristics are expected to depend on the relative location of the fibers and the stimulating electrodes. Consequently, it is conceivable that the answer to the question whether approaching the modiolus with the electrode array is favorable may depend on the species-specific anatomy of the cochlea. Cochlear anatomy differs between humans and nonhuman primates and also between humans and most other species, including guinea pigs and cats, in ways quite apart from size (Fig. 5.1). In humans the second and third turns

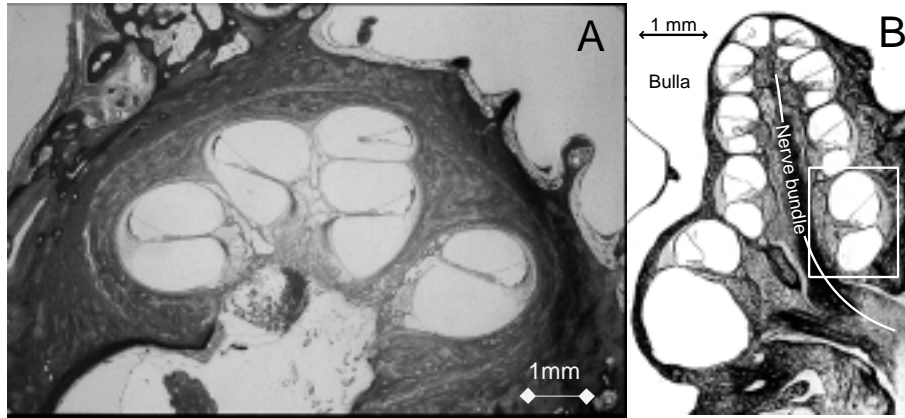


Figure 5.1: A: Midmodiolar cross-section of the human cochlea, showing the large distance between the basal turn and the central modiolar axis. All turns have a specific shape of the three scalae and the apical turns are more or less embedded in the basal turn (Courtesy of Dr F. Linthicum, House Ear Institute). The white bar with diamond-shaped endings has a length of 1 mm and indicates the magnification. B: A similar cross-section through the guinea pig cochlea, in which the anatomy of all turns, including their relative distance to the modiulus, is grossly equal apart from a scaling factor. The much smaller size of the guinea pig cochlea is illustrated by the scaling bar in the upper left corner. The white rectangle indicates the turn to which the basic slice is fitted, which is used for the construction of the model.

are more or less embedded in the basal one, and each turn has its own shape, whereas in the guinea pig all turns are stacked on top of one another and are almost uniformly shaped.

This study addresses the role the species-specific anatomy of the cochlea plays as a determinant of the spatial selectivity and dynamic range attainable with multichannel cochlear implants. For this purpose, fully three-dimensional computer models of the human and the guinea pig cochlea, implanted with clinically relevant macroelectrodes in lateral and modiulus-hugging positions, are compared. The results are discussed in the light of currently available and future electrode geometries.

5.2 Materials and Methods

A computational model of the implanted cochlea was used, which was developed to provide more insight into the fundamentals of functional electrical stimulation of the auditory nerve. The conceptual framework behind this two-step model is as follows: The speech processor delivers the stimulus current via the electrode system, which induces a potential field in the cochlea. This potential field, as computed by the volume conduction model, forms the input of the nerve fiber model that predicts which auditory nerve fibers will be excited. The information conveyed to the brain is characterized by the number, location and firing pattern of these fibers, the model's output. This method has been used successfully before (Frijns et al., 1995; Frijns et al., 1996a; Frijns et al., 2000a; Briaire and Frijns, 2000b), and here we describe only the essentials and the newly introduced methodologic aspects.

5.2.1 Three-dimensional volume conduction model of the human and guinea pig cochlea

The calculation of the potential distribution induced by the currents on the stimulating electrodes is especially intricate in the case of cochlear implants because of the complex geometry of both the inner ear and the electrodes. The boundary element method (BEM) with quadratic interpolation functions for the surface and the potential (Frijns et al., 2000b) was used to solve this problem, as was done in our previous studies. The cochlea is considered to be purely resistive, and capacitive effects (e.g., at the electrode-fluid interface) were not included, because measurements have shown that this assumption is valid for frequencies up to 100 kHz (F. Spelman, personal communication). The conductivity parameters for the various media were those used in our previous studies. The BEM requires discretization of the boundaries between media of different conductivity rather than subdivision of the media themselves. It combines relative ease of mesh generation with the opportunity to deal easily with multielectrode arrays (Briaire and Frijns, 2000a).

The model representations of the human and guinea pig cochlea are based on the histological cross-sections shown in Figure 5.1^A and Figure 5.1^B, respectively. The resulting human mesh has a two and three-quarters turn and is defined by 4,476 surface elements (Fig. 5.2^A). Figure 5.2^B shows how closely the midmodiolar cross-section of this mesh matches the histological slide of Figure 5.1^A. In the model, as in vivo, the higher cochlear turns are more or

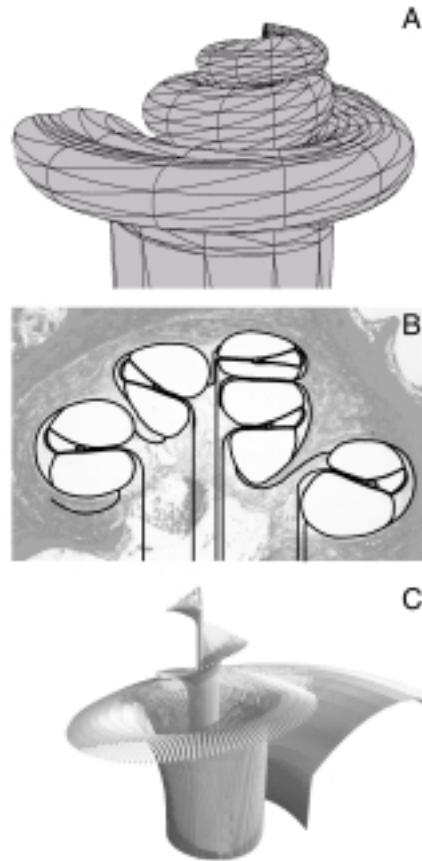
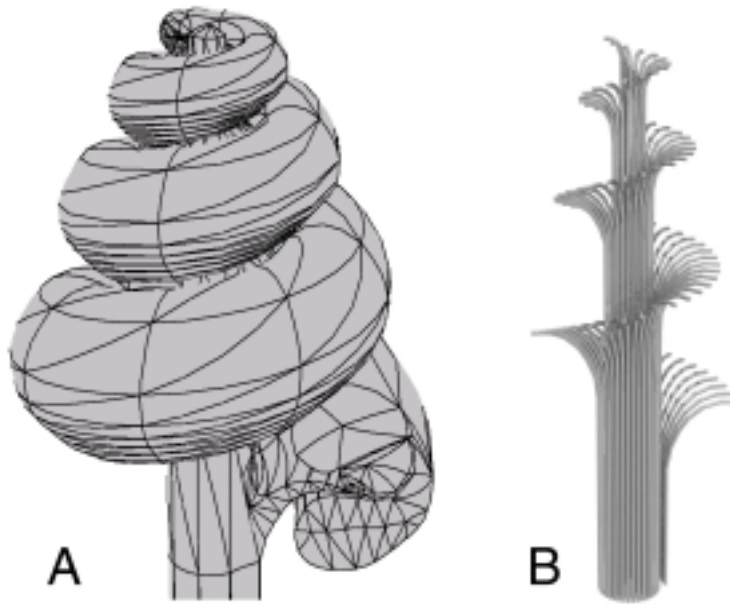


Figure 5.2: A: The boundary element mesh with curved triangular surface elements of the human cochlea as used in the computations. It was constructed on the basis of the histological cross-section of Figure 1A. B: The equivalent midmodiolar cross-section of the human cochlea mesh superimposed upon the histological slice of Figure 1A. The solid lines in the modiolus, exiting the osseous spiral lamina, indicate the course of the nerve fibers. C: Location of the primary auditory nerve fibers in the human cochlea model.



*Figure 5.3: **A:** The boundary element method mesh of the guinea pig cochlea as used in the computations **B:** Location of the primary auditory nerve fibers in the guinea pig cochlea model.*

less embedded in the basal one. Figure 5.2^C shows the spatial distribution of the modeled nerve fibers, which are distributed equidistantly along the basilar membrane with a spacing of approximately $115 \mu\text{m}$ (the unmyelinated terminals of the fibers [see Fig. 5.5] are spaced at $100 \mu\text{m}$). This means that each of the 299 nerve fibers in the simulations represents approximately 100 actual nerve fibers.

Similarly, Figure 5.3 shows the mesh (A) and the fiber distribution (B) in the guinea pig model. This model is somewhat more simplified than the human model, because it was constructed by scaling, and a combination of translation and rotation of a single slice fitted to the boxed part of the histological cross-section as shown in Figure 5.1^B. The details of this procedure, including the anatomically based scaling function, have been published elsewhere (Briaire and Frijns, 2000a). Therefore, the model is slightly limited in its description of

the hook region, but nevertheless it closely resembles the in vivo situation. It has three and a half cochlear turns and includes 405 nerve fibers, with their peripheral endings spaced uniformly every $40 \mu\text{m}$. The most striking difference between this guinea pig model and the human counterpart is the fact that the cochlear turns are stacked on top of one another and that the nerve fibers of all turns, including the basal one, are rather closely packed in the modiolus.

In the human, as well as in the guinea pig, each position in the cochlea is referred to in terms of its rotational position Υ , defined as the number of turns between that position and the basal end of the cochlea. This implies that the rotational position of the apex of the human cochlea is 2.75, whereas it is 3.5 in the guinea pig.

5.2.2 Simulated electrode configurations

In our previously published studies, we used bipolar point current sources rather than realistically shaped (banded) intracochlear electrode arrays. This simplification was dictated by the fact that at that time our software did not allow us to perform calculations with the large meshes that are necessary to include sufficient detail in these electrodes and to achieve the numerical accuracy required for adequately calculating neural responses.

In this study, however, we were interested in the effect of modern modiolus-hugging electrodes, like the Clarion HiFocus device, which have their electrode contacts at the modiolar side of an insulating carrier. This carrier impedes the current flow in the lateral direction, and as expected, this is reflected in the potential distribution in the neural compartment of the cochlea. Therefore, it was necessary to include realistic representations of the electrodes under study, at the cost of increasing the numerical effort involved in the calculations.

Figure 5.4 shows the model representation of the Clarion HiFocus electrode as used in the present study. The human model has 16 rectangular electrode contacts of $0.4 \times 0.5 \text{ mm}$, regularly spaced at 1.1 mm , at the medial side of a Silastic carrier. This slightly tapered carrier has small bulbs medially between the electrode contacts, preventing the electrode surfaces themselves from coming into direct contact with the modiolus. The mesh for this electrode array is defined by 1,678 triangles, adding to a total of 11,483 equations and unknowns to be solved for a solution for this electrode in the human cochlea. The conductivity of the carrier was defined as $10^{-5} (\Omega \cdot \text{m})^{-1}$ and that of the electrode contact as $100 (\Omega \cdot \text{m})^{-1}$. This is an empirical tradeoff between using the actual conductivities (0 and $\pm 10^7 (\Omega \cdot \text{m})^{-1}$ respectively) and avoiding the

numerical errors inherent in the use of large conductivity differences between neighboring media with the BEM. In this way, the conductor is approximately two decades more conductive than the surrounding perilymph, and the insulator is roughly three decades less conductive than the membranes surrounding the scala media.

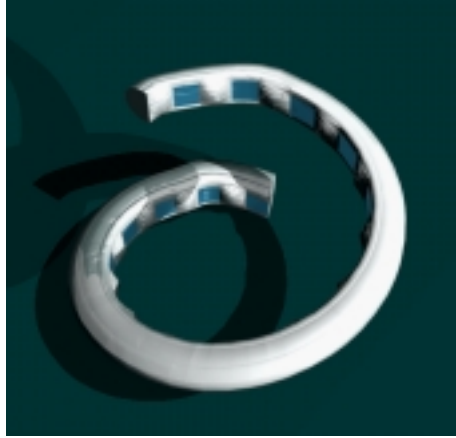


Figure 5.4: Model representation of the new Clarion HiFocus electrode, which has 16 rectangular surface contacts, located at the modiolar side of a silastic carrier. It is intended to be displaced to the modiolar wall of the scala tympani by a positioner, which is introduced separately along the outer curvature. The size of the contacts is 0.4×0.5 mm for the human and 0.18×0.23 mm for the guinea pig model.)

If this electrode is inserted along the outer wall into the scala tympani of the human cochlea model (insertion depth 23.7 mm = 1.03 turn), it is referred to as human lateral. The situation is referred to as human medial if the electrode is inserted alongside the modiolar wall (to a maximum depth of $\Upsilon=1.48$), together with a model replica of the so-called positioner, which has a medial concavity in which the electrode fits neatly. In fact, we fused the meshes of this Silastic strip and the electrode before starting the simulations to avoid unnecessary computations and numerical errors. The corresponding situations in the guinea pig are referred to as GP lateral and GP medial, respectively.

Because the guinea pig cochlea is much smaller than the human one, we downsized the guinea pig electrode and positioner in such a way that they fit into the scala tympani in a similar way as in the human situation. The electrode

contacts were 0.18×0.23 mm in the guinea pig model.

As indicated above, the insertion of a positioner into the cochlea has two mechanical effects: pushing the electrode into a modiolus hugging-position and causing a deeper insertion into the cochlea. The main purpose of this study was to observe the effect of lateral-to-medial displacement, rather than the effect of deeper electrode insertion. However, in vivo in humans, as well as in both modeled cochleae, the rotational position of the most basal electrode contact (No. 16) was negligibly changed by the positioner, allowing for a direct comparison of the results for this contact with and without a positioner. For more apical contacts, which are inserted considerably (up to half a turn) deeper, this is not a valid procedure, because it implies interference between the effects of the tapering of the scala tympani and the effects that result directly from the lateral-to-medial displacement of the electrode. Therefore, each comparison between situations with and without a positioner was carried out while looking at a fixed rotational position of the stimulated electrode (thereby changing the number of the stimulated electrode between situations).

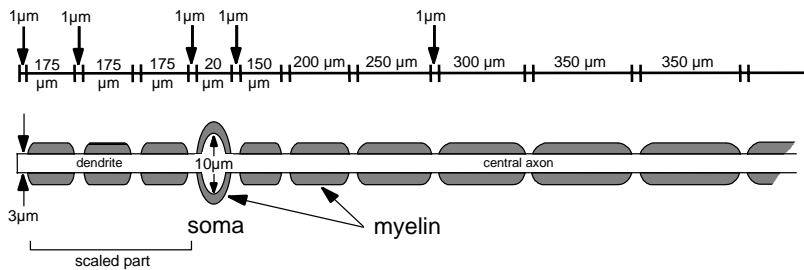


Figure 5.5: The morphology of the generalized Schwarz & Eikhof-Frijns auditory nerve fiber model as used in the calculations. The lengths of the three internodes in the so-called dendrite were scaled to adapt the fibers to the cochlea meshes.

5.2.3 Calculating the neural responses

The nonlinear generalized Swartz & Eikhof-Frijns model of primary auditory nerve fibers was used to simulate the response to time-varying potential fields in the cochlea. The model equations of this auditory nerve fiber model, which has nodal kinetics based on voltage clamp data in the rat (Schwarz and Eikhof,

1987), are described in detail elsewhere (Frijns et al., 1995) and are not reproduced here.

Figure 5.5 shows the morphology of the bipolar high spontaneous rate auditory fibers used in the calculations. These fibers, which were also used in our previous studies (Frijns et al., 1995; Frijns et al., 1996a; Frijns et al., 2000a; Briaire and Frijns, 2000b), consist of a peripheral and a modiolar axon with a diameter of 3 μm , interconnected by a cell body with a diameter of 10 μm . The gap width of the nodes of Ranvier is 1 μm . To accommodate the fibers to the cochlear meshes, we positioned the peripheral ending and the cell body of each fiber to their histologically correct positions and scaled the internodal lengths of the peripheral process accordingly.

5.3 Results

For all simulations presented here, we used cathodic-first symmetric biphasic current pulses (200 $\mu\text{s}/\text{phase}$) injected in a monopolar stimulation mode — i.e., against a far-field point current source — at different electrode contacts. The neural responses were plotted as I/O curves (Figs. 5.7 and 5.9), showing the fraction of all fibers that were excited as a function of stimulus level. By their nature, these I/O curves are closely related to the I/O curves calculated from electrically elicited whole nerve action potentials. The simulated I/O curves were computed on the basis of the underlying excitation profiles (Figs. 5.6 and 5.8, respectively), which show which fibers (ordered according to their rotational position Υ) are excited at each stimulus level. In these excitation profiles the part of the fiber (peripheral process, cell body or central axon) where the initial excitation takes place is indicated by gray shading. A narrow peak around the stimulated electrode in an excitation profile indicates that that mode of stimulation is selective. Such a selective stimulation is reflected in a relatively shallow slope of the I/O curve for stimulus levels immediately above threshold.

Figure 5.6 shows the excitation profiles computed for the Clarion HiFocus electrode without (GP lateral, A and C) and with (GP medial, B and D) positioner in the guinea pig cochlea. Figure 5.6^{A,B}, shows the computation for the most basal electrode (No. 16, $\Upsilon=0.4$), and Figure 5.6^{C,D}, shows the data for $\Upsilon=1.4$ turn (electrodes No. 1 and No. 5, respectively). The corresponding I/O curves are shown in Figure 5.7. In these figures it is readily seen that shifting the electrode from a conventional (lateral) to a modiolus-hugging position did not

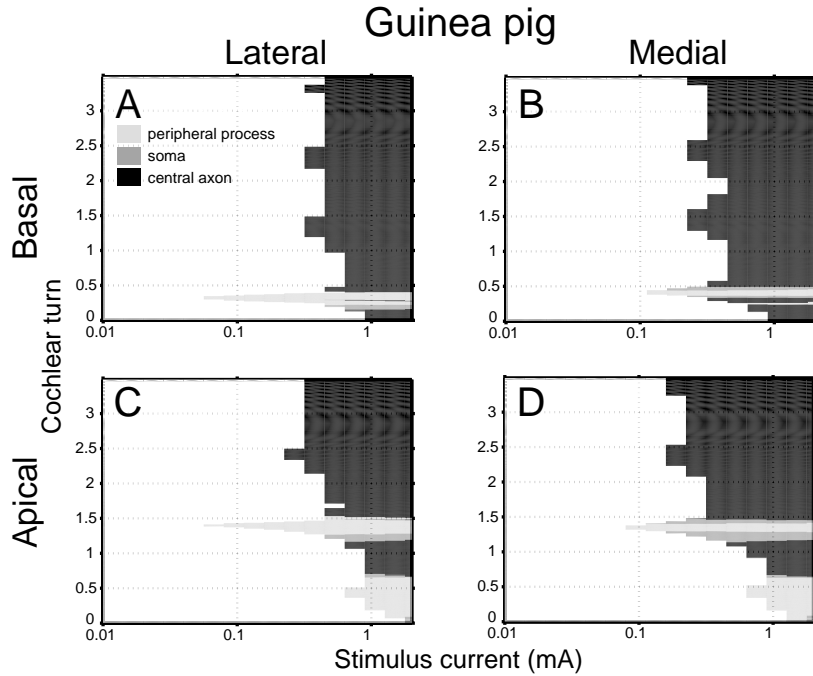


Figure 5.6: Excitation profiles for monopolar electrode configurations (cathodic-first biphasic current pulses, $200 \mu\text{s}/\text{phase}$) with the guinea pig equivalent of the Clarion HiFocus electrode in a lateral position (**A** and **C**) and with positioner (**B** and **D**). The location of the part of the nerve fiber where the initial excitation takes place is indicated by gray shading. **A** and **B** were computed for the most basal electrode contact (No. 16, $\Upsilon=0.4$) and **C** and **D** for the more apical contact at rotational position $\Upsilon=1.4$ (No. 1 and No. 5, respectively).

necessarily produce the desired reduction in threshold. On the contrary, for electrode No. 16 it even resulted in a considerable upward threshold shift. As can be seen by comparison of Figure 5.6^A and with Figure 5.6^B, this unexpected result is the consequence of the fact that the predicted site of excitation changes from the peripheral process (lateral position) to the cell body and modiolar part of the nerve fibers. This effect is less prominent for the apical electrodes, where the excitation threshold for the fibers at the same rotational position as the electrode is only marginally influenced by the lateral-to-medial shift. For both the apical and the basal electrodes, however, the modiolus hugging position leads to lower excitation thresholds for the fibers originating in more apical turns, which encode for lower frequencies in the physiologic situation. This so-called ectopic or cross-turn excitation occurs in the modiolus, where their central axons pass near the site of the stimulated electrode.

In humans, most excitation thresholds are higher (by a factor up to 10) as can be seen in the excitation profiles of Figure 5.8 and the corresponding I/O curves in Figure 5.9. This is not surprising, because the dimensions of the human cochlea are larger than those in the guinea pig counterpart. Especially for lateral electrode positions, this also leads to a somewhat larger range of stimulus levels before generalized excitation, as indicated by the steep part of the I/O curve, occurs. However, medializing the electrode with the positioner reveals a more striking difference between the human and animal model: With electrode No. 16 ($\Upsilon=0.2$, i.e., in the basal turn) in the human model, it reduces the excitation threshold for the fibers in the implanted turn by a factor of 4, whereas the threshold for cross-turn excitation is reduced by no more than a factor of 2 (Fig. 5.8^{A,B}). This means that in contrast to the guinea pig the lateral-to-medial displacement here reduces the amount of current needed to reach threshold and increases the dynamic range, while retaining the spatial selectivity. In the lateral position lower excitation thresholds are found for apical electrode No. 1 ($\Upsilon=1.0$) than for basal electrode No. 16 ($\Upsilon=0.2$) as a consequence of the smaller dimensions of the scala tympani. In the modiolus-hugging position, the threshold is further reduced, but with it the thresholds for fibers originating in the most apical turn are lowered as well. Unfortunately, this leads to a smaller range of stimulus levels before cross-turn excitation occurs. Thus, with respect to apical electrodes, the human situation is grossly comparable with the guinea pig equivalent.

Figure 5.10 gives the explanation for the different behavior in both species for basal and apical electrodes. It shows the potential distribution caused by a current of 1 mA injected into the cochlea through basal and apical electrodes in the monopolar mode in the GP medial and the human medial situations.

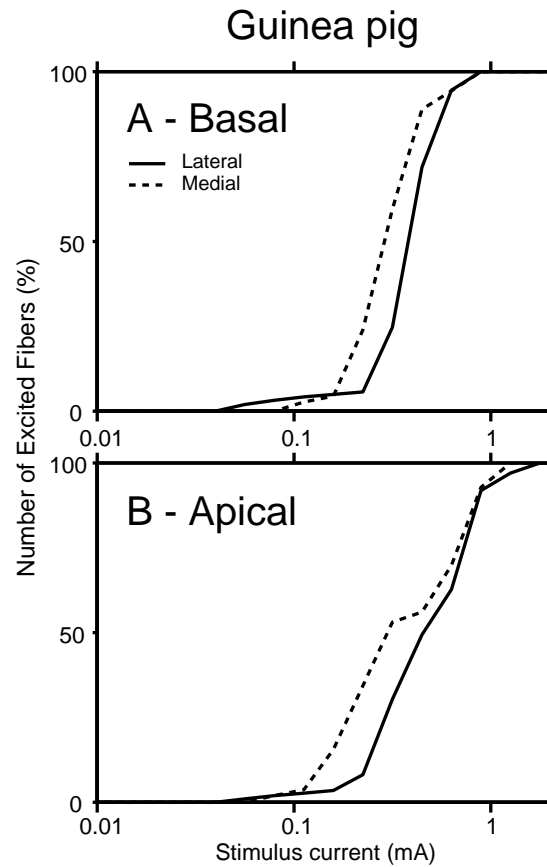


Figure 5.7: The effect of lateral-to-medial displacement in the guinea pig of the Clarion HiFocus electrode on threshold and slope of the I/O curve, which shows the fraction of the nerve fibers that is excited as a function of the stimulus level. **A**: Basal electrode contact (No. 16, $\Upsilon=0.4$), cathodic-first biphasic current pulses, $200 \mu\text{s}/\text{phase}$. **B**: As in **A** but now for the electrode contact at $\Upsilon=1.4$ (No. 1 in the lateral and No. 5 in the medial position).

For a correct interpretation of this figure, it is important to realize that not the absolute potential but the so-called activating function (Rattay, 1989) (roughly speaking, the [spatial] rate with which the potential gradient changes along the nerve fiber) is the main force leading to excitation of the nerve fibers. From Figure 5.10^A (GP medial situation, contact No. 16) it is clear that all fibers, regardless their site of origin, are exposed to fields with high gradient variations when they pass by the basal turn in the modiolus. The situation in Figure 5.10^C (human medial, contact No. 16) is fairly different: Fibers from the second turn pass through the outskirts of the potential field and follow almost the course of equipotential lines, whereas fibers from the apical region are even less likely to be stimulated. Comparison between Figure 5.10^B and Figure 5.10^D, showing the computations for apical electrodes, leads to a different analysis: For such apical electrode contacts, the implant sets up large potential gradients in the modiolus for both species, leading to a large likelihood of cross-turn stimulation for more apical turns. The fact that cross-turn stimulation is not an issue with regard to more basal turns in all species (Fig. 5.6^{C,D}; Fig. 5.8^{C,D}) is clarified further by Figure 5.10^{B,D}. This phenomenon requires direct stimulation of the dendritic part of the fibers in the turn immediately below the stimulated electrode. These fibers are relatively far away and are shielded from the electrode contact by the electrode carrier and — especially in the guinea pig — the insulating membranes surrounding the scala media.

5.4 Discussion and Conclusions

The main purpose of this modeling study was to obtain a better understanding of the circumstances under which modiolus-hugging scala tympani electrodes provide improvements over electrodes close to the lateral wall. The results suggest that the specific human cochlear anatomy, especially that of the basal turn, is a key factor in the potential success of approaching the modiolus as attempted with several modern electrode arrays (Gstoettner et al., 1999; Kuzma and Balkany, 1999; Aschendorff et al., 1999). The model predicts that the proximity of the electrode contacts to the excitable elements in the modiolus leads to reduced current thresholds while retaining a good dynamic range and spatial selectivity, at least for electrode contacts in the basal turn. To arrive at this conclusion, we introduced in this study a new volume conduction model of the human cochlea. Because the aim of this study did not allow ignoring the influence of the insulating electrode carrier, we included a detailed model of the Clarion HiFocus electrode array.

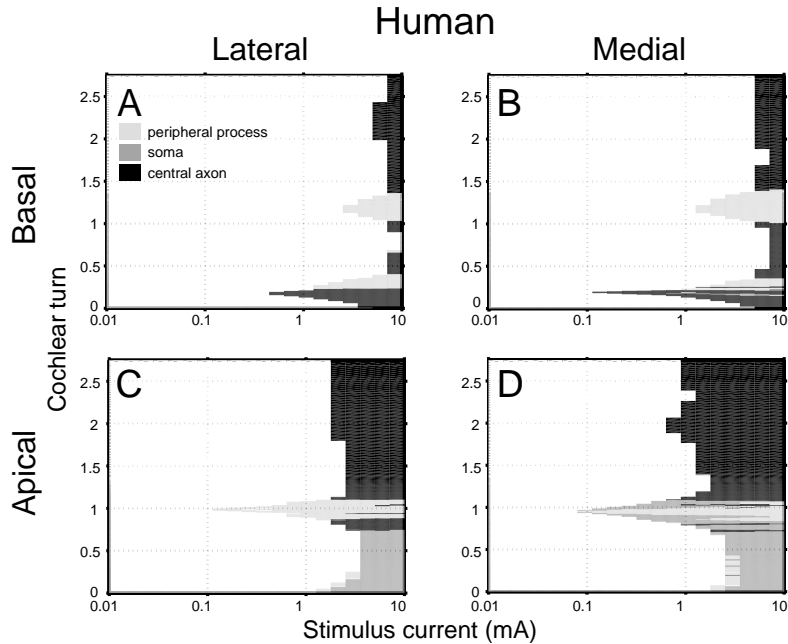


Figure 5.8: Excitation profiles for monopolar electrode configurations (cathodic-first biphasic current pulses, $200 \mu\text{s}/\text{phase}$) with the Clarion HiFocus electrode in a lateral position (**A** and **C**) and with the positioner (**B** and **D**) in the human cochlea. **A** and **B** were computed for the most basal electrode contact (No. 16, $\Upsilon=0.2$) and **C** and **D** for the more apical contact at rotational position $\Upsilon=1.0$ (No. 1 and No. 5, respectively).

The same electrode design (scaled down in size to fit the smaller cochlea) was tested in a model with the anatomy of the guinea pig cochlea, based on the previously validated (Frijns et al., 1995; Frijns et al., 1996a; Frijns et al., 2000a) numerical methods and parameters. This led to the somewhat paradoxical conclusion that approaching the modiolus does not necessarily lower the threshold level as it does in the human basal turn, whereas the dynamic range can be seriously reduced by the occurrence of cross-turn stimulation via the modiolus. The phenomenon of cross-turn stimulation is expected to lead to perceptual difficulties, because gradually increasing the stimulus level will suddenly lead to excitation of fibers that are physiologically associated

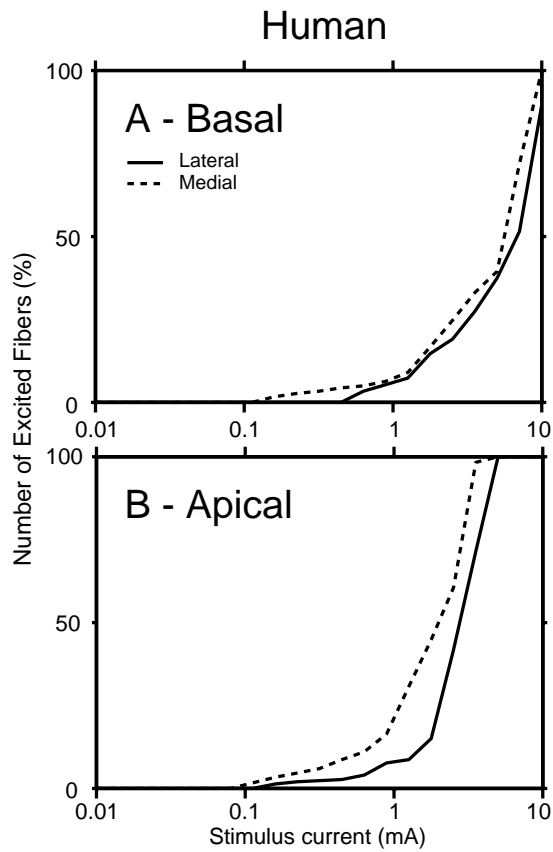


Figure 5.9: The effect of lateral to medial displacement in the human cochlea of the Clarion HiFocus electrode on threshold and slope of the I/O curve. **A**: Basal electrode contact (No. 16, $\Upsilon=0.2$), cathodic-first biphasic current pulses, $200 \mu\text{s}/\text{phase}$. **B**: As in **A** but now for the electrode contact at rotational position $\Upsilon=1.0$ (No. 1 in the lateral and No. 5 in the medial position).

with far lower frequencies. Such an effect has been reported in humans. Interestingly, that effect was more marked for wide bipolar stimulation than for monopolar stimulation (Cohen et al., 1996). As for the Clarion HiFocus electrode in humans, the fact that its apical electrode contacts perform better in a lateral position, while modiolus-hugging is better for the contacts in the basal turn, also has implications for safety: There is no advantage in pushing the positioner farther than one turn into the scala tympani, so one should avoid the risk of causing damage to the cochlear structures by exerting too much force on them when trying to obtain an unnecessarily deep insertion of the positioner. Future research with more sophisticated modes of stimulation than the monopolar mode we used may identify other ways to increase the spatial selectivity further, especially for more apical fibers.

An important body of cochlear implant research is formed by electrophysiologic studies in laboratory animals. Obviously, the underlying assumption is that the auditory system of the animals used in the studies is sufficiently comparable to the human equivalent to warrant a meaningful extrapolation of the results to the situation in deaf patients. In their recent study, Miller et al. (1999) found support for this hypothesis for psychophysical strength-duration functions. The strikingly different results between the human model and the guinea pig model pose some questions concerning the validity of this assumption for other aspects of electrical stimulation, especially because other species commonly used in auditory electrophysiology, like the cat, have many anatomical properties in common with the guinea pig. However, we also found that the guinea pig cochlea is a good model for the more apical parts of the human cochlea. Therefore, we conclude that one should always be cautious before interpreting animal experiments in terms of human applications. A computational model like the one used in this study, allowing manipulation of individual parameters while all the others are kept constant, may help to justify or reject such an extrapolation. In this study, the analysis of the potential distributions associated with the various electrode conditions in both species (Fig. 5.10) gave insight into the processes underlying results that were at first sight somewhat paradoxical.

As discussed in previous reports (Frijns et al., 1995; Frijns et al., 2000a), the exact value of the current thresholds predicted by the model is limited, because it is still a simplification of reality, dependent on many parameters that are not yet fully known. One of the known differences between the model and the *in vivo* situation in humans is the fact that the cell bodies in the spiral

ganglion are not myelinated (Arnold, 1987). Preliminary simulations, however, showed that this only slightly influences the threshold for situations without neuronal degeneration, although it has marked influence on spike timing. In spite of these limitations, the model is applicable to testing different electrode designs against one another under identical, fully controlled conditions. By contrast with animal experiments and clinical experiments in humans, one does not have to deal with interindividual variations or difficulties in manufacturing or implanting (miniaturized versions of) electrodes. For example, one of the main electroanatomical differences between the Clarion HiFocus electrode with positioner tested in this study and a new precurved intracochlear electrode with stylet from Cochlear Corp. (Melbourne, Australia) (Aschendorff et al., 1999) is the absence of a positioner lateral to the electrode in the latter case. The model allowed performing simulations with the Clarion HiFocus electrode in the medial position without the presence of the space-occupying positioner, thereby increasing the similarity with the precurved array with stylet. We found the same excitation thresholds and spread of excitation with increasing stimulus levels as with the positioner for all electrode contacts tested. In the human cochlea, the Silastic positioner appears to act as an insulator that shields the peripheral processes of the fibers one turn above the electrodes in the basal turn from direct excitation at higher stimulus levels, thereby increasing the dynamic range before ectopic stimulation occurs (Fig. 5.10^C).

We have also performed calculations with the precurved Clarion electrode array, which has ball contacts located below the dendrites and at the modiolar side of a tapered cylindrical carrier. Clinically, this electrode has been implanted with the same positioner as used with the Clarion HiFocus electrode (Kuzma and Balkany, 1999) in an attempt to take advantage of the modiolus-hugging effect. Although radiography revealed that the electrode was in the correct place, and a deeper insertion was obtained with the positioner (T. Balkany, personal communication), the effect on excitation thresholds was not unequivocal. This observation is in accordance with our simulation results, which show that the excitation thresholds are virtually unchanged, at least with the bipolar modes of stimulation used clinically. The main effect of the positioner is that less current is necessary to excite increasing numbers of nerve fibers. Clinical experience has shown that this should be interpreted not as a degradation of spatial selectivity but as a way to obtain a reasonable loudness growth with moderate current levels.

The main conclusion to be drawn from this study is that the specific anatomy of

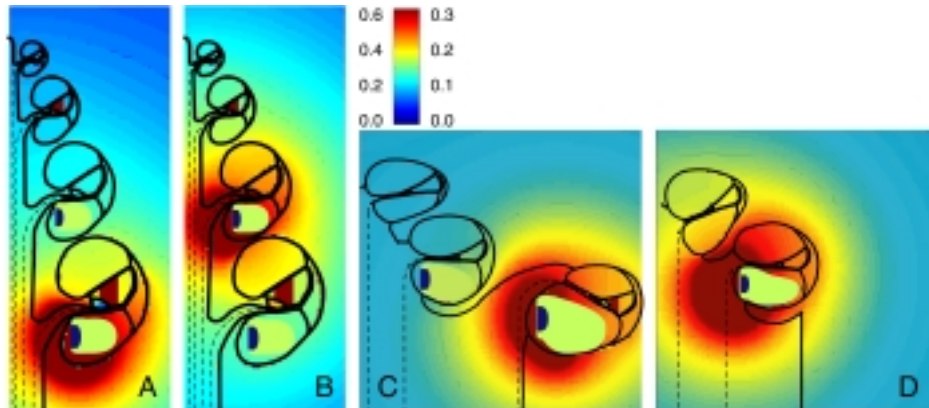


Figure 5.10: Potential plots for monopolar stimulation (1 mA) of the Clarion Hi-Focus electrode with positioner. The potential (in V) associated with the various gray levels is indicated by the color bar (the values to its left pertain to **A** and **B**; to the right, to **C** and **D**). The dashed lines illustrate the course of the primary auditory nerve fibers from the various turns. **A**: Basal electrode contact (No. 16, $\Upsilon=0.4$) in the guinea pig cochlea. **B**: Apical electrode contact (No. 5, $\Upsilon=1.4$) in the guinea pig cochlea. **C**: Basal electrode contact (No. 16, $\Upsilon=0.2$) in the human cochlea. **D**: Apical electrode contact (No. 5, $\Upsilon=1.0$) in the human cochlea.

the human cochlea has important beneficial implications for the clinical applicability of multichannel cochlear implants. The results shown in this study indicate that modiolus-hugging per se is not a universal remedy but is a promising method, to be tested in the basal turn with well-designed electrode arrays in humans rather than in animal models.

5.5 Acknowledgement

The authors thank Dr. F. Linthicum of the House Ear Institute for kindly providing the histologic cross-section used to construct the human mesh.

Chapter 6

Initial evaluation of the Clarion CII cochlear implant: Speech perception and neural response imaging

Johan H.M. Frijns, Jeroen J. Briaire, Jan A.P.M. de
Laat and Jan J. Grote
Ear and Hearing (2002), 23(3), 184-197

Abstract

Objective: The Clarion CII is a promising cochlear implant with which our first ten patients have obtained excellent speech perception results. The NRI system yields high quality signals with a limited number of sweeps at a high sampling rate.

Design: The speech perception scores on CVC words without lip reading were monitored prospectively for the ten postlingually deaf patients implanted with the Clarion CII device in the period July 2000 until May 2001 in the Leiden University Medical Center. Peroperative and postoperative NRI recordings were made, applying various combinations of monopolar stimulating and recording electrodes with the alternating polarity paradigm available in the test bench software.

Results: Nine patients preferred the CIS, one the PPS strategy, none the SAS strategy. With their favorite strategy they acquired significant open set speech understanding within a few weeks, resulting in an average CVC phoneme score of 84% (word score 66%) at the end of the study (follow-up 3 to 11 mo). In speech-shaped noise, the average phoneme recognition threshold (PRT) was reached at a signal to noise just below 0 dB. The NRI recordings had clear N_1 and P_1 peaks if there was at least one contact between the stimulating and recording electrodes, necessitating just 15 sweeps for a reliable recording. We observed considerable inter-patient and inter-electrode variability, but for a given situation NRI input/output curves were stable over time. More apical contacts generally elicited larger eCAPs. Response amplitudes tended to peak at recording sites around apical and basal stimulating electrodes, suggesting a limited spread of excitation. Preliminary recordings with the forward masking paradigm were consistent with the ones with the alternating polarity scheme.

Conclusions: The Clarion CII is a promising cochlear implant with which our first ten patients have obtained excellent speech perception results. The NRI system yields high quality signals with a limited number of sweeps at a high sampling rate.

6.1 Introduction

Since the introduction of the first single-channel device in the mid-seventies cochlear implants have undergone a wide range of technical improvements, and speech perception performance has been increasing steadily. Now multi-channel cochlear implants are firmly established as effective options in the habilitation and rehabilitation of adults and children with bilateral profound hearing impairment (NIH Consensus Statement, 1995). They aim to stimulate the primary auditory nerve fibers in the cochlea by injecting electric currents into the inner ear.

Animal experiments (Shepherd et al., 1993) and computational models (Frijns et al., 1995; Frijns et al., 1996a) initially suggested a considerable influence on implant function of the exact position of the electrode in the scala tympani. The latest devices are designed to be in a peri-modiolar (also called modiulus hugging) position rather than lying along the outer wall of the scala tympani (Gstoettner et al., 1999; Tykocinski et al., 2001; Kuzma and Balkany, 1999). The possible advantages of being in a peri-modiolar position, i.e. closer to the nerve fibers to be stimulated, include a reduction of the stimulus thresholds and stimulating currents, a higher selectivity of stimulation and an increased dynamic range. Preliminary clinical experience with the Clarion HiFocus and the Nucleus[®] Contour[®] electrodes suggests that at least some of the advantages sought with peri-modiolar electrodes (esp. reduced thresholds) can be reached (Tykocinski et al., 2001; Kuzma and Balkany, 1999). In a recent article (Frijns et al., 2001) we compared the Clarion HiFocus electrode in the lateral and modiulus hugging position in our computational model of the electrically stimulated cochlea. We concluded that modiulus hugging in the basal turn favorably influences spatial selectivity and dynamic range. This is a consequence of the specific anatomy of the human cochlea. As contrasted to other species, in humans the distance from the medial wall of the scala tympani to the nerve bundle in the modiulus is much larger in the basal turn than in the middle and apical turns. In more apical sites a position near the outer wall is therefore more desirable to avoid so-called cross-turn stimulation of fibers in the modiulus.

Improved implant electronics and speech processing strategies are other technical aspects contributing to the clinical success of multi-channel implants. A major breakthrough was achieved by the introduction of the CIS (Continuous Interleaved Sampling) strategy (Wilson et al., 1991). This strategy avoids electrode interactions by nonsimultaneous stimulation of the different electrode contacts in the array. There is laboratory evidence that increasing the rate of

stimulation in CIS may further increase speech performance (Rubinstein et al., 1999b).

With the increasing numbers of prelingually deaf children that are implanted, there has been growing interest in objective measures of the electrode to neural interface such as stapedius reflex thresholds (Almqvist et al., 2000), the electrical auditory brainstem response (EABR)(Shallop et al., 1991) and the electrically evoked compound action potential (eCAP) of the auditory nerve. Initially, eCAP recordings could only be made intraoperatively (Gantz et al., 1994) or from cochlear implants that used a percutaneous plug to connect the speech processor with the internal electrode array (Brown et al., 1990). Since 1998 such recordings are possible from most patients and most electrodes with the Nucleus CI24M implant, through a system called Neural Response Telemetry (NRT®)(Abbas et al., 1999). Although the shapes of NRT threshold curves are roughly the same as subjectively determined threshold and most comfortable level curves, some additional behavioral information is still needed to program the processor reliably.

In the present article we present the initial clinical experience in the Leiden University Medical Center with the Clarion CII implant (Advanced Bionics Corp., Sylmar, CA), which combines the HiFocus electrode with positioner with newly designed electronics, which is capable of high-rate and/or simultaneous stimulation through 16 independent current sources. Its hardware also features new telemetry options, including recording of eCAPs via the intracochlear electrode array (called Neural Response Imaging, NRI). Here we will present speech perception data in quiet and in noise obtained with the new device, programmed in a mode that emulates the previous Clarion (CI) device. In addition we will demonstrate and discuss some of the possibilities for objective assessment of the electrode-to-neural interface, emerging from the NRI technique.

6.2 Patients, Materials and Methods

6.2.1 The Clarion CII Cochlear Implant

All patients in this study have been implanted by a single surgeon at the Leiden University Medical Center with the Clarion CII cochlear implant in the period immediately following the CE (Conformité Européenne) approval (July 2000) for its clinical use in deaf adults and children in the European Community. This

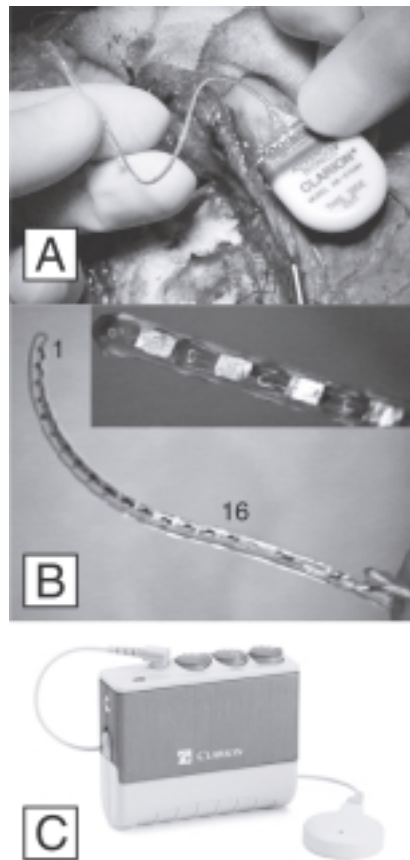


Figure 6.1: A The new implantable electronics of the Clarion CII implant (Advanced Bionics Corp., Sylmar, CA) is encased in the same ceramic housing as the previous Clarion Multi-Strategy implant. B The modiolus hugging HiFocus electrode has 16 electrode contacts (0.4x0.5 mm), equidistantly spaced at 1.1 mm. The most apical contact is numbered 1, the most basal one 16. C All patients in this study used the new Platinum speech processor.

implant, which obtained FDA approval in March 2001, is shown in Fig. 6.1. It incorporates the HiFocus electrode, which is brought into a modiolus hugging position by secondary insertion of a so-called positioner. The electrode contacts are numbered from 1 at the tip of the electrode to 16 at the basal end (Fig. 6.1^B).

The implanted electronics uses less power than its predecessor (referred to as the CI) and is driven by the Platinum[®] speech processor (PSP) shown in Fig. 6.1^C. The implanted circuitry contains 16 independent current sources (versus eight in the CI), which can be driven simultaneously. These linear current sources have an 11-bit (including sign bit) DAC, yielding a best resolution of 0.25 μA in the lowest of their 4 output ranges. The current sources in the CI had a log-based amplitude scale (9 bits including sign bit) with a 0.3 dB current step. With a 10 k Ω load the new current sources reach 63% of their final value in less than 1 μsec , which compares favorably with the 5 μsec needed in the CI. This improvement in the current source allows better timing of the pulses in a CIS type strategy. The basic design of the implant differs from all previous devices in the way the stimulus information is transmitted from the speech processor to the current sources. Traditionally, cochlear implants work by continuously updating the complete stimulus information from external components. This implant system first transfers a so-called pulse table containing the processing scheme (stimulus waveforms, pulse durations and/or update rates) into a memory bank in the internal electronics. During normal use, the speech processor transmits only amplitude information through the RF link to the internal electronics. This enables the total system to operate at rates up to 373,000 pulses per second, because it is less constrained by the limited bandwidth of the RF link. Currently, however, software limitations require the implant to operate in a mode that emulates the output of the conventional Clarion (CI) implant, allowing for a maximum of 8 active contacts and a maximum non-simultaneous update rate of 6500 biphasic pulses per second (75 $\mu\text{sec}/\text{phase}$) (Kessler, 1999).

6.2.2 Patient Demographics and Follow-Up

Here we report the 3 to 11 mo follow-up data of the first ten Clarion CII recipients (labelled consecutively A to J) implanted between July 2000 and May 2001 in the ENT department of the Leiden University Medical Center. They enrolled in the program of the Cochlear Implant Rehabilitation Center Leiden-Effatha (CIRCLE), run in collaboration with the Institute for the Deaf Effatha in Zoetermeer. As shown in Table 6.1 all patients were postlingually deafened

Table 6.1: Patient demographics of the 10 postlingually deafened implantees involved in the clinical study, listed in order of surgical implantation.

Patient	Gender	Age at implantation (yr)	Duration of deafness (yr)	Hearing loss (dB HL)	Contralateral Ear Hearing Loss (dB HL)	Etiology
A	F	62	2	115	>120	Progressive
B	M	43	>30	>120	115	Hereditary
C	F	38	>30	115	115	Hereditary
D	F	39	35	>120	115	Aminoglycosides
E	M	59	1	105	100	Ménière's disease
F	F	49	15	>120	>120	Progressive
G	F	52	23	>120	>115	Unknown
H	F	28	3	>120	>120	Hereditary
I	F	51	33	>120	110	Syndromal
J	M	14	2 months	>120	>120	Meningitis

Duration of deafness denotes the duration of the period of severe-to-profound hearing loss. The hearing loss is the average pure tone hearing loss in both ears for 1, 2 and 4 kHz rather than the conventional Fletcher Index (based upon the PTA thresholds for 0.5, 1 and 2 kHz), since these frequencies are more relevant for the speech reception in quiet and in noise.

(9 adults, 1 child) with a wide variety of etiologies. The preoperative objective assessment of the hearing loss with DPOAE's, ABR and ECoG responses (Schoonhoven et al., 1999) confirmed the pure tone hearing thresholds listed in Table 6.1. Preoperative CAT and MRI scans did not show any anatomical abnormalities, in 8 patients. In patient E a very anterior bulging of the sigmoid sinus and a slit-like narrowing of the scala tympani in the vicinity of the round window was observed. In patient J, deafened due to meningococcal meningitis, there were signs of intracochlear ossification in both cochleae.

Preoperative speech perception scores were measured in a free-field condition with adequately fitted hearing aids using the standard CVC word lists (pre-recorded female speaker) of the Dutch Society of Audiology at 65 dB SPL (Smooenburg, 1992). As contrasted with normal clinical use, the results of four lists (each 11 words, i.e., 33 phonemes) were averaged to obtain a single data point to increase the accuracy. If the candidates did not have adequately fitted hearing aids, their speech perception was tested with newly fitted ones after a trial period of at least 6 wk. The same test was used to evaluate the postoperative performance with the implant. If applicable, noise with a long-term frequency spectrum equal to speech (as available on the same CD used to present the words) was added to test the performance with the implant in background noise. As shown in Fig. 6.3 the average preoperative phoneme score was 8% (range: 0 to 23%), and the word scores were between 0 and

2%.

Preoperatively, using both hearing aids, seven patients could not complete a speech-tracking task without the help of lipreading at a speed higher than 10 words correct per minute (the point below which we discontinued the measurement). This test, which aims at measuring performance in real-life conditions (De Filippo and Scott, 1978), is more difficult to standardize than, e.g., CVC word tests. To minimize biases the test was conducted according to the protocol formulated by Matthies and Carney (1988), including their prompting and stopping rules. We used a live presentation of selected everyday texts (of 100-110 words, 7-10 words per phrase) by a single female speaker other than the speech therapist they trained with. After completion of the full text the total number of words was divided by the time it took to complete the test, yielding a score in words per minute (wpm). In the present paper we will present results for the sound-only condition. In this condition the scores of normally hearing listeners range between 90 and 100 wpm.

We also used sentence materials to test the postoperative performance of the patients in noise. For this purpose we presented the sentence test developed by Plomp and Mimpen (1979) from the standard CD (female speaker) in a free field condition. The standard 2 dB up (wrong result), 2 dB down (correct result) paradigm on sets of 13 sentences was used to adjust the level of the speech in standardized steady-state speech noise (65 dB SPL) in search of the speech reception threshold (SRT). In this relatively difficult test an answer is only scored as correct if the whole sentence is repeated flawlessly. Scores are considered to be reliable if the intra-test standard deviation is less than 3.0 dB. For normally hearing subjects the SRT is reached at a signal to noise ratio of approximately -5 dB.

In the CIRCLE program the rehabilitation starts immediately after the fitting, four to six wk after surgery. This newly developed training program (Frijns-van Putten et al., 2005) has a structure with ten levels of increasing difficulty, starting with simple discrimination tasks, and (if possible) building up to open set speech perception in noisy circumstances. The training does include listening to VCVs and CVCs, but the therapist never uses any words from the test materials to avoid biasing the test results. The training is given by a speech therapist and has an intensive start with 20 sessions of 30 minutes in the first two wk and 10 such sessions in the next two wk. In the next two mo up to 15 additional sessions take place, gradually diminishing in frequency. In the same 3-mo period each patient undergoes approximately 12 fitting sessions. Five of these are scheduled in the first week, and all patients are offered CIS, SAS

as well as PPS processing strategies in this early phase. When making decisions on the parameters we always paid attention to maximizing the amount of high frequency information, like commonly done when adjusting conventional hearing aids to optimize speech perception in noise. For this purpose we tried to maximize the upper limit of the dynamic range (the M-level) for the basal-most electrodes or electrode pairs, even though patients often initially did not like the overall sound. At the same time we also tried to avoid cross-turn stimulation, which is expected to occur at more elevated stimulus levels, especially at apical electrode contacts (Frijns et al., 2001). This phenomenon results from excitation of modiolar parts of nerve fibers, originating from more apical cochlear turns than the one the stimulating contact is in. Due to the tonotopic organization of the cochlea such cross-turn stimulation is expected to produce lower-pitched sensations. Whenever patients reported such percepts for a particular electrode we reduced the M-level for that electrode (Frijns and Braire, 2001). A detailed description of the fitting strategy is beyond the scope of the present article and will be published elsewhere.

6.2.3 Neural Response Imaging

One of the new features of the Clarion CII implant is the built-in capability to measure the electrically evoked compound action potential (eCAP) of the auditory nerve through the intracochlear electrodes, denoted by Neural Response Imaging (NRI). In itself such a measure of the electrode to neural interface is not new, as it was already available (as Neural Response Telemetry, NRT) in the Nucleus CI24M implant (Cochlear Corp, Sydney, Australia) (Abbas et al., 1999). The Clarion CII has an on-chip differential amplifier with multiplexed inputs, which returns from an overload condition due to a stimulus artefact within 20 μ sec, thereby eliminating the need to switch off the inputs during stimulus delivery. The responses are captured with a 9-bit (8 bits plus sign) analog-to-digital converter, operating at sampling rates up to 60 kHz. This high rate is achieved by first storing the sampled data in the same piece of memory that is used to store the pulse tables for stimulation (see above) before transferring them on a sweep-by-sweep basis (approximately 1 per second) to the external computer for averaging. The present study mainly used the alternating polarity paradigm (Finley et al., 1997), an artefact rejection scheme, which is commonly used in acoustical CAP measurements (Versnel et al., 1992). According to this paradigm the responses to anodic-first and cathodic-first pulses are averaged, which eliminates the artefact, while the biological signals—which

have the same polarity for both stimulus conditions—are retained. Alternatively, we performed some preliminary measurements with a forward masking paradigm (Brown and J., 1990), which makes use of the refractory properties of the auditory nerve.

For all NRI recordings we used biphasic pulses with 37.5 μ sec phase duration and we averaged 15 sweeps (± 1 sweep per second) of each stimulus presentation. In this study we used monopolar stimulation and recording modes. We short-circuited the stimulus and recording electrodes during approximately 190 μ sec immediately preceding the stimulus onset to discharge them before each NRI sweep. It turned out that the device produced an internal interference signal, which was synchronous with the sweeps but independent of the stimulus strength, allowing us to subtract a so-called system signature from each sweep before further processing. In fact, this “system signature” was an NRI recording with the stimulus amplitude set to zero. Next, the recording was digitally blanked until 200 μ sec after stimulus onset to prevent any residual artefact from disturbing the further post-processing, which consisted of zero-phase shift filtering based on a fourth order Butterworth low-pass filter with a cut-off frequency of 6 kHz. The effect of the different processing steps, which were performed in MatLab[®] version 5.3 (The MathWorks, Inc., Natick, MA), is illustrated in Fig. 6.2.

6.3 Results

During surgery no additional anatomical abnormalities were encountered. In subject E an “egg shell” like decompression of the sigmoid sinus was performed and the sinus was temporarily impressed during the formation of the posterior tympanotomy, the cochleostomy and the electrode insertion. The basal most end of his scala tympani had to be widened over a length of approximately 5 mm. In nine patients a complete and uneventful insertion of the HiFocus electrode was achieved, but in patient J, just 13 contacts could be inserted after a drill-out of the basal scala tympani. A postoperative CAT scan showed an insertion of approximately 270 degrees in the latter patient.

In line with our findings in the computational model (Frijns et al., 2001) we aimed to get the electrode in a modiolus hugging position only in the basal turn, while at the same time avoiding unnecessary damage to the intracochlear

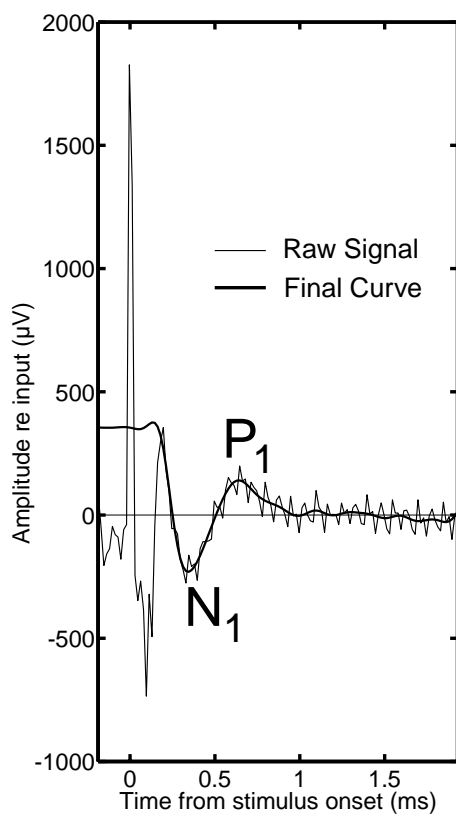


Figure 6.2: After subtraction of a “system signature” the recorded NRI data are first digitally blanked until 200 μ s after stimulus onset ($t=0$). Then the signal is low-pass filtered using a zero-phase shift filter to eliminate high-frequency noise. Before the stimulus delivery the stimulating and recording electrodes are short-circuited to remove residual charge that might interfere with the NRI recording.

structures. Therefore, the insertion of the positioner was stopped if any increased resistance was felt, resulting in a 3 to 6 mm (8mm in patient J) protrusion of the positioner from the cochleostomy. A postoperative plain radiograph or CT confirmed the correct position of the electrode. We did not observe any postoperative complications.

6.3.1 Speech Perception in Quiet and in Background Noise

At the time of removal of the pressure bandage, seven days after surgery, a preliminary fitting with the CIS strategy was performed. At that time 5 of the 10 patients had considerable open set sentence recognition without lip reading within 10 minutes after hook-up. The final fitting took place 5 wk later. Then, the patients were fitted with an 8-channel monopolar CIS, and an 8-channel bipolar SAS strategy. After 1 week the strategy that resulted in the lower speech perception (which always happened to be the strategy the patients liked less) was replaced by an 8-channel monopolar PPS strategy. Surprisingly, nine patients after three mo had a definitive preference for the CIS strategy, and one (G) for the PPS strategy. Figure 6.3 shows the results for the CVC word test as obtained for all patients with their preferred strategy. The minimum follow-up was 3 mo, the longest 11 mo. The bars show the average scores at predetermined intervals (1 and 2 wk, 1, 2, 3 and 6 mo). For most patients an additional data point is available, measured with their implant still in emulation mode, immediately before they entered another study (not reported here), employing more electrodes, higher pulse rates, and shorter pulses. Figure 6.3^A shows the phoneme scores, as is the standard with this test in the Dutch setting, while Figure 6.3^B displays the same data as word scores, which is a more common way to look at these data in Anglo-Saxon countries. Both figures show a rapid increase in performance, which reaches an average of 80% for the phoneme scores and of 62% for the word scores at three mo, the longest follow-up completed by all patients. The average of the last phoneme scores obtained for all patients is 84% (Table 6.2), the corresponding word score 66%. It is noteworthy that patient J, who had a partial insertion of 270 degrees (13 contacts) fits in with the group so well.

The speech-tracking results (only measured at the predetermined follow-up intervals listed above) are shown in Figure 6.4. The steadily increasing scores (up to 66 wpm on the average at three mo) in this figure reflect the increased ease of listening subjectively reported by the patients. The tendency of the speech tracking performance to drop slightly for most patients from 3 to 6 mo may reflect the fact that none of the patients received formal training in this

Table 6.2: The phoneme scores on the NVA CVC word test (65dB SPL, free field, sound only, 44 words per data point) at the end of the follow-up period (second column) in quiet and in speech noise with Signal-to-Noise ratios (SNR) of +10, +5 and 0 dB. The SNR for which 50% of the phonemes are correctly understood (column "SRT (CVC)") was calculated by linear interpolation. Similarly, the Phoneme Recognition Threshold (PRT) was calculated by linear interpolation of the phoneme scores, normalized by the data in quiet. The column SRT (Plomp) gives the Speech Reception Threshold (i.e., the average SNR for two consecutive measurements with 13 different sentences) for the Plomp & Mimpfen (1979) sentences presented at 65 dB SPL. The bottom row shows the mean data for each column.

Patient	Duration of follow-up (wk)	SNR(dB) ∞ (%)	SRT (CVC)				SRT (Plomp)		
			+10 dB (%)	+5 dB (%)	0 dB (%)	-5 dB (%)	(dB)	(dB)	(dB)
A	48	93	70	58	52	21	-0.3	-0.9	+5.5 ^a
B	43	91	79	54	49	28	+1.0	-0.8	+4.6 ^a
C	43	71	51	52	40	21	+4.2	-1.2	na
D	39	89	75	50	49	30	+5.0	-1.2	+7.0 ^b
E	35	89	81	69	66	39	-3.0	-4.0	+3.6 ^b
F	26	93	81	74	53	22	-0.5	-1.0	+2.2 ^b
G	22	90	79	71	52	40	-0.8	-2.9	+9.6 ^b
H	22	81	70	50	27	nt	+5.0	+2.9	+4.2 ^c
I	13	63	46	35	22	nt	+11.2	+3.7	na
J	13	79	58	43	23	nt	+7.3	+4.1	na
Mean		84	69	56	43	29^d	+2.9	-0.1	5.2^d

^a 26 weeks of follow-up

^b 13 weeks of follow-up

^c 8 weeks of follow-up

^d over tested patients

na = not available (even without noise not reliable)

nt = not tested

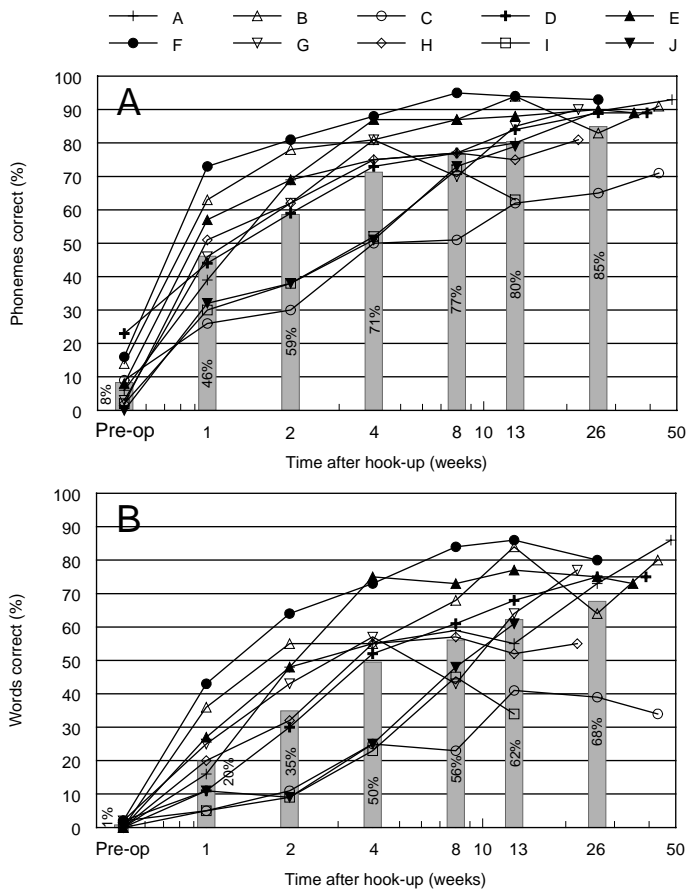


Figure 6.3: A Phoneme scores on a CVC word test in quiet (free field, sound only, 65 dB SPL) as measured pre operatively, at 1 and 2 wk, and after 1, 2 and 3 mo for the ten patients in this study. The individual scores are shown as lines, the average scores as bars. B Word scores on the same CVC word test in quiet as A.

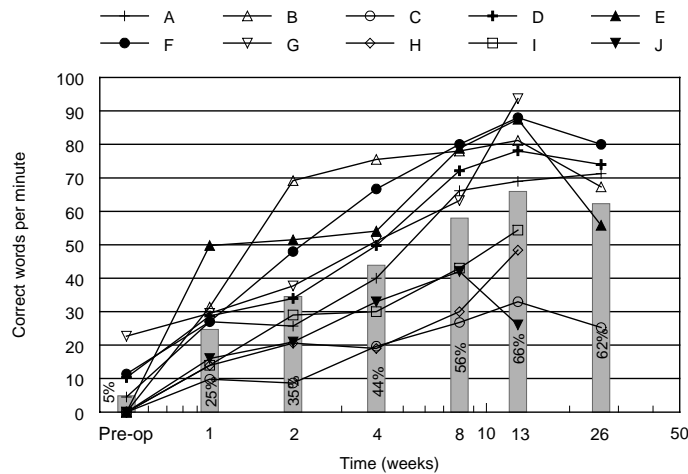


Figure 6.4: Results for the ten patients in Figure 3 of a speech-tracking test (sound only condition) as a function of time after hook-up. The individual scores are shown as lines, the average scores as bars.

period. However, the effect is small and it may be just coincidental, given the known limitations of the speech-tracking procedure. Despite these limitations, it measures other capabilities than just hearing (such as the ability to use contextual information) and the performance ranking of the individual patients is somewhat different from that with the CVC word test.

Table 6.2 summarizes the performance in noise for the ten patients included in the study. Relative to the performance on the CVC test in quiet, all subjects show a significant decrease in performance at a +10 dB signal to noise ratio. The performance gradually decreases if the noise is increased in steps of 5 dB. At a +5 dB signal to noise ratio 8 of the 10 patients have phoneme scores above 50%, while four of them are still performing above this level at 0 dB signal to noise ratio. Generally speaking, the poorest performers in noise are the ones with the shorter follow-up (subjects H, I and J). Their scores were below 30% at the 0 dB level, and they were not tested at a -5 dB signal to noise ratio. As shown in Table 6.2, the 50% phoneme score, also known as the Speech Reception Threshold (SRT) is reached at a +2.9 dB signal to noise ratio (range: -3.0 to 11.2 dB) on average.

Table 6.2 also shows an estimate of the average phoneme recognition threshold (PRT) for each patient. The PRT is defined as the signal to noise ratio that produces 50% of the performance level in quiet (Fu and Shannon, 1999). In our group, the values range between -4.0 and + 4.1 dB (average -0.1 dB). The SRT as measured with the Plomp and Mimpen (1979) sentence test varied between +2.2 and +9.6 dB (average +5.2 dB). The three patients (C, I and J), who could not complete the latter task reliably, not even without noise, are the poorest performers. They have a phoneme score in quiet below 80%. With these patients the results depended strongly on the starting level of the speech for the first sentence.

6.3.2 Neural Responses

Figure 6.5 demonstrates the ability to record NRI input/output curves, both peroperatively and in awake patients. In these recordings the monopolar stimulating (#7) and recording (#5) electrodes were located in the middle of the array. To avoid subjective interpretation errors we developed software to determine the N_1 to P_1 peak-to-peak amplitude of the eCAP automatically. This amplitude shows a monotonic increase (up to a certain saturation level) with stimulus amplitude (Fig. 6.5^{A&B}), while the latency of both peaks is hardly influenced by both stimulation intensity and time (Fig. 6.5^C). As illustrated in Figure 6.5^B the NRI threshold and the slope of the I/O curve are robust over time. This is remarkable, since the electrode impedances change rapidly after implantation, partly due to deposition of body substances, scar tissue formation and the formation of iridiumoxide on the contact surface after electrode activation (Peeters et al., 1998). Furthermore, these impedance changes explain the differences at high stimulus levels between the curves in Figure 6.5^B. While the current source did not reach its upper voltage compliance limit ($\pm 8V$) at the time of implantation, it did at the first fitting, since the impedance of the stimulating electrode had risen from 3.1 k Ω to 10.9 k Ω . In line with this observation the patient did not perceive any increase in loudness for stimulus currents above 1 mA. However, after 2 weeks of usage the impedance had fallen to 8.7 k Ω , and the patient could no longer stand the high loudness associated with stimulus levels of 1 mA and above.

We also recorded I/O-curves in the other patients using various electrode combinations. Some typical results are shown in Figure 6.6. These recordings were in line with the observations in Figure 6.5^B, although there are large inter-patient variations in the eCAP amplitude, which also varies considerably with the position of the stimulating and recording electrode. In most cases

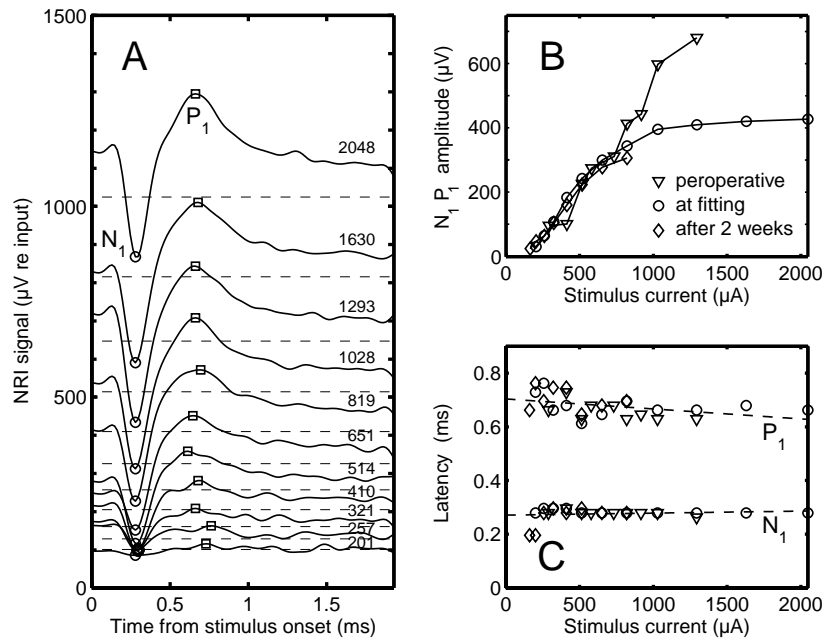


Figure 6.5: NRI recordings of patient F from the middle of the electrode array (alternating polarity paradigm, stimulating electrode 7, recording electrode 5).

A Traces for varying stimulus intensity recorded at the time of fitting. The N_1 (circles) and P_1 (squares) peaks have been determined automatically. To enhance the visibility the individual traces have been level shifted proportionally to the stimulus strength as indicated by the dashed lines. The numbers to the right indicate the stimulus current in μA .

B The $N_1 P_1$ amplitude of the eCAP as a function of stimulus level, measured at three moments in time.

C The latency of the N_1 and the P_1 peak of the eCAP as a function of stimulus level for the same recordings as used in B. The symbols designate the moment the recording was made, as indicated by the legend in B. The dashed lines are the linear regression lines based upon all data.

however, more apical stimulating and recording contacts result in larger NRI response amplitudes, possibly due to the smaller cochlear dimensions in the apex and consequently the closer proximity of apical electrodes to the auditory nerve in the modiolus. Patient D, in whom we were not able to record a reliable NRI with electrode 7 as the stimulating electrode, forms an interesting exception. Since this patient produced normally shaped eCAPs for the other electrodes tested, including the neighboring electrode combination 10-8 this lack of response may be an indication of localized ganglion cell loss or other cochlear damage. The subjective T- (threshold) and M-levels for electrode 7, however, are not essentially different from its neighbors, while its pitch ranking is between them as expected.

Most NRI responses and subjective loudness saturate for stimulus levels above $\pm 700 \mu\text{A}$. This is in line with the above-mentioned concept of reaching the compliance limit of the current sources, as electrode impedances around $10 \text{ k}\Omega$ are found after some time of usage in most patients. The latency of the N_1 and P_1 peaks (not shown in Figure 6.6), is much less variable than their amplitude and conforms with the range of values shown in Fig. 6.5^C.

In an attempt to document the spread of excitation we recorded NRI responses with all available electrodes for stimulating electrodes at apical, intermediate and basal positions in the cochlea (electrodes 3, 7 and 15 respectively). A typical result is shown in Fig. 6.7, where the eCAP amplitudes peak around the stimulating electrode for stimulating electrodes 3 and 15. This is in line with the expectations. However, for electrode 7 the response amplitudes increase gradually from basal to apical recording locations and there is certainly no peak around the stimulating electrode. This same result, that eCAP amplitudes do not peak around stimulating contacts in the middle of the array, occurred for all patients in which we could measure the NRI for this electrode. In many cases it was not possible to make reliable recordings with electrode contacts neighboring the stimulating contact, since the amplifier was driven into overload by the stimulus artefact. Therefore we routinely performed the measurements with one contact between the stimulating and the recording contacts.

Figure 6.8 shows the eCAP waveforms we recorded in three patients with a forward masking protocol as used with the Nucleus system (Abbas et al., 1999) with inter pulse intervals (IPIs) between the (equal intensity) masker and probe pulses of 350 and 500 μsec . This figure also shows the recordings with the alternating stimulus protocol, obtained in the same session with the same stimulation and recording contacts. The I/O-curves based upon the

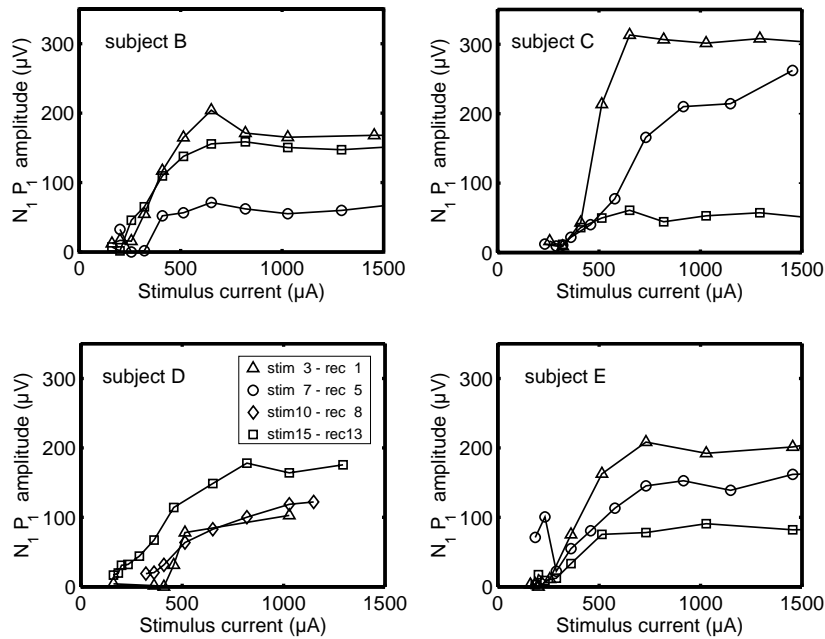


Figure 6.6: The N_1P_1 amplitude of the eCAP as a function of stimulus level as measured with the alternating polarity paradigm in four awake patients with stimulus and recording electrodes in three positions (Δ = apical, \circ & \diamond = middle, \square = basal) along the electrode array. Saturation of the curves is due to the current source reaching its voltage compliance limit rather than due to saturation at a neural level.

N_1P_1 amplitudes of these recordings are shown in Figure 6.9. Patients B and C yielded clear responses, but the (intra-operative) recordings in patient G contained more noise and did not show any saturation in the I/O-curves for any paradigm. In all patients the alternating polarity paradigm yielded smaller N_1P_1 amplitudes than the forward masking protocol, especially at higher stimulus levels. In addition, the amplitude of the responses for the two forward masking paradigms tended to saturate at much higher stimulus levels than with the alternating stimulus paradigm (patients B and C). At such high stimulus levels we observed a steeply rising slope between the N_1 and P_1 peaks, often without a clearly visible N_1 peak, a phenomenon that never occurred with the alternating polarity paradigm. At lower stimulus levels the eCAP

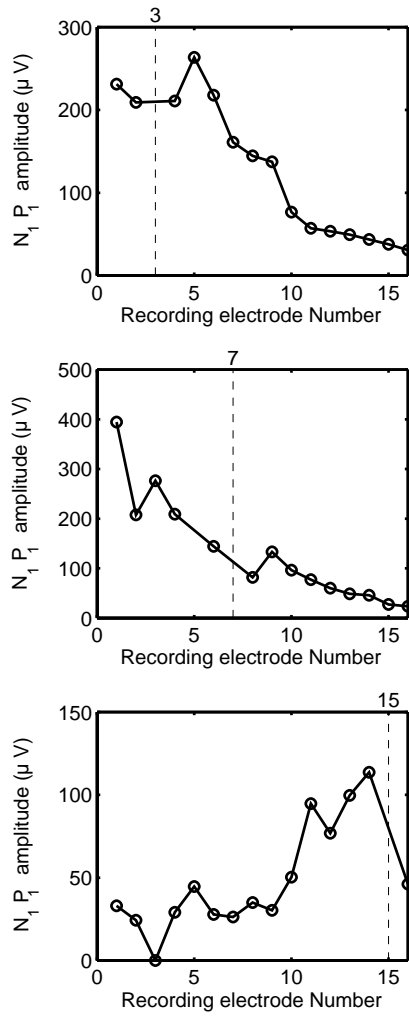


Figure 6.7: The eCAP amplitude (alternating polarity paradigm, stimulus level 731 μ A) in patient E with stimulating electrode 3, 7 and 15, respectively, recorded from all other electrodes in the array.

waveforms were surprisingly comparable for the alternating polarity and both forward masking paradigms, while the slope of the I/O-curves was slightly lower with the alternating polarity paradigm. NRI-thresholds, determined by downward extrapolation of these curves, were almost identical for all three paradigms.

6.4 Discussion and Conclusions

In this article we presented the first clinical results obtained in the Leiden University Medical Center with the Clarion CII cochlear implant, which combines a modiolus hugging electrode with newly designed implant electronics and a new, externally worn, (“platinum”) sound processor. Although the CII implant contains 16 independently driven current sources and is technically capable of high update rates, its clinical use is currently limited to a so-called emulation mode of the previous Clarion HiFocus implant. Surprisingly, in light of the favorable results reported for the SAS strategy with the original Clarion CI implant (Battmer et al., 1999), 9 subjects in our small but diverse group of 10 postlingually deafened adults had a definitive final preference for the CIS strategy over the SAS and PPS strategies, while 1 patient’s final preference was the PPS strategy. With their preferred strategy we found quickly improving and ultimately excellent speech scores, both in quiet and in noise. In a recent survey Shannon (Shannon, 2001) found an ever-increasing performance for each generation of implants, up to a level of 45% words correct for a CVC word test in quiet with the newest Nucleus Countour and the original Clarion HiFocus implants. A highly comparable outcome was reported by Hamzavi et al. (2001) for postlingually deaf adults implanted with the MedEl® Combi 40/40+® cochlear implant after a follow-up of one y. Within 3 mo 8 of the 10 patients in our series scored 52% to 86%, which is 7 to 41 percentage points above the level of performance for CVCs reported by Shannon. Two subjects scored (4 and 11 percentage points) below this average level. The average phoneme and word scores on this test were somewhat higher (84% and 66%, respectively) when measured at the end of the follow-up period (i.e., after 3-11 mo, Table 6.2). Therefore, it is likely that the scores of most patients will improve further with additional listening experience, although we are certainly observing ceiling effects on the tests in silence.

Unlike other studies, in most patients the speed of improvement for phoneme scores seems to slow down already after 1 mo (Fig.6.3^A). For word scores such a plateau is not discernible (Fig.6.3^B). With speech tracking the upper

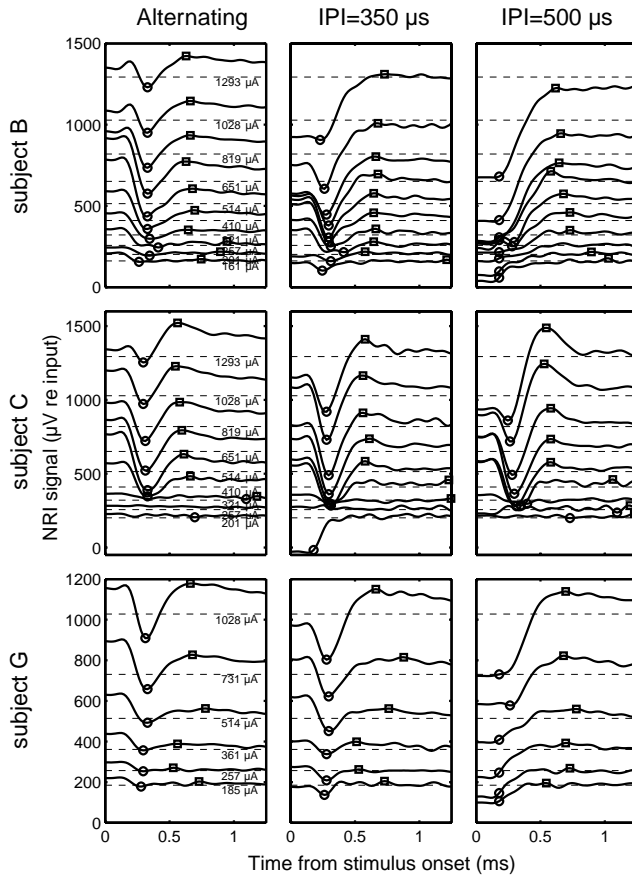


Figure 6.8: NRI recordings for patient B, C and G at various stimulus levels for stimulation electrode 3 and recording electrode 1. To enhance the visibility the individual traces have been level shifted proportionally to the stimulus strength as indicated by the dashed lines. The numbers to the right indicate the stimulus current in μA . For each patient the left most panel shows the results obtained with the alternating polarity paradigm, while the middle and right most panels show data obtained with the forward masking paradigm with a masker-probe interval of $350 \mu\text{s}$ and $500 \mu\text{s}$, respectively.

limit of performance seems to be approached after approximately 2 mo (Fig. 6.4). An interesting observation in this small group of patients with little or no residual hearing is the fact that the time course of speech perception improvement, especially when measured as phoneme scores with CVC words (Fig. 6.3^A), shows a limited inter-patient variability despite their different preoperative conditions. Also, duration of deafness is not correlated with final performance for our subjects. The five next patients implanted in our clinic (with a follow-up of 2 wk to 2 mo), although fitted with a higher rate CIS strategy (1430 pps per contact, 8-16 contacts), confirmed this trend of limited patient variability, but of course larger series are needed to validate this observation.

The CVC word tests used in the present study are the common way to measure speech perception in the Netherlands and Flanders, both in routine clinical practice and with cochlear implant users. The standardized way is to report phoneme scores rather than word scores. Unfortunately, there are few published studies using this test material that allow a direct comparison with the data presented here. Mens (2001) used the same test material, presented at 70 dB SPL, and found phoneme scores between 0 and 80% (average 47%, equivalent word score $\pm 24\%$) in all 20 postlingually deafened patients implanted in the Nijmegen clinic who use the CIS strategy with a follow-up of 1 y or more. There may be some bias in his patient group, since he does not report any speech perception data on the 15 SAS users in his clinic (implanted with a Clarion CI with positioner). Wouters and van den Berghe (2001) report average phoneme scores around 61% (equivalent word score $\pm 34\%$) on the Flemish version of the NVA test for four good performers with the LAURA implant, which is in line with the results reported by Smoorenburg et al. (2001), who used the same speech material as we did and reported an average phoneme score of 65% in 10 Dutch users of the Nucleus CI24M implant. All in all, these results support the conclusion that the good results reported here are not caused by language or test differences.

We also tested the performance in background noise with CVC words (Table 6.2) and found a phoneme recognition threshold (PRT) of approximately 0 dB, and an SRT of approximately +3 dB. This is a good result in light of those reported by Fu and Shannon (1999), who found PRT values around +5 dB for Nucleus22 patients using a 4 channel CIS strategy. Wouters and van den Berghe (2001) report an SRT of nearly +10 dB for conditions similar to the ones used in the present study (speech and sound from the same direction) with four good performers with the CIS strategy on the LAURA prosthesis using the Flemish version of the NVA CVC word list.

One should keep in mind that all these results are far below the performance of normally hearing listeners, who have an average SRT (and PRT, since they score 100% in quiet) on the NVA CVC word test of -11 dB (-9 dB on the Flemish version; Wouters et al. (1994)). On the other hand, many patients wearing a conventional hearing aid for perceptible losses of 60 dB or above do not perform better than our Clarion CII users (Bosman and Smoorenburg, 1999).

Hamzavi et al. (2001) reported a 50% degradation of performance on German sentence material at signal to noise ratios between +10 and +15 dB. Although the test conditions are different, the performance of our group, with an average SRT around +5 dB on the Plomp and Mimpen (1979) sentence test, is probably more resistant to noisy listening conditions. Unfortunately, there is no literature on the use of this Dutch test on cochlear implantees, but it has been used in other centers in the Netherlands, where SRT's around +10 dB were found (Smoorenburg, personal communication).

There are a number of possible factors that may have contributed to the good clinical outcome for this group. First, there may be demographic factors. This is a small initial group, and the patients are relatively young (mean age at implantation 44 yr). However, none of the patients had any useful residual hearing, and the average duration of deafness (with a variety of causes) is approximately 17 yr. Second, there may be technical factors related to the implant or the fitting strategy. Although the implant was operated in a mode intended to mimic the original Clarion HiFocus implant, its electronics has been fully redesigned. As described above, the current sources have higher impedances and produce pulses with rise times around 1 μ sec instead of 5 to 10 μ sec as their predecessors did. This means that the non-simultaneous stimulation of the CIS-strategy is more precisely achieved with the CII implant.

Part of the relative insensitivity of speech perception to noise may be related to the fact that we deliberately maximized the dynamic range for the more basal electrodes, encoding for frequencies of 2 kHz and above (Frijns and Briaire, 2001), despite of the fact that the patients initially did not like those highly pitched sounds. Such a policy, which is common practice when fitting conventional hearing aids, is not generally used with cochlear implants. In general, hearing-impaired subjects tend to prefer speech signals with a high-frequency emphasis. The improvement of their speech-intelligibility performance with hearing aids can be accounted for by the amount of low-frequency cutoff, as published by Versfeld et al. (1999). In this respect the surgeon's policy not to

insert the positioner too deep to avoid lower-pitched percepts due to cross-turn stimulation may have added value. As described in the section Patients, Materials and Methods, awareness of and elimination of cross-turn stimulation is another mainstay of the new fitting method used in our clinic. It will be described in detail in a future publication.

Finally, other center-specific factors such as the intensive start of the rehabilitation program with 2 half-hour training sessions per day during the first two wk and 1 such session per day during the next two wk, may account for the relatively rapid rise in performance with time. The initially frequent fitting sessions (5 in the first week) may also contribute to the rapid rise in performance. This cannot, however, explain the large amount of open set speech recognition found in five of the patients immediately following hook-up.

In this study we also performed an initial test with an important new feature of the Clarion CII implant, viz. its ability to record electrically evoked compound action potentials of the auditory nerve. Using the test bench (revision 3.45) of the system in combination with our own post-processing software we could record NRI responses with the alternating polarity paradigm at a sampling rate of 60 kHz. Unlike the Nucleus NRT system (Abbas et al., 1999), which has an internal sampling rate of 10 kHz, the internal amplifier in the Clarion CII does not require blanking during stimulus delivery. With its amplification set to 300, averaging 15 sweeps per stimulus presentation eliminated the noise sufficiently. Compared with the NRT system the recordings in the CII are much more detailed due to the higher sampling rate and the 9-bit ADC (Figure 6.5). However, despite of the fact that the required number of sweeps is much lower than the 50 to 200 commonly used with the NRT system, the test bench NRI system is effectively slower as the communication between the implant and the personal computer does not allow for more than one sweep per second rather than the 35 to 80 sweeps in the NRT system. Future versions of the interface are expected to allow higher sweep rates.

An interesting observation is that the overall shape of the signals obtained with the alternating stimulus paradigm does not depend on the stimulus intensity. They always show clear N_1 and somewhat broader P_1 peaks, and the latency of the peaks is virtually independent of stimulus levels. With the forward masking paradigm highly comparable responses are obtained for stimulus levels below 700 μA , but at higher levels the response has a steep slope between the (often hardly discernible) N_1 and P_1 peak. This dependence of the response morphology on stimulus intensity resembles the effects shown by Abbas et al. (1999); their Fig. 6.4). The fact that this phenomenon turns

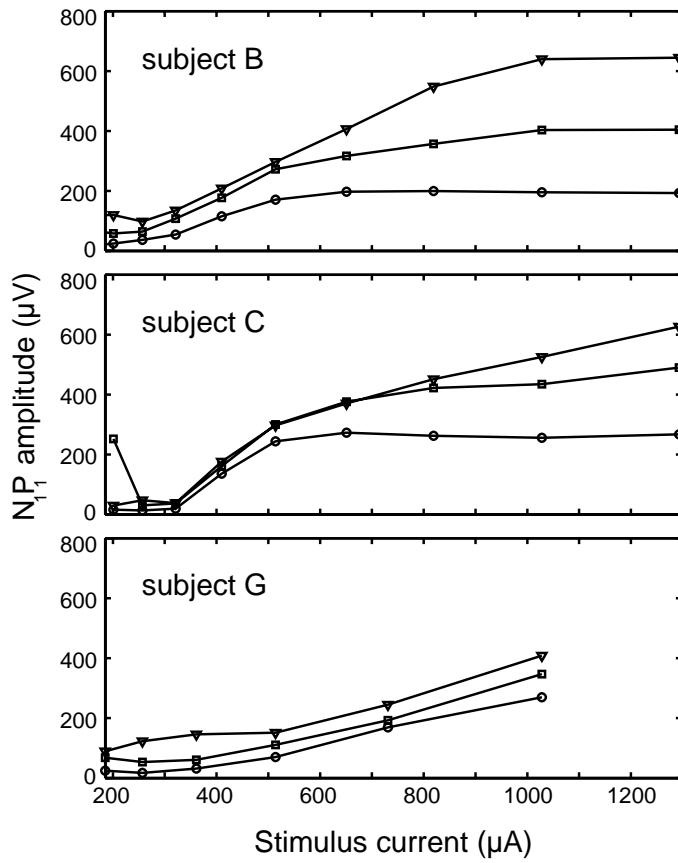


Figure 6.9: The N_1P_1 amplitude of the eCAPs shown in Figure 8 as a function of stimulus level. For all three patients (B,C and G) the data points for the alternating polarity paradigm are marked with open circles (\circ), while those for the forward masking paradigm are marked with a square (\square , IPI=350µs) and a triangle (∇ , IPI=500µs), respectively.

out to occur in two implant systems with completely different designs, could mean that true electrophysiological processes inherent to the forward masking paradigm rather than technical limitations of the implant systems underly it. On the other hand, the fact that the distorted waveforms become apparent at current levels at or above what seems to be the voltage compliance limit of the current sources, may indicate that indeed a non-linearity of the recording system is responsible, as suggested by Abbas et al. (1999). A further analysis of the differences between the two recording paradigms is beyond the scope of the present article, but it is one of the topics currently under study in our laboratory, both in humans as well as in animal and computational models (Klop et al., 2004).

The ultimate goal of all objective measures in cochlear implantation is to derive parameters from them allowing for a reliable initial fitting of children. Currently such a paradigm is not yet available and the NRT system is mainly applicable to determine the shape and possibly the slope of the curves describing the threshold and maximum output level (Smooenburg et al., 2001).

An important finding for the predictive use of NRI-recordings, especially per-operative ones, is the fact that our results are stable over time despite varying impedances of both the recording and stimulating electrodes (Fig. 6.5). This observation and the fact that NRI amplitudes vary unpredictably between patients and electrodes are consistent with the findings of Abbas et al. (1999). We find, however, a tendency for the largest responses to be recorded from the more apical recording sites, not only with apical stimulation (Fig.6.6) but also for stimulating electrodes in the middle of the array (7 in Figure 6.7). This may be due to the smaller dimensions in the apical turn relative to the basal turn, and to the slight embedding of the apical turn in the basal turn of the human cochlea (cf. Frijns et al. (2001)). As a result, apical recording electrodes are closer to the fibers excited in the modiolus, leading to a larger amplitude of the recorded eCAP. Of course the amplitude and shape of the eCAP also depend on the trajectory of the nerve fibers carrying the action potentials relative to the recording electrode. Future studies with computer models of the electrically implanted cochlea may lead to more definitive conclusions on the underlying volume conduction aspects of neural recording.

Similarly, such computer simulations will be of great value for the interpretation of NRI recordings with all nonstimulated electrodes, like the ones shown in Figure 6.7. Such recordings are intended to serve as an objective tool to measure the spread of neural excitation. However, while the patients report clear perceptual differences between all electrodes, the preliminary results in

Figure 6.7 suggest large overlap of the regions excited by neighboring electrodes. Therefore, we infer that the peaks that are found with this method are considerably broader than the actual neural response patterns. Another intriguing effect is the absence of any evidence for tuning around stimulating electrodes in the middle of the array, which subjectively do have clear tuning. Future research will have to explain this finding, which has also been reported by Battmer et al. (2001).

Based on the results presented in this article of the first patients implanted with the Clarion CII implant, we conclude that the Clarion CII is capable of delivering high amounts of speech information, even when operated in an emulation mode that mimics its predecessor, the Clarion HiFocus (CI) implant. We found very high open-set speech understanding, in a number of cases even without training. It is expected that the results can be further improved if the full technical potential of the implant is unleashed, e.g., with higher update rates or simultaneous use of all current sources. Although the clinical value of eCAP recordings still needs to be proven, we have shown that the NRI system yields a good signal quality and that its design has a great deal of flexibility. However, the current version of the NRI test bench imposes considerable limits on the speed of eCAP recordings.

6.5 Acknowledgement

This research was financially supported by grants from the Hoogenboom-Beck-Fund and the Heinsius Houbolt Fund. The authors wish to thank Peter-Paul Boermans, MSc and the other members of the CIRCLE team for their invaluable assistance in patient care and evaluation. They also gratefully acknowledge Charlie Finley, PhD, for providing the NRI test bench software.

Chapter 7

The relative value of predictive factors of cochlear implant performance depends on follow-up time

Jeroen J. Briaire and Johan H.M. Frijns

Abstract

Objective: Although cochlear implantation is widely applied, its outcomes are not very predictable on an individual basis. Several factors, such as the duration of deafness and the pre-operative speech understanding, have been identified as potential predictors. However, the relative value of these predictors varies between studies. This study evaluated the effect of the duration of post-operative follow-up on the value of pre-operative predictors.

Study Design: 91 subjects implanted between 2000 and 2005 with a HiRes90K or CII implant with a HiFocus I electrode array were included in this study. The group was divided into subpopulations of positioner users ($n=28$) and non-positioner users ($n=63$), as well as into young implanted (< 65 yr, $n=66$) and late implanted (> 65 yr, $n=25$). Speech understanding was evaluated using a CD to present CVC words in free field at 65 dB SPL. Testing was conducted at increasing intervals from 1 wk to 2 yr following hook-up. Correlations with the duration of deafness, age at implantation and pre-operative CVC scores were calculated directly. Multiple regression analysis were applied using the Iowa predictive model directly, or with this model extended to consider age at implantation or the presence of an electrode positioner. All analysis were performed on the entire population and for the subgroups described above.

Results: While age at implantation showed no correlation with speech perception in the first year after implantation, after 2 yrs a negative correlation was found ($r=-0.25$; $p < 0.05$). Inversely age at onset of deafness showed a strong correlation in the initial phase ($r=0.4$; $p < 0.0001$ at 2wk) but this correlation diminished with longer implant use ($r < 0.01$; $p > 0.5$ at 2yr). Duration of deafness showed a similar decrease in correlation with longer follow up time, remaining only barely significant after 2 yr ($r=0.25$; $p < 0.05$). No significant correlation was found between pre- and post-operative speech understanding. In line with these findings, the coefficients of the Iowa predictive model turned out to be heavily dependent upon the implant experience accrued before an evaluation was conducted.

Conclusion: The relative importance of predictive factors is highly dependent on the post-operative experience. Therefore, predictive models should be based on follow-up times of at least 2 years to allow poorer performers approach their ultimate performance level. This is especially so for the duration of deafness: recipients with a longer duration of deafness have a much shallower learning curve, yet finally obtain similar results to those with shorter durations of deafness. Implantation at an older age limits the long term speech understanding improvement, resulting in a significantly poorer score after 2 yr

of implant use compared to those implanted at a younger age. When dealing with non-controlled retrospective studies, multiple regression analysis should be used to extract the influence of, for instance, electrode array design, or age at implantation, on the speech understanding scores; while reducing the effect of other non-controlled parameters such as duration of deafness.

7.1 Introduction

Cochlear implants (CI) have provided the opportunity for post-lingually deafened adults to regain a part of their auditory communicative skills. Despite the significant improvements in average performance there remains a considerable amount of unpredictable inter-subject variability. Most previous studies seeking to predict post-operative speech understanding pre-operatively have been handicapped by heterogeneous patient populations with variable devices, speech processing strategies, speech discrimination tests, or clinical rehabilitation programs. The use of varying clinical programs, particularly different devices, can influence the usefulness of performance predictors. Electronics and electrode designs have evolved over time (Kuzma and Balkany, 1999; Frijns et al., 2002; Patrick et al., 2006), leading to improved speech perception for the whole group of cochlear implant recipients. Outcomes produced by older device technology can partially invalidate predictions of the outcomes of current devices.

In this study an in many aspects homogeneous group of CII or HiRes90K users was analyzed. There were no functional differences between the CII and HiRes90K devices. The CII had all electronics housed in a ceramic case while the HiRes90K used a titanium case with an external receiver coil. All subjects were implanted and rehabilitated at the Leiden cochlear implant center in the period from 2000 to 2005. In all subjects a HiFocus 1 electrode array was used, an array with 16 electrode contacts directed towards the inner wall of the scala tympani (Frijns et al., 2002). The only variation in implant type is the use of the electrode positioning system in the first 28 subjects. As reported in a previous study (van der Beek et al., 2005) the positioner users showed a significantly better speech understanding after one year of implant use. For this reason all analyses were performed separately for this group, to identify any further differences.

Another significant difference between the positioner and non-positioner group described by van der Beek et al. (2005) was age, the latter group being significantly older. A number of implant centers report that with time the average age of the implanted adult recipients rises. Recent research has shown that elderly implant users perform just as well as younger users of cochlear implants (Labadie et al., 2000; Pasanisi et al., 2003; Haensel et al., 2005; Leung et al., 2005; Chan et al., 2007). To investigate the importance of age on outcome, outcomes will be analyzed for the age at implantation, a factor with reports of inverse or insignificant correlations (Oh et al., 2003; Pasanisi et al., 2003; Ruffin et al., 2007).

The only parameters consistently predicting outcome of cochlear implantation in numerous studies is the duration of deafness which is reported to influence outcomes adversely (Gantz et al., 1993; Summerfield and Marshall, 1995; Waltzman et al., 1995; Albu and Babighian, 1997; Rubinstein et al., 1999a; Gomma et al., 2003; Friedland et al., 2003; Chan et al., 2007). The same correlation was found in Dutch studies (van Dijk et al., 1999; Mens, 2001). However, recently several studies report no significant correlation for performance with the duration of deafness in their cohorts (Ruffin et al., 2007; Francis et al., 2005). Rubinstein et al. (1999a) and Friedland et al. (2003) used multiple regression analysis with both pre-operative sentence scores and the duration of deafness to predict the postoperative word scores. This model was extended to include the age at implantation (Leung et al., 2005); this parameter only showed a significant result if used as a step function for younger (<65 yr) and older (>65 yr) implantees. As mentioned above, the use of processor variations or different electrode array types could well have influenced these outcomes. Another factor that may influence the outcome of these predictive studies was the time at which performance was evaluated. It was observed that some users need more time to approach their plateau performance level. However, long term follow up studies indicate that there was no further change in performance after 2 years of CI use (Ruffin et al., 2007; Oh et al., 2003).

To summarize, the purpose of this study was to evaluate the known preoperative predictors of cochlear implant performance (Duration of deafness, pre-operative speech perception score, age at implantation) and their stability over the first two years of implant use in a homogeneous group of implant users. In addition, the improvement of elderly cochlear implant recipients and the use of an electrode positioning system were analyzed separately.

7.2 Materials and Methods

7.2.1 Participants

The study group comprised 91 sequentially implanted post-lingually deafened adolescents and adults who underwent implantation with an Advanced Bionics (Sylmar, CA) HiFocus CII or HiRes90K implant at the Leiden cochlear implant center between 2000 and 2005. Inclusion criteria for this study were: use of the HiRes stimulation strategy for more than one year, normal cognitive function and native Dutch language. As may be seen in table 7.1 the subjects form a heterogeneous group in terms of duration of deafness (mean 16.8 years,

range 0.7-58 years) and age at implantation (mean 52.6 years, range 14-86 years). The boundary of 65 years of age was used as a criterion to divide the group into two separate subpopulations (Leung et al., 2005; Haensel et al., 2005): $n=66$ and $n=25$ for <65 years and ≥ 65 years respectively. The placement of a positioner during surgery was used as a second way to divide the population into two groups: $n=28$ and $n=63$ for with and without positioner respectively.

Table 7.1: Characteristics of the entire population and of the subgroups analyzed.

	Total	Age groups		Positioner groups	
		< 65 yr	> 65 yr	with	without
# patients	91	66	25	28	63
Age at implantation, y					
Mean (SD)	52.6 (16.2)	45.2 (12.8)	71.4 (5.1)	46.6 (13.1)	55.0 (16.9)
Range	14-86	14-64.6	65-86	14-68	14-86
Duration of deafness, mean (SD), yr	16.8 (14.6)	18.6 (14.6)	12.3 (13.3)	19.1 (14.2)	15.8 (14.6)
Preoperative CVC phoneme score					
Mean (SD)	20.3 (18.2)	20.7 (16.9)	22.3 (19.9)	14.9 (16.5)	23.8 (17.6)
Range	0-70	0-70	0-70	0-70	0-70
Preoperative CVC word score					
Mean (SD)	7.4 (10.3)	6.6 (8.3)	8.3 (12.1)	5.7 (9.9)	7.8 (9.3)
Range	0-49	0-40	0-49	0-49	0-40

There are some other demographic differences between the sub-groups. The age division naturally produces a significant difference in age at implantation, but also a difference in the age at onset of deafness. In other words, the years with auditory input was significantly different ($p < 0.001$) with on average 59 yr before onset of deafness for the older group and 27 yr for the younger group. The same significant relations, although less strong ($p < 0.05$), were found for the positioner vs. non positioner group, mean age at onset of deafness 27 yr and 39 yr for the positioner and non-positioner group respectively. The fact that age at onset of deafness and age at implantation are significantly co-varying is illustrated in figure 7.1^A, the scatter plot and linear regression line for these variables. The regression line shows a highly significant correlation between the two variables ($p < 0.00001$).

With the exception of the pre-operative phoneme scores between the positioner and non-positioner groups all other variables were not significantly different. The positioner group had an pre-operative phoneme score of 14.9 %

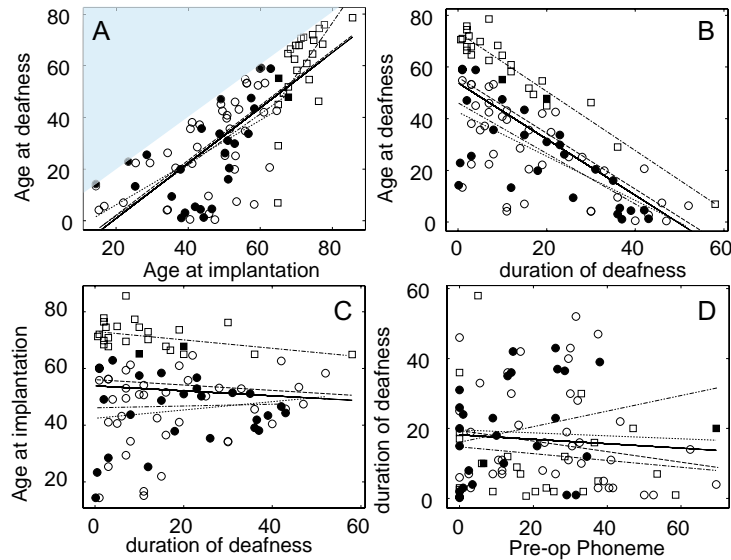


Figure 7.1: Scatter plots between various pre-operative predictive variables. The symbols differentiate the subjects into the four groups (circles: < 65 yr, squares: > 65 yr, open: non-positioner, filled: positioner). **A** age at implantation vs. age at onset of deafness, **B** duration of deafness vs. age at onset of deafness, **C** duration of deafness vs. age at implantation and **D** pre-operative phoneme scores vs. duration of deafness). The lines are linear regression lines of the various groups: solid the entire population, dashed the non-positioner subjects, the dash double dotted the positioner subjects, the dotted the subjects implanted < 65 yr, and dash dotted the subjects implanted > 65 yr.

correct, while the non-positioner population scored 23.8 % correct ($p < 0.05$). This difference was not found in the word scores ($p > 0.7$) because of the lower sensitivity of the word test at low levels of speech perception.

Preoperative speech perception scores were measured in a free-field condition with optimally fitted hearing aids using the standard CVC word lists (prerecorded female speaker) of the Dutch Society of Audiology at 65 dB SPL (Smooenburg, 1992). The lists consisted of 4 sub-lists, each containing eleven Dutch three-phoneme monosyllables. The same test was used to evaluate postoperative performance with the implant at fixed time intervals: 1wk, 2wk, 1mo, 2mo, 3mo, 6mo, 1 yr and 2 yr post hookup. As shown in Table 7.1, the average preoperative phoneme score was 20.3 % (range: 0 to 70 %), and the average word score was 7.4 % (range 0 to 49 %). There were some missing data points within the dataset. Although all subjects were invited to their regular testing sessions, some did not participate at every evaluation session. These subjects have not been excluded from this study, to avoid bias via a criterion based on motivation. Table 7.2 shows the number of subjects included in the study groups at the various test intervals.

Table 7.2: Number of subjects which participated in the scheduled evaluation sessions.

	Total	Age groups		Positioner groups	
		< 65 yr	> 65 yr	with	without
Total included	91	66	25	28	63
1 wk	88	64	25	28	60
2 wk	90	66	24	28	62
1 mo	90	66	24	28	62
2 mo	87	63	24	27	60
3 mo	87	64	24	28	60
6 mo	85	60	25	27	58
1 yr	89	65	25	28	62
2 yr	73	54	19	25	48

As mentioned above, only subjects using the HiRes speech coding strategy for more then one year were included in the analysis. All subjects were programmed with the Bionic Ear Programming System (BEPS), all except one used a HiRes program in mono-polar sequential mode. The one exception used a paired pulsatile program. The first 18 subjects started in emulation mode (Kessler, 1999), using 8 channels with 75 μ s/phase pulses, but were switched over to HiRes mode in a later stage (Frijns et al., 2003). The rate of

stimulation used in all programs did not exceed 1500 pulses per second per channel in sequential mode. The majority of the subjects used a pulse width of 21 μ s per phase, with 12 active electrode contacts. The overall stimulation rate was lowered when less electrodes were used by the inclusion of inter pulse intervals. The fitting method used in our center did not involve setting individual M-levels or loudness balancing, as will be described in the next section.

7.2.2 Fitting procedure using the profile fitting method

The first step in the fitting procedure was to determine the threshold (T) level for each electrode contact. The T-levels were found using an up-down-up procedure while delivering 300 ms duration pulse trains of bi-phasic pulses. Increasing the level back towards threshold was not done too slowly so as to avoid the subject forgetting the percept associated with this electrode. Typically, the T-levels followed a smooth curve along the array. This helped to predict the approximate threshold value for the next electrode and allowed one to quickly increase stimulus levels to that point. In this way, finding the threshold at the initial stimulation took 5-6 minutes for all 16 electrode contacts.

The next step in the fitting method was to determine the M (most comfortable) levels. At our center, the initial M-levels were set in a smooth line, with a slightly increasing emphasis for the higher frequencies. This approach was based on experience with hearing aids, where increases in high frequency information lead to improved speech understanding in noise (Versfeld et al., 1999). The shape was based on the average of the previously fitted users; initially, the overall level was set well below the likely actual M-level.

The program was further adjusted in live speech mode. First, the T-levels were adjusted to compensate for systematic errors from the up-down-up procedure and for loudness integration (McKay et al., 2001). With the processor volume turned down completely and the processor in live speech mode, the subject hears a constant noise without modulation. Normally, the loudness of this noise reduces slowly in the first minute, likely due to neural adaptation. When the noise persisted, it was removed by lowering all T-levels simultaneously.

To determine the final M-levels, first the volume control was slowly increased to its center position. While a speech signal was delivered at normal voice level (live speech), the M-levels for all electrodes were increased simultaneously, taking care to avoid over-stimulating, until speech was reported to be comfortably loud. At this stage, the subject gave an assessment of sound quality. If the percept had a very low or muffled quality, the M-levels of the low

frequency electrodes were reduced, while maintaining a smooth M-level profile. If the sound was described as too sharp, the slope of the M-level profile was lowered, but never further than a straight horizontal line.

If impulsive sounds (i.e., putting a cup on a table) gave an uncomfortable sensation, the M-level of the most basal electrode was reduced slightly. In a very short time (below 15 min), it was possible to adjust the levels to give the subject a acceptable sound percept. Most cochlear implant recipients had only low frequency residual hearing prior to implantation. It may therefore, take time for the recipient to become accustomed to the new high frequency sound. Hence, it is useful to try to increase M-levels for the basal electrodes over the initial fittings. For most subjects, the overall M-level was increased slightly at the beginning and then stabilized after one or two weeks.

Some subjects (especially the ones with positioner) reported a dominating low pitched echo or booming noise when sound was delivered. Based on our previous modeling studies, we believe this to result from cross-turn stimulation (Frijns et al., 2001). This percept could easily dominate forcing the recipient to use a reduced electrical dynamic range, since the low tones were very quickly found to be uncomfortable and determined the overall loudness of sound. While fitting these cases, the stimulation level where the percept changed was used as M-level and additional clipping levels were applied to prevent sound from going above this level. This ensured that these potentially disrupting percepts were avoided. In most cases, the overall volume had to be increased afterwards.

7.2.3 Statistical Analysis

A two-tailed t-test was used to evaluate differences between groups, pre-operative data and scores at the test intervals. Regression analysis was used to determine the predictive value of variables such as age at implantation (*AgeImp*), duration of deafness (*DUR*) and preoperative speech perception (*PreOp*) scores on post-operative speech perception outcomes (*PostOp*). Multiple regression analysis was used to evaluate the predictive model presented by Rubinstein et al. (1999a) and Friedland et al. (2003). The model has been adapted to use pre-operative phoneme or word scores in place of the CID sentence scores, which has no equivalence in Dutch.

$$PostOp = A + (B \cdot DUR) + (C \cdot PreOp) + D \cdot \frac{DUR}{1 + PreOp} \quad (7.1)$$

This model was extended by Leung et al. (2005) to:

$$PostOp = A + (B \cdot DUR) + (C \cdot PreOp) + D \cdot \frac{DUR}{1 + PreOp} + E \cdot AgeImp, \quad (7.2)$$

$$PostOp = A + (B \cdot DUR) + (C \cdot PreOp) + D \cdot \frac{DUR}{1 + PreOp} + E' \cdot z, \quad (7.3)$$

to include the age at implantation (AgeImp) as a variable or as a step function z where $z=0$ if age is younger than 65 years and $z=1$ if age is 65 years or older. All regressions were calculated for the entire study population but also for the groups divided by age and positioner vs. non-positioner use separately. The positioner factor can also be included in the prediction model as a second step function:

$$PostOp = A + (B \cdot DUR) + (C \cdot PreOp) + D \cdot \frac{DUR}{1 + PreOp} + E \cdot z + F \cdot Pos, \quad (7.4)$$

where Pos indicates the use of a positioner during surgery (Pos=1 for positioner used, zero otherwise). To study the effect of the positioner independently from the age of implantation, the model equation was also formulated without the age at implantation variable:

$$PostOp = A + (B \cdot DUR) + (C \cdot PreOp) + D \cdot \frac{DUR}{1 + PreOp} + F \cdot Pos. \quad (7.5)$$

All statistical analyses were performed with Matlab 7 (The MathWorks, Inc.), including the statistical toolbox.

7.3 Results

7.3.1 Group comparisons

Figure 7.2 shows the speech perception scores in phonemes (Fig. 7.2^A) and in words (Fig. 7.2^B) correct, pre-operatively and at the set post operative intervals. The study population performance increased from 45.3 % phonemes correct (21.1 % words correct) one week post hook-up to 77.4 % phonemes correct (58.6 % words correct) 2 yr post-hook-up.

The four sub-groups have been plotted in the same figure. For the two age groups, it can be seen that, initially the older (> 65 yr) group performed slightly (non-significantly) better than the younger group. After 3 mo, however, the growth in performance diminishes for the older group. Ultimately, the trend inverted and led to a significantly poorer performance for the older group at 2 yr post-hookup ($p < 0.05$). This finding was true for both phoneme and word scores. Excluding the subjects which missed the data points at 2 yr from the study groups did not change the values or the significance levels at earlier test intervals; again only the outcome at 2 yr follow up showed a significant difference. The difference between the positioner and non positioner groups became larger with increasing follow up time. At three and six mo follow up the difference approached significance ($0.1 > p > 0.05$). The one and two yr post-hookup test interval difference became significant for both phoneme and word scores ($p < 0.05$ and $p < 0.01$ for 1 yr and 2 yr respectively). Excluding the subjects without data points at 2 yr did not change this finding. Only the word scores at 3 mo follow up reached significance ($p=0.04$) in that reduced population.

Table 7.3: The regression coefficients (r , p and slope) corresponding to the linear regression lines in figure 7.1, correlating the various pre-operative parameters. Horizontally the various pre operative parameters tested and vertically the different evaluation sessions. The line types represent: solid the entire population, dashed the non-positioner subjects, the dashed double dotted the positioner subjects, dotted the subjects implanted < 65 yr, and dash dotted the subjects implanted > 65 yr.

		Age at implantation			Duration of deafness		
		r	p	slope	r	p	slope
Age at deafness	Tot	0.77	5E-19	1.1	0.7	2E-14	-1.1
	noP	0.78	5E-14	1.1	0.69	6E-10	-1.1
	Pos	0.67	9E-05	0.98	0.73	1E-05	-0.98
	< 65	0.59	2E-07	0.81	0.7	5E-11	-0.85
	> 65	0.64	5E-04	2	0.96	8E-14	-1.1
		Duration of deafness			Pre-op Phonemes		
		r	p	slope	r	p	slope
Age at Implant	Tot	0.08	0.5	-0.09	0.08	0.5	-0.06
	noP	0.08	0.5	-0.09	0.18	0.2	-0.15
	Pos	0.02	0.9	0.02	0.26	0.2	0.22
	< 65	0.17	0.2	0.15	0.05	0.7	-0.04
	> 65	0.39	0.05	-0.15	0.14	0.5	-0.09

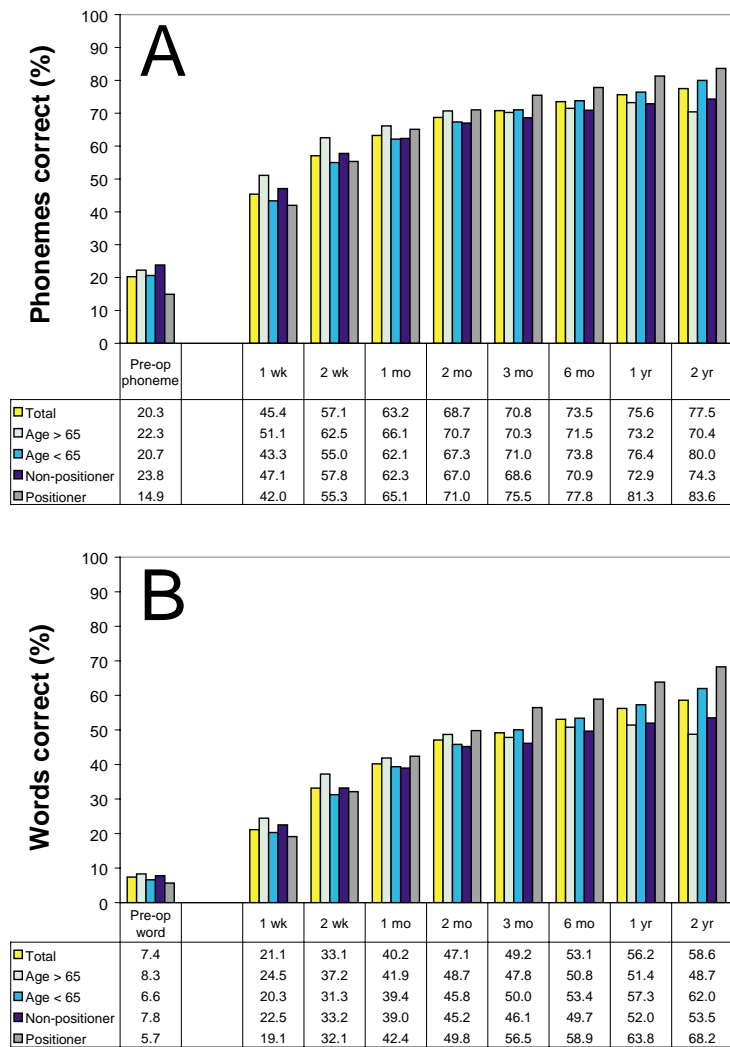


Figure 7.2: The speech perception scores in phonemes (A) and in words (B) correct, pre-operative and at the set post operative intervals for the entire population and the scores for the four subgroups.

7.3.2 Bivariate regression analyses

Pre-operative values

As already described in the Materials and Methods section, there is a significant relation ($r=0.77$; $p < 0.0001$) between age at onset of deafness and age at implantation (Fig. 7.1^A; Table 7.3). The upper left part of this scatter plot is empty; age at implantation is always greater than the age at onset of deafness. A similar plot (Fig. 7.1^B), also with a highly significant correlation ($r=0.7$; $p < 0.0001$), is found comparing the age at onset of deafness with the duration of deafness. These two variables exhibit a similar restriction; duration of deafness combined with the age at onset of deafness can never exceed the age of the patient, leaving the upper right part of the plot empty, in other words: Here is an inherent dependence between the two parameters. Consequently this dependence introduces a correlation between the two variables. The two variables along the horizontal axis in figure 7.1^A and 7.1^B, age at implantation and the duration of deafness, are however, independent of each other, both for the total population ($p=0.5$) and for the four sub-groups ($p > 0.05$) (Fig. 7.1^C; Table 7.3), although also for these variables a underlying restriction is present, duration of deafness can never exceed the age at implantation.

As expected various pre-operative audiometric tests, tone audiometry, speech understanding test both under headphones and aided in free field were correlated ($p < 0.01$); data not presented for brevity. Figure 7.1^D shows the scatter plot with regression line for duration of deafness against pre-operative phoneme score. Table 7.3 shows the corresponding outcomes of the regression analysis. The pre-operative word and phoneme scores are both independent ($p > 0.3$ and $p > 0.5$ respectively) of the other pre-operative measures (duration of deafness, age at onset of deafness and age at implantation). Also, within the various sub-groups no significant correlations were found between the speech perception variables.

Pre- and post operative correlation

Figure 7.3^{A,B,C,D} shows the scatter plots, including regression lines, for the age at implantation with the CVC phoneme scores at 2wk, 3mo, 1yr and 2 yr post-hookup. Table 7.4 shows analyses for the total population and the four sub-groups. There was a significant negative correlation between both phoneme ($r = -0.25$; $p < 0.05$; -2.4 % per decade) and word scores ($r=-0.24$; $p < 0.05$; -3.4 % per decade) and age at implantation at the 2yr follow up

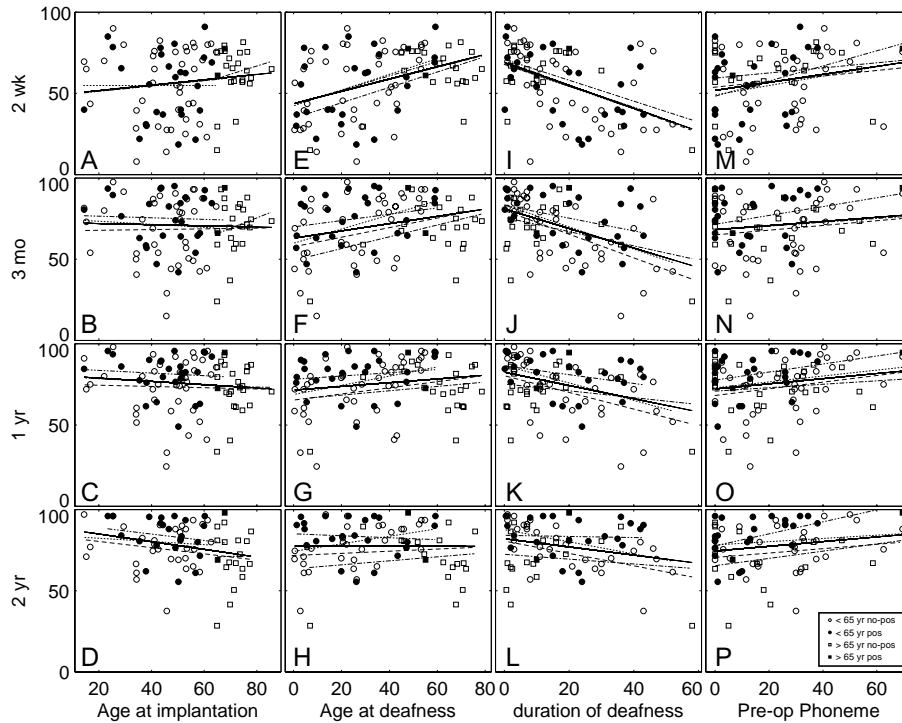


Figure 7.3: Post-operative speech scores recorded after various durations of implant use (rows: 2 wk, 3 mo, 1 yr and 2 yr) as a function of the Pre-operative predictive variables (columns: age at implantation, age at onset of deafness, duration of deafness and pre-operative phoneme scores). Lines and symbols are as in figure 7.1.

interval. Performance recorded at earlier intervals did not show this significant correlation.

Figure 7.3^{E,F,G,H} shows the CVC phoneme scores at 2wk, 3mo, 1yr and 2 yr respectively as a function of the age at onset of deafness. Again table 7.4 shows regression analysis for the entire population and the individual sub-groups. In contrast to age at implantation, the correlation between age at onset of deafness and performance decreased with increasing implant use. While there was a good correlation ($r > 0.3$; $p < 0.001$) up to 2 mo, the correlation gradually reduced to $p < 0.01$ ($r=0.28$) at 3 mo, with no correlation remaining after 2 yr ($p > 0.9$; $r=0.002$). The same trend was seen for word scores. Analyzing this finding for the four sub-groups, it was observed that the older group showed no correlation for word score with age at onset of deafness at any test interval. There were however, some weak correlations for phoneme scores up until 2 mo post hookup. The younger group showed a significant positive correlation between performance and age at onset of deafness, even after 2 yr of implant use ($r=0.3$; $p < 0.05$; 2.3 % phonemes per decade; $r=0.3$; $p < 0.05$; 3.8 % words per decade). This correlation became weaker with increasing implant use. The non-positioner users were very similar to the older group, while the positioner users followed the trend of the entire population. This observation was in accordance with the positioner group being significantly younger than the non-positioner group.

Figure 7.3^{I,J,K,L} shows the CVC phoneme scores at 2wk, 3mo, 1yr and 2 yr respectively as a function of the duration of deafness. Analysis relating to the regression lines for the entire population and the four subgroups are shown in table 7.4. As for age at onset of deafness, the correlation with duration of deafness gradually decreases from $r=-0.49$ ($p < 10^{-6}$) at two weeks post hookup to $r=-0.25$ ($p < 0.05$) after 2 yr of implant use. Initially duration of deafness influenced outcome at -6.9 % per decade, reducing to -2.5 % per decade after 2 years of implant use. After two years subjects with a longer duration of deafness gradually increased in average performance while the subjects with a short duration of deafness reached a plateau much faster. The same correlations held for the word scores ($r=-0.43$; $p < 0.0001$; -5.3 % words correct per decade 1 wk post hookup and $r=-0.25$; $p < 0.05$; -0.37 % words correct per decade 2 yr post hookup). Again the older subject group did not follow the trend of the overall population. For word scores there were no significant correlations at all; for phonemes only weak significant correlations up to 2 mo post hookup ($p < 0.05$). A similar split was observed for the positioner group which showed a correlation with duration of deafness, while the non-positioner group did not.

Figure 7.3^{M,N,O,P} showed the CVC phoneme scores at 2wk, 3mo, 1yr and 2 yr respectively as a function of the aided free field pre-operative phoneme scores. Again, the regression line analysis for the entire population and the four subgroups are detailed in table 7.4. There were no significant correlations between the pre-operative score and the outcome measures in phonemes ($r < 0.22$; $0.35 > p > 0.04$) or in words correct ($r < 0.26$; $0.19 > p > 0.02$). Although there were some 'incidental' significant values, the scatter plots did not show a clear trend and the significance was not repeated systematically over time.

Table 7.4: The regression coefficients (r , p and slope) corresponding to the linear regression lines in figure 7.3, correlating the post-operative performance scores with pre-operative parameters. Horizontally, the various pre-operative parameters tested and vertically the different evaluation sessions. The line types represent: solid the entire population, dashed the non-positioner subjects, the dashed double dotted the positioner subjects, the dotted the subjects implanted < 65 yr, and dash dotted the subjects implanted > 65 yr.

		Age at implantation			Age at deafness			Duration of deafness			Pre op Phonemes		
		r	p	slope	r	p	slope	r	p	slope	r	p	slope
2 wk	Tot	0.13	0.2	0.17	0.41	6.00E 05	0.38	0.49	9.00E 07	0.7	0.21	0.05	0.25
	noP	0.13	0.3	0.16	0.42	0.0007	0.37	0.51	2.00E 05	0.73	0.14	0.3	0.16
	Pos	0.1	0.6	0.16	0.39	0.04	0.43	0.43	0.02	0.65	0.36	0.06	0.46
	65	0.01	1	0.01	0.39	0.001	0.48	0.47	7.00E 05	0.71	0.22	0.07	0.29
	65	0.15	0.5	0.48	0.46	0.02	0.47	0.5	0.01	0.62	0.18	0.4	0.15
3 mo	Tot	0.03	0.8	0.04	0.28	0.01	0.22	0.47	3.00E 06	0.6	0.13	0.2	0.13
	noP	0.02	0.9	0.02	0.36	0.01	0.3	0.56	3.00E 06	0.74	0.13	0.3	0.14
	Pos	0.03	0.9	0.04	0.24	0.2	0.2	0.36	0.06	0.39	0.3	0.1	0.28
	65	0.06	0.7	0.08	0.39	0.002	0.41	0.52	1.00E 05	0.69	0.12	0.4	0.13
	65	0.2	0.4	0.64	0.36	0.09	0.36	0.36	0.09	0.44	0.15	0.5	0.13
1 yr	Tot	0.1	0.3	0.1	0.16	0.1	0.11	0.37	0.0003	0.41	0.18	0.09	0.16
	noP	0.03	0.8	0.03	0.26	0.04	0.19	0.45	0.0002	0.51	0.23	0.08	0.22
	Pos	0.09	0.7	0.08	0.16	0.4	0.1	0.29	0.1	0.25	0.33	0.08	0.25
	65	0.06	0.6	0.08	0.33	0.01	0.3	0.46	0.0001	0.52	0.2	0.1	0.19
	65	0.01	1	0.04	0.15	0.5	0.14	0.19	0.4	0.21	0.15	0.5	0.11
2 yr	Tot	0.25	0.03	0.24	0.002	1	0.001	0.25	0.03	0.25	0.17	0.1	0.14
	noP	0.21	0.2	0.19	0.1	0.5	0.07	0.38	0.007	0.37	0.16	0.3	0.14
	Pos	0.19	0.4	0.2	0.09	0.7	0.06	0.05	0.8	0.04	0.5	0.01	0.36
	65	0.09	0.5	0.09	0.3	0.03	0.23	0.41	0.002	0.37	0.14	0.3	0.11
	65	0.03	0.9	0.11	0.11	0.6	0.12	0.12	0.6	0.14	0.25	0.3	0.21

Table 7.5: Outcomes of the multiple regression analysis using speech scores in phonemes (top) and words (bottom) measured after 2 yr of implant use. Model 1 is the lowa predictive model using a constant (A), duration of deafness (B), pre-operative speech scores (C) and a compression factor (D). Models 2 and 3 are extentions including the age at implantation (E) or a step function differentiating the two age groups (E'). Models 4 and 5 include a parameter marking use of the electrode positioner (F).

Phonem	Model 1		Model 2		Model 3		Model 4		Model 5	
	R ²	overall p	R ²	overall p	R ²	overall p	R ²	overall p	R ²	overall p
	Coefficient	pValue	Coefficient	pValue	Coefficient	pValue	Coefficient	pValue	Coefficient	pValue
A	77.59	1.9E-32	91.29	3.8E-21	81.61	2.7E-33	76.43	2.8E-29	72.43	4.3E-30
B	-0.30	0.02	-0.17	0.22	-0.36	0.003	-0.37	0.001	-0.33	0.005
C	0.19	0.07	0.25	0.2	0.19	0.06	0.25	0.01	0.27	0.01
D	0.29	0.21	-0.16	0.42	0.32	0.14	0.35	0.1	0.33	0.13
E			-0.22	0.05						
E'					-11.51	0.003	-8.48	0.02		
F							9.5	0.01	11.86	0.001

Word	Model 1		Model 2		Model 3		Model 4		Model 5	
	R ²	overall p	R ²	overall p	R ²	overall p	R ²	overall p	R ²	overall p
	Coefficient	pValue	Coefficient	pValue	Coefficient	pValue	Coefficient	pValue	Coefficient	pValue
A	60.87	4.8E-20	77.36	6.4E-11	65.98	1.1E-20	59.2	3.8E-17	54.84	6.1E-18
B	-0.23	0.27	-0.27	0.18	-0.35	0.09	-0.35	0.07	-0.28	0.15
C	0.4	0.18	0.42	0.15	0.45	0.12	0.49	0.07	0.47	0.09
D	-0.2	0.49	-0.15	0.61	-0.1	0.72	-0.1	0.7	-0.16	0.55
E			-0.31	0.07						
E'					-14.87	0.01	-9.95	0.08		
F							14.69	0.01	17.43	0.001

7.3.3 Multiple regression analysis

Five predictive models were described in the material and methods section with a progressively increasing number of parameters. The bivariate regression analysis, presented above, have illustrated that the three preoperative parameters (duration of deafness, pre-operative CVC scores and age at implantation) are independent variables and hence can safely be used in a multiple regression analysis. In table 7.5 the outcomes from the multiple regression analysis for each of the five models have been summarized for the phoneme scores recorded after two years of implant use. The overall accuracy of the

model fit improved with increasing number of parameters. The amount of post-operative score variance described by the model increased from 11 % (Model 1) to 30 % (Model 4), while the significance improved from $p=0.04$ to $p < 0.0005$. The same can be seen for the word scores (lower half of table 7.5), where both the R^2 and the p values were slightly less favorable.

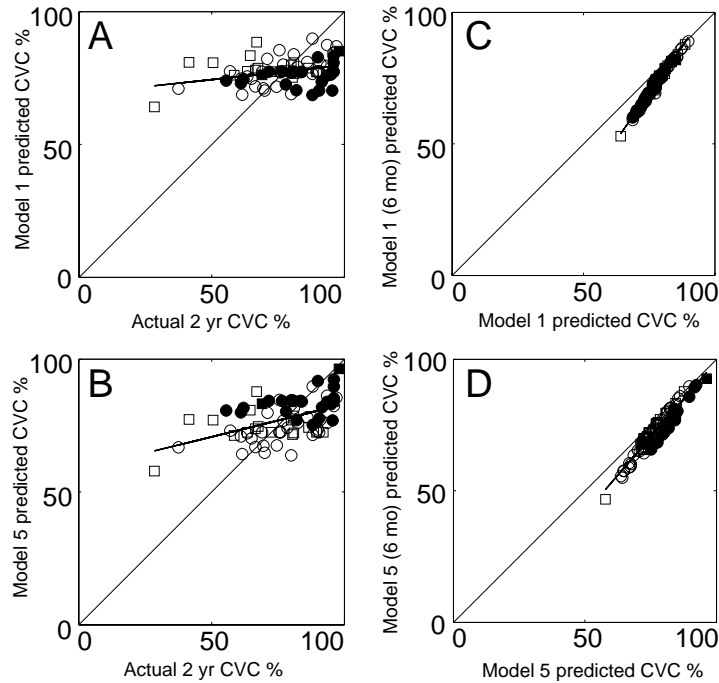


Figure 7.4: The predicted CVC phoneme scores as a function of the actual CVC scores for model 1 (A) and model 5 (B). Scatter plots of the predictor based on 6 mo data and the predictor based on 2 yr data for model 1 (C) and model 5 (D)

In table 7.5 the individual coefficients of the model predictions based on phoneme scores and their corresponding significance may also be found. The offset parameter (A) has the best predictive value ($p < 10^{-20}$) for all five models. In model 1 (equation 7.1), only the duration of deafness (parameter B) showed significance ($p < 0.05$) with a 3.0% reduction of phonemes correct per decade. The age at implantation (parameter E) was the only, just, significant predictor for model 2. In model 3 the use of the step function to discriminate

between the two age groups, proved to provide an improvement in fit. Subjects with the same pre-operative demographics, but implanted after the age of 65, scored 11.5 % worse than their younger counterparts ($p=0.003$). In this equation also the duration of deafness had a significant negative influence (-3.6% per decade; $p < 0.005$). Models 4 and 5 considered the influence of the positioner. As mentioned above, there was a significant difference between these groups. For both models four and five, all predictors became significant, with the exception of the compression factor (parameter D). The parameters in model 4 indicated that being implanted without positioner at greater than 65 years of age reduced the postoperative phoneme score with $8.5+9.5\%$ compared to the same subject demographics implanted below the age of 65 and implanted with a positioner. It should be noted that, although model 4 is highly significant, only 30 % of the variance in the data is described by this equation.

In figure 7.4^{A,B} the predictive values of model 1 and model 5 respectively are illustrated. Scatter plots show the predicted CVC scores as a function of the actual CVC scores. The correlation line is much flatter than the $x=y$ line; the predictor had difficulty in accurately predicting the outcome for the lower performing subjects. Due to the positioner parameter, the subjects with a positioner (filled symbols) are predicted to have better scores and shift up within the group.

In the lower half of table 7.5 the same coefficients and significance analysis are presented for word, as opposed to phoneme, scores. The overall trend is the same. However, as for overall significance, the individual parameters are also less reliable. Where, with phoneme scores the duration of deafness and pre-operative scores were significant predictors in models 4 and 5, with word scores the p values were all above 0.05; only presence of the positioner remained a significant predictor.

Table 7.6 presents comparable multiple regression data from the phoneme scores but calculated with 6 mo data. Models 1 and 2 demonstrated a higher correlation coefficient and higher significance levels compared to the 2 yr data. The other models were comparable. Looking at the individual components, the duration of deafness particularly has a much higher significance for each of the models. On the other hand, the parameter for age at implantation (E or E') did not reach significant levels and their absolute values were much smaller, indicating a smaller difference between the two age groups (e.g. model 3: -11.5% at 2 yr vs. -6.5% at 6 mo).

Figure 7.4^{C,D} shows scatter plots of the postoperative predictions from model 1 and model 5 respectively, plotting the 6 mo against the 2 yr data. All points lie

below the $x=y$ line, while the regression line crosses the $x=y$ close to the 100 % point. In other words, the 6 mo data model predicts lower scores, especially for the poorer performing subjects.

Table 7.6: Similar to table 7.5 but using the 6 mo post-hookup data, rather than 2 yr data, in the analysis

Phonemes	Model 1		Model 2		Model 3		Model 4		Model 5	
	R ²	overall p	R ²	overall p	R ²	overall p	R ²	overall p	R ²	overall p
	Coefficient	pValue	Coefficient	pValue	Coefficient	pValue	Coefficient	pValue	Coefficient	pValue
	0.16	0.002	0.18	0.003	0.19	0.002	0.25	0.0003	0.24	0.0001
A	74.75	2.1E-34	81.64	2.8E-20	77.07	2.7E-33	71.94	1.9E-28	70.27	3.9E-31
B	-0.45	0.001	-0.33	0.02	-0.5	0.0002	-0.52	0.00009	-0.49	0.0001
C	0.23	0.04	0.31	0.12	0.25	0.03	0.31	0.01	0.31	0.01
D	0.33	0.21	-0.2	0.37	0.35	0.19	0.37	0.16	0.36	0.16
E			-0.07	0.54						
E'					-6.48	0.1	-3.48	0.38		
F							9.68	0.01	10.67	0.004

Word	Model 1		Model 2		Model 3		Model 4		Model 5	
	R ²	overall p	R ²	overall p	R ²	overall p	R ²	overall p	R ²	overall p
	Coefficient	pValue	Coefficient	pValue	Coefficient	pValue	Coefficient	pValue	Coefficient	pValue
	0.19	0.001	0.15	0.03	0.22	0.001	0.26	0.0002	0.25	0.0001
A	58.8	8.5E-23	62.25	1.4E-9	62.11	6.7E-22	57.26	7.0E-18	54.79	3.7E-20
B	-0.48	0.02	-0.49	0.01	-0.57	0.01	-0.57	0.004	-0.52	0.01
C	0.51	0.07	0.52	0.06	0.56	0.04	0.61	0.03	0.58	0.03
D	-0.2	0.5	-0.19	0.54	-0.15	0.62	-0.15	0.6	-0.18	0.53
E			-0.06	0.67						
E'					-8.97	0.1	-5.34	0.34		
F							10.71	0.04	12.27	0.01

Models 1, 2 and 3 can also be used to examine the individual positioner and non-positioner groups. In the positioner group the significance of the overall fit is very poor. Only model 2 just barely reaches a significance level ($p < 0.05$) with an R^2 value of 0.4. Next to the overall level parameter (A), the pre-operative score parameter (C) showed the highest significance for models 1 and 4 ($p < 0.05$). In the non-positioner group it was the duration of deafness parameter that reached significance. For this group, model 3 had the best predictive value ($R^2=0.33$; $p = 0.002$). The duration of deafness had a negative correlation with a slope of -5.3 % per decade ($p=0.0003$), while the age groups (E') differed with -10.9 % in favor of the younger population ($p = 0.01$).

Likewise models 1, 2 and 5 can be used on the two age groups. In the older (very small) group none of the models reached significance. The group with subjects implanted before the age of 65, showed a significant correlation for

models 1 and 5 ($R^2=0.19$; $p=0.02$ and $R^2=0.29$; $p=0.002$ respectively). Again, the duration of deafness was a significant coefficient in both of these models ($p < 0.002$). Model 5 had the best predictive value, where the positive influence of the use of a positioner (F) was 9.3 % ($p=0.01$).

7.4 Discussion

These data indicate that outcome with a cochlear implant is correlated with duration of deafness, age at implantation and the modiolar proximity of the electrode array. The correlations change, however, over time. Where the correlations with age at implantation and the use of a positioner become larger with greater implant experience, the correlation with duration of deafness reduces gradually. Using early outcome measures as a basis for predictive analyses of post operative outcome underestimates the ultimate outcome and inflates the influence of certain pre operative predictive factors.

The duration of deafness has been highlighted in numerous studies (Gantz et al., 1993; Summerfield and Marshall, 1995; Waltzman et al., 1995; Albu and Babighian, 1997; Rubinstein et al., 1999a; Gomaa et al., 2003; Chan et al., 2007) as, "a consistent and the most significant determinant of postoperative speech recognition" (Friedland et al., 2003). The duration of post-operative follow up in most of these studies was between 3 mo and 1 yr. For instance, all studies using the Iowa predictive model (Rubinstein et al., 1999a) used the best post-operative score within the first year (Rubinstein et al., 1999a; Friedland et al., 2003; Gomaa et al., 2003; Leung et al., 2005). Studies with a long follow-up time indicate, however, that performance has not yet stabilized at these early evaluation points, but continues to improve for at least the first 2 years (Ruffin et al., 2007; Oh et al., 2003). Our bivariate data with the duration deafness (fig. 7.3^{I,J,K,L}) clearly indicate that with increasing implant use the correlation with the duration of deafness reduces. In a recent study with a very long follow up time, up to 10 yr, the same trend is noted; at 3 and 6 mo a significant negative correlation was found but with longer implant use the correlation was absent (Ruffin et al., 2007). From the individual scatter plots, it can be noted that the subjects with the longer duration of deafness continue improving over time, while the subjects with a short duration of deafness plateau in performance much more quickly. This fact can lead to an over estimation of the influence of the duration of deafness on post-operative performance when using only a short follow-up period.

The validity of these changes in correlations coefficients depend on the normality of the distributions indicating if the performance plateau seen in the group with a shorter duration of deafness is just a ceiling effect or really the end of the learning curve. Analysis of the normality of the distribution for the phoneme scores revealed an asymmetric distribution (skewness < -0.7) towards the higher scores for all test moments for the group with a short duration of deafness (< 20 yr). The group with longer duration of deafness has a relatively symmetric score distribution up till 3 mo of implant use (skewness > -0.2), but with increasing implant use the asymmetry increases (< -0.9). This suggests some ceiling effects or at least a non-linearity in the test outcomes. Word scores differentiate better than phoneme scores for high performing patients; the distributions based on word scores are much more symmetric, the skewness in the group with the shorter duration deafness is between 0 and -0.4 . The group with the long duration of deafness starts out with an asymmetric distribution towards the 0% score (skewness around 1), in line with the poor sensitivity of this test towards the lower scoring patients. After 2 yrs. of implant use the distribution has become much more symmetric (skew -0.3). The normal distributions in the word scores indicate that the found diminishing correlation with the duration of deafness, for both phoneme and word scores, is a true phenomenon, not caused by ceiling effects in the test material.

The same argument holds for the age at implantation. There is no significant difference between those implanted before the age of 65 and the group implanted after reaching this age, for implant use of less than 2 yr. Looking closely at the outcome changes over time, one sees an equal performance until 6 mo. At that time the older group stabilizes in performance, while the younger group continues to improve. After 2 years of implant use the performance difference becomes significant (9.5 % in phonemes and 13.3 % in words, fig 7.2). Several studies indicating that there was no significant difference in performance for elderly subjects (Pasanisi et al., 2003; Haensel et al., 2005; Leung et al., 2005) used a follow-up time of only one year, with the exception of the study by Chatelin et al. (2004) which demonstrated a significant difference between the two age groups at the 12 mo post operative session. A study comparing a group of 14 elderly implant users from Hong Kong showed that the younger group performed better on a tone identification task 2 yr post hookup (Chan et al., 2007). Here also multiple regression analysis was performed, however, using only 12 mo sentence recognition data.

The implant experience accrued at the time of assessment is also of influence on the components of the multiple regression analysis. The component corresponding to the duration of deafness found by Rubinstein et al. (1999a) and

(Friedland et al., 2003) was -0.42 % words correct/yr and -0.56 % words correct/yr respectively. These are much larger than the -0.23 % words correct/yr found in this study. The value at the 6 month postoperative evaluation for our population was -0.48 % words correct/year, a value in line with those found by Rubinstein and Friedland. The extension of the Iowa model to include age at implantation (Leung et al., 2005), yielded -0.005%/yr of subject age or, -4.6 % in the binary condition. This appears very different from our coefficients at 2 yr post hookup: -0.31 %/yr in model 2 and -14.9 % in the binary model 3. The analyses with the 6 mo data, show much more similar data points to Leung: -0.06 %/per year in model 2 and -8.9 % in model 3.

The Iowa regression model was further extended in this study to encompass the presence of the positioner. The group comparisons (fig. 7.2) already indicated that a significant difference existed between the positioner and non-positioner groups (9.3 % phonemes, 14.7 % words correct, $p < 0.01$) in favour of the positioner group. There were however, additional differences between these groups that could have interfered with the outcome (Table 7.1), the average age at implantation was significantly younger ($p < 0.05$) and the pre-operative phoneme score was significantly worse ($p < 0.05$) for the positioner group. As described above, the age factor is in favor and the pre-operative score is in disfavor of the performance of the positioner group. Multiple regression analyses model 4 illustrates a difference of 9.5 % ($p < 0.01$) and 14.7 % ($p < 0.01$) in favor of the positioner group in phoneme and word scores respectively (Table 7.5). Both of these values are very similar to the values found from simple group comparisons (van der Beek et al., 2005): apparently both the effects of age at implantation and pre-operative scores are in balance. The effect of the positioner, without taking age at implantation into account, is larger: 11.9 % and 17.4 % in phoneme and word scores respectively, indicating that both parameters do influence outcome.

Although there is a large difference between the lateral wall and the perimodiolar electrode array, the other predictive variables in the multiple regression analysis do not change overly with the inclusion of implant type. However, both the predictive value and significance level improves on consideration of electrode array location. Studies evaluating predictors of cochlear implantation efficacy, including the impact of implant type, could improve their analysis by inclusion of these differences. Friedland et al. (2003) for instance, uses the Iowa predictive model in a population consisting of several devices, 23 Nucleus devices (Cochlear Corporation, Lane Cove, Australia), 34 Clarion devices (Advanced Bionics, Sylmar, CA, USA) and one Med-El device. From the data presented it becomes clear that the Clarion users perform 10 % worse

then their Cochlear counterparts (his figure 3). Since most studies comparing improved electrode array designs with their predecessors are retrospective studies, and are thus not well controlled with randomized groups, a multiple regression analysis could more accurately highlight the difference between any two devices.

Conversely, other parameters could be changed unintendedly through mixing implant types. For instance, the present study shows a significant difference between the group implanted before the age of 65 and the group implanted at a later age; a difference of 11.5 % phonemes or 14.9 % words correct (table 7.5). Comparing the multiple regression models 3 and 4, one notices that part of this difference can be attributed to the positioners placed in a relatively younger subject group. The remaining difference is 8.5 % phonemes and 10.0 % words correct.

Figure 7.4 shows the accuracy of the model predictions. As already indicated, the predictive model over-estimates outcome from the poorer performers. All subjects received a final predictive score well above 50 % phonemes correct, while the real range is much broader: 30 % to 98 % phonemes correct. This indicates that the factor determining why these subjects are poorer performers is not included in the parameter set, an additional parameter being required to shift these poor performers away from the average value set with parameter A. The same limitation can be seen in other predictive formulas, the predictor presented by Friedland et al. (2003) has a limited range between 5 % and 60 % words correct while the actual CVC data have a range from 0% to 95 % words correct. The large factor relating to the good performers is missing in the formula.

7.5 Conclusions

The relative importance of predictive factors is highly dependent on the follow-up time considered. Therefore, predictive models should be based on follow-up times of at least 2 years to allow the poorer performers to approach their plateau performance level. This is especially so with regard to the duration of deafness. Those with a longer duration of deafness have a much shallower learning curve, but ultimately reach similar scores to those with shorter durations of deafness. High age at implantation limits the long term speech understanding improvement, resulting in a significantly poorer score after 2 yr of implant use. Multiple regression analysis should be used to extract the

influence of, for instance, the electrode array design or, age at implantation in non-controlled retrospective studies. This will reduce the effect of other parameters such as the duration of deafness on the final outcome.

7.6 Acknowledgement

This research was financially supported by grants from the Heinsius Houbolt Fund.

Chapter 8

Unraveling the Electrically Evoked Compound Action Potential

Jeroen J. Briaire and Johan H.M. Frijns
Hearing Research (2005), 205(1-2), 143-156

Abstract

With the advent of eCAP recording tools such as NRT and NRI for cochlear implants, neural monitoring has become widely used to ascertain the integrity of the neural/electrode interface as well as for assisting in the setting of program levels. The basic concepts of eCAP recordings are deduced from the acoustical equivalent of the electrocochleogram. There are, however, indications that under electrical stimulation some of these do not hold, like the unitary response concept (i.e., the principle that every fiber produces the same contribution to the eCAP). Computer modeling has proven to be a valuable tool for gaining insight into the functioning of electrical stimulation. In this study the extension of a three-dimensional human cochlea, incorporating back-measuring capabilities, is described. Using this new model, the contribution of single fiber action potentials (SFAPs) to the measured eCAP is investigated. The model predicts that contrary to common belief- the compound action potential as measured by the cochlear implant system does not necessarily reflect the propagated action potential along the auditory nerve.

8.1 Introduction

The recording of electrically evoked compound action potentials (eCAPs) of the auditory nerve has become widespread since the introduction of Neural Response Telemetry (NRT) by Cochlear Ltd. (Sydney, Australia) and Neural Response Imaging (NRI) by the Advanced Bionics corporation (Sylmar, CA, USA). These systems allow easy acquisition of the eCAP through the cochlear implant system without the need of extra recording or stimulating electrodes such as a trans-tympanic needle. The fundamentals of auditory CAP recordings are known from the acoustically evoked equivalent, which is the electrocochleogram. The latter is used in clinical practice as a reliable way to measure a frequency specific objective audiogram (Schoonhoven et al., 1996; Schoonhoven et al., 1999). Stimuli with alternating polarity are used in such acoustically evoked recordings to remove the cochlear microphonic (CM), which results from outer hair cell responses. One of the mainstays of these recordings is that the CAP response can be described as a superposition of unitary responses, meaning that each nerve fiber contributes equally to the signal (Versnel et al., 1992; Goldstein and Kiang, 1958), and that the amplitude of the recorded fiber response correlates with the number of excited nerve fibers. The recording of eCAPs gives rise to some specific issues compared to the electrocochleogram, e.g., now the electrical artifact has to be suppressed instead of the CM. The question that remains is whether all the other principles of acoustical CAP recordings are applicable for eCAP recordings. Moreover, to date the clinical value of using eCAP input/output functions and thresholds to set processor parameters remains limited to finding contours for the levels in the programs. These objective data have to be supplemented by behavioral data to get functional programs (Abbas et al., 1999; Seyle and Brown, 2002; Smoorenburg et al., 2002). It remains unclear, however, what the fundamental problems are why it is not possible to build programs that patients prefer based only on eCAPs. Additionally, the ability to measure refractory properties (Miller et al., 2000) and the possibility to obtain objective measures of spatial selectivity (Cohen et al., 2003; Abbas and Brown, 2000; Frijns et al., 2002) are not yet sufficiently validated in terms of their clinical applicability. More specific questions that need to be answered are, to what extent these objective measures are applicable to the fitting of children or can be used to assess neural degeneration in regions of the cochlea.

To gain further insight into the working mechanisms of electrical stimulation of the auditory nerve by a cochlear implant, a detailed computer model of the cochlea has been developed at the Leiden University Medical Center (Frijns et

al., 2000a; Briaire and Frijns, 2000a). The model consists of two parts, a 3D volume conduction model and an active auditory nerve fiber model. The volume conduction part provides insight into the distribution of the current through the cochlea (Briaire and Frijns, 2000b) and how this distribution can be influenced by, for example, electrode orientation. In and of itself however, the potential distribution does not tell which fibers will react and how the stimulus waveform affects the response. For this purpose the nerve fiber model is used. Using the potential distribution along the nerve fibers for its input, this model calculates which fibers and what part of these fibers will be excited (Frijns and ten Kate, 1994; Frijns et al., 1995). Initially, both models were based upon the cochlea of a guinea pig, our experimental animal, with corresponding fiber morphology and nodal kinetics. The presence of cross-turn stimulation, the unintended and unwanted activation of nerve fibers from a higher turn than where the stimulating electrode is located, and the influence of the electrode position were the main outcomes of this initial model (Frijns et al., 1995; Frijns et al., 1996a). To generate an applicable human model, the animal volume conduction model was extended to use realistic electrode geometries and to match the human cochlear anatomy. This also gave us a tool to investigate the validity of transferring results obtained from animal experiments to the human situation (Frijns et al., 2001). Recently, one of the main outcomes of this study, a decrease in threshold and an increase in neural excitation at a fixed current level when the electrode is moved to a more peri-modiolar position, was confirmed with intra-operative electrically evoked auditory brainstem response (EABR) measurements with the HiFocus electrode in lateral and medial positions by Firszt et al. (2003).

Previous studies, with integrated use of neural and volume conduction models from a number of groups (Hanekom, 2001; Rattay et al., 2001a), typically focused on the so-called forward problem, i.e., predicting the neural excitation pattern. To our knowledge, the first attempt to simulate eCAPs was a preliminary study with a guinea pig model that was in itself just capable of solving the forward problem (Frijns et al., 1996b). It used the assumption that the unitary response concept was also valid for the electrically stimulated cochlea and led to the conclusion that just the site of excitation along the auditory nerve fiber cannot account for the latency differences observed. To answer more subtle questions about the value and possibilities of eCAP recordings and the validity of the unitary response concept a more sophisticated model is needed, which is able to solve the full backward problem, i.e., the calculation of the eCAP response as recorded via intra-cochlear electrode contacts.

As stated above, the geometry of the cochlea and the implant used in our

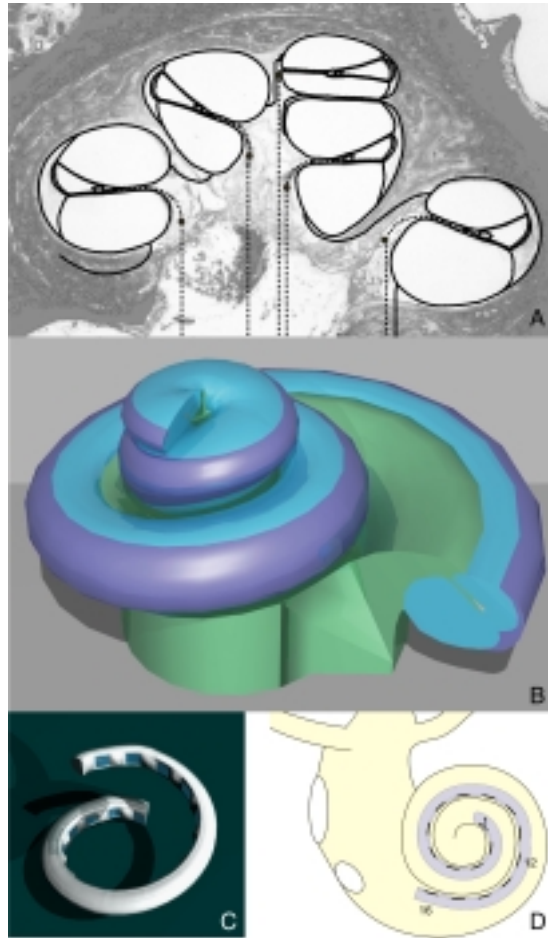


Figure 8.1: **(A)** Mid-modiolar cross-section of the human cochlea with the cross-section of the volume conduction model shown in bold lines. In the modiolar part of the cochlea the positions of the nerve fibers have been plotted (dotted lines) as well as the approximate locations of the cell-bodies within the spiral ganglion (indicated by solid circles). **(B)** A three-dimensional representation of the cochlear model. **(C)** Model representation of the HiFocus electrode array as used for the simulations. **(D)** Schematic representation of the electrode array in the cochlea, with contacts 1, 12 and 16 numbered.

previous studies were already in line with the human anatomy. However, the kinetics and morphology of the nerve fibers were still based on the guinea pig, which likely compromised the applicability of the findings to humans. The main anatomical difference between the guinea pig and human primary auditory nerve fiber is the morphology of its cell body, which is unmyelinated in humans as contrasted with all other mammals. From Rattay's model study (Rattay et al., 2001b) it is known that the unmyelinated cell body in the human fiber is likely to play an important functional role, as it induces a delay in the conduction of the action potential (AP) along the fiber. Also the length of the peripheral process in humans is much longer than in guinea pigs. Therefore, there are presumably more than three (the value used in the guinea pig models) inter-nodal segments in the human peripheral process, although there is no formal histological evidence available.

The present study aims at deriving a fundamental understanding of the processes underlying eCAP recordings in humans, both in terms of the contributions of the individual nerve fibers to the overall signal as well as to what extent this signal yields clinically relevant information about functional aspects of electrical stimulation. For this purpose the neural model has been extended to incorporate an unmyelinated cell body and an unmyelinated pre-somatic region. In addition, the algorithms of the volume conduction model have been upgraded to calculate the eCAP from single fiber responses in order to generate simulated wave forms that can be compared with actual recordings.

8.2 Materials and methods

8.2.1 The forward problem: simulating neural excitation in the human cochlea

The computational model of the electrically stimulated human cochlea as described in Frijns et al. (2001) forms the basis of the computational model used in the present study. The model geometry is a realistic three-dimensional representation of the human cochlea with a model representation of the Clarion HiFocus cochlear implant (Fig. 8.1^{A,B,C}). Details of this geometry have been published in the aforementioned paper. Unless stated otherwise, the implant array is in a peri-modiolar position in the scala tympani throughout the present study, as it is expected to be clinically when a peri-modiolar electrode array is used (Fig. 8.1^D). The nerve fibers are located in the modiolus and radiate

out into the osseous spiral lamina, with the tips of their peripheral processes evenly distributed below the organ of Corti with a spacing of $100\mu\text{m}$. This leads to a total of 299 modeled fibers in the entire cochlea. Each fiber in the model represents a group of 100 actual nerve fibers, limiting the amount of computational effort while preserving sufficient spatial resolution. All simulations in this study are performed with biphasic current pulses with a phase duration of $37.5\mu\text{s}$ on contact 12 of the array, approximately in the middle of the basal turn. The most apical contact #1, with an insertion of approximately 1.5 turns, is used as recording contact. This situation will be referred to as 'standard conditions'.

As explained in section 8.1, the model consists of two sub-models: First, the volume conduction step calculates the potential distribution and the current spread through the various tissues incorporated in the cochlea model (Briaire and Frijns, 2000a; Briaire and Frijns, 2000b) as a result of the current injected through a stimulated electrode. Thereby, the (quasi-static) volume conduction model calculates the potential $V_{f,k}^{stim}$ on every node of Ranvier k of each fiber f induced by a unit current from the stimulating electrode $stim$, yielding the resistance matrix R^{stim} with elements $R_{f,k}^{stim}$. This matrix serves as the transfer function between the stimulating electrode and the nodes of Ranvier. Then Ohm's law yields the time-varying potential $V_{f,k}^{stim}(t)$ due to a time-varying current stimulus $I(t)$, injected from the stimulating electrode:

$$V_{f,k}^{stim}(t) = R_{f,k}^{stim} I(t) \quad (8.1)$$

The second sub-model is an active, non-linear nerve fiber model, which calculates the neural response elicited by the stimulus. Compared to our previous studies the morphology has been upgraded to get a better representation of the human nerve fiber. Fig. 8.2 shows the fiber morphology as used in this study. It represents a bipolar high spontaneous rate (HSR) nerve fiber with a uniform axon diameter of $3\mu\text{m}$, an inter-nodal length varying between 50 and $350\mu\text{m}$ and a nodal gap width of $1\mu\text{m}$. As contrasted to our previous studies, the fiber model now includes a $10\mu\text{m}$ thick, cell body (CB) preceded by a thin (axon diameter $2\mu\text{m}$) pre-somatic compartment as initially used by Rattay et al. (2001b). These two segments have been modeled as unmyelinated segments in the so-called unmyelinated cell body (UMCB) condition. In this condition the fiber morphology is in accordance with known human data (Nadol, 1988). The importance of these changes to the modeled fiber morphology was reported by Rattay et al. (2001b), who showed the influence

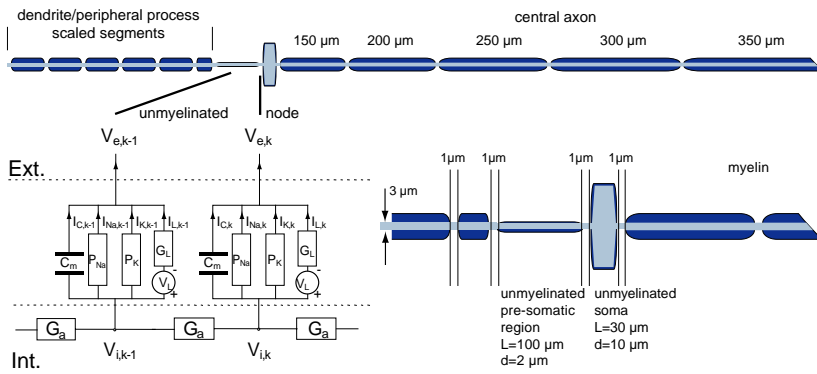


Figure 8.2: Representation of the nerve fiber morphology. The peripheral process consists of 6 scalable segments to adjust for the variable length from the organ of Corti to the cell body. In the UMCB condition the pre-somatic region and the cell body were modeled as active segments with a capacitance and ionic currents. In the MCB condition these two segments behaved as fully isolated elements.

of the unmyelinated cell body on the spike propagation. The need for the unmyelinated pre-somatic region is also explained in that study, showing that this region is needed for the action potential to bridge the large capacitor formed by the unmyelinated cell body. It forms a safety factor to ensure the propagation of the AP along the nerve fiber. Similar to Rattay et al. (2001b), both on the soma and on the pre-somatic region 4 myelin wraps are included to enable AP propagation across the cell body. This thinly myelinated situation is called unmyelinated for clarity and in accordance with the description and naming in Rattay et al. (2001b). To model the cell body and the presomatic region, nodes of Ranvier, were added to these segments with corresponding diameters. The myelin wraps (N) can be seen as a series of membranes, each with the same capacitance and conductance. Using the scale factor $\frac{1}{1+N}$ the capacitance and conductance could be calculated for a certain number of myelin wraps (with 4 myelin layers this leads to $C_m = 3.52pF$ and $G_L = 0.75n\Omega^{-1}$ for the presomatic region and $C_m = 5.28pF$ and $G_L = 1.13n\Omega^{-1}$ for the cell body). The current strengths of the ionic currents were however reduced by an extra factor 30 compared to the nodes of Ranvier (inset Fig. 8.2). To investigate to what extent the UMCB contributes to the observed differences between eCAP recordings between animals and humans, also a myelinated cell body (MCB) condition was used, where the cell body and the pre-somatic region are fully myelinated. As in the model of Rattay et al. (2001b) the number of inter-nodes

in the peripheral process for both the MCB and UMCB condition has been increased from 4 to 6 to deal with the fact that the trajectory from the tip of the fiber to the cell body is much larger in humans than in guinea pigs. However, although more inter-nodal segments are used in the peripheral process, the position of the cell bodies in the spiral ganglion is in accordance with histological data like in our previous studies with a human cochlear geometry (Frijns et al., 2001). To fit the peripheral process into the anatomically correct position its length is scaled to match the trajectory from the spiral ganglion to the organ of Corti. The nodes of Ranvier and the unmyelinated segments include a membrane capacitance, active sodium and potassium ionic channels and a passive leak conductance (Fig. 8.2, inset). The equations governing the kinetics of this so-called generalized Schwarz-Eikhof-Frijns (GSEF) auditory nerve fiber model are described in detail elsewhere (Frijns et al., 1994; Frijns et al., 1995; Frijns et al., 2000a) and will not be repeated here.

8.2.2 The backward problem: calculation of the compound action potential

Essentially, an AP is a depolarization of the cell membrane at the nodes of Ranvier, which propagates along the nerve fiber. The processes of depolarization and repolarization are characterized by current flowing into and out of the fiber through the nodal membrane. In fact, recording the eCAP is the simultaneous registration at a single recording electrode of the potentials induced by these nodal currents. In the computational model this concept of eCAP generation is applied, while taking into account four different current components in each modeled node of Ranvier (inset of Fig. 8.2) viz. the current $I_k^C(t)$ through the membrane capacitance, $I_k^{Na}(t)$ and $I_k^K(t)$ through the sodium and potassium ionic channels and $I_k^L(t)$ through the leak conductance. This means that the contribution of a single node of Ranvier k is given by the net current $I_{f,k}(t)$ leaving the fiber f through this node as a function of time t :

$$I_{f,k}(t) = -(I_{f,k}^C(t) + I_{f,k}^{Na}(t) + I_{f,k}^K(t) + I_{f,k}^L(t)) \quad (8.2)$$

The potential at the recording electrode as induced by each nodal current $I_{f,k}(t)$ can be calculated by application of the reciprocity theorem: the same transfer resistance that exists between a stimulating electrode and a particular node of Ranvier gives the relationship between a current through that node of Ranvier and the electrode when used to record the eCAP:

$$V_{f,k}^{rec}(t) = R_{f,k}^{rec} I_{f,k}(t), \quad (8.3)$$

where $V_{f,k}^{rec}(t)$ is the potential on the recording electrode *rec* induced by $I_{f,k}(t)$ and R^{rec} is the corresponding resistance matrix (standard electrode #1 is used). To obtain the single fiber action potentials of each fiber $SFAP_f^{rec}(t)$ on the recording electrode the contributions of all the nodes of Ranvier of a fiber are combined

$$SFAP_f^{rec}(t) = \sum_k V_{f,k}^{rec}(t). \quad (8.4)$$

Finally, all SFAPs must be combined to create the potential $V^{rec,total}(t)$ as would be measured at a recording electrode as a function of time:

$$V^{rec,total}(t) = \sum_f SFAP_f^{rec}(t). \quad (8.5)$$

The above summation has to be performed at each moment in time where the eCAP has to be calculated. Since each fiber in the simulation represents 100 actual fibers, $V^{rec,total}(t)$ has to be multiplied by this factor for comparison with actual measurements. All eCAP responses in this paper were sampled at $10\mu s$ intervals, although the integration of equations governing the individual nerve fibers took place with a fourth order Runge-Kutta method with adaptive step size control in order to ensure numerical accuracy (Frijns and ten Kate, 1994). Therefore, fourth order polynomial interpolation was used to obtain the nodal current strengths in all the fibers at the predefined, evenly spaced time intervals.

8.2.3 The use of an artifact rejection scheme

Although the capacitance at the level of the electrode to fluid interface (the main source of stimulus artifacts in actual eCAP recordings) is not incorporated in the present model, there turned out to be a considerable stimulus artifact in the simulated eCAPs. This artifact is caused by the membrane capacitance of the nodes of Ranvier and especially in the unmyelinated cell body. This artifact is up to an order of magnitude larger than the neural response and can obscure or disfigure it just as is the case in actual recordings. We concluded that the simulations too would benefit from an artifact rejection scheme.

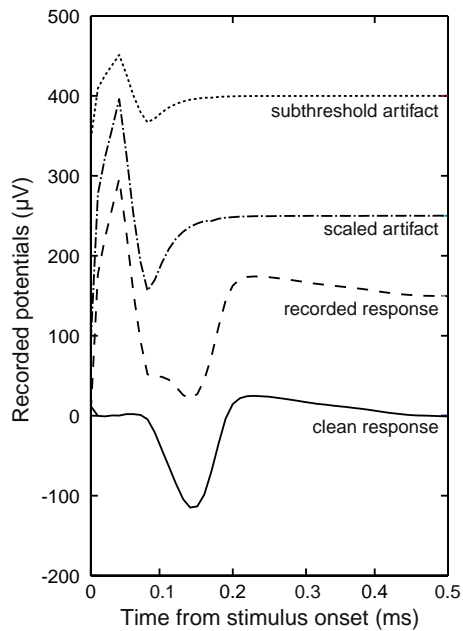


Figure 8.3: Visualization of the scaled artifact method. The response of a subthreshold stimulation is recorded (dotted line) and scaled (dash dotted line) to fit the amplitude of the artifact in the supra-threshold recording (dashed line). By subtracting the scaled artifact from the recorded response, a response without artifact is obtained (solid line)

From experimental studies three artifact rejection schemes are known: alternating polarity, forward masking (MP3) and scaled artifact; all three are based on different neural properties. All three methods have been tested with the model, and lead to the conclusion that the clinical drawbacks of each of the different methods (Klop et al., 2004) also apply to the model situation. The alternating polarity paradigm uses the fact that the polarity of the CAP is equal for anodic and cathodic stimuli while the artifact polarity is linked to that of the stimulus. However, there are fundamental differences in the neural response to cathodic and anodic stimulation, making this paradigm less appropriate for a theoretical study like the present one. The forward masking paradigm uses the refractory period of the nerve fibers to create a stimulus artifact without an eCAP which is then used to cancel the artifact of the intended eCAP response. For several reasons this paradigm, which is clinically the most widely

used, is also not optimal for the present study. First, the timing of the pulses in this paradigm is dictated by the refractory behavior of the neural elements. In the model, this refractory behavior has not been fully evaluated yet and is subject of ongoing research in our laboratory. Second, the calculation of the response to a double pulse takes 4-5 times more time than determining the response to a single pulse. Such an increase in calculation time is a considerable drawback of this method. Therefore, the scaled artifact paradigm is used throughout this study. It uses the artifact from a sub-threshold stimulus, scaled to fit the artifact of the response under study, which is then subtracted from the calculated eCAP to remove the artifact (Fig. 8.3). Clinically, the validity of this method is limited by the intrinsic non-linearity of the electrode to fluid interface, the uncertainty that the artifact is really without a neural response and the fact that the noise in the recording of the artifact is scaled with the artifact. In the present model the electrode to tissue interface is not incorporated, which eliminates the major flaws of the method. In addition, for the model situation, recording noise and unknown fiber excitation do not exist. The calculated SFAPs change less than 1% when the step size of the fiber models is reduced by a factor 10, indicating sufficient numerical accuracy.

8.3 Results

The most detailed presentation of the outcome of the forward problem is the so-called excitation profile as shown in Fig. 8.4. Such a plot depicts which nerve fibers get excited at various stimulus levels. The location of the initial excitation (peripheral process, cell body or modiolar axon) is indicated by the degree of shading. Fig. 8.4^A shows such an excitation profile for the standard conditions as defined in section 8.2, as calculated with the old, guinea pig based, fiber (GSEF) used in previous human model studies (Frijns et al., 2001; Frijns and Briaire, 1999). Fig. 8.4^B shows the same result for the present human nerve fiber morphology (UMCB condition). It is clear from these figures that the shapes of the profiles are very similar. The main differences are an upward shift in threshold for the UMCB fiber, and a change in excitation site, especially along the edges of the excitation area where the fibers are stimulated just above threshold level. In the GSEF fiber morphology the peripheral process is excited at threshold level, where it is the central axon in the human fibers. The excitation profile for the MCB condition is not presented, since it resembles the presented plots very closely: the thresholds for the MCB and UMCB fibers are almost identical, while the initial excitation

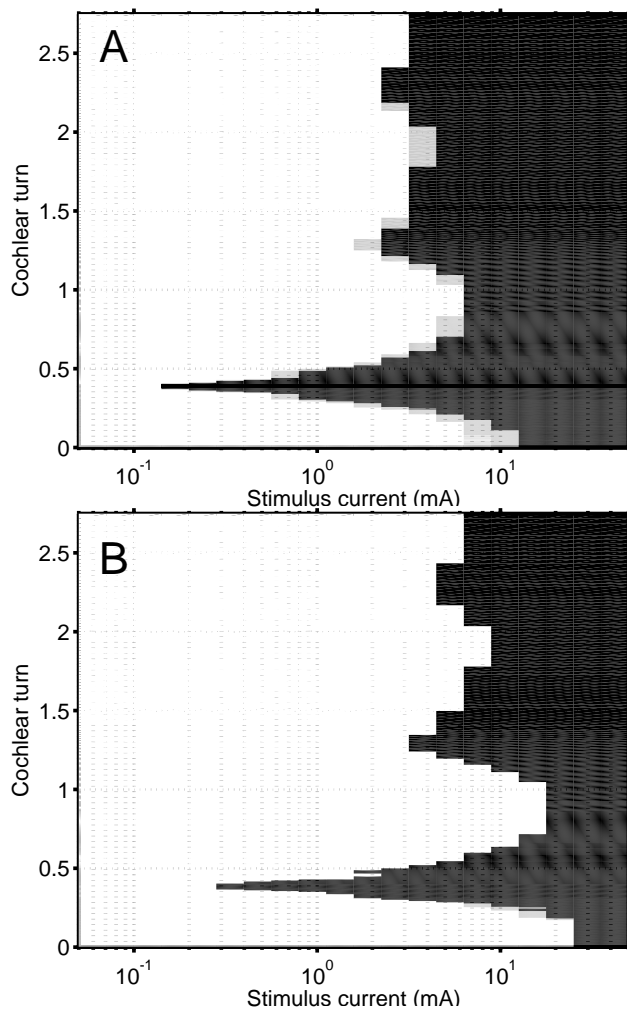


Figure 8.4: Excitation profile for the nerve fiber used in previous studies (**A**) and for the UMCB condition (**B**). In these profiles is depicted which nerve fibers get excited for a certain current strength. The location where the initial excitation occurs is indicated by the degree of shading (light gray: peripheral process and black the modiolar axon). For this setting there is no initial excitation on the cell body and the surrounding nodes.

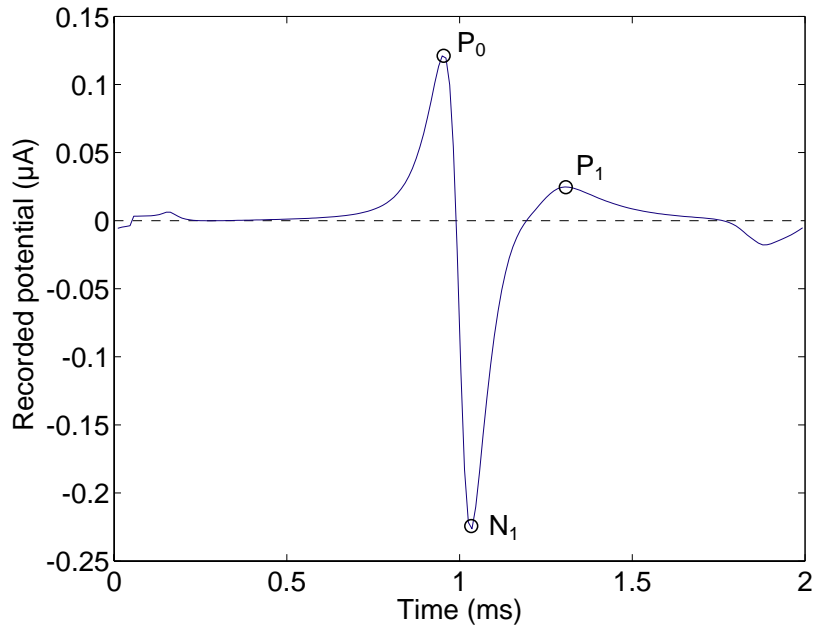


Figure 8.5: Single fiber action potential (SFAP) from a straight uniform nerve fiber (with 100 segments of $350 \mu\text{m}$, like the central axon of the used auditory nerve fiber) in a infinite homogeneous medium. The recording electrode is placed 17.5 mm from the tip of the nerve fiber and 0.6 mm from the fiber axis.

site for the MCB tends to shift to the cell body for the fibers along the edges of the excitation area. These observations indicate that previously published conclusions based on excitation profiles computed with the GSEF fiber are still in line with the present results.

As described in the previous section, obtaining the eCAP with the model involves a sequence of calculation steps. First, the currents from all the nodes of Ranvier have to be calculated. Next, their contribution on the potential at the recording electrode has to be computed, yielding the SFAPs for each fiber. Finally, all SFAP contributions must be superimposed to get the final eCAP, Eq. (8.5). As an initial validation of the principle of calculating the eCAP in the way described above, the procedure was tested in a single uniform nerve fiber in an infinite, homogeneous medium. The segments of this uniform nerve fiber are the same as the axonal part of the MCB and UMCB auditory nerve fiber (with an inter-nodal length of $350 \mu\text{m}$). According to the theories developed for

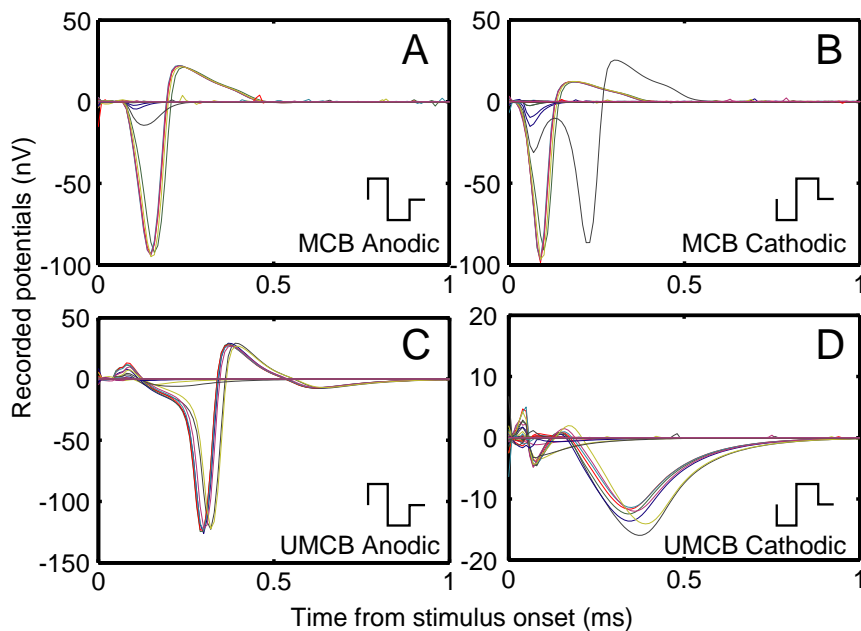


Figure 8.6: All the SFAPs as recorded from the most apical contact at approximately 1.5 turns insertion depth induced by a current, 6 dB above threshold for the (A) MCB anodic-first, (B) MCB cathodic-first, (C) UMCB anodic-first and (D) UMCB cathodic-first condition.

EMG recordings (Schoonhoven and Stegeman, 1991) an asymmetric triphasic SFAP is expected for relatively small recording distances as used in this test. The simulated SFAP is plotted in Fig. 8.5. When the AP gets close to the recording electrode a sharp positive peak (P_0) becomes apparent followed by a large negative peak (N_1). When the AP finally propagates away from the recording electrode a more shallow positive P_1 peak is induced. Therefore, the test case behaves in line with the theoretical expectations. From this and similar experiments we concluded that the algorithm for the backward problem is conceptually correct.

In Fig. 8.6 the full volume conduction and neural model with the MCB and UMCB auditory fiber morphology were used to calculate SFAPs for anodic-first and cathodic-first biphasic current pulses. These calculations were made for a stimulation level that was 6 dB above the threshold (the current strength at which the first modeled fiber is excited) for the standard condition of the model. For the anodic-first MCB condition (Fig. 8.6^A) the first positive peak

P_0 is not discernible in these responses, as can be expected from the fact that the AP cannot really propagate towards the recording electrode. This is the consequence of the fact that the excitation site is close to the recording electrode. The N_1 and P_1 peaks are clearly visible, with absolute latencies of N_1 and P_1 , around 0.15 ms and 0.24 ms after stimulus onset respectively. In Fig. 8.6^B the SFAPs for a cathodic-first stimulus are plotted. Again, no P_0 peak is observed, but the majority of the responses have shorter latencies with N_1 at 0.1 ms, i.e., very close to the artifact, and P_1 at approximately 0.18 ms. This means that these latencies are 50-60 μ s shorter than the ones found for the anodic-first condition. There is one SFAP with a longer latency. This originates from the nerve fiber at the edge of the excitation area. This fiber is stimulated just above threshold level and it takes some time before the AP starts propagating.

To clarify the mechanism underlying these latency differences between cathodic- and anodic-first stimulation, the propagation of the AP along a fiber at the center of the excitation area was analyzed in so-called AP-plots (Figs. 8.7^{A,B}). In these plots the deviation (V_k) of the transmembrane potential from the resting membrane potential is plotted for all nodes of Ranvier as a function of their position along the nerve fiber. The tip of the peripheral process is located at 0 mm, the cell body at approximately 2 mm. For the fiber under study the stimulating electrode is located near the cell body, i.e., at approximately 2 mm along the fiber. The different curves in Fig. 8.7 represent V_k at 10 μ s intervals:

$$V_k = V_i - V_e - V_r \quad (8.6)$$

with V_i the internal potential, V_e the external potential and V_r the resting membrane potential. The first curve is taken at stimulus onset, i.e. at the start of the first stimulus phase. For clarity a thick line has been added in each of the two stimulus phases. For instance, during an anodic stimulus (first three lines in Fig. 8.7^A), the external potential is elevated ($V_e \uparrow$), with a much lower internal potential, resulting (Eq. (8.6)) in a negative V_k at the stimulus site. At the same time, because of the potential difference, current is flowing into the nerve fiber, thereby increasing the internal potential at the stimulus site. This current is then transported along the nerve fiber, increasing V_i at the nodes surrounding the stimulus site. At these nodes V_e is only slightly elevated due to the stimulus, leading to a net raise of the transmembrane potential V_k on both sides of the stimulation site (visible in the dashed line of Fig. 8.7^A). However,

the nerve fiber only starts reacting after the second stimulus phase, which induces a positive V_k at the excitation node. After the stimulus, this positive V_k is maintained at the excitation node and the region of positive V_k 's even broadens due to the active processes in the nerve fiber. This process continues until 50 μ s after the end of the stimulus. The peak then splits in two, and two APs start propagating in opposite directions. For clarity the propagating APs have been indicated with gray bars in the plots.

The AP-plot for the cathodic-first MCB condition, where SFAPs with a short latency were found (Fig. 8.6^B), is shown in Fig. 8.7^B. The fiber is stimulated most in the nodes of the central axon next to the cell body at 2.1 mm from the tip of the fiber. This excitation site is due to the use of a peri-modiolar electrode array in this study. The fibers on the edge of the excitation area are excited in the peripheral process, as can be seen in the excitation plots. The first negative stimulus phase induces a positive V_k , leading to a depolarization. Thus the fiber reacts immediately on the first negative stimulus phase and two APs occur, one moving antidromically toward the organ of Corti and one (orthodromic) along the central axon. The second stimulus phase helps to split up the two APs. The difference in AP arrival at the central end of the modeled fiber is approximately 70 μ s, where the cathodic-first situation is the earlier one. The hypothesis that the fiber is initiated during the cathodic phase of the stimulus in both the anodic- and cathodic-first stimulus conditions can not account for this large delay, since the phase duration is as short as 37.5 μ s. In fact, the initiation process is different, and this adds a major contribution to the delay, which is also reflected in the latency difference between the SFAPs from the anodic- and cathodic-first stimulation (Fig. 8.6^A vs. 8.6^B).

The SFAP responses from UMCB condition of the fiber morphology, as shown in Fig. 8.6^{C,D}, have completely different characteristics compared to the MCB condition. The anodic-first stimulus leads to a delayed response with the N_1 peak around the 0.3 ms, followed by a P_1 peak at 0.45 ms. The cathodic-first response (Fig. 8.6^D) shows only a very broad and shallow N_1 peak. Again, the corresponding AP-plots (sub-figures 8.7^{C,D}) will be used to get a better understanding of these wave forms. For the anodic-first stimulus the downward (orthodromic) propagating AP in the UMCB condition (Fig. 8.7^C) behaves similar to the orthodromic AP in the MCB condition (Fig. 8.7^A). On the other hand, the AP propagating upward (antidromic) to the peripheral process is delayed by the cell body. The timing of the delayed SFAP shown in Fig. 8.6^C fits best to this AP, moving to the tip of the fiber. To get an indication of the delay induced by the cell body the AP-plot of a fiber excited at the peripheral process by an apical lateral wall electrode (contact #1) at threshold

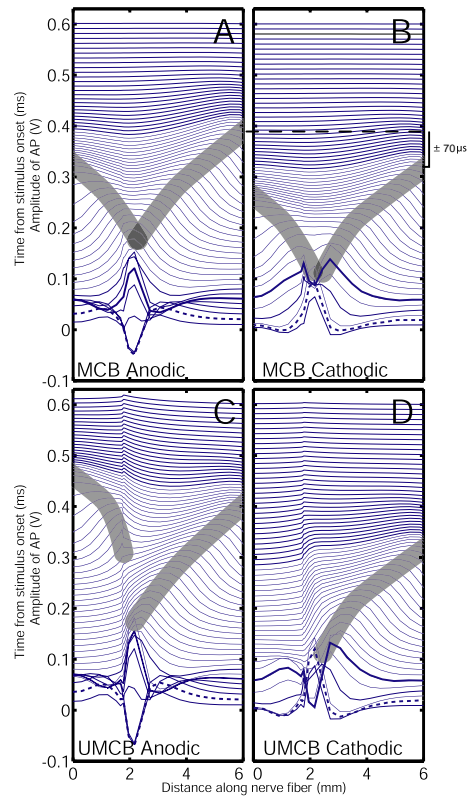


Figure 8.7: In these AP-plots the intracellular potential of a fiber at the center of the excitation area is plotted as a function of the distance along the nerve fiber from peripheral process (0mm) to the cell body at approximately 2 mm and further along central axon (> 2.1 mm). The different lines represent different time steps of $10\mu s$ each, with the bottom line $t=0$. A dashed and a solid line have been added at the end of respectively the first and second phase of the stimulus. The gray bars indicate the trajectory of the AP along the nerve fiber. The excitation is induced by a current 6 dB above threshold in the (A) MCB anodic-first, (B) MCB cathodic-first, (C) UMCB anodic-first and (D) UMCB cathodic-first condition.

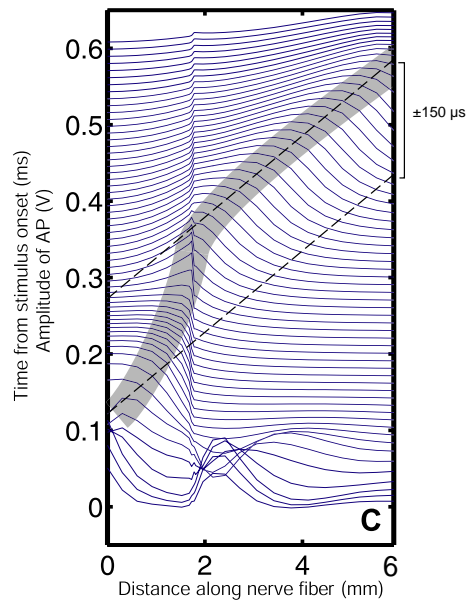


Figure 8.8: The AP-plot for a nerve fiber excited at the peripheral process by an apical contact along the medial wall. The gray bar indicates the trajectory of the AP along the nerve fiber. By extrapolating the trajectory of the AP it is estimated that the delay induced by the unmyelinated cell body is approximately $150 \mu\text{s}$.

level is shown in Fig. 8.8. Without obstructions the AP propagates with a constant velocity, in other words along a straight line. This is clearly the case for distances above 2 mm along the nerve fiber. By extrapolating the trajectory of the AP in the peripheral process it is possible to get an indication of the delay induced. By measuring the vertical distance between the actual trajectory and the extrapolated trajectory, a somatic delay of approximately $150 \mu\text{s}$ is found, which roughly corresponds with the delay found in the calculated SFAPs.

In the case of a cathodic-first stimulus (Fig.8.7^D) the second AP, propagating to the dendrite is not able to cross the cell body, and the potential slowly decreases back to the resting state (Fig. 8.6^D). The first cathodic phase depolarizes the nerve fiber and two APs are initiated as usually. The antidromic AP is propagating very slowly through the cell body. The second positive phase has a negative effect on the depolarization of the unmyelinated elements and leaves a charge on the capacitors, cancelling the sodium influx. In addition, contrary to the situation with an orthodromic AP crossing the cell body, there

is also no pre-somatic region helping the AP to cross the unmyelinated cell body in antidromic direction. This combination makes that the nodes in the peripheral process are not depolarized and the AP is aborted.

All SFAPs described above were calculated at a current strength of 6dB above threshold. Clinically the NRT or NRI capabilities of the implants are mostly used to record IO-curves, which in turn are used to determine the corresponding thresholds. The same experiment has been simulated with the computer model. Clinically, the use of anodic-first pulses is preferable for eCAP measurements because of their slightly longer latencies compared to the cathodic-first pulses (Klop et al., 2004), reducing the interference of the stimulus artifact. Therefore, also for this experiment anodic-first biphasic pulses have been used to calculate five eCAPs at different current strengths with 3 dB intensity steps. In Fig. 8.9 these eCAPs have been plotted for the MCB condition. The bottom line was calculated for the lowest current strength, and shows a small eCAP consisting out of an N_1 and P_1 peak. When the current levels rise, the latency of both peaks is slightly reduced and the peaks become larger. At the highest levels the P_1 peak becomes less pronounced and even the amplitude of the N_1 peak starts to reduce. At the same time a very sharp P_0 peak shows up. The corresponding IO-curve, which depicts the N_1P_1 amplitude, is plotted in Fig. 8.10 together with the same curve, now based on the number of excited nerve fibers. For the lower current strengths both curves are very similar. At higher current levels, however, the calculated N_1P_1 amplitude decreases while the number of fibers that get excited keeps increasing monotonously. The same phenomenon can be seen in the calculated UMCB responses (not shown), where the N_1P_1 amplitude starts to reduce at even lower current strengths. In both cases the reduction of the N_1P_1 amplitude is accompanied by a growing P_0 peak. To get insight in the causes of this phenomenon, the distributions of the MCB SFAPs contributing to the eCAP induced by an anodic-first stimulus have been plotted in Fig. 8.11. The amplitude is color-coded with red designating a positive amplitude and blue a negative one, while the SFAPs are ordered for fibers from base to apex along the vertical axis. Horizontally the time has been plotted. For low stimulation levels (Figs. 8.11^{A,B,C}) the single fiber contributions are very homogeneous, first a blue negative part (N_1) followed by a red positive potential (P_1). When the current strength increases, however (Fig. 8.11^{D,E}), the of the response of the center part changes, and adds a highly different contribution to the eCAP, which leads to the P_0 peak. Similar observations were done for cathodic-first and anodic-first stimulation of the UMCB nerve fibers (not plotted here), but this effect was not detected at all in the cathodic-first stimulation of MCB nerve fibers.

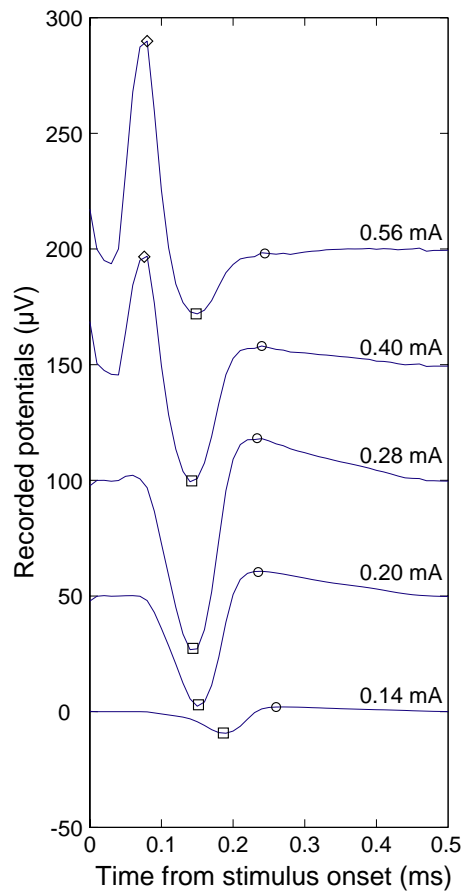


Figure 8.9: The calculated eCAP responses for the MCB condition, as induced by anodic-first biphasic current pulses for five current strengths. The N_1 and P_1 peaks are indicated by squares and circles, respectively. The P_0 visible at higher current strengths are indicated by a diamond.

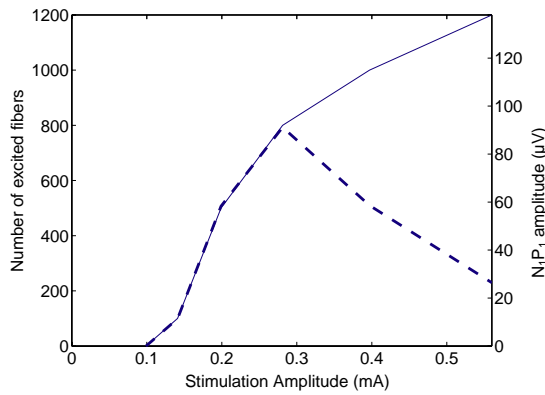


Figure 8.10: The response amplitude (N_1-P_1 difference) (dashed line) and the number of excited nerve fibers against the current strength (solid line) as a function of the stimulation strengths.

The explanation why the fibers in the center of the excitation area have a different contribution to the eCAP at higher stimulus levels, becomes clear from Fig. 8.12. In Fig. 8.12^A the AP plot of an MCB fiber (anodic-first stimulation) at the center of the excitation area is plotted. Due to the large stimulation currents used (0.40 mA, cf. Figs. 8.9 and 8.11^D), the orthodromic AP starts further away from the site where the current is injected, while the antidromic AP is indiscernible. The propagating orthodromic AP is already too far away along the central axon to have any significant contributions to the SFAP as recorded on contact #1. The resulting SFAP is characterised by a large P_0 peak followed by a shallow N_1 peak. The nerve fibers at the border of the excitation area have a very similar AP propagation (Fig. 8.12^B) as the fibers at the center when lower current strengths are used (Fig. 8.7^A). In summary the P_0 peak only occurs at the higher current strengths and originates from the fiber population at the center of the excitation area for both the MCB and UMCB condition.

8.4 Discussion

In this study the mechanisms behind the eCAP are investigated with a computational model. The model consists of a realistic three-dimensional cochlea

model combined with an active, non-linear nerve fiber model. To be able to calculate the eCAP properly, the model had to be extended to allow for recording of the currents generated in the nerve fiber model through the volume conduction model of the cochlea. The generated currents and the recording algorithm used in a long and homogeneous nerve fiber produce SFAPs (Fig. 8.5) with a shape very comparable with more fundamental predictions and actual measurements (Schoonhoven and Stegeman, 1991). From this elementary experiment we conclude that the described algorithm for SFAP calculation from an active nerve fiber model is functioning correctly.

The peak latencies found in the full model, however, do not match the human situation (Frijns et al., 2002; Abbas et al., 1999). The latencies are short, and fit much closer to recorded eCAPs from the guinea pig (Klop et al., 2004). The changes made to the morphology, i.e., adding more segments in the peripheral process, increasing the size of the cell body and removing the myelin layers from the cell body and pre-somatic region, as was indicated by the study of Rattay et al. (2001a), did not yield more accurate eCAPs or SFAPs. However, the changes did result in an upward threshold shift because the capacitance of the cell body worked as a drain for the stimulating current. The main effect ascribed to the unmyelinated cell body by Rattay et al. (2001a), the somatic delay in AP propagation, does occur with the UMCB morphology as can be seen clearly from Fig. 8.8, where is shown that the cell body in our UMCB model causes a delay of approximately 150 μ s.

It seems that, although the morphology has been adapted to the human situation, the shape of the calculated eCAP and thus also the shape of the AP resembles more closely the animal situation on which the nodal kinetics are based (Schwarz and Eikhof, 1987). The amplitude of the calculated response is also smaller (factor 2-4) than the recorded human eCAP response. The various changes to the morphology lead to specific effects in the behavior of especially the UMCB fiber, such as the somatic delay described by Rattay et al. (2001a), but do not lead to an accurate human eCAP response. This somatic delay induces an increased overall latency of the SFAP responses as plotted in Fig. 8.6^C for the UMCB fiber, but the inter-peak interval invariably remains too short. Current investigation at our center focuses on implementing human kinetics (Wesselink et al., 1999) into our nerve fiber model, which appears to influence the shape and propagation speed of the AP and may lead to a more realistic eCAP wave form.

In spite of the fact that the delayed SFAPs as shown for the UMCB condition with anodic first stimulation (Fig. 8.6^C) correlates with the above mentioned

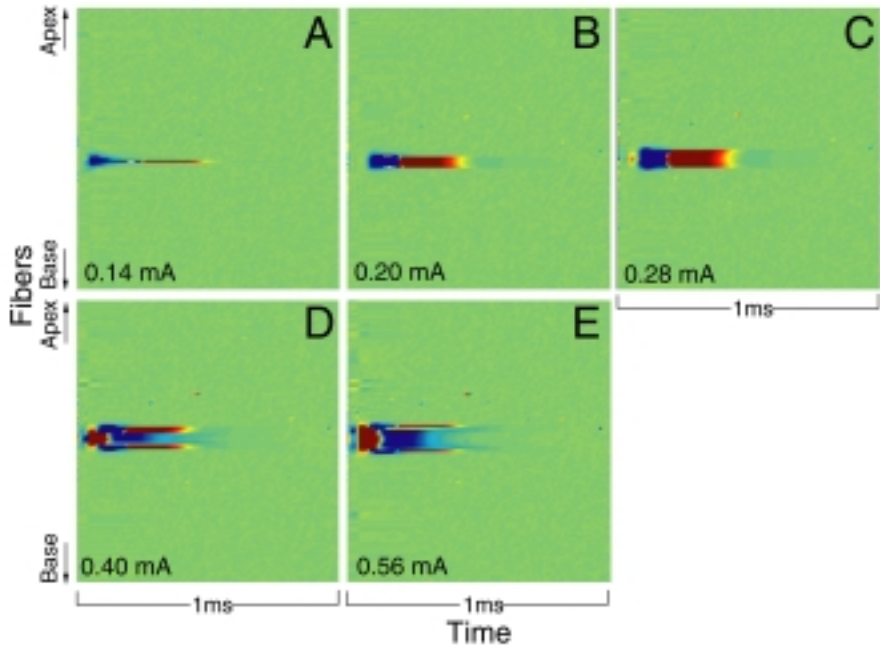


Figure 8.11: The SFAPs for the nerve fibers ordered from base to apex as a function of the time. The amplitude is color-coded with blue a negative potential and red a positive potential. The SFAP-distribution is plotted for the same five different anodic-first biphasic current steps in the MCB condition used to get the IO-curve of Fig. 8.10.

somatic delay, the excitation of the orthodromic AP takes place directly in the central axon, and this AP can thus propagate to the brain without passing the delaying cell-body. The same observation holds for the cathodic-first stimulation (Fig. 8.6^D). In this situation a very normal AP propagates along the central axon as can be seen from the AP-plot (Fig. 8.7^D). Nevertheless a distorted eCAP wave form is recorded (Fig. 8.6^D). Looking closely to the two AP-plots (Fig.s 8.7^{C,D}) one notices that for the anodic-first situation the antidromic AP does have a delay corresponding to the delayed SFAP response, while the antidromic AP is abortive in the case of cathodic-first stimulation. Such a terminated AP could be responsible for the small negative potential seen in the SFAP plot. From these observations one can deduce that the current emitted by the unmyelinated cell body dominates the response in the UMCB condition. The AP trajectory plotted in Fig. 8.7^D might closely resemble the AP plot for degenerated nerve fibers (i.e., without peripheral processes). This could explain the absence of NRI or NRT responses in some patients with neural degeneration while they have very normal auditory sensations and good performance. A recent paper about antidromic action potentials (Miller et al., 2004) already indicated that two APs are present and that the initial positive peak in the eCAP originates from antidromic APs originating from a relatively central site of excitation. This corresponds in part with our finding that the dendrite is responsible for the generation of the P_0 peak. The presence of the P_0 peak at higher current strengths, which originates from the central part of the excitation area, is subject of ongoing model studies. That study indicates that the state of neural degeneration of the fibers has a big influence on the presence of the P_0 peak.

The dominance of the response by the current from the cell body could be reduced if a leaking cable model were used. In that way the whole fiber would emit more current and the SFAP would give a more balanced view on the behaviour of the fiber as a whole. With the current model (Frijns and ten Kate, 1994; Frijns et al., 1994; Frijns et al., 1995), based on the work of Schwarz and Eikhof (1987), it is not possible to add these leaking compartments while maintaining realistic AP conditions without increasing the nodal current densities. This problem was solved by Rattay, who uses a Hodgkin and Huxley (1952) based model, by increasing the sodium, potassium and leakage conductance by a arbitrary factor 10, thereby assuming higher channel densities in the nodes of Ranvier. We hope to be able to add the leaking compartments and a conduction layer between the myelin and the central axon (Halter and Clark, 1991) with the new human kinetics.

Although the morphology of the MCB condition is more like the fiber found in

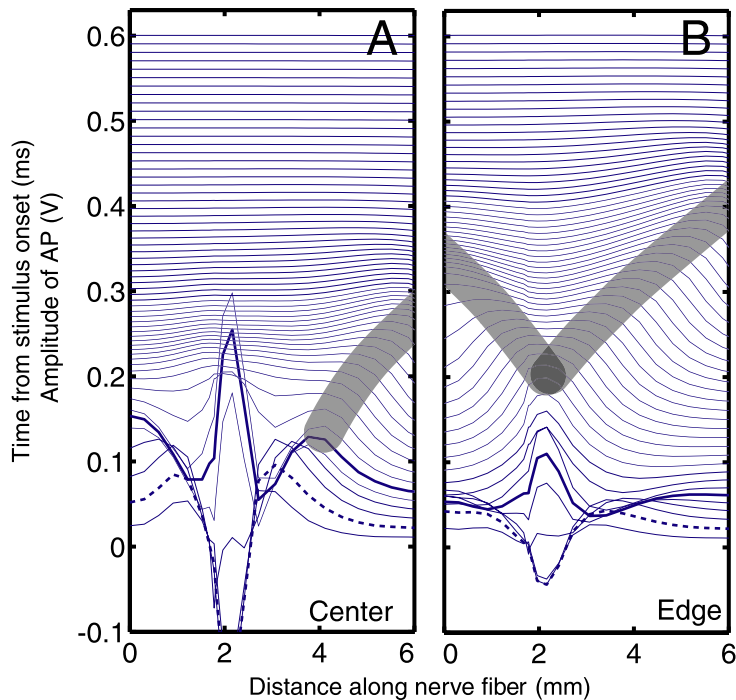


Figure 8.12: The AP-plots for (A) a fiber at the center of the excitation area and (B) a fiber at the edge of the excitation area for a large stimulus current (12 dB above threshold) where the center part of the fibers does not give a contribution to the eCAP response.

animal experiments, it is still a valuable tool to get understanding of the processes occurring during electrical stimulation and their effect on eCAP recordings. For example, an influence of stimulus polarity on the in vivo recorded eCAP was observed (i.e., anodic-first stimulation resulted in a response, which was delayed approximately 60 μs longer than that with cathodic-first stimulation). This has been a topic of recent studies (Klop et al., 2004; Miller et al., 1998), especially since there are direct consequences for using the alternating polarity artifact rejection scheme to measure the eCAP. In our model we find a very similar result (Fig. 8.6^{A,B}) with a delay of 50-60 μs . From the analysis of the AP-plots (Fig. 8.7^{A,B}) it becomes clear that the initiation process of the AP explains the latency shift. The anodic-first stimulus excites the nerve fiber at one place close to the electrode contact, while the cathodic-first stimulus induces two APs just next to the stimulation site. This behavior is similar to that

seen in responses to mono-phasic stimulation with the polarity of the second stimulus phase.

From these AP-plots it is also clear that in most cases for a peri-modiolar electrode array there are two simultaneous APs, one orthodromic, and one antidromic. Both can induce a biphasic response on a recording electrode. As mentioned above, for the UMCB condition the presented responses are actually dominated by the antidromically propagating AP. With this in mind it can be expected that the exact placement of the recording electrode is also of importance. In this study the most apical electrode has been used as the recording contact, probably giving a preference to the antidromic AP because of the proximity and the perpendicular orientation of the peripheral process, while the central axon is directed away from the recording contact. It is conceivable that the ortho- and antidromic APs have a varying relative contribution to the eCAP recorded at the various recording contacts along the array when a scanning method is used to measure spatial selectivity (Frijns et al., 2002; Abbas and Brown, 2000). Apical recording contacts will preferably register the upward moving AP where the basal recording electrodes will mainly see the downward propagating signal. The situation as plotted in Fig. 8.8 with only one AP moving along the fiber is only found in lateral wall electrodes or more apical contacts where the initial excitation occurs in the peripheral process .

It has been indicated above that the currents of the cell body and the surrounding nodes dominate the overall eCAP response. This is deduced from the fact that the latencies of the calculated eCAPs match with the propagation of the antidromic AP passing through these segments. Differentiating between the contributions to the SFAP of various nodes of a nerve fiber is very difficult, because the potentials induced by a single node on the recording contact are some magnitudes larger than the final SFAP. The SFAP is defined by the very small differences between the contributions of the individual nodes. Blocking some nodes for instance from contributing to the SFAP, in an attempt to differentiate between the various segments, disrupts this balance and makes the outcome useless. This makes it impossible to exactly indicate what part of the fiber, or AP trajectory is responsible for a certain change in the recorded SFAP.

The nerve fibers turned out to give other SFAPs at high (Fig. 8.11^C) than at low (Fig. 8.11^D) current strengths. This is also reflected in the AP plot (Fig. 8.12^A vs. 8.12^B). At high stimulation levels the AP is initiated further along the nerve fiber, causing it not to contribute to the N_1P_1 complex of the eCAP. Such high currents induce a mono-phasic neural potential on the recording contact. The nerve fibers at the edges of the excitation area only receive a current

just above threshold due to the distance from the stimulating electrode, and they will produce normal SFAPs. Their contribution to the eCAP is similar to the one seen close to the stimulating contact for low current strengths. The consequence of this behavior for clinical practice is that during eCAP measurements the slope of the IO-curve is shallower than that predicted by the increase of the number of excited nerve fibers. Moreover, the amplitude of the response can saturate or even decrease for larger current strengths. The same phenomenon has also been reported in cat experiments by Miller et al. (1998) (their Fig. 8) who found a decrease in the eCAP amplitude-level function at higher current strengths. He observes, that saturation of the IO-curve does not automatically indicate that all fibers are active and contributing to the recorded eCAP response.

The mono-phasic contribution of fibers from the center of the excitation area resembles a P_0 peak as can be seen clearly in Fig. 8.9. Theoretical models of neural excitation (Schoonhoven and Stegeman, 1991) also predict the presence of such a peak, but then it originates from the AP approaching the recording site. This mechanism was also demonstrated with the current model using a homogeneous nerve fiber (Fig. 8.5). In an actual recording it would not be possible to discriminate between the two sources of the P_0 peak. One would only record its presence. By investigating the individual contribution of the nerve fibers and the trajectories of the APs it becomes clear that the P_0 peak from our model simulations is not the effect of an AP propagating toward the recording electrode but of the initiation of an orthodromic AP further along the nerve fiber, deep in the modiolus.

This necessarily means, that for electrical stimulation, the unitary response theory (i.e., where every fiber contributes the same amount to the whole nerve response) is not valid. The fibers from the center of the excitation area give a different, mono-phasic, contribution where the edges give a bi-phasic response with a typical N_1P_1 pattern. For an electrode, located near the lateral wall, the model predicts excitation in the peripheral processes. In this situation the somatic delay will be added as an extra delay to the AP propagation. This would result in a further delayed SFAP, which also does not fit into the unitary response concept. This variation of the SFAP contributions is less when a recording contact further away from the cochlea, for instance along the auditory nerve trunk is used, like in some animal experiments (Miller et al., 2003; Houben et al., 2000). These remote recording sites are probably better than intracochlear electrodes to study neural recruitment and latency shifts as observed by the brain.

The model extension to allow for eCAP response calculations allows us to study the fundamental principles underlying the eCAP response. The newly introduced fiber morphology with an unmyelinated cell body and pre-somatic region, functions correctly for studies of excitation and propagation of the AP. The dominance of the cell body on the simulated eCAP should however be further investigated and validated. Future studies must incorporate a more realistic human fiber model, which produces more correct latencies. The simulations give insight in the differences between the SFAPs and indicate that at high current strengths the center part of the excitation area does not contribute to the N_1P_1 complex in recorded eCAP responses but gives rise to a P_0 peak. They also explain a negative slope of IO-curves, in spite of monotonously increasing numbers of excited fibers.

8.5 Acknowledgement

This research was financially supported by grants from the Hoogenboom-Beck-Fund and the Heinsius Houbolt Fund. We thank Prof. Dr. J.J. Grote, former head of our department, for his continuing support.

Chapter 9

The consequences of neural degeneration regarding optimal cochlear implant position in scala tympani: A model approach

Jeroen J. Briare and Johan H.M. Frijns
Hearing Research (2006), 214(1-2), 17-27

Abstract

Cochlear implant research endeavors to optimize the spatial selectivity, threshold and dynamic range with the objective of improving the speech perception performance of the implant user. One of the ways to achieve some of these goals is by electrode design. New cochlear implant electrode designs strive to bring the electrode contacts into close proximity to the nerve fibers in the modiolus: this is done by placing the contacts on the medial side of the array and positioning the implant against the medial wall of scala tympani. The question remains whether this is the optimal position for a cochlea with intact neural fibers and, if so, whether it is also true for a cochlea with degenerated neural fibers. In this study a computational model of the implanted human cochlea is used to investigate the optimal position of the array with respect to threshold, dynamic range and spatial selectivity for a cochlea with intact nerve fibers and for degenerated nerve fibers. In addition, the model is used to evaluate the predictive value of eCAP measurements for obtaining peri-operative information on the neural status.

The model predicts improved threshold, dynamic range and spatial selectivity for the peri-modiolar position at the basal end of the cochlea, with minimal influence of neural degeneration. At the apical end of the array (1.5 cochlear turns), the dynamic range and the spatial selectivity are limited due to the occurrence of cross-turn stimulation, with the exception of the condition without neural degeneration and with the electrode array along the lateral wall of scala tympani. The eCAP simulations indicate that a large P_0 peak occurs before the N_1P_1 complex when the fibers are not degenerated. The absence of this peak might be used as an indicator for neural degeneration.

9.1 Introduction

Cochlear implants are widely used as a means to restore at least some hearing in children and post linguually deafened adults. Although there is no absolute pre-operative measure to predict the outcome after cochlear implantation there are some pre-operative parameters that have a predictive value on the performance after cochlear implantation: the duration of deafness and the amount of residual hearing (Gantz et al., 1993; Summerfield and Marshall, 1995; Waltzman et al., 1995; Albu and Babighian, 1997; Rubinstein et al., 1999a; Gomaa et al., 2003; Friedland et al., 2003). From histological studies (Schuknecht, 1993; Nadol, 1990) it has become apparent that unstimulated nerve fibers degenerate after some time, first the peripheral process, also called dendrite, followed by the cell body and the remainder of the nerve fiber. One can conclude from these two facts, the reduced performance after a long duration of deafness and the neural degeneration, that the loss of dendrites is an important cause of the reduced performance obtained with cochlear implants in patients with a long duration of deafness. The question arises if it is possible to adapt the electrode design in such a way that it optimally stimulates the nerve fibers in the cochlea, while neural excitation patterns in patients with degenerated cochleae are also satisfactory.

It is presumed that placing the electrode contacts closer to the modiolus would reduce thresholds and increase the spatial selectivity. The various cochlear implant manufacturers have concentrated on changing the electrode design to direct the contacts towards the modiolus and to place the electrode array in a peri-modiolar position. Advanced Bionics Corporation (Sylmar, CA, USA) tried to accomplish this by inserting an Electrode Positioning System (EPS). The EPS is inserted after implantation of the electrode array along the lateral wall of the cochlea, thus pushing the contacts against the modiolus, while increasing the insertion depth (Kuzma and Balkany, 1999). Cochlear Limited (Sydney, Australia) uses a pre-curved electrode array, the Nucleus Contour, to achieve medial placement. For insertion the Contour is loaded on a stylet, straightening the array. The stylet is removed during the insertion, returning the array to its pre-curved shape in the cochlea and placing it in a peri-modiolar position (Cohen et al., 2002).

The effect of the positioning tools like the EPS or the stylet on the position of the implant in the cochlea can be studied with radiographic imaging or histological studies. From such studies it is apparent that in the case of the EPS the electrode is moved towards the modiolus at the basal part of the cochlea while the most apical electrode contact remains along the lateral wall (Frijns

et al., 2002). The Contour electrode on the other hand tends to be more medial at the apical part of the cochlea while the more basal contacts remain in a more lateral position (Saunders et al., 2002). To obtain information on the functional effects a comparison of patient groups is needed or preferably direct measure of the effects of electrode placement in individual patients. From the patient trials (Saunders et al., 2002; Tykocinski et al., 2001; Donaldson et al., 2001; Cohen et al., 2001) and animal experiments (Cords et al., 2000; Shepherd et al., 1993) it becomes apparent that the modiolar position at least leads to lower thresholds and improved spatial selectivity (Cohen et al., 2003).

The same result was found in various studies comparing eABR recordings during surgery, both with and without the EPS and after stylet removal (Pasanisi et al., 2002; Wackym et al., 2004; Firszt et al., 2003). This allows a direct measure in the same patients for the two electrode positions. In the last two studies the thresholds of the basal electrodes of the HiFocus implant system decreased, while the threshold of the apical electrode reduced significantly with the Nucleus Contour implant system: this is consistent with the imaging evidence that at these positions the implants are placed closer to the modiolus. However, these threshold values tell nothing about the performance of the patients or about the optimal electrode position. Would the best performance be obtained for an electrode array placed uniformly against the modiolus or would it be preferable for it to be placed more laterally in some region of the cochlea?

The main problem with studies describing the above-mentioned comparisons within one patient or effects between groups (van der Beek et al., 2005), is that more than just the radial position of the contacts changes by inserting the EPS or removing the stylet. At the same time, the insertion depth is increased. For instance, is the increased wave V amplitude in the apex of the Contour electrode found by Wackym et al. (2004) the effect of the peri-modiolar position or of the deeper insertion? This is illustrated in a recent study by van der Beek et al. (2005), comparing two patient groups, one with and one without the EPS. In the non-EPS group higher thresholds were found at the basal end of the cochlea. A comparison between the threshold level and the insertion depth, indicated a correlation. It turned out that the elevated threshold without EPS could be compensated for by the surgeon by inserting the HiFocus electrode array further into the cochlea. In other words, the insertion depth can account for some of the reported changes. But for this example one should remember that pushing the electrode in further also results in a reduction of radial distance to the modiolus for the basal contacts.

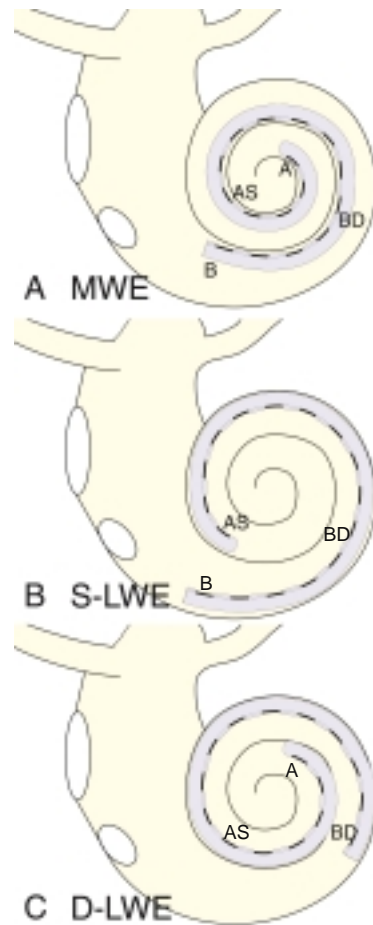


*Figure 9.1: Schematic representation of the electrode positions. In panel **A** the medial wall electrode (MWE) condition and in panels **B** and **C** the shallow and deep lateral wall electrode (LWE) condition respectively. The four different rotational angles along the cochlear duct that are used for the calculations are indicated by letters: **B** ($\Upsilon = 0.2$), **BD** ($\Upsilon = 0.38$), **AS** ($\Upsilon = 1.0$) and **A** ($\Upsilon = 1.48$).*

The individual differences between patients and the amount of neural degeneration is still not accounted for. It could very well be that the optimal position of the electrode array in a cochlea without neural degeneration is different from a situation where most fibers are degenerated. It is, however, at the time of implantation not known where and to what extent the nerve fibers have degenerated. It would, for instance, be valuable to know this during surgery, so that the insertion depth or maybe in the future the radial position of the electrode array may be adjusted during surgery. At this stage, there are only very limited tools available that might be useful for determining the presence of the peripheral processes. One of those tools is the recording ability of the implant (Neural Response Imaging (NRI) in the Advanced Bionics implant systems and Neural Response Telemetry (NRT) in the Cochlear Limited devices) to measure the electrically evoked compound action potential (eCAP) through one of the electrode contacts. There have been some studies that ascribed differently-shaped eCAP responses to the presence of peripheral processes (Stypulkowski and van den Honert, 1984; Lai and Dillier, 2000). The assumption made in these studies is that the cell body induces a delay on the action potential, resulting in multiple-peaked responses when the fiber is excited on the peripheral process combined with fibers excited directly at the modiolar axon.

To find the optimal position of the implant system and study the effects of neural degeneration, a detailed computational model of the human cochlea was used. Within the model, the exact position of the electrode contacts can be controlled and therefore the effect on the neural response of electrode longitudinal and radial locations can be studied. It is also possible to remove the peripheral processes from the nerve fibers and study, again, the effect of electrode locations. To test the usability of eCAP recordings for determining peripheral process survival patterns, the individual contributions of the nerve fibers to the eCAP are calculated both for intact fibers and for fibers without peripheral processes.

9.2 Materials and Methods

The three-dimensional computer model of the human cochlea, as used in this study, consists out of two parts, a geometrical part simulating the volume conduction and a neural part simulating the reaction of the nerve fibers to the induced potential distribution. The geometrical model simulates the electric

conduction through a cochlea, and can be used to study the difference between cochlear shapes, for instance between the cochlea of a guinea pig, a widely used experimental animal for cochlear implants, and the human cochlea (Frijns et al., 2001). In this study the volume conduction model is used to model the difference of the electric conduction through a realistic representation of a human cochlea with a Clarion HiFocus implant (Frijns et al., 2002) at various stimulus locations. To investigate the effects of insertion depth and lateral/medial placement of the electrode contacts, the potentials are calculated for a contact at both the medial and the lateral wall for four different rotational angles (Υ), defined as the insertion in turns measured from the basal end of the cochlea (Briaire and Frijns, 2000a).

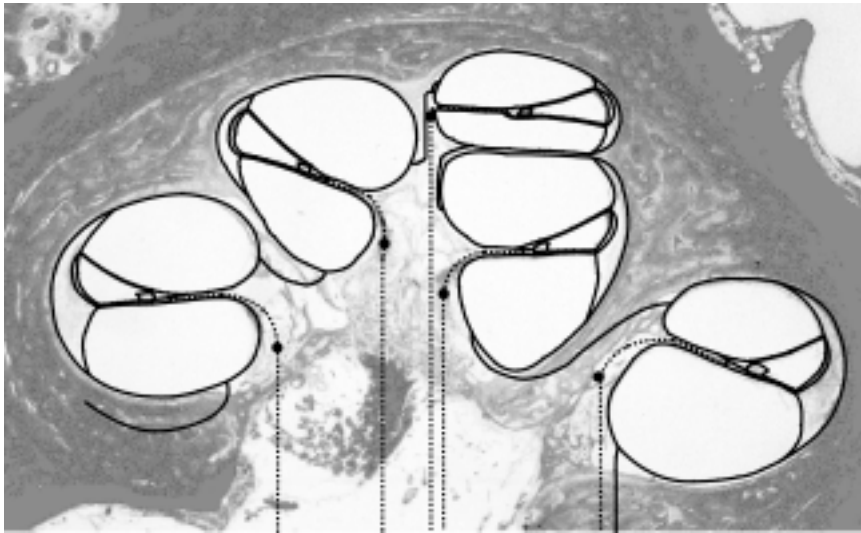


Figure 9.2: Mid-modiolar cross-section of the human cochlea with the cross-section of the volume conduction model shown in bold lines. In the modiolar part of the cochlea the positions of the nerve fibers have been plotted (dotted lines) as well as the approximate locations of the cell bodies within the spiral ganglion (indicated by solid circles)

The first two angles are the places of the most basal contact (B, $\Upsilon = 0.2$) and the most apical contact (A, $\Upsilon = 1.48$) of the electrode along the medial wall (MWE). Fig. 9.1^A shows a schematic representation of the electrode position. Due to the different curvature, the electrode along the lateral wall will not have the same span of rotational angles as the MWE. To compensate for this

problem, the lateral wall electrode (LWE) is computed for two different insertion depths, corresponding to what was done in our clinic to compensate for the threshold rise at the basal end of the electrode array: A shallow insertion (S-LWE) (Fig. 9.1^B) and a deep insertion (D-LWE)(Fig. 9.1^C). The insertion depths of the lateral wall electrodes have been chosen in such a way that the most basal electrode of the S-LWE has the same rotational angle as B and the apical contact of the D-LWE has the same rotational angle as A. The two other positions are then the basal electrode of D-LWE (BD) at $\Upsilon = 0.38$ and the apical electrode of S-LWE (AS) at $\Upsilon = 1.0$. This results in four different rotational angles along the cochlear duct B ($\Upsilon = 0.2$), BD ($\Upsilon = 0.38$), AS ($\Upsilon = 1.0$) and A ($\Upsilon = 1.48$). At each of these positions a contact is matched in both the MWE and the two LWEs. With these locations it is possible to gain insight into what differences can be expected as a function of insertion depth for lateral wall electrodes (S-LWE vs. D-LWE) or the changes that can be expected to occur when an EPS is inserted into the cochlea (contacts B, BD and AS along the lateral wall vs. B and BD along the medial wall and A of the D-LWE).

The calculated potential distributions are used by the neural model to calculate which fibers will react to the stimulus. The nerve fibers are located in the modiolus of the cochlea model with a cell body at the height of scala tympani in Rosenthal's canal and the peripheral process radiating out into the osseous spiral lamina. The tips of the fibers are evenly distributed below the organ of Corti with a spacing of 100 μm . This leads to a total of 299 modeled fibers in the entire cochlea where each modeled fiber represents a group of 100 actual nerve fibers. The peripheral processes are scaled to obtain the correct length for each fiber maintaining the position of the tip as well of the cell body. Fig. 9.2 and 9.3^A show a graphical representation of the geometric position of the nerve fibers.

The neural morphology has been updated to gain a better representation of the human nerve fiber (Briaire and Frijns, 2005). The morphology of the bipolar high spontaneous rate nerve fiber is depicted in Fig. 9.4. The main improvement is the use of an unmyelinated cell body preceded by an also unmyelinated pre-somatic region. These unmyelinated segments have capacitance and resistance related to the number of myelin layers: for this study four layers were used on the cell body and the pre-somatic region. A second minor change concerns the peripheral process which has been divided into six smaller segments rather than the four used in previous studies. These changes are according to the study by Rattay et al. (2001b) who indicated that this is a more realistic representation of the human situation. The details of this model are beyond the scope of this study and are published elsewhere

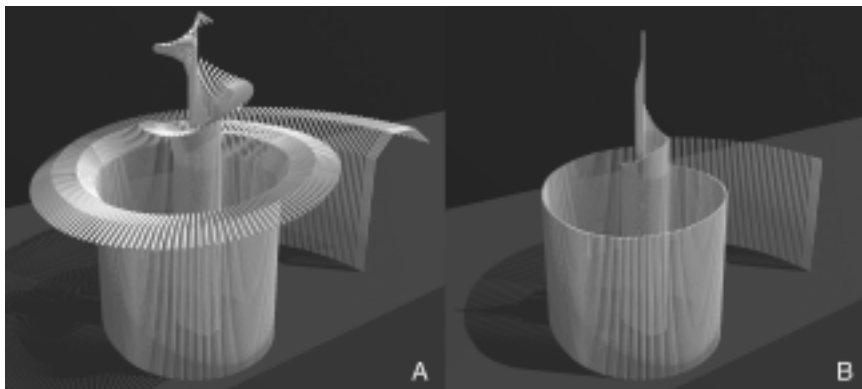


Figure 9.3: A graphical representation of the nerve fibers in the cochlea model. Panel **A** shows the fibers with peripheral processes radiating out of the modiolus and panel **B** the degenerated condition.

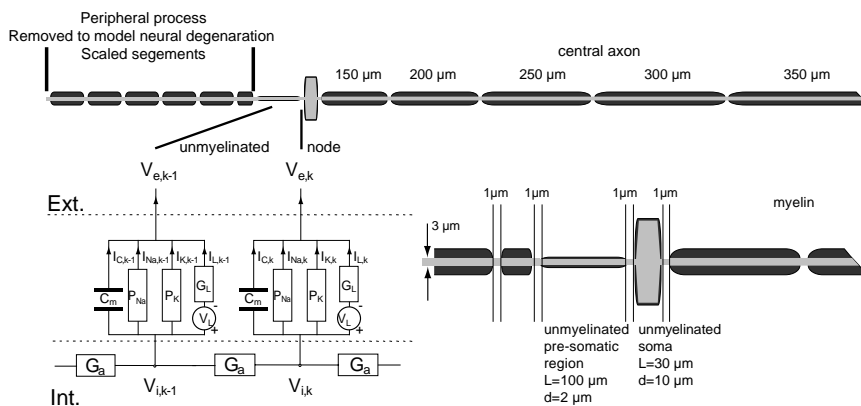


Figure 9.4: The morphology of the bipolar high spontaneous rate nerve fiber. The unmyelinated segments were modeled by adding extra nodes with capacitor and resistor values relative to the number of layers. The peripheral process is divided into six segments. These segments have been removed to model the degenerated fiber state.

(Briaire and Frijns, 2005; Briaire and Frijns, 2000a; Frijns et al., 2000a; Frijns et al., 2001). To study the effect of neural degeneration, all calculations were performed for nerve fibers without peripheral processes (figure 9.3^C).

The results of the computational model are presented in excitation plots. These plots illustrate which fibers fire at a certain current strength by placing all the nerve fibers ordered from base to apex as a function of the distance along the organ of Corti on the vertical axis and the current strength along the horizontal axis. In this study 37.5 μ s/phase cathodic-first biphasic current pulses, without an inter-phase gap, are used. A gray scale is used to represent the initial excitation site.

In clinical practice it is not possible to measure an actual excitation profile. As previously mentioned it is only possible to record the eCAP through the implant system. To provide insight in what can be expected from these recorded eCAPs in case of neural degeneration, the eCAP is calculated from the model nerve fibers. To obtain the eCAP, as would be recorded from one of the electrode contacts, the potential contributions induced by the currents from each of the nodes of Ranvier of all the nerve fibers have to be calculated at the position of the recording contact. To compute these contributions, the currents of the ionic channels in the individual nodes of Ranvier are combined to get the total current at the nodes. These currents are used as input for the volume conduction model. The volume conduction model then gives the potential contribution of all nodes and fibers on the recording contact. These contributions are then superimposed to obtain the overall potential induced by the nerve fibers. The time-dependent eCAP response is derived by computing these potentials at fixed time intervals (Briaire and Frijns, 2005).

9.3 Results

In Fig. 9.5^A the excitation profile is plotted for the basal electrode in the lateral position. The main excitation site is visible around 5 mm ($\Upsilon = 0.2$), defining the threshold at approximately 1.1 mA. A second excitation peak occurs one turn higher (approximately at 20 mm), originating from the close proximity of the modiolar part of these nerve fibers to the stimulating electrode: this effect is known as cross-turn stimulation. These cross-turn excited nerve fibers causes a rapid increase in the number of excited fibers and in this way limit the dynamic range. A dashed line indicates the threshold level, the level at

which the first fibers become excited. A second dashed line indicates the current level at which 40 of the modeled fibers become excited, corresponding with an excitation area of 4 mm along the organ of Corti (I_{4mm}) or the area spanned by approximately 5 electrode contacts. The difference between the threshold and the I_{4mm} level is used as a measure for the maximum dynamic range.

When the electrode is placed in a peri-modiolar position (Fig. 9.5^B) a lower threshold and a lower cross-turn stimulation threshold occurs. The main excitation peak in the medial position is also sharper, in other words more selective. An increase in dynamic range is achieved by placing the electrode against the medial wall. In both positions the main excitation site is directly in the modiolar axon as can be seen from the color. The main excitation site of the cross-turn stimulation is at the peripheral process, this is due to the cochlear anatomy where the basal turn lies further away from the modiolus and encompasses the second turn, as can be clearly seen from the histological cross-section in Fig. 9.2. Scala tympani of the second turn functions as a conductive pathway to the fibers in this turn. The threshold of this cross-turn stimulation is higher when an actual positioner is taken into account, filling up scala tympani with insulator.

For contacts deeper in the cochlea the excitation site of the cross-turn stimulation shifts from the peripheral process to the central axon, as can be seen in the excitation patterns for the contact BD at $\Upsilon = 0.4$ (Fig. 9.5^{C,D}). These more apical contacts have broader excitation peaks compared to the more basal contacts, indicating a more rapid neural recruitment and less spatial selectivity. The lateral wall electrode has the same threshold as the most basal electrode contact, but because of the broader excitation peaks the dynamic range is slightly smaller. The medial electrodes showed a decrease in threshold, but with a constant dynamic range compared to the basal contact.

The observed decrease in threshold when the contacts are moved against the modiolus is still clearly visible at this ($\Upsilon = 0.4$) rotational angle. The same cannot be said for the contacts at $\Upsilon = 1.0$ (AS). Here the thresholds are almost equal for medial and lateral position (Fig. 9.5^{E,F}), only slightly lower on the medial side. Considering the contacts at larger rotational angles, it is clear that the diminished threshold difference between medial and lateral positions is caused by a large reduction of the threshold of the lateral wall contact. In addition, the site of excitation has also changed. The LWE primarily excited the peripheral-process in contrast to the MWE which tended to stimulate in the central axon.

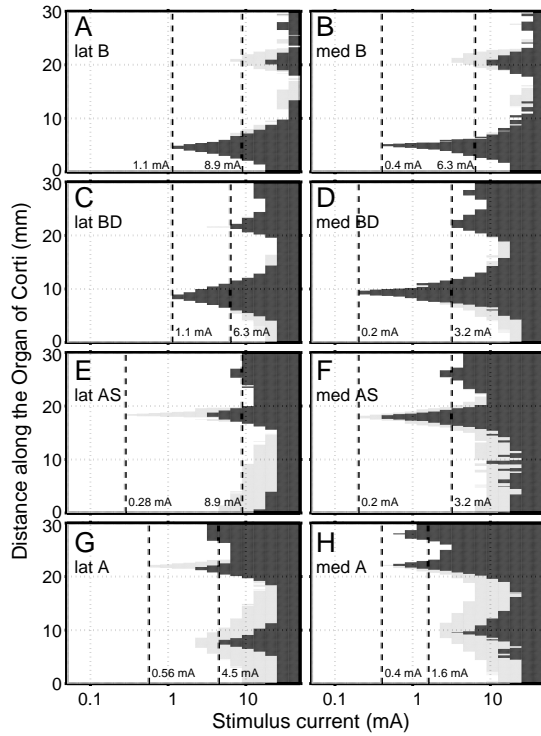


Figure 9.5: Excitation profiles computed with cathodic-first biphasic current pulses of $37.5 \mu\text{s}/\text{phase}$ in the fiber model with peripheral processes. The profile indicates which nerve fibers are excited and where the initial excitation site is (gray shading: peripheral process = light gray, central axon = black, around the soma = intermediate) at a certain current strength. The dashed lines indicate the threshold level and the current level at which at least 40 modeled fibers are excited, equivalent to an excitation area of 4 mm along the organ of Corti. The left column is for positions along the lateral wall of the cochlea, the right column for the peri-modiolar positions. The various rows indicate the rotational angle of the used electrode: **A,B** position B at $\Upsilon = 0.2$, **C,D** position BD at $\Upsilon = 0.38$, **E,F** position AS at $\Upsilon = 1.0$ and **G,H** position A at $\Upsilon = 1.48$.

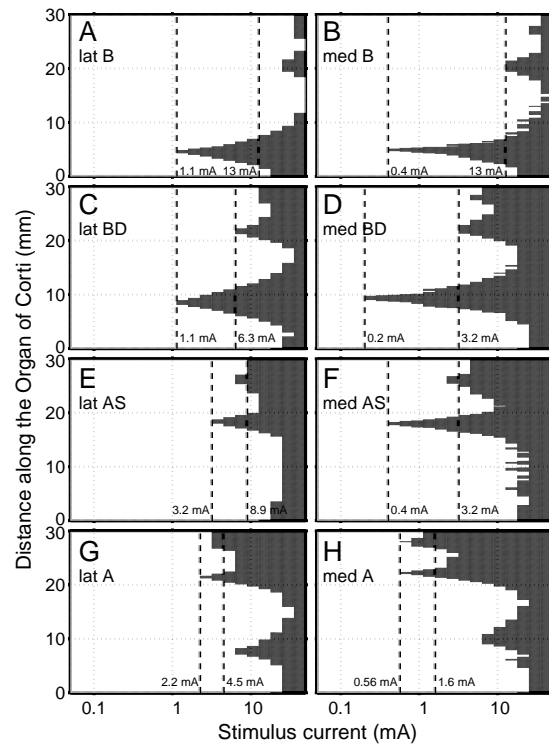


Figure 9.6: The same as Fig. 9.5, but for the degenerated nerve fiber model.

At the position of the most apical contact for both the MWE and LWE the dynamic range is reduced. It is not a broadening of the main excitation peak that causes this reduced dynamic range, but the decrease of the cross-turn stimulation threshold (Fig. 9.5^{G,H}). For the contact A of MWE the difference between the threshold and the cross-turn threshold even reduces to almost zero. The threshold of the medial wall electrode continues to be lower than the corresponding contact at the lateral wall, although the difference becomes very small. The stimulation of the main excitation peak is again mainly in the peripheral process for the LWE. For a cochlea without the peripheral processes due to neural degeneration this has large consequences as can be seen in the outcomes of the model without peripheral processes (Fig. 9.6). In this figure the excitation plots are depicted for the same eight locations in the cochlea as in the previous figure but are calculated with a degenerated nerve fiber model.

For the four basal electrode positions (Fig. 9.6^{A,B,C,D}) there are only minimal changes compared to the full model. The main excitation peaks remain unchanged, as would be expected from the fact that the central-axon is the main excitation site. There is a reduction of cross-turn stimulation, because these fibers were stimulated in the peripheral process. The more apical electrodes depended more on the excitation of the peripheral processes. In Fig. 9.6^E the excitation plot for the truncated nerve fiber model is plotted for the lateral wall electrode at position AS. In the full fiber model it is shown that the threshold is low and the dynamic range large because of the excitation in the peripheral process. Here, however, with neural degeneration the threshold has increased dramatically and the dynamic range is greatly reduced. The MWE at the same position also has an increased threshold, but the change is of a much smaller magnitude. Also in the most apical electrodes 9.6^{G,H} differences in thresholds can be detected. In the degenerated cochlea only a very small functional dynamic range remains for both electrode configurations. In both positions cross-turn stimulation will occur almost at the same current level as the direct stimulation.

As stated above, it might be possible to use eCAP measurements to ascertain the presence of peripheral processes, perhaps even during surgery. Therefore, the neural responses corresponding to the above excitation profiles have been calculated at 9 dB above threshold for both the full nerve fiber model (Fig. 9.7) and the case without the peripheral processes (Fig. 9.8), with the exception of the most apical contact along the lateral wall (Fig. 9.8^C) which has been calculated at 6dB above threshold because of the very limited dynamic range. For brevity, only the results of the two extremes, contacts B ($\Upsilon = 0.2$) and A

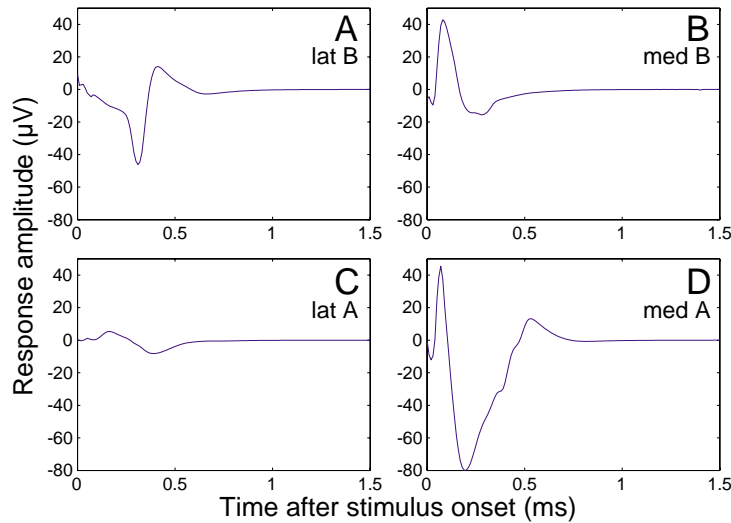


Figure 9.7: The calculated eCAP responses in the non-degenerated cochlea at 9dB above threshold for the basal electrode (**A,B**) and the apical electrode (**C,D**) for the lateral wall position (left panels) and medial wall position (right panels).

($\Upsilon = 1.48$), will be presented. In Fig. 9.7^A the eCAP is plotted for the basal contact of the LWE. There are clear N_1 and P_1 peaks visible at 0.32 ms and 0.41 ms after stimulus onset respectively. When moving toward more apical electrodes the P_1 peak disappears and at the same time a P_0 peak becomes apparent (Fig. 9.7^C). The overall eCAP amplitude also reduces toward the apex.

The medial contact in the base (Fig. 9.7^B) shows directly the P_0 - N_1 combination with the absence of peak P_1 . The amplitude is comparable with the lateral contact. The responses of the electrodes towards the apex have a stable response shape, comparable to Fig. 9.7^B with the exception of the response of the most apical contact: at that position the P_1 peak appears (Fig. 9.7^D). At this apical position at 9dB above threshold a significant amount of cross-turn excitation occurs (Fig. 9.5^H). From the single fiber contributions it can be seen that the P_1 peak originates from these fibers linked to the organ of Corti one turn above the main excitation site.

A main difference between the responses from the fiber model with and without the peripheral processes is the absence of the P_0 peak at all positions

(Fig. 9.8). There is also a large amplitude difference at the basal contacts (Fig. 9.8^{A,B}), the responses being 5-10 times smaller than for the full model (Fig. 9.7^{A,B}). This amplitude difference is not visible at the apical electrodes (Fig. 9.8^{C,D}). This is mainly due to the occurrence of cross-turn stimulation, with many more fibers being included in the eCAPs of the degenerated model at 9 or 6 dB above threshold. Again a small P_1 peak is visible at the medial contact in the apex, originating from fibers connected to the higher turns. Another abnormality is the N_1 peak at the basal end of the cochlea (Fig. 9.8^A), it shows a very irregular pattern, like a double peak. This is also visible for the BD contact (not presented), for which the latter of the two peaks has become the most prominent.

9.4 Discussion

This study describes the effects of the position of the electrode array in scala tympani and the consequences of peripheral process loss on the patterns of neural excitation produced by cochlear implants. The neural responses have been calculated for an electrode array, based on the Clarion HiFocus I, placed in a medial wall position, a lateral wall and a deeply inserted lateral wall position. Cochlear geometry in the base and apex are very different (Frijns et al., 2001) and therefore four longitudinal cochlear positions have been analyzed. This makes it possible to make predictions and describe the changes when an electrode is moved from a lateral wall to a medial wall position as is done when an EPS is placed or a stylet is removed during implantation. The goal is to find the optimal electrode position with a minimum of influence of neural degeneration. Therefore all calculations have also been performed with the degenerated nerve fiber model.

As mentioned in section 9.1, one of the expected gains of a peri-modiolar position should be an improved spatial selectivity (Tykocinski et al., 2001; Kuzma and Balkany, 1999; Aschendorff et al., 1999). The width of the main excitation peak, for instance 9 dB above threshold, is a good measure for the spread of excitation. There is a difference between the basal and apical electrodes: from Figs. 9.5 and 9.6 it is clear that the basal electrodes are more selective when placed medially than laterally, in accordance with the findings of Cohen et al. (2003). However, apically ($\Upsilon > 1$ turn) the excitation from a lateral wall contact is in the peripheral process resulting in a very selective excitation peak. Placing the array against the modiulus, this benefit is lost and the excitation peak broadens significantly. At the same time cross-turn excitation thresholds

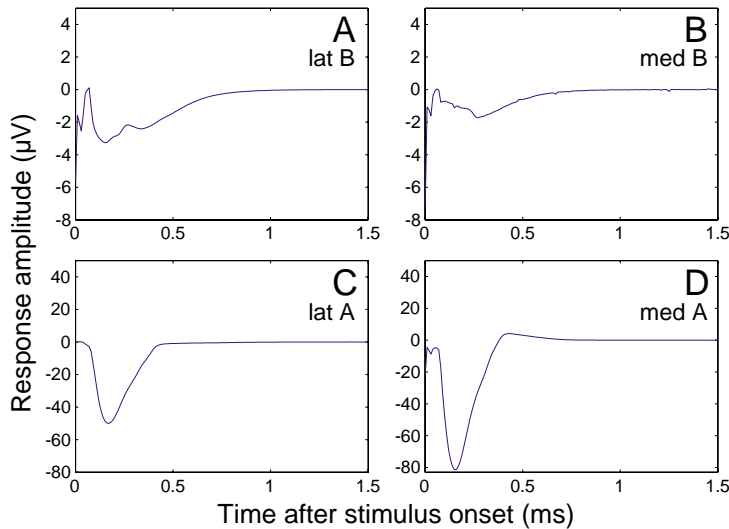


Figure 9.8: The same as in Fig. 9.7, but for the degenerated fiber model, with the exception that the response in panel C is calculated at 6 dB above threshold.

become an influential factor, as they approach the “local” threshold, and thus spreading the excitation to more apical regions.

The best described benefit of the lateral to medial wall placement is the lower threshold, as found in clinical practice (Donaldson et al., 2001; Cohen et al., 2001; Firszt et al., 2003; Wackym et al., 2004), animal experiments (Cords et al., 2000; Shepherd et al., 1993) and initial model studies (Frijns et al., 1995; Frijns et al., 1996a; Frijns et al., 2001). Our model results show a very clear 9-15 dB threshold difference at the basal end of the cochlea for both the full nerve model as well as the degenerated nerve fiber model (Figs. 9.5^{A,B,C,D} and 9.6^{A,B,C,D}). At the apical part of the cochlea, peri-modiolar benefits with respect to thresholds and selectivity are less clear. In the cochlea without peripheral processes the large difference in threshold is still the same (Fig. 9.6^{E,F,G,H}). In the non-degenerated cochlea however, the benefit becomes much smaller, around 3 dB (Fig. 9.5^{E,F,G,H}). This reduced benefit of threshold difference for the medial contact can be explained by the fact that the site of excitation changes for these apical contacts from the peripheral processes to the central axon when the array is moved to a peri-modiolar position. In other words the distance from the electrode contact to the actual excitation site does not change as much as in the basal end of the cochlea where all

excitation takes place in the central axon.

These findings are in accordance with the threshold differences found by Firszt and co-workers (Firszt et al., 2003; Wackym et al., 2004), who reported a significant lower eABR thresholds for the middle and basal electrodes of a HiFocus implant when the contacts are pushed closer to the modiolus with an EPS. They found no significant difference at the apex where there is only a minimal lateral to medial displacement because the EPS does not reach that high into the cochlea.

An effect not taken into account during the two mentioned studies is the change in rotational angle of the electrode contacts. The lateral and medial contacts at the basal end can easily be compared. However, the contacts at the apex also shift to a much higher turn when the array is placed in a perimodiolar position. Contact # 1 of the lateral electrode (Fig. 9.5^E) at $\Upsilon = 1$ shifts upward to $\Upsilon = 1.48$ when pushed toward the modiolus (Fig. 9.5^H). Comparing these two outcomes, a small difference in threshold is visible but also a big reduction in spatial selectivity. In clinical practice it is almost impossible to correct these position changes as the exact position is not known during surgery.

With the model there is no such restriction. With the presented excitation profiles it is possible to investigate what is the optimal location, with respect to selectivity and dynamic range of the implant system. It is even possible to take into account the presence of neural degeneration. In the basal part of the cochlea it is a straightforward decision: the medial contacts have favorable thresholds, are more selective and there is minimal influence of neural degeneration.

From recent studies of Boëx (Boëx et al., 2003) it is shown that it can be favorable to switch off the most apical electrodes when there is much neural interaction. One can see from the excitation profiles at $\Upsilon = 1.48$ (Figs. 9.5^{G,H} and 9.6^{G,H}), that in the apex much neural interaction can be expected. The dynamic range at these high cochlear turns is limited, and the excitation area becomes very broad after the first few current steps due to cross-turn excitation. The exception for this observation is the lateral position without neural degeneration (Fig. 9.5^G), where the excitation takes place in the peripheral process. From these results one could conclude that deep insertion only makes sense with some residual hearing and with an electrode array along the lateral wall of scala tympani.

The profiles at $\Upsilon = 1$ (Figs. 9.5^{E,F} and 9.6^{E,F}) are a transition from the basal

to the apical part of the cochlea. Intact nerve fibers are beneficial for the lateral wall contact, while the medial contacts still have the benefit of an improved threshold. At this rotational angle, the cross-turn threshold starts to decrease, but there is still a large dynamic range left. The exception is the case without peripheral processes and the implant placed along the lateral wall (Fig. 9.6^E): here the dynamic range is very small. At this position there is no clear preference for a medial or lateral wall position, although neural degeneration could reduce the dynamic range for the lateral position.

It would be ideal to know during insertion where the nerve fibers are degenerated and where they are not. At present only the neural response recordings of the implant systems are at our disposal. Stypulkowski and van den Honert (1984) observed that the recorded eCAP sometimes had a double positive peak and suggested that this response arises from two components, delayed responses from fibers excited in the peripheral process and responses with shorter latencies excited in the central axon. This concept is supported by Lai and Dillier (2000) who showed with a simple computational model that it is possible to produce such double peaked responses by combining two $N_1 P_1$ responses with different latency and amplitude. From the excitation profiles it becomes unlikely that this phenomenon can help identify the presence of neural degeneration with implants that mainly excite the nerve in the central axon and where most fibers have the same latency. At the same time it is possible that the fibers at the edges of the excitation area are excited in the peripheral process and the center fibers in the central axon (Fig. 9.5^F) and produce double peaked responses without neural degenerations.

The absence of the P_1 peak in the responses without a peripheral process could be a better indication although this condition also occurs in the non-degenerated model. A close examination of the AP-trajectory along the nerve fiber indicated that these responses without P_1 very often originate from a discharge of the cell body (Briaire and Frijns, 2005). That study suggests that the main source of the eCAP recording by intracochlear contacts originates from the cell body, and in the case of direct stimulation in the central axon, from the antidromic AP propagating toward the peripheral process. This is in correspondence with the responses presented in this paper where only very small “discharge shaped” responses are found in the fibers without a peripheral process (Fig. 9.8^B). It is not possible for an AP to move through a cell body when there are no segments on the other side. In the situation of the non-degenerated model the AP can approach the cell body and move through it to the peripheral process, explaining the P_0 peak. The presence of the P_0 peak can therefore only occur in the fibers with the peripheral process. In a recent

study Miller et al. (2004) also found a P_0 peak preceding the N_1P_1 complex with anodic monopolar stimulation. Similar to our findings he suggests that the excitation in the central axon produces both orthodromic and antidromic action potentials. In this case, the antidromic AP, the one going through the cell body, dominates the recorded intracochlear potential. The actual recording of this peak is difficult due to the stimulus artifact in real measurements, but it is worthwhile to investigate this phenomenon .

For more detailed and more accurate predictions from the computational model more refinements have to be incorporated. Improvements currently built into the model are adaptations of the kinetics to match the human fiber more accurately (Wesselink et al., 1999). Secondly the myelin sheaths are improved to simulate a more realistic leaking transmission line-like model (Halter and Clark, 1991). Ideally these improvements will lead to eCAP responses with more accurate inter-peak latencies and will reduce the dominance of the cell body on the response a little, although the fact that the cell body is unmyelinated will result in a much larger current ejecting from this part of the nerve fiber than out of the peripheral process and the central axon. Increasing the number of calculated nerve fibers should enable us to study the differences of the fiber behavior at the edges and the center of the excitation area.

The differences between degenerated nerve fibers and the complete fiber calculation could also explain why it is possible to have a subjective percept in patients without being able to record any eCAP with the use of intra cochlear contacts. The responses of the degenerated fibers are much smaller and are hard to identify when a stimulus artifact is also present. An improved back-measuring system is needed to be able to record these responses in actual patients.

The model is used in this study to investigate the optimal placement of the electrode array with respect to the threshold, spatial selectivity and the dynamic range. Guided by these findings a new electrode design is being developed based on the original HiFocus concept. The new electrode array, HiFocus 4L, aims at a medial position on the basal end of the cochlea and a lateral wall position for the most apical contacts. Initial temporal bone studies have indicated that the target positions are achieved with the new electrode array and that minimal damage is done to the cochlear structures (Frijns et al., 2004). The starting point for this study was the existing HiFocus electrode design with contacts directed towards the modiolus. This contact orientation is also present in the Nucleus Contour electrode array with the difference that the contacts are slightly rounded at the edges. Other, older electrode designs

also used contacts directed in other directions: the Clarion pre-curved and the Laura electrode array. In contrast, the Nucleus straight array used bands around the carrier. In this study the radial position of the contacts was used to investigate the effects on the excitation patterns, but additional variables, like the contact orientation, could be considered in a effort to further optimize the electrode design.

9.5 Acknowledgment

This research was financially supported by grants from the Hoogenboom-Beck-Fund and the Heinsius Houbolt Fund. We wish to thank Prof. Dr. J.J. Grote, for his continuing support.

Chapter 10

Concept and initial testing of a new, basally perimodiolar electrode design

J.H.M. Frijns, J.J. Briaire, A. Zarowski, B.M. Verbist
and J. Kuzma

In R.T. Miyamoto (ed.), Cochlear Implants, Vol. 1273
of International Congress Series (2004), Elsevier

Abstract

A recent study showed that 25 patients with the CII cochlear implant system (HiFocus I electrode) with partially inserted positioner obtained a significantly better speech perception than a demographically identical group (20 patients) with the electrode alone. CT-scans in the positioner group showed basally a perimodiolar, and apically a lateral electrode position. A computational model of the human cochlea also predicted that a perimodiolar position of the electrode array is best for basal contacts, while a lateral position is preferable for more apical ones. This study reports the concept and initial testing of a new, one-piece, electrode design, intended to yield a similar position of the contacts and suitable for cochleae of all sizes with minimal insertion trauma. Prototype electrodes were inserted in fresh human temporal bones and the position of the contacts was verified with multi-slice and high-resolution CT-scans prior to a careful dissection, documenting the insertion trauma. This showed that the new electrode is able to attain the desired position with minimal damage to the intracochlear structures. It is concluded that the new electrode meets its design criteria, and is worth a clinical evaluation as it promises good speech perception results without the negative effects reported for the positioner.

10.1 Introduction

Perimodiolar (also called modiolus hugging) electrodes are intended to place the contacts in close proximity to the excitable nerve fibers in the modiolus in order to reduce stimulation levels, to produce more selective stimulation and -ultimately- to achieve better speech understanding. Frijns et al. (2002) reported good speech perception outcomes in an initial group of patients implanted with the Clarion CII implant with HiFocusI electrode with separate positioner. The positioner was deliberately only inserted partially, in order to achieve a perimodiolar position for the basal contacts, while the more apical contacts were intended to be in an outer wall position. This was based on a computational modeling study (Frijns et al., 2001), which predicted that a perimodiolar position increases the spatial selectivity and the dynamic range in the basal turn. Moreover, it predicted for apical positions that modiolar proximity will not lower the excitation threshold, but that it will reduce the dynamic range.

This is a consequence of the specific anatomy of the human cochlea. As contrasted to other species, in humans the distance from the medial wall of the scala tympani to the nerve bundle in the modiolus is much larger in the basal turn than in the middle and apical turns. In more apical sites a position near the outer wall is therefore more desirable to avoid so-called cross-turn stimulation. This phenomenon results from intra-modiolar excitation nerve fibers, originating from more apical cochlear turns than the one the stimulating contact is in, unintentionally leading to lower-pitched sensations.

In July 2002 the positioner was withdrawn from the market as it was identified as one of the possible causes of post-implantation meningitis (Cohen et al., 2004), and from thereon the HiFocusI electrode was used without positioner. A recent comparison of the outcomes of demographically comparable groups of 25 patients with and 20 patients without a positioner (Van der Beek et al., submitted) showed a significantly ($p < 0.05$) reduced speech perception for the group without positioner. At 3 months post hook-up the monosyllabic CVC word scores (sound only) were 60% and 45%, respectively. This difference persisted after 6 and 12 months. The main differences between the electrode positions are illustrated in Fig.10.1: With partially inserted positioner the basal part of the array is close to the modiolus, as intended, while the entire array is located near the outer wall without positioner. In addition, the insertion depth without positioner is typically reduced by 90° to 180° since the electrode follows the outer curvature.

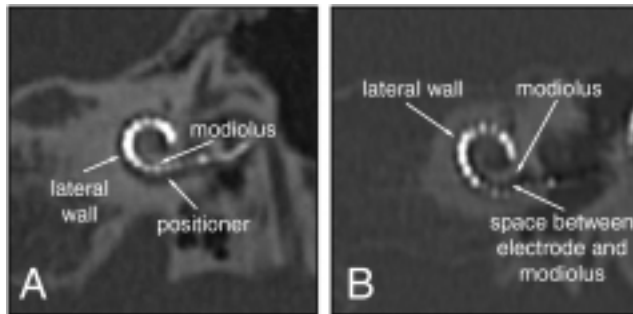
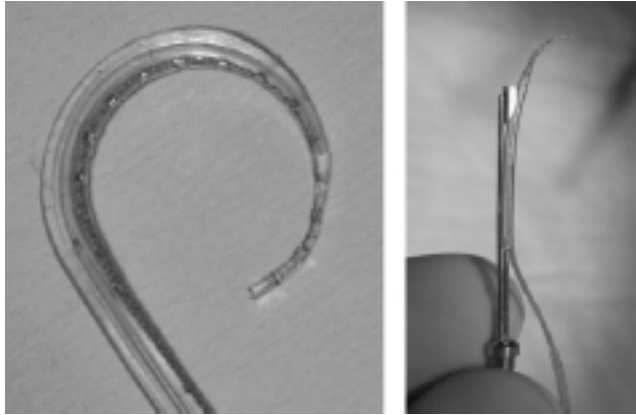


Figure 10.1: A. Multi-slice CT of a typical patient implanted with the HiFocus1 electrode and separate positioner B. Multi-slice CT of a typical patient implanted with the HiFocus1 electrode without positioner

To overcome these shortcomings a new electrode array was designed, called the HiFocus4L. This is a one-piece electrode, intended to yield a similar position of the contacts as the HiFocus1 with partially inserted positioner and suitable for cochleae of all sizes. This paper presents an analysis of electrode position and insertion trauma in temporal bones, using CT-scans and micro-dissection.

10.2 Materials and methods

Two fresh human temporal bones were prepared and scanned with a micro-CT-scanner and with a clinical multi-slice CT-scanner using our clinics routine protocol with 0.5mm slice thickness (Verbist et al., submitted). After the formation of a cochleostomy (1.1x1.5mm), which included the round window, the HiFocus4L electrode (Fig.10.2^A) was inserted with the insertion tool shown in Fig.10.2^B. The cochleostomy was sealed with soft tissue and the electrode lead sutured to the bone. Immediately thereafter the bones were scanned with both scanners and a careful microdissection, documenting any intracochlear damage, was performed.



*Figure 10.2: **A.** The HiFocus4L electrode has contacts directed towards the modiolus. It has a very thin tip and is broader at the base. It is precurved with a large radius to follow the outer wall curvature. The electrode dimensions are chosen in such a way that it fits in even the smallest cochleae. **B.** The electrode is inserted with a special tool. It is pushed off a stilet, which does not reach the tip of the electrode.*

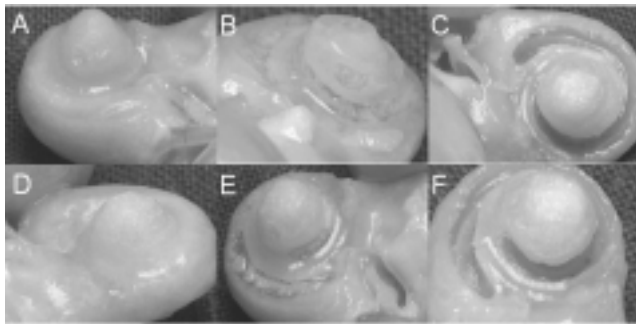


*Figure 10.3: **A.** After electrode insertion the cochleae were isolated from the temporal bones. **B** Next, the endosteum of the scala vestibule was exposed. **C.** Looking through the intact basilar membrane the electrode is shown to be in the desired position. **D.-F.** The same as A.-C., now for the second temporal bone.*

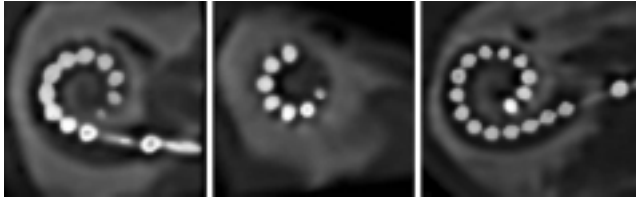


Figure 10.4: **A.** Multi-slice CT (MSCT) of the basal part of the first temporal bone, showing good modiolar proximity. **B** MSCT of the apical portion of the first temporal bone, showing 530° insertion depth and a lateral position of the apical half of the array. **C.** MSCT of the second temporal bone, showing the position of all individual electrode contacts.

10.3 Results

The insertions were uneventful and the tool handling turned out to be easily performed single-handedly. Microdissection (Fig.10.3) showed full scala tympani insertions and did not reveal any damage to the intracochlear structures, apart from a minor lifting of the basilar membrane without further damage at 180° insertion depth in one temporal bone. Both transillumination of the temporal bones and the multi-slice CT-scans (Fig.10.4) demonstrated that the electrode contacts were close to the modiolus in the basal turn and gradually more lateral in more apical portions. The insertion depth was at least one turn in both cases. The micro-CT-scans confirmed these findings.

10.4 Discussion

The abovementioned observations (van der Beek et al., submitted) that speech perception with basally perimodiolar electrodes is better than with conventional, outer wall electrodes, are in line with earlier model predictions. The HiFocus4L electrode, tested in the present study, is a single-piece design, intended to achieve the same contact positions as with the HiFocus1 with partially inserted positioner. This study has shown that it meets its design criteria without causing substantial intracochlear damage. Therefore, the design will be evaluated further in a histological study. The next step will be a clinical

evaluation of its potential to improve speech perception.

10.5 Acknowledgment

The authors want to acknowledge the Heinsius-Houbolt fund for their funding.

Chapter 11

The model as a clinical tool: General discussion and future perspectives

The development of a computer model, from a rotationally symmetrical guinea pig cochlea model to a fully three dimensional human cochlea model with realistic implants and eCAP recording capabilities, has been described in this thesis. This comprehensive model can be used for clinical applications and evaluation of implant design changes. In the final chapter of this thesis the capabilities of the current model are described as well as the steps needed to produce more accurate predictions and allow for for patient specific simulations.

With the current model it is possible to calculate the excitation patterns of various electrode arrays placed at different positions in the scala tympani (chapters 5 and 9). In chapter 10 an implant design is presented which is created on the basis of insights in modeling such as shown in chapter 9. Data from the same model can be used to analyze the outcomes of clinical studies describing the performance and parameters of different implants (van der Beek et al., 2005).

The simulated eCAP recordings allow detailed analysis of the single fiber contributions to the overall eCAP. The findings of chapter 8 are in substantial agreement with eCAP data from animal experiments in our center (Westen et al., in preparation). The animal experiences show strong non-linearities in the I/O-curves at high current levels. With the same eCAP simulation method, more complex experiments can be analyzed like a dual-masker ‘apple-core’ selectivity measurement (Klop et al., in preparation). The eCAP analysis gives also insight in the psychophysical equivalent of the apple core eCAP recordings (Dingemans et al., 2006).

The results obtained with the new human cochlea model are also used to get insight into the fundamental working of speech coding strategies. For a long time, multi-polar stimulation has been used to improve spatial selectivity of electrical stimulation. An alternative way to use multi-polar stimulation is by simultaneous stimulation of two neighboring electrodes, so-called current steering (Donaldson et al., 2005). In this way it appeared to be possible to elicit an intermediate percept between the two contacts. Our model gave insight in the excitation patterns during current steering with respect to changes in loudness and pitch (Frijns et al., 2005; Briare et al., 2006). One remarkable finding is that the generally valued high spatial selectivity is a drawback for improving frequency information through current steering. The model data are now used to set up detailed psychophysical experiments.

11.1 Tuning the implant

Although cochlea models can be used to understand stimulation patterns and current pathways, there are still some improvements needed before predictions for individual patients can be made. The nerve fibers in the computational model have a straight trajectory from the organ of Corti to the modiolus. In the *in vivo* situation, the fibers are bundled when they pass the habenula perforata. Recent histological findings have also shown that the length of the spiral ganglion is shorter than the organ of Corti (Sridhar et al., 2006). This length difference is generally due to the course of more apical nerve fibers. To be able to predict accurately the functioning of deeply inserted electrode arrays, these discrepancies have to be taken into consideration.

The main consequence of the torqued trajectory of the apical fibers is probably a shift in the tonotopy of the excitation function. The Greenwood tonotopic distribution, along the length of the organ of Corti (Greenwood, 1990) is generally used to estimate the frequency distribution along the electrode array. The excitation profiles in chapter 9 show clearly that in most situations the nerve is excited in or just after the spiral ganglion. In other words, the Greenwood map does not describe the frequency distribution along the length of a cochlear implant. As a consequence, when being fitted according to Greenwood's formula, patients are expected to have a distorted frequency alignment across the electrode contacts (Dorman et al., 2007; Boëx et al., 2006). This causes higher harmonics of a presented signal to be presented at the wrong place by the implant, and consequently at the wrong pitch, making the signal sound out of tune.

Although the current model can predict the site of excitation the length difference between the Spiral Ganglion and the organ of Corti has not been taken into account. It could also be reasoned that specific anatomical variations can have an influence on the exact excitation area of a specific electrode contact. Computational modeling can help to map the correct frequencies to the excitation site of the individual patient, but a detailed model of the implanted cochlea of each individual patient is required to accomplish this.

11.2 The individual patient's cochlear model

A considerable problem in obtaining a patient's individual cochlear model is the cochlear size. Until now, only one single cochlear model is used for all

calculations. This is sufficient for general trends and predictions. However, to achieve patient specificity, the cochlear size and the model size have to match. For instance, the insertion depth or the modiolar distance will vary depending on the cochlear size (Postnov et al., 2006). This implies that if the size or the shape of the cochlea is variable, the anatomy has to be analysed, for instance, on the basis of CT images. In chapter 5 is indicated that the shape of the cochlea can also have a large impact on the outcome of electrical stimulation.

To estimate the cochlear size and the exact location of the electrode contacts, detailed pre- and post-operative CT or MRI images are needed. In a recent study in cooperation with the department of Radiology, the detail of multi slice CT images has been improved (Verbist et al., 2005). This improvement allows assessment of the precise intra-cochlear position of the electrode array and visualization of individual electrode contacts. An implementation must be made to be able to match the geometry of the cochlea model and the implant position to the data from the patient's CT scans. CT scans can also be used to visualize extra-cochlear structures. These extra-cochlear structures can influence the current pathways or cause unwanted side effects of the electrical stimulation. For instance, when the facial nerve is in close proximity of the cochlea, it can function as a current pathway out of the cochlea. This can result in unwanted stimulation of the facial muscles. These current drains through the facial nerve canal can also be identified by Electrical Field Imaging (EFI) measurements (Vanpoucke et al., 2004), an objective potential recording through the implant device.

11.3 Objective measures

EFI records the potential distribution through the scala tympani by measuring the potential on all contacts along the electrode array when a single contact is stimulated. With this technique, short circuits and possible extra-cochlear current drains can be located. It may even be possible to visualize ruptures in the basilar membrane, created when the electrode was inserted. With some minor adjustments, the volume conduction part of the computer model can predict EFI responses from various electrode positions and extra-cochlear current drains. The influence of these extra-cochlear structures on excitation patterns can be analyzed with our cochlear model by incorporating the extra-cochlear structures. These additions to our model are comparable amendments to the investigation of the effects of the bulla around the guinea pig cochlea described in chapter 3. Based on the results described in chapter

3, one could predict only minor changes to the excitation pattern. However, specific placement of the reference electrode contact in the skull and some favorable current pathway, like through the facial nerve, could result in a local change in threshold.

The eCAP simulation capabilities, described in chapter 8, are a valuable tool for the investigation and development of new recording paradigms. For instance the non-linearities which cause ceiling effects in the I/O-curves, as mentioned at the beginning of this chapter, have always been ascribed to current source saturation. The model analysis described in this thesis indicates that the reduced amplitude is the result of overstimulated fibers in the center of the excitation area. This assumption led us to initiate an animal experiment in order to prove the existence of these non-contributing nerve fibers in the center of the excitation area. The same experiment was also performed in the computer model (Westen et al., in prep). This is an example of how model findings can direct eCAP recordings while on the other hand, eCAP recordings can eventually validate the model outcomes.

It should be noted that most eCAP recordings are performed on relatively high stimulation levels, as has been shown in chapter 6. The subjective threshold is always much lower than the recorded objective threshold. One of the findings is that eCAP recordings at such high current levels are less reliable, because multiple different single fiber contributions are combined in a single eCAP. To obtain really functional eCAP recordings, the stimulus level for eCAP recordings will have to be lowered to approximately this subjective threshold, in order to record from very small sub-populations of excited nerve fibers. Therefore, it is essential that in the future the recording capabilities of the cochlear implants are improved to be able to record eCAPs at appropriately low current levels.

Although the model used in this thesis calculates the eCAP responses, there exists a discrepancy between the N_1 and P_1 peak latencies of human recordings and their simulated counterparts. The calculated responses have latencies that correlate more closely to the guinea pig nerve than to the human one, even with the inclusion of a human-like non-myelinated cell body (chapter 8). This may be explained by the kinetics which underlies the nerve fiber model. These are based on voltage clamp measurements in rat and cat motor nerve fibers at mammalian body temperature (Schwarz and Eikhof, 1987; chapter 2). To improve the accuracy of the eCAP calculations, the kinetics underling the nerve fiber model has to be updated to the human situation (Wesselink et al., 1999; Schwarz et al., 1995). Further model improvements can be made by including leakage through the myelin sheath and a conduction layer between

the axon and this neurilemma (Halter and Clark, 1991).

11.4 Keeping up the pace

The neural kinetics used in the model has also a large influence on the refractory properties of the nerve fiber. With the increased stimulation rates of modern processors, this neural property has become more and more important. For instance, the Clarion CI implant used stimulation rates up to 6.5 kHz, the new HiRes 90K implant (equal to the CII) from Advanced Bionics is capable of a sustained stimulus rate of 92 kHz (chapter 6). There is no clear understanding how these very high rates may influence the much slower nerve fibers.

With the Conditioned CIS (CCIS) strategy the slow recovery property of the nerve is used to reintroduce stochasticity in the implanted cochlea. With CCIS, a high rate unmodulated pulse train puts all nerve fibers in a refractory state. The variable recovery time of the individual fibers introduces a stochastic distribution of those fibers which are excited by the relatively low-rate speech carrying stimulus. The CCIS principle, possibly leading to the occurrence of so-called stochastic resonance, has been examined extensively in a very detailed nerve fiber model (Rubinstein et al., 1999b), on a supercomputer.

Although our model has refractory properties, stochastic behavior is not incorporated. The detailed model of Rubinstein (Rubinstein et al., 1999b), which includes individual ion channels, does not easily coexist with the large number of fibers needed in our full cochlea simulations. Therefore, an approximation is required, which introduces stochastic behavior without the obligation of extreme computational efforts. With such an improved fiber model, neural behavior induced by the new high rate stimulation modes can be analyzed.

11.5 The future of cochlear implants

Optimizing the implant capabilities after implantation, neglects the opportunity of optimizing the position of the electrode array in the cochlea for a specific patient. With the right imaging techniques (Verbist et al., 2005) it should be possible to obtain detailed pre-operative information on the cochlear anatomy, these data could then be used to find the optimal electrode placement for the individual patient. Current manufacturing processes are focused on a limited

number of electrode designs, following the “one fits all” principle. With the current manufacturing processes individualizing contact locations would require unrealistic efforts and costs to produce the numerous design variations.

All currently produced clinical electrode arrays are manufactured by hand, have the same wire bundle principle and use the same materials (silicone and platinum iridium) as the arrays produced in the last 20 years (Spelman, 2006). Alternatives are being developed but are until now not used in humans. For instance Corbett et al. (2004) developed a flexible, layered array on substrates of biocompatible dielectric material. An other approach is using thin film electrodes, like the high-density electrode array with 32 stimulating sites, described by Bhatti et al. (2005). These arrays could be build with microcircuit techniques. Micro-electro-mechanical (MEMs) manufacturing techniques, would not allow only automatic fabrication or an increase in the number of electrode contacts, but also integration of other circuits into the array (Wang et al., 2005a).

To optimize the array to a specific patient's cochlea, one should be able to control the direction the electrode contact is oriented. An electrode array with integrated circuits could provide a programmable number of electrode contacts. This would potentially allow for controlling the orientation of the contacts even after implantation with a single electrode design (Harrison et al., 2005). The inclusion of piezoresistive polysilicon sensors in an array can give information on shape of the array during insertion and the amount of tip contact with the cochlear structures. In turn, this would allow for active feedback on the status of the electrode array during the surgery (Wang et al., 2005b; Wang et al., 2005a; Tang et al., 2005). This could be of help with the extraction of the stylet with pre-curved electrode arrays like the Contour Advanced electrode from Cochlear Ltd. or the Helix from Advanced Bionics Company. Future arrays might even be guided around the corner and towards the modiolus with for instance shape memory material (Spelman et al., 1998). This would eventually lead to an implant that can be inserted without damaging the delicate cochlear structures at all and with contacts that are positioned in the most favorable orientation for the individual patient.

Another source of cochlear damage after cochlear implantation is the adhesion of for instance blood or bone dust on the electrode array. These inserted particles, but also the array itself, can become a source for inflammatory reactions, fibrous tissue growth or even ossification inside the cochlea resulting in structural changes or nerve fiber damage. Because of the ever shifting criteria for implantation, more and more patients are implanted with residual

hearing, and these damaging effects are becoming more important. These effects could be suppressed for instance by coating the array with corticosteroids (Paasche et al., 2006a; De Ceulaer et al., 2003). There are indications that these single dose drug delivery methods have a favorable effect on the electrode impedance. By incorporating the drug in for instance a dissolving polymer the delivery time could be spread out over several weeks. Continuous delivery or multiple dose delivery would require a drug delivery canal into the cochlea (Paasche et al., 2006b; Jolly and Hochmair, 2006). The Med-El company is developing a clinical array with a drug delivery canal that can be attached to a drug delivery pump through a micro-septum connector, allowing for exchange or removal of the drug pump without opening a canal, which would be a pathway for bacteria, directly to the perilymph (Jolly and Hochmair, 2006).

These long term drug delivery systems are of importance for the application of neurotrophic factors. Neurotrophic factors have protective effects on auditory neurons, which are considered to be among the key factors defining the efficacy of cochlear implantation (Richardson et al., 2006; Gillespie and Shepherd, 2005; McGuinness and Shepherd, 2005). One step further along the line is not just maintaining the spiral ganglion cells but to actually regenerate them (Rask-Andersen et al., 2005). This process requires pharmacologic intervention to actuate and to maintain the newly formed fibers. Although new auditory fibers would give functional benefit for cochlear implants, the final stage would be to also regenerate the hair cells (White et al., 2006; Izumikawa et al., 2005; Kawamoto et al., 2003). Some initial work on producing easily available stem-cells for the regeneration of spiral ganglion cells is in progress at our oto-biological laboratory (Huisman et al., 2006).

As mentioned above, new areas of interest in the field of cochlear implants will arise, such as new micro-electro-mechanical (MEM) arrays with control circuitry build into the array, large number of electrode contacts, drug delivery systems and regeneration techniques. Some of these advancements can already be investigated with the current model, like the various new electrode designs and contact arrangements. Some questions will demand further improvement and expansion of the cochlear model, for instance the effects of new fiber growth. Computational modeling of the cochlea provides the means to investigate the feasibility and efficacy of new ideas, even in the stage before implementation. It can formulate guidelines along which new concepts and insights can be developed and validated. Such insights serve as the starting point for clinical trials, psychophysical tests, objective recording paradigms and animal experiments ultimately leading to better electrode designs and

speech processing algorithms. All in all, computational modeling forms a theoretical guideline along which cochlear implants can be improved.

Bibliography

- Aarnink, R. , 1991. *Finite element modeling of the inner ear, with respect to electrical stimulation of the deaf ear*, Master's thesis, University Twente.
- Abbas, P. J. and Brown, C. J. , 2000. Electrophysiology and device telemetry, in S. B. Waltzman and N. L. Cohen (eds), *Cochlear Implants*, Thieme, chapter 7, pp. 117–133.
- Abbas, P. J., Brown, C. J., Shallop, J. K., Firszt, J. B., Hughes, M. L., Hong, S. H. and Staller, S. J. , 1999. Summary of results using the Nucleus CI24M implant to record the electrical evoked compound action potential, *Ear Hear* 20, 45–59.
- Albu, S. and Babighian, G. , 1997. Predictive factors in cochlear implants, *Acta Otorhinolaryngol Belg* 51(1), 11–16.
- Almqvist, B., Harris, S. and Shallop, J. K. , 2000. Objective intraoperative method to record averaged electromyographic stapedius muscle reflexes in cochlear implant patients, *Audiology* 39, 146–152.
- Andreev, A. M., Gersuni, G. V. and A., V. A. , 1935. On the electrical excitability of the human ear: On the effect of alternating currents on the affected auditory apparatus, *J Physiol USSR* 18, 250–265.
- Arnold, W. , 1987. Myelination of the human spiral ganglion, *Acta Otolaryngol (Stockh.)* Suppl.436, 76–84.
- Aschendorff, A., Richter, B. Stecker, M. and Laszig, R. , 1999. First results in implanting a new precurved intracochlear electrode with stiletto, *Abstracts of the 1999 Conference on Implantable Auditory Prostheses*, Asilomar Conference Center, Pacific Grove, CA, USA, p. 56.
- Balkany, T. J. , 1986. Cochlear implants, *Otolaryngol Clin North Am* 19(2), 215–449.

- Ballantyne, J. C., Evans, E. F. and Morrison, A. W. , 1978. Electrical auditory stimulation in the management of profound hearing loss. report to the department of health and social security on visits in october 1977 to centres in the u.s.a. involved in cochlear implant prostheses., *J Laryngol Otol Suppl* 1, 1–117.
- Ballantyne, J. C., Evans, E. F. and Morrison, A. W. , 1982. Electrical auditory stimulation in the management of profound hearing loss. an up-dated report to the department of health and social security., *J Laryngol Otol* 96(9), 811–816.
- Banfai, P., Karczag, A., Kubik, S., Luers, S. P. and Surth, W. , 1985. Extra-cochlear eight-channel electrode system. report on 104 patients., *Acta Otorhinolaryngol Belg* 39(4), 720–734.
- Battmer, R. D., Büchner, A., Frohne-Büchner, C., Tasche, C. and Lenarz, T. , 2001. Telemetric measurement of the compound action potential in Clarion and Nucleus cochlear implant systems., *Abstracts of the 2001 Conference on Implantable Auditory Prostheses*, Asilomar Conference Center, Pacific Grove, CA, USA, p. 74.
- Battmer, R. D. and Zilberman, Y., Haake, P. and Lenarz, T. , 1999. Simultaneous Analog stimulation (SAS)-Continuous Interleaved Sampler (CIS) pilot comparison study in Europe., *Ann Otol Laryngol* 108(suppl. 177), 69–73.
- Békésy, G. v. , 1960. *Experiments in Hearing*, Acoustical Society of America.
- Bhatti, P. T., Pflingst, B. E., Anderson, D. J. and Wise, K. D. , 2005. A 128-site, 16-channel electrode array for a cochlear prosthesis, *Annual report 2005*, Engineering Research Center for Wireless Integrated MicroSystems.
- Binns, K. L., Lawrenson, P. J. and Trowbridge, C. W. , 1992. *The Analytical and numerical Solution of Electric and Magnetic Fields*, Wiley & Sons, New York.
- Black, R. C., Clark, G. M., Tong, Y. C. and Patrick, J. F. , 1983. Current distributions in cochlear stimulation, *Ann NY Acad Sci* 405, 137–145.
- Blume, S. S. , 1995. *Sources of Medical Technology: Universities and Industry*, National Academy Press, chapter Cochlear Implantation: Establishing Clinical Feasibility, 1957-1982.
- Boëx, C., Baud, L., Cosendai, G., Sigrist, A., Kos, M. I. and Pelizzone, M. , 2006. Acoustic to electric pitch comparisons in cochlear implant subjects with residual hearing, *J Assoc Res Otolaryngol* 7(2), 110–124.

- Boëx, c., Kos, M. I. and Pelizzone, M. , 2003. Forward masking in different cochlear implant systems, *J Acoust Soc Am* 114(4 Pt 1), 2058–2065.
- Bosman, A. J. and Smoorenburg, G. F. , 1999. Predictors of cochlear implant performance, *Audiology* 38(2), 109–116.
- Brebbia, C. A. and Dominguez, J. , 1992. *Boundary Elements - An Introductory Course*, McGraw-Hill, New York.
- Briaire, J. J. and Frijns, J. H. M. , 1998a. The influence of electrode dimensions of cochlear implants on the spatial selectivity, *Ned Tijdsch Geneeskd* 142, 613.
- Briaire, J. J. and Frijns, J. H. M. , 1998b. What are the consequences of intrascalar ossification for the outcome of cochlear implantation? - a model study, *Abstracts of the 4th European Symposium on Pediatric Cochlear Implantation*, Den Bosch, p. 88.
- Briaire, J. J. and Frijns, J. H. M. , 2000a. 3d mesh generation to solve the electrical volume conduction problem in the implanted inner ear, *Simulat Pract Theory* 8, 57–73.
- Briaire, J. J. and Frijns, J. H. M. , 2000b. Field patterns in a 3d tapered spiral model of the electrically stimulated cochlea, *Hear Res* 148, 18–30.
- Briaire, J. J. and Frijns, J. H. M. , 2005. Unraveling the electrically evoked compound action potential, *Hear Res* 205(1-2), 143–156.
- Briaire, J. J., Kalkman, R. K. and Frijns, J. H. M. , 2006. Model insights in the excitation patterns of current steering, *Abstracts of the 8th European Symposium on Pediatric Cochlear Implantation*, Lido di Venezia, Italy.
- Brown, C. J., Abbas, P. J. and Gantz, B. J. , 1990. Electrically evoked whole-nerve action potentials i.data from human cochlear implant users, *J Acoust Soc Am* 88(3), 1385–1391.
- Brown, C. J., Abbas, P. J. and Gantz, B. J. , 1998. Preliminary experience with neural response telemetry in the Nucleus CI24M cochlear implant., *Am J Otol* 19(3), 320–327.
- Brown, C. J. and J., A. P. , 1990. Electrically evoked whole-nerve action potentials: parametric data from the cat, *J Acoust Soc Am* 85(5), 2205–2210.
- Brown, M. C. , 1987. Morphology of labeled afferent fibers in the guinea pig cochlea, *J Comp Neurol* 260, 591–604.

- Bruce, I. C., Irlicht, L. S., White, M. W., O'Leary, S. J., Dynes, S. and Clark, G. M. , 1999a. A stochastic model of the electrically stimulated auditory nerve: Single-train response, *IEEE Trans Biomed Eng* 46(6), 630–637.
- Bruce, I. C., Irlicht, L. S., White, M. W., O'Leary, S. J., Javel, E. and Clark, G. M. , 1999b. A stochastic model of the electrically stimulated auditory nerve: Single-pulse response, *IEEE Trans Biomed Eng* 46(6), 617–629.
- Brummer, S. B. and Turner, M. J. , 1977. Electrochemical considerations for safe electrical stimulation of the nervous system with platinum electrodes, *IEEE Trans Biomed Eng* 24, 59–62.
- Chan, V., Tong, M., Yue, V., Wong, T., Leung, E., Yuen, K. and van Hasselt, A. , 2007. Performance of older adult cochlear implant users in hong kong., *Ear Hear* 28(2 Suppl), 52S–55S.
- Charlet de Sauvage, R., Cazals, Y., Erre, J. P. and Aran, J. M. , 1983. Acoustically derived auditory nerve action potential evoked by electrical stimulation: An estimation of the waveform of single unit contribution, *J Acoust Soc Am* 73(2), 616–627.
- Chatelin, V., Kim, E. J., Driscoll, C., Larky, J., Polite, C., Price, L. and Lalwani, A. K. , 2004. Cochlear implant outcomes in the elderly., *Otol Neurotol* 25(3), 298–301.
- Chatterjee, M. , 1999. Effects of stimulation mode on threshold and loudness growth in multielectrode cochlear implants, *J Acoust Soc Am* 105, 850–860.
- Clark, G. M. , 1999. Cochlear implants in the third millenium, *Am J Otol* 20, 4–8.
- Cohen, L. T., Busby, P. A., Whitford, L. A. and Clark, G. M. , 1996. Cochlear implants place psychophysics. 1. pitch estimation with deeply inserted electrodes, *Audiol Neurotol* 1, 265–277.
- Cohen, L. T., Richardson, L. M., Saunders, E. and Cowan, R. S. , 2003. Spatial spread of neural excitation in cochlear implant recipients: comparison of improved ecap method and psychophysical forward masking, *Hear Res* 179(1-2), 72–87.
- Cohen, L. T., Saunders, E. and Clark, G. M. , 2001. Psychophysics of a prototype peri-modiolar cochlear implant electrode array., *Hear Res* 155(1-2), 63–81.

- Cohen, N. L., Roland, J. T. Jr. and Fishman, A. , 2002. Surgical Technique For The Nucleus® Countourtm Cochlear Implant, *Ear Hear* 23 Supplement(1), 59–66S.
- Cohen, N. L., Roland, J.T. Jr. and Marrinan, M. , 2004. Meningitis in cochlear implant recipients: the north american experience, *Otol Neurotol* 25(3), 275–281.
- Colombo, J. and Parkins, C. W. , 1987. A model of electrical excitation of the mammalian auditory-nerve neuron, *Hear Res* 31, 287–312.
- Corbett, S. S., Johnson, T. J., Clopton, B. M., Spelman, F. A., Strole, J. A. and Ketterl, J. R. , 2004. Method of making high contact density electrode array, United States Patent # 6,782,619.
- Cords, S. M., Reuter, G., Issing, P. R., Sommer, A., Kuzma, J. and Lenarz, T. , 2000. A silastic positioner for a modiolus-hugging position of intracochlear electrodes: electrophysiologic effects, *Am J Otol* 21(2), 212–217.
- Dallos, P., Popper, A. N. and Fay, R. R. (eds) , 1996. *The Cochlea*, Vol. 8 of *Springer handbook of auditory research*, Springer, New York.
- Davies, A. J. , 1980. *The finite element method: a first approach*, Clarenton Press, Oxford.
- Davis, H. , 1935. The electrical phenomena of the cochlea and the auditory nerve, *J Acoust Soc Am* 6(4), 205–215.
- De Ceulaer, G., Johnson, S., Yperman, M., Daemers, K., Offeciers, F. E., O'Donoghue, G. M. and Govaerts, P. J. , 2003. Long-term evaluation of the effect of intracochlear steroid deposition on electrode impedance in cochlear implant patients., *Otol Neurotol* 24(5), 769–74.
- De Filippo, C. L. and Scott, B. L. , 1978. A method for training and evaluating the reception of ongoing speech, *J Acoust Soc Am* 63, 1186–92.
- Dingemanse, J., Frijns, J. H. M. and Briaire, J. J. , 2006. Psychophysical assessment of spatial spread of excitation in electrical hearing with single and dual electrode contact maskers., *Ear Hear* 27(6), 645–657.
- Djourno, A. and Eyries, C. , 1957. Auditory prosthesis by means of a distant electrical stimulation of the sensory nerve with the use of an indwelt coiling, *Presse Med* 65, 1417.

- Donaldson, G. S., Kreft, H. A. and Litvak, L. , 2005. Place-pitch discrimination of single- versus dual-electrode stimuli by cochlear implant users (I)., *J Acoust Soc Am* 118(2), 623–626.
- Donaldson, G. S., Peters, M. D., Ellis, M. R., Friedman, B. J., Levine, S. C. and Rimell, F. L. , 2001. Effects of the Clarion Electrode Positioning System on auditory thresholds and comfortable loudness levels in pediatric patients with cochlear implants, *Arch Otolaryngol Head Neck Surg* 127(8), 956–960.
- Dorman, M. F., Hannley, M. T., Dankowski, K., Smith, L. and McCandless, G. , 1989. Word recognition by 50 patients fitted with the symbion multichannel cochlear implant., *Ear Hear* 10(1), 44–49.
- Dorman, M. F., Spahr, T., Gifford, R., Loiselle, L., McKarns, S., Holden, T., Skinner, M. and Finley, C. , 2007. An electric frequency-to-place map for a cochlear implant patient with hearing in the nonimplanted ear, *J Assoc Res Otolaryngol* 8(2), 234–240.
- Dowell, R. C., Mecklenburg, D. J. and Clark, G. M. , 1986. Speech recognition for 40 patients receiving multichannel cochlear implants., *Arch Otolaryngol Head Neck Surg* 112(10), 1054–1059.
- Doyle, J. H., Doyal, J. B. and Turnbull, F. M. , 1964. Electrical stimulation of the eighth cranial nerve, *Arch Otolaryngol* 80, 388–391.
- Eddington, D. K. , 1980. Speech discrimination in deaf subjects with cochlear implants., *J Acoust Soc Am* 68(3), 885–91.
- Ferguson, A. S. and Stroink, G. , 1997. Factors affecting the accuracy of the boundary element method in the forward problem—i:calculating surface potentials, *IEEE Trans Biomed Eng* 44(11), 1139–1155.
- Fernández, C. , 1952. Dimensions of the cochlea (guinea pig), *J Acoust Soc Am* 24(5), 519–523.
- Finley, C. C. F., Wilson, B. S., Van den Honert, C. and Lawson, D. , 1997. Speech processors for auditory prosthesis, sixth quarterly progress report, *Technical report*, Research Triangle Institute, NC., <http://npp.ninds.nih.gov/ProgressReports/SpeechProcessorsforAuditoryProsthesesDC52103/qpr6/qpr6.html>.
- Finley, C. C., Wilson, B. S. and White, M. W. , 1990. Models of neural responsiveness to electrical stimulation, in J. Miller and F. Spelman (eds),

- Cochlear Implants: Models of the Electrically Stimulated Ear*, Springer-Verlag, New York, pp. 55–96.
- Firszt, J. B., Wackym, P. A., Gaggl, W. and Burg, L. S. and Reeder, R. M. , 2003. Electrically evoked auditory brain stem responses for lateral and medial placement of the Clarion HiFocus electrode, *Ear Hear* 24(2), 184–190.
- Firszt, J., Rotz, L. A., Reeder, R., Novak, M. A. and Koch, D. , 1999. Electrically evoked auditory brainstem responses measured during cochlear-implant surgery with and without the Clarion® electrode positioning system, *Abstracts of the 1999 Conference on Implantable Auditory Prostheses*, Asilomar Conference Center, Pacific Grove, CA, USA, p. 56.
- Fourcin, A. J., Rosen, S. M., Moore, B. C., Douek, E. E., Clarke, G. P., Dodson, H. and Bannister, L. H. , 1979. External electrical stimulation of the cochlea: clinical, psychophysical, speech-perceptual and histological findings., *Br J Audiol* 13(3), 85–107.
- Francis, H. W., Yeagle, J. D., Bowditch, S. and Niparko, J. K. , 2005. Cochlear implant outcome is not influenced by the choice of ear., *Ear Hear* 26(4 Suppl), 7S–16S.
- Frankenhæuser, B. and Huxley, A. F. , 1994. The action potential in the myelinated nerve fiber of *xenopus laevis* as computed on the basis of voltage clamp data, *J Physiol (London)* 171, 302–315.
- Friedland, D. R., Venick, H. S. and Niparko, J. K. , 2003. Choice of ear for cochlear implantation: effect of history and residual hearing on predicted postoperative performance, *Otol Neurotol* 24(4), 582–529.
- Frijns, J. H. M. , 1995. *Cochlear Implants: A Modelling Approach*, PhD thesis, Rijksuniversiteit Leiden.
- Frijns, J. H. M. and Briaire, J. J. , 1999. The consequences of species differences in cochlear anatomy on the portability of animal data to the outcome of cochlear implantation in man, *Abstracts of the 1999 Conference on Implantable Auditory Prostheses, Asilomar, California*, Asilomar Conference Center, Pacific Grove, CA, USA.
- Frijns, J. H. M. and Briaire, J. J. , 2001. New insights in the fitting strategy yield improved speech recognition after cochlear implantation, *Clinical Otolaryngology Abstracts of the 198th Meeting of the Dutch ENT Society*.

- Frijns, J. H. M. and ten Kate, J. H. , 1994. A model of the myelinated nerve fibres for electrical prosthesis design, *Med Biol Eng Comput* 32, 391–398.
- Frijns, J. H. M., Briaire, J. J. and Grote, J. J. , 2001. The importance of human cochlear anatomy for the results with modiolar hugging multi-channel cochlear implants, *Otol Neurotol* 22(3), 340–349.
- Frijns, J. H. M., Briaire, J. J. and Schoonhoven, R. , 2000a. Integrated use of volume conduction and neural models to simulate the response to cochlear implants, *Simulat Pract Theory* 8, 75–97.
- Frijns, J. H. M., Briaire, J. J., de Laat, J. A. and Grote, J. J. , 2002. Initial evaluation of the Clarion CII cochlear implant: speech perception and neural response imaging, *Ear Hear* 23(3), 184–197.
- Frijns, J. H. M., Briaire, J. J., Zarowski, A., Verbist, B. and Kuzma, J. , 2004. Concept and initial testing of a new, basally perimodiolar electrode design, in R. T. Miyamoto (ed.), *Cochlear Implants*, Vol. 1273 of *International Congress Series*, Elsevier.
- Frijns, J. H. M., de Snoo, S. L. and Schoonhoven, R. , 1995. Potential distributions and neural excitation patterns in a rotationally symmetric model of the electrically stimulated cochlea, *Hear Res* 87, 170–186.
- Frijns, J. H. M., de Snoo, S. L. and Schoonhoven, R. , 2000b. Improving the accuracy of the boundary element method by the use of second order interpolation functions, *IEEE Trans Biomed Eng* 47(10), 1336–1346.
- Frijns, J. H. M., de Snoo, S. L. and ten Kate, J. H. , 1996a. Spatial selectivity in a rotationally symmetric model of the electrically stimulated cochlea, *Hear Res* 95, 33–48.
- Frijns, J. H. M., Kalkman, R. K., van den Hooff, R. and Briaire, J. J. , 2005. Implications of the non-linear tonotopic relationship between the human spiral ganglion and organ of corti, *Abstracts of the 2005 Conference on Implantable Auditory Prostheses*, p. 46.
- Frijns, J. H. M., Klop, M. C., Bonnet, R. M. and Briaire, J. J. , 2003. Optimizing the number of electrodes with high-rate stimulation of the Clarion CII cochlear implant, *Acta Otolaryngol* 123(2), 138–142.
- Frijns, J. H. M., Mooij, J. and ten Kate, J. H. , 1994. A quantitative approach to modelling mammalian myelinated nerve fibres for electrical prosthesis design, *IEEE Trans Biomed Eng* 41(6), 556–566.

- Frijns, J. H. M., Schoonhoven, R. and Grote, J. J. , 1996b. The influence of stimulus intensity on spike timing and the compound action potential in the electrically stimulated cochlea: a model study, *IEEE 18th annual international conference of the Engineering in Medicine and Biology Society*, no 17, p. 2 pages.
- Frijns-van Putten, A. A. M. E., Beers, M., Snieder, S. G. and Frijns, J. H. M. , 2005. Hoortraining voor volwassen ci-dragers: Het cochleaire leermodel (in dutch), *Logopedie en Foniatrie* 77, 50–59.
- Fu, Q. J. and Shannon, R. V. , 1999. Effect of acoustic dynamic range on phoneme recognition in quiet and noise by cochlear implant users, *J Acoust Soc Am* 106(6), L65–70.
- Gantz, B. J., Brown, C. J. and J., A. P. , 1994. Intraoperative measures of electrically evoked auditory nerve compound action potential, *Am J Otol* 15, 137–144.
- Gantz, B. J., Woodworth, G. G., Knutson, J. F. and et al. , 1993. Multivariate predictors of audiological success with multichannel cochlear implants, *Ann Otol Rhinol Laryngol* 102(12), 909–916.
- Gillespie, L. N. and Shepherd, R. K. , 2005. Clinical application of neurotrophic factors: the potential for primary auditory neuron protection., *Eur J Neurosci* 22(9), 2123–33.
- Girzon, G. , 1987. *Investigation of current flow in the inner ear during electrical stimulation of intracochlear electrodes*, Msc thesis, Massachusetts Institute of Technology.
- Gleich, O. and Wilson, S. , 1993. The diameters of guinea pig auditory nerve fibres: Distribution and correlation with spontaneous rate, *Hear Res* 71, 69–79.
- Goldstein, M. H. J. and Kiang, N. Y. S. , 1958. Synchrony of neural activity in electric response evoked by transient acoustic stimuli, *J Acoust Soc Am* 30, 107–114.
- Gomaa, N. A., Rubinstein, J. T., Lowder, M. W., Tyler, R. S. and Gantz, B. J. , 2003. Residual speech perception and cochlear implant performance in postlingually deafened adults, *Ear Hear* 24(6), 539–544.
- Graham, J. M. , 2003. Graham fraser memorial lecture 2002. from frogs' legs to pieds-noirs and beyond: some aspects of cochlear implantation., *J Laryngol Otol*.

- Greenwood, D. D. , 1990. A cochlear frequency-position function for several species—29 years later., *J Acoust Soc Am* 87(6), 2592–2605.
- Gstoettner, W., Franz, P., Hamzavi, J., Plenk, H., Baumgartner, W. and Czerny, C. , 1999. Intracochlear position of cochlear implant electrodes., *Acta Otolaryngol (Stockh)* 119, 229–233.
- Haensel, J., Ilgner, J., Chen, Y. S., Thuermer, C. and Westhofen, M. , 2005. Speech perception in elderly patients following cochlear implantation., *Acta Otolaryngol* 125(12), 1272–1276.
- Halter, J. A. and Clark, J. W. J. , 1991. A distributed-parameter model of the myelinated nerve fiber, *J Theor Biol* 148(3), 345–382.
- Hamzavi, J., Franz, P., Baumgartner, W. D. and Gstoettner, W. , 2001. Hearing performance in noise of cochlear implant patients versus severely-profoundly hearing-impaired patients with hearing aids, *Audiology* 40(1), 26–31.
- Hanekom, T. , 2001. Three-dimensional spiraling finite element model of the electrically stimulated cochlea, *Ear Hear* 22(4), 300–15.
- Harrison, W. V., Griffith, G. A. and Faltys, M. A. , 2005. High contact count, sub-miniature, full implantable cochlear prosthesis, United States Patent # 6,980,864.
- Hodgkin, A. and Huxley, A. F. , 1952. A quantitative description of membrane current and its application to conduction and excitation in nerve, *J Physiol* 117, 500–544.
- Houben, V., Van Immerseel, L. and Peters, S. , 2000. Comparing stimulation and recording strategies with eap measurements, *Abstracts of the 5th European Symposium on Paediatric Cochlear Implantation*, Antwerp, Belgium, p. 41.
- House, W. F. , 1995. *Cochlear Implants: My Perspective*, AllHear, Inc.
- House, W. F. and Urban, J. , 1973. Long term results of electrode implantation and electronic stimulation of the cochlea in man, *Ann Otol* 82, 504–517.
- Huisman, M. A., Heller, S. and Frijns, J. H. M. , 2006. Beschadigde binnencellen: is er therapie op komst? (in dutch), *Ned Tijdschr. KNO*.
- Ifukube, T. and White, R. L. , 1987. Current distributions produced inside and outside the cochlea from a scala tympani electrode array, *IEEE Trans Biomed Eng* 34(11), 883–890.

- Izumikawa, M., Minoda, R., Kawamoto, K., Abrashkin, K. A., Swiderski, D. L., Dolan, D. F., Brough, D. E. and Raphael, Y. , 2005. Auditory hair cell replacement and hearing improvement by *atoh1* gene therapy in deaf mammals., *Nat Med* 11(3), 271–6.
- Jolly, C. and Hochmair, I. , 2006. Implantable fluid delivery apparatuses and implantable electrode, United States Patent # 7,044,942.
- Jolly, C. N., Spelman, F. A. and Clopton, B. M. , 1996. Quadrupolar stimulation for cochlear prostheses: Modeling and experimental data, *IEEE Trans Biomed Eng* 43(8), 857–865.
- Jones, R. C., Stevens, S. S. and Lurie, M. H. , 1940. Three mechanisms of hearing by electrical stimulation, *J Acoust Soc Am* 12(2), 281–290.
- Kawamoto, K., Ishimoto, S., Minoda, R., Brough, D. E. and Raphael, Y. , 2003. *Math1* gene transfer generates new cochlear hair cells in mature guinea pigs in vivo., *J Neurosci* 23(11), 4395–400.
- Kessler, D. K. , 1999. The Clarion multi-strategy cochlear implant, *Ann Otol Laryngol* 108(suppl.177), 8–16.
- Kiang, N. Y. S. and Moxon, E. C. , 1972. Physiological considerations in artificial stimulation of the inner ear, *Ann Otol Rhinol Laryngol* 81(5), 714–730.
- Klop, W. M. C., Hartlooper, A. and Briaire, J. J. and Frijns, J. H. M. , 2004. A new method for dealing with the stimulus artefact in electrically evoked compound action potential measurements, *Acta Otolaryngol* 124(2), 137–143.
- Kral, A., Hartmann, R., Mortazavi, D. and Klinke, R. , 1998. Spatial resolution of cochlear implants: the electrical field and excitation of auditory afferents, *Hear Res* 121, 11–28.
- Kuzma, J. A. and Balkany, T. J. , 1999. New generation Clarion electrodes for highly focused stimulation, *Abstracts of the 1999 Conference on Implantable Auditory Prostheses*, Asilomar Conference Center, Pacific Grove, CA, USA, p. 60.
- Labadie, R. F., Carrasco, V. N. and Gilmer, C. H. Pillsbury, H. C. r. , 2000. Cochlear implant performance in senior citizens., *Otolaryngol Head Neck Surg* 123(4), 419–424.

- Lai, W. K. and Dillier, N. , 2000. A simple two-component model of the electrically evoked compound action potential in the human cochlea, *Audiol Neurootol* 5(6), 333–45.
- Leung, J., Wang, N. Y., Yeagle, J. D., Chinnici, J., Bowditch, S., Francis, H. W. and Niparko, J. K. , 2005. Predictive models for cochlear implantation in elderly candidates., *Arch Otolaryngol Head Neck Surg* 131(12), 1049–1054.
- Lieberman, M. C. and Oliver, M. E. , 1984. Morphometry of intracellularly labeled neurons of the auditory-nerve: Correlations with functional properties, *J Comp Neurol* 223, 163–176.
- Maniglia, A. J., Abbass, H., Azar, T., Kane, M., Amantia, P., Garverick, S. and Ko, W. H. , 1999. The middle ear bioelectric microphone for a totally implantable cochlear hearing device for profound and total hearing loss, *Am J Otol* 20(5), 602–611.
- Matthies, M. L. and Carney, A. E. , 1988. A modified speech tracking procedure as a communicative performance measure, *J Speech Hear Res* 31, 394–404.
- McGuinness, S. L. and Shepherd, R. K. , 2005. Exogenous bdnf rescues rat spiral ganglion neurons in vivo., *Otol Neurotol* 26(5), 1064–72.
- McKay, C. M., O'Brien, A. and James, C. J. , 1999. Effect of current level on electrode discrimination in electrical stimulation, *Hear Res* 136, 159–164.
- McKay, C. M., Remine, M. D. and McDermott, H. J. , 2001. Loudness summation for pulsatile electrical stimulation of the cochlea: effects of rate, electrode separation, level, and mode of stimulation, *J Acoust Soc Am* 110, 1514–24.
- Meijs, J. W. H., Weier, O. W., Peters, M. J. and van Oosterom, A. , 1989. On the numerical accuracy of the boundary element method, *IEEE Trans Biomed Eng* 36(10), 1038–1049.
- Mens, L. , 2001. Verbeterde overdracht van spraak met een cochleair implantaat: Waar is de flessenhals?, *Klinische Fysica* 2001/2, 10–14.
- Miller, A. L., Smith, D. W. and Pflugst, B. E. , 1999. Across-species comparisons of psychophysical detection thresholds for electrical stimulation of the cochlea: II. strength-duration functions for single, biphasic pulses, *Hear Res* 135, 47–55.

- Miller, C. A., Abbas, P. J. and Brown, C. J. , 2000. An improved method of reducing stimulus artifact in the electrically evoked whole-nerve potential, *Ear Hear* 21(4), 280–290.
- Miller, C. A., Abbas, P. J., Hay-McCutcheon, M. J., Robinson, B. K., Nourski, K. V. and Jeng, F. C. , 2004. Intracochlear and extracochlear escape suggest antidromic action potentials, *Hear Res* 198(1-2), 75–86.
- Miller, C. A., Abbas, P. J., Nourski, K. V., Hu, N. and Robinson, B. K. , 2003. Electrode configuration influences action potential initiation site and ensemble stochastic response properties, *Hear Res* 175(1-2), 200–214.
- Miller, C. A., Abbas, P. J., Rubinstein, J. T., K., R. B., Matsuoka, A. J. and Woodworth, G. , 1998. Electrically evoked compound action potentials of guinea pig and cat: responses to monopolar, monophasic stimulation, *Hear Res* 119(1-2), 142–154.
- Mooij, J. , 1992. *Simulation of action potentials in auditory nerve fibres*, Master's thesis, Technical University of Delft.
- Motz, H. and Rattay, F. , 1986. A study of the application of the Hodgkin-Huxley and the Frankenhaeuser-Huxley model for electrostimulation of the acoustic nerve, *Neuroscience* 18, 699–712.
- Nadol, J. B. J. , 1990. Degeneration of cochlear neurons as seen in the spiral ganglion of man, *Hear Res* 49(1-3), 141–154.
- Nadol, J. J. , 1988. Comparative anatomy of the cochlea and auditory nerve in mammals, *Hear Res* 34(3), 253–265.
- NIH Consensus Statement , 1995. Cochlear implants in adults and children, 13(2), 1–30.
- Nijdam, H. F. , 1982. *Auditory Sensory Cell Pathology in the Waltzing Guinea Pig*, PhD thesis, Groningen University.
- Oh, S. H., Kim, C. S., Kang, E. J., Lee, D. S., Lee, H. J., Chang, S. O., Ahn, S. H., Hwang, C. H., Park, H. J. and Koo, J. W. , 2003. Speech perception after cochlear implantation over a 4-year time period., *Acta Otolaryngol* 123(2), 148–153.
- O'Leary, S. J., Black, R. C. and Clark, G. M. , 1985. Current distributions in the cat cochlea: A modelling and electrophysiological study, *Hear Res* 18(3), 273–281.

- Paasche, G., Bockel, F., Tasche, C., Lesinski-Schiedat, A. and Lenarz, T. , 2006a. Changes of postoperative impedances in cochlear implant patients: the short-term effects of modified electrode surfaces and intra-cochlear corticosteroids, *Otol Neurotol* 27(5), 639–47.
- Paasche, G., Bogel, L., Leinung, M., Lenarz, T. and Stover, T. , 2006b. Substance distribution in a cochlea model using different pump rates for cochlear implant drug delivery electrode prototypes., *Hear Res* 212(1-2), 74–82.
- Pasanisi, E., Bacciu, A., Vincenti, V., Guida, M., Barbot, A., Berghenti, M. T. and Bacciu, S. , 2003. Speech recognition in elderly cochlear implant recipients., *Clin Otolaryngol Allied Sci* 28(2), 154–157.
- Pasanisi, E., Vincenti, V., Bacciu, A., Guida, M. and Bacciu, S. , 2002. The nucleus contour electrode array: an electrophysiological study, *Laryngoscope* 119(9), 1653–1656.
- Patrick, J. F., Busby, P. A. and Gibson, P. J. , 2006. The development of the nucleus freedom cochlear implant system., *Trends Amplif* 10(4), 175–200.
- Peeters, S., Marquet, J., Officiers, F. E., Bosiers, W., Kinsbergen, J. and Van Durme, M. , 1989. Cochlear implants: the laura prosthesis., *J Med Eng Technol* 13(1-2), 76–80.
- Peeters, S., Van Immerseel, L., Zarowski, A., Houben, V., Govaerts, P. and Offeciers, E. , 1998. New developments in cochlear implants, *Acta Otorhinolaryngol Belg* 52, 115–127.
- Plomp, R. and Mimpen, A. M. , 1979. Improving the reliability of testing the speech reception threshold for sentences., *Audiology* 18, 43–52.
- Postnov, A., Zarowski, A., De Clerck, N., Vanpoucke, F., Offeciers, F. E., Van Dyck, D. and Peeters, S. , 2006. High resolution micro-ct scanning as an innovatory tool for evaluation of the surgical positioning of cochlear implant electrodes., *Acta Otolaryngol* 126(5), 467–474.
- Pullan, A. , 1996. A high-order coupled finite element/boundary element torso model, *IEEE Trans Biomed Eng* 43(3), 292–298.
- Rask-Andersen, H., Bostrom, M., Gerdin, B., Kinnefors, A., Nyberg, G., Engstrand, T., Miller, J. M. and Lindholm, D. , 2005. Regeneration of human auditory nerve. in vitro/in video demonstration of neural progenitor cells in adult human and guinea pig spiral ganglion., *Hear Res* 203(1-2), 180–91.

- Rattay, F. , 1989. Analysis of models for extracellular fiber stimulation, *IEEE Trans Biomed Eng* 36, 676–692.
- Rattay, F. , 1993. Simulation of artificial neural reactions produced with electric fields, *Simulat Pract Theory* 1(3), 137–152.
- Rattay, F., Leao, R. N. and Felix, H. , 2001a. A model of the electrically excited human cochlear neuron. ii. influence of the three-dimensional cochlear structure on neural excitability, *Hear Res* 153, 64–79.
- Rattay, F., Lutter, P. and Felix, H. , 2001b. A model of the electrically excited human cochlear neuron. i. contribution of neural substructures to the generation and propagation of spikes, *Hear Res* 153, 43–63.
- Richardson, R. T., Noushi, F. and O'leary, S. J. , 2006. Inner ear therapy for neural preservation., *Audiol Neurootol* 11(6), 343–356.
- Rubinstein, J. T., Parkinson, W. S., Tyler, R. S. and Gantz, B. J. , 1999a. Residual speech recognition and cochlear implant performance: effects of implantation criteria, *Am J Otol* 20(4), 445–452.
- Rubinstein, J. T., Wilson, B. S., Finley, C. C. and Abbas, P. J. , 1999b. Pseudospontaneous activity: stochastic independence of auditory nerve fibers with electrical stimulation, *Hear Res* 127, 108–118.
- Ruffin, C. V., Tyler, R. S., Witt, S. A., Dunn, C. C., Gantz, B. J. and Rubinstein, J. T. , 2007. Long-term performance of clarion 1.0 cochlear implant users., *Laryngoscope* 117(7), 1183–1190.
- Sapozhnikov, A. , 1990. *Computer modelling of the implanted cochlea*, Bsc thesis, University of Melbourne.
- Saunders, E., Cohen, L., Aschendorff, A., Shapiro, W., Knight, M., Stecker, M., Richter, B., Waltzman, S., Tykocinski, M., Roland, T., Laszig, R. and Cowan, R. , 2002. Threshold, comfortable level and impedance changes as a function of electrode-modiolar distance, *Ear Hear* 23(1 Supplement), 28–40S.
- Schoonhoven, R. and Stegeman, D. F. , 1991. Models and analysis of compound nerve action potentials, *Crit Rev Biomed Eng* 19(1), 47–111.
- Schoonhoven, R., Lamoré, P. J. and de Laat, J. A. P. M. and J., G. J. , 1999. The prognostic value of electrocochleography in severely hearing-impaired infants, *Audiology* 38(3), 141–54.

- Schoonhoven, R., Prijs, V. F. and Grote, J. J. , 1996. Response thresholds in electrocochleography and their relation to the pure tone audiogram, *Ear Hear* 17(3), 266–275.
- Schuknecht, H. F. , 1993. *Pathology of the ear*, Lea & Febiger, Philadelphia.
- Schwarz, J. R. and Eikhof, G. , 1987. Na currents and action potentials in rat myelinated nerve fibres at 20 and 37°C., *Pflügers Arch* 409, 569–577.
- Schwarz, J. R., Reid, G. and Bostock, H. , 1995. Action potentials and membrane currents in the human node of ranvier., *Pflügers Arch* 430(2), 283–292.
- Seyle, K. and Brown, C. J. , 2002. Speech perception using maps based on neural response telemetry measures, *Ear Hear* 23(1), 72S–79S.
- Shallop, J. K., VanDyke, L., Goion, D. W. and Mischke, R. E. , 1991. Prediction of behavioral threshold and comfort values for Nucleus 22-channel implant patients from electrical auditory brain stem response test results, *Annals of Otol, Rhinol and Laryngol* 100, 896–898.
- Shannon, R. V. , 2001. Overview of cochlear implant technology and research: Cochlear implant basics, cochlear implant results, research issues. short course on non-syndromic deafness, *ARO Midwinter Meeting*, St. Petersburg Beach, Florida.
- Shepherd, R. K., Hatsushika, S. and Clark, G. M. , 1993. Electrical stimulation of the auditory nerve: The effect of electrode position on neural excitation, *Hear Res* 66, 108–120.
- Simmons, F. B. , 1985. *Schindler RA, and Merzenich, MM (eds) Cochlear Implants*, Raven Press., chapter History of cochlear implants in the United States: A personal perspective, pp. 1–7.
- Simmons, F. B., Epley, J. M., Lummis, R. C., Guttman, N., Frishkopf, L. S., Harmon, L. D. and Zwicker, E. , 1965. Auditory nerve: Electrical stimulation in man, *Science* 148, 104–106.
- Simmons, F. B., Mongeon, C. J., Lewis, W. R. and Huntinton, D. A. , 1964. Electrical stimulation of acoustical nerve and inferior colliculus, *Arch Otolaryngol* 79, 559–568.
- Smoorenburg, G. F. , 1992. Speech reception in quiet and in noisy conditions by individuals with noise-induced hearing loss in relation to their tone audiogram, *J Acoust Soc Am* 91(1), 421–423.

- Smoorenburg, G. F., Willeboer, C. and Dijk, J. E. v. , 2001. Speech reception with ecap based processor fitting., *Abstracts of the 2nd Int. Symp. on Objective Measures in Cochlear Implantation*, Lyon, p. 65.
- Smoorenburg, G. F., Willeboer, C. and van Dijk, J. E. , 2002. Speech perception in Nucleus CI24M cochlear implant users with processor settings based on electrically evoked compound action potential thresholds, *Audiol Neurootol* 7(6), 335–347.
- Spelman, F. A. , 2006. Cochlear electrode arrays: past, present and future., *Audiol Neurootol* 11(2), 77–85.
- Spelman, F. A., Clopton, B. M. and Pflugst, B. E. , 1982. Tissue impedance and current flow in the implanted ear. implications for the cochlear prosthesis, *Ann Otol Rhinol Laryngol Suppl.* 98, 91, 3–8.
- Spelman, F. A., Clopton, B. M., Voie, A., Jolly, C. N., Huynh, K., Boogaard, J. and Swanson, J. W. , 1998. Cochlear implant with shape memory material and method for implanting the same, United States Patent # 5,800,500.
- Sridhar, D., Stakhovskaya, O. and Leake, P. A. , 2006. A frequency-position function for the human cochlear spiral ganglion., *Audiol Neurootol* 11(Suppl 1), 16–20.
- Stevens, S. S. , 1937. On hearing by electrical stimulation, *J Acoust Soc Am* 8(3), 191–195.
- Strelhoff, D. , 1973. A computer simulation of the generation and distribution of cochlear potentials, *J Acoust Soc Am* 54, 620–629.
- Stypulkowski, P. H. and van den Honert, C. , 1984. Physiological properties of the electrically stimulated auditory nerve. i. compound action potential recordings, *Hear Res* 14(3), 205–23.
- Suesserman, M. F. , 1992. *Noninvasive Microelectrode Measurement Technique for Performing Quantitative, in Vivo Measurements of the Inner Ear Tissue Impedances*, PhD thesis, University of Washington.
- Suesserman, M. F. and Spelman, F. A. , 1993. Lumped-parameter model for in vivo cochlear stimulation, *IEEE Trans Biomed Eng* 40(3), 237–245.
- Summerfield, A. Q. and Marshall, D. H. , 1995. Preoperative predictors of outcomes from cochlear implantation in adults: performance and quality of life, *Ann Otol Rhinol Laryngol* 166(Suppl.), 105–108.

- Tang, Y., Aslam, D. M., Wang, J. and Wise, K. D. , 2005. Technology and integration of poly-crystalline diamond piezoresistive position sensors for a cochlear implant probe, *Digest Int. Conf. on Solid-State Sensors, Actuators, and Microsystems (Transducers'05)*, Seoul, pp. 543–546.
- Tykocinski, M., Saunders, E., Cohen, L. T., Treaba, C., Briggs, R. J., Gibson, P., Clark, G. M. and Cowan, R. S. , 2001. The contour electrode array: Safety study and initial patient trials of a new perimodiolar design, *Otol Neurotol* 22, 33–41.
- van den Honert, C. and Stypulkowski, P. H. , 1987. Single fiber mapping of spatial excitation patterns in the electrically stimulated auditory nerve, *Hear Res* 29, 195–206.
- van der Beek, F. B., Boermans, P. P. B. M., Verbist, B. M., Briaire, J. J. and Frijns, J. H. M. , 2005. Clinical evaluation of the Clarion CII HiFocus 1 with and without positioner, *Ear Hear* 26(6), 577–592.
- van Dijk, J. E., van Olphen, A. F., Langereis, M. C., Mens, L. H., Brokx, J. P. and Smoorenburg, G. F. , 1999. Predictors of cochlear implant performance, *Audiology* 38(2), 109–116.
- van Oosterom, A. , 1991. Mathematical aspects of source modeling, *Acta Otolaryngol (Stockh.) Supp* 491, 70–79.
- Vanpoucke, F., Zarowski, A., Casselman, J., Frijns, J. and Peeters, S. , 2004. The facial nerve canal: an important cochlear conduction path revealed by clarion electrical field imaging., *Otol Neurotol* 25(3), 282–289.
- Verbist, B. M., Frijns, J. H. M., Geleijns, J. and van Buchem, M. A. , 2005. Multisection ct as a valuable tool in the postoperative assessment of cochlear implant patients., *Am J Neuroradiol* 26(2), 424–429.
- Versfeld, N. J., Festen, J. M. and Houtgast, T. , 1999. Preference judgments of artificial processed and hearing-aid transduced speech, *J Acoust Soc Am* 106, 1566–1578.
- Versnel, H., Prijs, V. F. and Schoonhoven, R. , 1992. Round-window recorded potential of single-fibre discharge (unit response) in normal and noise-damaged cochleas, *Hear Res* 59(2), 157–170.
- Volta, A. , 1800. On the electricity excited by mere contact of conducting substances of different kinds, *Royal Soc Philos Trans* 90, 403–431.

- Wackym, P. A., Firszt, J. B., Gaggl, W., Runge-Samuels, C. L., Reeder, R. M. and Raulie, J. C. , 2004. Electrophysiologic effects of placing cochlear implant electrodes in a perimodiolar position in young children, *Laryngoscope* 114(1), 71–76.
- Waltzman, S. B., Fisher, S. G., Niparko, J. K. and Cohen, N. L. , 1995. Predictors of postoperative performance with cochlear implants, *Ann Otol Rhinol Laryngol* 104(Suppl 165), 15–18.
- Wang, J., Gulari, M. N. and Wise, K. D. , 2005a. An integrated position-sensing system for a mems-based cochlear implant, *Electron Devices Meeting, 2005. IEDM Technical Digest. IEEE International*, Miami, Florida, pp. 121– 124.
- Wang, J., Gulari, M. N., Bhatti, P. T., Arcand, B. Y., Friedrich, C. R. and Wise, K. D. , 2005b. A cochlear electrode array with built-in position sensing, *IEEE International Conference on Micro Electro Mechanical Systems (MEMS)*, Miami, Florida, pp. 786–789.
- Warman, E. N., Grill, W. M. and Durand, D. , 1992. Modeling the effects of electric fields on nerve fibers: Determination of excitation thresholds, *IEEE Trans Biomed Eng* 39(12), 1244–1254.
- Wesselink, W. A., Holsheimer, J. and B., B. H. , 1999. A model of the electrical behaviour of myelinated sensory nerve fibres based on human data, *Med Biol Eng Comput* 37(2), 228–235.
- White, P. M., Doetzlhofer, A., Lee, Y. S., Groves, A. K. and Segil, N. , 2006. Mammalian cochlear supporting cells can divide and trans-differentiate into hair cells., *Nature* 441(7096), 984–7.
- Wilson, B. S., Finley, C. C., Lawson, D. T., Wolford, R. D., Eddington, D. K. and Rabinowitz, W. M. , 1991. Better speech recognition with cochlear implants, *Nature* 352(6332), 236–238.
- Wouters, J. and van den Berghe, J. , 2001. Speech recognition in noise for cochlear implantees with a two- microphone monaural adaptive noise reduction system, *Ear Hear* 22, 420–430.
- Wouters, J., Damman, W. and Bosman, A. J. , 1994. Vlaamse opname van woordenlijsten voor spraakaudiometrie, *Logopedie* 7(6), 28–33.
- Zhou, H. and Oosterom, A. v. , 1994. Application of the boundary element method to the solution of anisotropic electromagnetic problems, *Med Biol Eng Comput* 32(4), 399–405.

Summary

Cochlear implants (CI) are by now an accepted form of rehabilitation for profoundly deaf patients. CI users regain part of their hearing by direct electrical stimulation of the auditory nerve. With modern cochlear implants most users are able to achieve open-set speech understanding and are able to use the telephone. There are, however, still a lot of unanswered questions regarding the optimal design, stimulation paradigms, fitting methods and objective measurements. With the development of a realistic computer model of the implanted cochlea, as described in this thesis, these questions are analyzed from a fundamental perspective. This realistic model enables the analysis of clinical devices and gives insight in discrepancies between human and animal results. Insights gained from the model are used to improve clinical practice. Based on the model outcomes presented the characteristics of an improved electrode design were defined, and finally tested in a temporal bone study.

Chapter 1 presented the basic principles of a cochlear implant and a historical overview of the development of this device, from experimental devices to well accepted commercial products. At the end of this chapter the thesis was outlined.

Chapter 2 described the basic principle of modeling cochlear implants with a two step model. The first step is the modeling of the electrical conduction through the cochlea, also known as the volume conduction problem. The second step is to model the behavior of the nerve fibers in response to the potential distribution calculated in the first step. This two step model was used throughout this thesis. The newly introduced spiral shaped cochlea model allows for the prediction of excitation thresholds and spatial selectivity in the implanted cochlea. The model outcomes describing differences between excitation areas for various electrode locations, were compared with electrophysiological experiments. It was concluded they showed good agreement.

In chapter 3 a detailed description was given of the volume conduction model with an explanation of how the spiral shaped cochlear meshes and implant designs used in this thesis were generated. The meshes have the flexibility to investigate clinically relevant issues. With this model of the guinea pig cochlea the insulating effects of the membranes surrounding the scala tympani have been investigated. The described mesh generating software has the flexibility to be used for the much more challenging creation of the human cochlea.

Chapter 4 described the potential distributions and current pathways in a spiral cochlear model as described in the previous chapters. The relatively well conducting scala tympani turned out to be the main one indeed, but the exponential decay ($J \sim e^{-z}$) of current was only a good description of the far-field

behavior. In the vicinity of the electrodes, i.e. near the fibers that are most easily excited, higher current densities were found, that were best described by a spherical spread of the current ($J \sim \frac{1}{R^2}$). We concluded that the current spread along the scala tympani and its dependence on the position of the current source in the cochlea is well described by the superposition of spherical and exponential decay.

In chapter 5 a comparison was made between the outcomes of a guinea pig computer model and a realistic model of the human cochlea, both implanted with a model of a HiFocus cochlear implant. Taking into account the large anatomical differences in size, location in the temporal bone and overall geometry of the cochlea and auditory nerve between both species. It turned out that a well-designed modiolus-hugging electrode yields reduced current thresholds and a high spatial selectivity without a reduction of the dynamic range. However, in the second turn of the human cochlea the outcome was less favorable: As in the guinea pig, cross-turn stimulation reduces the dynamic range in the perimodiolar position substantially. We concluded that the clinical success of cochlear implantation in man and the promising results with modiolus-hugging devices depend largely upon typically human cochlear anatomy.

The clinical evaluation of the HiFocus electrode array with electrode positioning system combined with the CII implant electronics is described in chapter 6. The speech perception scores on CVC words without lip reading were monitored prospectively for the ten postlingually deafened patients. After one week all patients but one were able to use the telephone functionally. At the end of the study (follow-up 3 to 11 mo) the average CVC phoneme score was 84% (word score 66%). The Phoneme Recognition Threshold (50% of the performance in silence) was reached for Signal-to-Noise ratios between 0 and 5dB. NRI recordings were obtained with both the alternating polarity and the forward masking paradigm. The NRI system, although somewhat slow, gives good results and offers the ability to measure I/O curves and neural tuning.

The study presented in chapter 7 evaluated the effect of the duration of post-operative follow-up on the value of pre-operative predictors. The performance outcomes of a group of 91 subjects, implanted between 2000 and 2005 with a HiRes90K or CII implant with a HiFocus I electrode array, were evaluated with univariate linear regression analysis and with multiple regression analysis based on the Iowa predictive model. The difference in learning curve between patients with a long and a short duration of deafness or with differences in implantation age introduces a dependence on the post-operative

experience on the relative importance of predictive factors. Therefore, predictive models should be based on follow-up times of at least 2 years to allow poorer performers approach their ultimate performance level. When dealing with non-controlled retrospective studies, multiple regression analysis should be used to extract the influence of, for instance, electrode array design, or age at implantation, on the speech understanding scores; while reducing the effect of other parameters such as duration of deafness.

In chapter 8 the extension of a the human cochlea model, incorporating recording capabilities, is described. This model is used to investigate the individual single fibre action potential (SFAP) contribution to the eCAP at various stimulation levels. The single fiber contributions indicated that at high current levels the fibers located centrally in the excitation area, close to the stimulating electrode, yield an atypical response, without a clear negative peak in the SFAP. The number of fibers with atypical responses also increased with stimulus level. Therefore, the overall eCAP amplitude decreases above a certain stimulus level. This phenomenon was recorded earlier, but was always regarded as a recording artifact.

Chapter 9 described an extensive model study on the consequences of the precise location of the electrode array in the scala tympani. The objective of this chapter was to find the optimal placement with respect to threshold, dynamic range and spatial selectivity for both, degenerated and non-degenerated cochleae. The model predicted reduced threshold, increased dynamic range and higher spatial selectivity for the peri-modiolar position at the basal end of the cochlea, with minimal influence of neural degeneration. At the apical end of the array (1.5 cochlear turns), the dynamic range and the spatial selectivity were limited due to the occurrence of cross-turn stimulation, with the exception of the condition without neural degeneration and with the electrode array along the lateral wall of scala tympani. The benefits of eCAP recordings with respect to intra-operated placement optimisation were investigated. The eCAP simulations indicated that a large P_0 peak occurs before the N_1P_1 complex when the fibers are not degenerated. The absence of this peak might be used as an indicator for neural degeneration.

Based on the design criteria described in chapter 9 a design change of the current HiFocus electrode array has been proposed which should have a perimodiolar position of the electrode array for the basal contacts, while a lateral position should be achieved for more apical ones. The initial temporal bone study with prototype electrodes meeting these criteria was described in chapter 10. The prototype electrodes were inserted in human temporal

bones and the position of the contacts was verified with high-resolution CT-scans prior to a careful dissection, documenting the insertion trauma. The new electrode was able to attain the desired position with minimal damage to the intracochlear structures.

In chapter 11 the capabilities of the current model are described as well as future steps needed for the creation of a patient specific model with direct clinical implications for the individual patient. Some of the ongoing developments leading to a new generation of cochlear implants are highlighted. It was concluded that computational modeling can form a theoretical guideline along which new experiments and new developments for cochlear implants can be directed.

Samenvatting

Cochleaire implantatie (CI) is een inmiddels geaccepteerde vorm van revalidatie voor dove en ernstig slechthorende patiënten. CI-dragers krijgen een deel van hun gehoor terug door directe elektrische stimulatie van de gehoorzenuw. Door middel van moderne cochleaire implantaten is voor de meeste gebruikers spraakverstaan weer mogelijk evenals telefoneren. Er zijn echter nog steeds veel onbeantwoorde vragen over het optimale ontwerp van het cochleaire implantaat, stimulatieparadigma's, inregelmethodes en objectieve meetmethodes. Met de ontwikkeling van een realistisch computermodel van de geïmplanteerde cochlea, zoals beschreven in dit proefschrift, kunnen deze vragen worden geanalyseerd vanuit een fundamenteel gezichtspunt. Dit realistische computermodel maakt de analyse van klinische protheses mogelijk en geeft inzicht in de afwijkingen tussen resultaten behaald bij mensen en proefdieren. Inzichten die voortkomen uit het model worden gebruikt bij de verbetering van de klinische praktijk. Als gevolg van het gebruik van het model zijn de eigenschappen van een verbeterd elektrodeontwerp vastgesteld en later getest in een studie op rotsbeenderen.

Hoofdstuk 1 gaat in op de uitgangspunten van een cochleair implantaat en blikt terug op de ontwikkeling van deze prothese van een experimenteel apparaat tot een zeer geaccepteerd commercieel product. Aan het eind van dit hoofdstuk wordt de inhoud van dit proefschrift beschreven.

Hoofdstuk 2 beschrijft het basisprincipe van het modelleren van cochleaire implantaten door middel van een model in twee stappen. De eerste stap is het modelleren van de elektrische geleiding door de cochlea, ook bekend als het volumegeleidingsprobleem. De tweede stap is het simuleren van het gedrag van de zenuwvezels in reactie op de potentiaal verstoring berekend in de eerste stap. Dit tweestappenmodel wordt overal in dit proefschrift gebruikt. De introductie van het spiraalvormige cochleamodel maakt het mogelijk excitatiedrempels en spatiële selectiviteit in de geïmplanteerde cochlea te voorspellen. De uitkomsten van het model, die verschillen laten zien tussen de excitatiegebieden van de verschillende elektrodelocaties, worden vergeleken met elektrofysiologische experimenten. Wij concluderen dat zij goede overeenkomsten laten zien.

Hoofdstuk 3 geeft een gedetailleerde beschrijving van het volumegeleidingsmodel met een uitleg hoe de spiraalvormige cochleaire meshes en de implantaatontwerpen in dit proefschrift zijn gegenereerd. De meshes bieden de flexibiliteit om klinisch relevante onderwerpen te onderzoeken. Door middel

van het model van een caviacochlea zijn de isolerende effecten van de membranen die de scala tympani omringen onderzocht. De beschreven mesh-genererendesoftware is flexibel genoeg om te worden gebruikt voor de meer uitdagende creatie van het menselijk cochlea.

Hoofdstuk 4 beschrijft de potentiaal distributie- en stroompaden in het spiraalvormige cochleaire model zoals beschreven in de voorgaande hoofdstukken. De relatief goed geleidende scala tympani blijken inderdaad zeer belangrijk te zijn. Het exponentiële verval ($J \sim e^{-z}$) van de stroom geeft echter alleen maar een goede omschrijving van het verrevelgedrag. In de nabijheid van de elektrodes, dan wel in de nabijheid van de gemakkelijkst te prikkelen vezels, worden hogere stroomdichtheden gevonden die het beste omschreven kunnen worden met een sferische spreiding van de stroom ($J \sim \frac{1}{R^2}$). We concluderen dat de stroomspreiding langs de scala tympani en diens afhankelijkheid van de positie van de stroombron in de cochlea goed wordt omschreven door de superpositie van het sferisch en exponentieel verval.

Hoofdstuk 5 beschrijft de vergelijking tussen de resultaten van een computermodel van het caviacochlea en een realistisch model van het menselijk cochlea. Beide zijn geïmplantéerd met een model van een HiFocus cochleair implantaat. Hierbij wordt rekening gehouden met de aanzienlijke anatomische verschillen in grote, locatie in het rotsbeen en de complete geometrie van de cochlea en de gehoorzenuw van beide soorten. Het blijkt dat een goed ontworpen perimodiolaire elektrode resulteert in stimulatiedrempels en een hoge spatiële selectiviteit zonder een verlaging van het dynamisch bereik. In de tweede winding van het menselijk cochlea zijn de resultaten echter minder gunstig. Evenals bij de cavia verlaagt cross-turn stimulatie het dynamisch bereik in de perimodiolaire positie substantieel. We concluderen dat het klinische succes van cochleaire implantatie bij de mens en de veelbelovende resultaten met de modiolaire elektrode grotendeels afhankelijk zijn van de typisch menselijke cochleaire anatomie.

De klinische evaluatie van de HiFocus elektrodearray met de positionering van het elektrodepositioneringssysteem gecombineerd met de CII-implantaat-elektronica is beschreven in hoofdstuk 6. De spraakperceptiescores op CVC-woorden zijn, zonder het gebruik van spraakafzien, geobserveerd bij tien postlinguaal doofgeworden patiënten. Na n week waren alle patiënten in staat de telefoon functioneel te gebruiken. Aan het eind van het onderzoek (3 tot 11 maanden na afloop) was de gemiddelde CVC-fonemenscore 84% (woordscore 66%). De Fonemen herkenningdrempel (50% van de uitvoering in stilte) wordt bereikt voor Signal-to-Noise ratio's tussen 0 en -5 dB. NRI-waarnemingen

worden bereikt met zowel de wisselende polariteit als het forward masking paradigma. Het NRI-systeem, alhoewel wat traag, geeft goede resultaten en biedt de mogelijkheid om I/O curves te meten en de neurale spreiding te bepalen.

Het onderzoek zoals beschreven in hoofdstuk 7 evalueert het effect van de duur van een post-operatieve follow-up op de waarde van de pre-operatieve voorspellers. De prestatieresultaten van een groep van 91 patiënten, geïmplanteerd tussen 2000 en 2005 met een HiRes90K of CII-implantaat met een HiFocus I elektrodearray, wordt geëvalueerd door middel van de uni-variate lineaire regressieanalyse en de multiple regressieanalyse gebaseerd op het Iowa voorspellend model. Het verschil in de leercurve tussen patiënten met een lange en korte duur van doofheid, of het verschil in implantatieleeftijd laat een afhankelijkheid zien van de postoperatieve ervaring op het relatieve belang van de voorspellende factoren. Om die reden moeten voorspellende modellen gebaseerd worden op follow-up tijden van minimaal twee jaar om patiënten die langzamer herstellen de mogelijkheid te geven hun maximale prestatieniveau te benaderen. Wanneer gebruik gemaakt wordt van niet gecontroleerde retrospectieve onderzoeken, zou de meervoudige regressieanalyse gebruikt moeten worden om de invloed van bijvoorbeeld, het ontwerp van het elektrodearray of de implantatieleeftijd op de spraakbegripscores te achterhalen. Daarmee wordt het effect van andere parameters zoals de duur van de doofheid gereduceerd.

Hoofdstuk 8 beschrijft de uitbreiding van het menselijk cochleamodel met het vermogen om responsen terug te kunnen meten. Dit model wordt gebruikt om de bijdrage van de individuele enkele vezel bijdragen (SFAP) aan de eCAP te onderzoeken bij wisselende stimulatieniveaus. De bijdrage van de individuele vezel laat zien dat bij hoge stroomniveaus centraal gelegen vezels in het excitatiegebied, dicht bij de stimulerende elektrode, een a-typische reactie vertonen zonder een duidelijke negatieve piek in de SFAP. Het aantal vezels met a-typische reacties neemt bovendien toe met het stimulatieniveau. Als gevolg hiervan neemt de algehele eCAP-amplitude af boven een zeker stimulatieniveau. Dit verschijnsel werd eerder waargenomen, maar werd altijd beschouwd als een waarnemingsartefact.

Hoofdstuk 9 beschrijft een uitgebreid modelonderzoek naar de consequenties van de exacte locatie van het elektrodearray in de scala tympani. Het doel van dit hoofdstuk is het bepalen van de optimale plaatsing met betrekking tot drempel, dynamisch bereik en spatiële selectiviteit voor zowel gedegeneerde als niet-gedegeneerde cochleae. Het model voorspelt een verlaagde

drempel, toegenomen dynamisch bereik en hogere spatiële selectiviteit voor de peri-modiolaire positie aan het basale einde van de cochlea. Hierbij treedt minimale invloed op van neurale degeneratie. Aan het apicale einde van de array (1,5 cochleaire windingen), waren het dynamisch bereik en de spatiële selectiviteit beperkt als gevolg van het optreden van cross-turn stimulatie. Uitzondering hierop is de situatie waarbij geen neurale degeneratie optreedt en de elektrodearray langs de laterale wand van de scala tympani is geplaatst. De voordelen van eCAP-waarnemingen met betrekking tot intra-operative plaatsingsoptimalisatie zijn onderzocht. De eCAP-simulaties geven aan dat een grote P_0 piek optreedt voor het N_1P_1 complex wanneer de vezels niet zijn gedegenerereerd. De afwezigheid van deze piek kan gebruikt worden als een indicator voor neurale degeneratie.

Gebaseerd op de ontwerpcriteria zoals beschreven in hoofdstuk 9 is een ontwerpwijziging in de huidige HiFocus elektrodearray voorgesteld met een peri-modiolaire positie van de elektrodearray voor de basale contacten, terwijl een laterale positie verkregen moet worden voor meer apicale posities. De initiële studie op rotsbeenderen met prototype elektrodes die tegemoed komen aan deze criteria is beschreven in hoofdstuk 10. De prototype elektrodes zijn geplaatst in menselijke rotsbeenderen en de positie van de contacten is geverifieerd met hoge resolutie CT-scans voorafgaand aan zorgvuldige dissectie en documentatie van het insertie trauma. De nieuwe elektrode is in staat de gewenste positie in te nemen met minimale schade aan intracochleaire structuren.

Hoofdstuk 11 beschrijft zowel de mogelijkheden van het huidige model als de toekomstige stappen voor de ontwikkeling van een patiëntspecifiekmodel met directe klinische gevolgen voor de individuele patiënt. Enkele van de lopende ontwikkelingen die leiden tot een nieuwe generatie cochleaire implantaten zijn toegelicht. Er wordt geconcludeerd dat het modelleren met behulp van computers een theoretische richtlijn kan geven waarlangs nieuwe experimenten en nieuwe ontwikkelingen voor cochleaire implantaten kunnen verlopen.

Curriculum vitae

Jeroen Johannes Briaire geboren op 31 Januari 1974 te Nootdorp heeft in 1991 zijn HAVO en in 1992 zijn VWO diploma gehaald aan het St. Maartens college te Voorburg. Hij heeft in 1997 zijn ingenieursdiploma Technische Natuurkunde gehaald aan de Technische Universiteit van Delft op het gebied van Fysische Technologie. Na zijn doctoraalexamen is hij als onderzoeker in opleiding begonnen bij de KNO-afdeling van het toenmalige AZL. Na enkele jaren onderzoek naar cochleaire implantaten met behulp van computermodellen is hij in juli 2001 naast zijn onderzoek in deeltijd begonnen met de opleiding tot klinisch fysicus in de audiologie. Per 7 september 2006 werd hij als zodanig geregistreerd. Sinds 2000 is hij werkzaam als audioloog, aanvankelijk in opleiding, voor het cochleaire implantatie team van het Leids Universitair Medisch Centrum. Momenteel is hij werkzaam als dagelijks leidinggevende van het CI-team en coördinator van het CI-gerelateerde onderzoek.